



STUDIA UNIVERSITATIS
BABEŞ-BOLYAI

Volume 67, No. 1 (2022)

Engineering



UNIVERSITATEA BABEŞ-BOLYAI
BABEŞ-BOLYAI TUDOMÁNYEGYETEM
BABEŞ-BOLYAI UNIVERSITAT
BABEŞ-BOLYAI UNIVERSITY
TRADITIO ET EXCELLENTIA



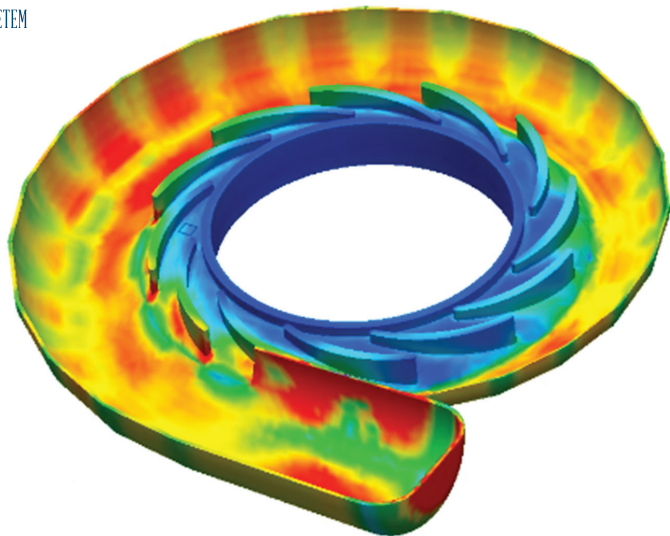
STUDIA UNIVERSITATIS
BABEŞ-BOLYAI
www.studia.ubbcluj.ro
51 B.P. Hasdeu Street, 400371
Cluj-Napoca, ROMANIA



CLUJ UNIVERSITY PRESS
www.editura.ubbcluj.ro

ISSN: 2734-7680

ISSN-L: 2734-7680





STUDIA UNIVERSITATIS
BABEŞ-BOLYAI

Engineering

The Journal of the Faculty of Engineering at Reşiţa
Babeş-Bolyai University from Cluj-Napoca

Volume 67, No. 1, 2022

doi:10.24193/subbeng.2022.1

Published Online: 2022-11-21

ISSN (Online): 2734-7680

EDITORIAL OFFICE:

Piața Traian Vuia, Nr. 1-4, 320085, Reșița,
Caraș-Severin, România
http://studia.ubbcluj.ro/serii/engineering/index_en.html

EDITOR-IN-CHIEF:

Nicoleta GILLICH

BBU University Center in Reșița – Romania
Faculty of Engineering
nicoleta.gillich@ubbcluj.ro

© Studia Universitatis Babeș-Bolyai, Babeș-Bolyai University
B.P. Hasdeu str. no. 51, 400371 Cluj-Napoca, Romania
Phone: +40-264-405300 *6452; Fax: +40-264-591906
e-mail: office@studia.ubbcluj.ro

Table of content

| | |
|---|-----------|
| <i>Alexandra-Teodora Aman, Cristian Tufisi, Gilbert-Rainer Gillich</i> Damage detection in simply supported beams using machine learning | 7 |
| <i>Olga-Ioana Amariei, Codruța-Oana Hamat, Alexandru-Victor Amariei</i> Analysis of the quality of the sales forecast | 16 |
| <i>Olga-Ioana Amariei, Andrea-Amalia Minda, Daniel-Mihai Amariei</i> Analysis of the optimal location of new facilities within a production section | 27 |
| <i>Carmen Nicoleta Debeleac</i> Sensitivity analysis on the vertical motion of heavy machine due to changing tires characteristics | 39 |
| <i>Nicolae Daniel Fita, Liliana Samoila, Dragos Pasculescu, Emilia Grigorie, Raluca Grigorie</i> Analysis of the energy security of the Republic of Moldova in the context of accesion and integration to the European Union | 45 |
| <i>Nicolae Daniel Fita, Mihai Sorin Radu, Dragos Pasculescu, Florin Mureșan, Danut Mircea Pinte</i> Analysis of power system of the Republic of Moldova in the context of the interconnection to ENTSO-E and accesion to European Union | 58 |

| | |
|--|------------|
| <i>Marius Lolea, Andrea Amalia Minda, Eva Barla, Andrei Sărăcuț-Ardelean, Emeric Szabo</i> | |
| The Electromagnetic Mapping of the City of Beiuș | 70 |
| <i>Octavian Mangos</i> | |
| Analysis of heat flows in the eddy current wind generator | 85 |
| <i>Calin-Octavian Miclosina, Alexandru-Stefan Filip, Vasile Cojocar, Daniel-Gheorghe Vela</i> | |
| On the Milling Process Simulation of an Injection Mold Part | 93 |
| <i>Ion-Cornel Mituletu, Alexandru Predica, Ionut Voina</i> | |
| Sine Wave Electromagnetic Generation Using H-Bridge and Microcontroller | 105 |
| <i>Daniela Negrea, Cornelia-Victoria Anghel-Drugărin, Marius Lolea, Emeric Szabo</i> | |
| About the availability of hydro-energy units from the Iad – Drăgan Hydropower Subsystem | 113 |
| <i>Adeolu Seun Obamehinti, Victor Eguavoen</i> | |
| A literature review of land title with the aim of maximising the benefits of Blockchain technology in the management of Land Title in Nigeria | 124 |
| <i>Michael Banji Olatunde, Faith Ozofu Olatunde, Henry Eronmosele Oriakhi</i> | |
| Street Guide Mapping of Auchi, Edo State, Nigeria | 136 |
| <i>Michael Banji Olatunde, Faith Ozofu Olatunde, Iyotor Thaddeus Eshiemokhai, Hussani Idris</i> | |
| Control Extension Using Global Navigation Satellite System Receivers in Auchi, Nigeria | 149 |

| | |
|--|------------|
| <i>Yahaya Olotu, Livinus Apebuamhe Izah, Moses Eromosele Eseigbe, Reuben Ishiekwene, John Friday Ogbodo</i> Re-calibration of an automatic evaporimeter | 162 |
| <i>Yahaya Olotu, Edwin Omozuapo Oyathelemi, Shaka Momoh, Olugbemiga Stephen Ifabiyi</i> Evaluation of the effects of non-revenue water on water security in Ondo State, Nigeria | 172 |
| <i>Yahaya Olotu, Reuben Ishiekwene, Mariam Abdul-Wajid Obomeghie, Stephen Korede Abolaji, Ferdinand Aleonokhu Aigbodoh</i> Development and Evaluation of a Digital MPF5-Moisture Meter | 182 |
| <i>Dan Alexandru Pîrşan</i> The influence of the Young modulus on two elements of a Warren truss on the dynamic behavior of the structure | 191 |
| <i>Zeno-Iosif Praisach, Dan Alexandru Pîrşan</i> The influence of the change of the longitudinal modulus of elasticity on the dynamic behavior of a Warren truss | 201 |
| <i>Marius-Florian Predus, Cristian-Mircea Muscai, Cornel Hatiegan</i> Simulation of electric field lines produced by electric point charges | 209 |
| <i>Liviu-Bogdan Protea, Cristian-Mircea Muscai</i> Design of low voltage electrical circuits for industrial receivers | 216 |
| <i>Elisabeta Spunei, Arpad Csepei, Ion Piroi, Florina Piroi, Mihai Rotaru</i> Study on the importance of upgrading public lighting systems | 224 |

| | |
|---|------------|
| <i>Mihaela Dorica Stroia, Cornel Hațiegan, Bogdan Daniel Borcilă</i> Application for speech assistance of people with hearing disability | 238 |
| <i>Stelică Timofte, Lenuța Cîndea, Cornel Hațiegan</i> Robot for tracking rectilinear motion | 246 |
| <i>Petru Todos, Ilie Nuca, Andrei Chiciuc, Vadim Cazac, Marcel Burduniuc</i> Electromechanical engineering education and science in Republic of Moldova | 256 |
| <i>Ion Voncilă, Elena Selim, Ion Paraschiv</i> Geometry influence of stator and rotor armatures on energy efficiency of induction motors | 268 |

Damage detection in simply supported beams using machine learning

Alexandra-Teodora Aman, Cristian Tufisi*, Gilbert-Rainer Gillich

Abstract. *The more our infrastructure is aging, the risk of structural failure is higher, making the detection of damage using modal parameters a very important factor that can be applied in structural health monitoring. The most desired way to assess the health of engineering structures during operation is to use non-destructive vibration-based methods. In the current paper, a modal approach using a machine learning technique by training a feedforward backpropagation neural network for detecting transverse damages in simple supported beam-like structures is presented. A method for analytical determination of the training data is used and the obtained dataset values are employed for training an ANN that will be used to locate and evaluate the severity of transverse cracks in cantilever beams. The output from the ANN model is compared by plotting the calculated error for each case in comparison with FEM results using the SolidWorks simulation software.*

Keywords: *damage detection, machine learning, natural frequency, structural health monitoring*

1. Introduction

Engineering systems rely on effective damage detection techniques to ensure their safe operation over time. In case of damage occurrence, the dynamic and static behavior of structures, such as natural frequencies, modal shape, stiffness, and the degree of damping are affected [1]. The development of the modern aeronautical industry, mechanical systems, and the civil industry generated a new trend for a more rigorous analysis of structures. The recent orientation in the development of damage detection methods in structures is characterized by using high-performance computers that engage numerical methods, including the finite element method, comparing the results with experimental data, and with different analytical methods [2].



The use of modal parameters in early-stage damage detection techniques has gained much attention in the last decades, as of the promising results obtained by several research [3]. Paper [4] presents a method to detect the location and severity of transverse cracks in a simply supported beam that uses the first three natural frequencies, and the method is validated through FEM, analytical and experimental data. The authors in paper [5] illustrate a damage detection method, capable of locating a crack in beams with any boundary conditions by considering the changes of the modal curvature. Because the computation performance of computers has increased, new methods that rely on intelligent algorithms that can handle large amounts of data, mainly by using modal parameters, have been developed for the detection of damages. In the paper [6], the authors present a method for detecting damages in cantilever beams by using artificial neural networks (ANN) that are trained using the mode shape displacements. In article [7], the authors successfully developed an ANN algorithm for detecting the presence of one or multiple cracks in structures using a metaheuristic training algorithm, and paper [8] demonstrates the possibility of locating and evaluating cracks by using ANN's even when the boundary conditions are uncertain. In the current research, we extend the method presented in [8] for developing an ANN using the MATLAB software that is capable of detecting, locating, and evaluating breathing transverse cracks, present along the whole width, in simply supported steel beams by employing the Relative Frequency Shifts (RFS).

2. Analytic approach

Damages decrease the overall capacity of a structure to retain energy, thus impacting its dynamic parameters. By using the RFS values caused by the occurrence of a crack, depending on its location and severity, a database of damage signatures can be easily created by analytical approaches.

In the current research, we utilize the methods shown in paper [9] to calculate the RFS values, for the first six weak-axis vibration modes, by considering the severity $\gamma(a)$ for a crack of depth a and the squared normalized modal curvature $[\overline{\phi}''(x)]^2$ for a known position x along the beam [10]. The RFS values for any crack severity can be found with the following relation (1) [10]:

$$\Delta_{f_i-D} = \gamma(a) \cdot [\overline{\phi}''(x)]^2 \quad (1)$$

By using the stiffness decrease method presented in paper [11], the severity for a certain crack depth can be calculated from the beam's deflection both in undamaged δ_u and damaged state δ_d , with the following relation (2):

$$\gamma(a) = \frac{\sqrt{\delta_D} - \sqrt{\delta_U}}{\sqrt{\delta_D}} \quad (2)$$

The normalized modal curvature is determined using eq. (3):

$$\varphi''(x) = -\sin(\alpha x) \quad (3)$$

In the present paper, the training dataset represents the RFS values calculated for the first six natural frequencies of the damaged beam, considering only the transverse vibration modes. The RFS values generated for training the ANN model are calculated using relations (1) to (3) for a transverse breathing crack that is present on a simply supported steel beam with its considered dimensions presented in mm in Figure 1.

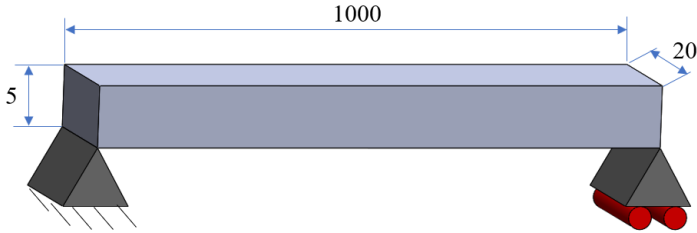


Figure 1. Main dimensions of the simply supported steel beam

The severity $\gamma(a)$ of the transverse crack is considered for a crack depth a between $a=0.1...0.28 \cdot H$, where H represents the beam's thickness as presented in Table 1. The ANN is trained to output the percent of the damage depth.

Table 1. Severity values used for calculating the RFS's

| Severity $\gamma(a)$ [-] | Crack depth [mm] | Crack depth [%] |
|-----------------------------|---------------------|--------------------|
| 0.00086654 | 0.5 | 10.00% |
| 0.00119113 | 0.6 | 12.00% |
| 0.00214098 | 0.8 | 16.00% |
| 0.00334597 | 1 | 20.00% |
| 0.00512393 | 1.2 | 24.00% |
| 0.00710485 | 1.4 | 28.00% |

The RFS's are calculated, for the six vibration modes, iteratively for all defined severity values considering several positions of the crack along the beam, starting from the left end with a step of 10 mm, thus obtaining 600 possible damage scenarios. The calculated RFS's for the six vibration modes are plotted and presented in Figure 2.

Because of the nature of the boundary conditions, as can be observed from Figure 2, the modal curvature will be symmetric relative to the axis of the beam, therefore the developed neural network will always output two possible damage locations, from which one location is the mirrored value of the true one.

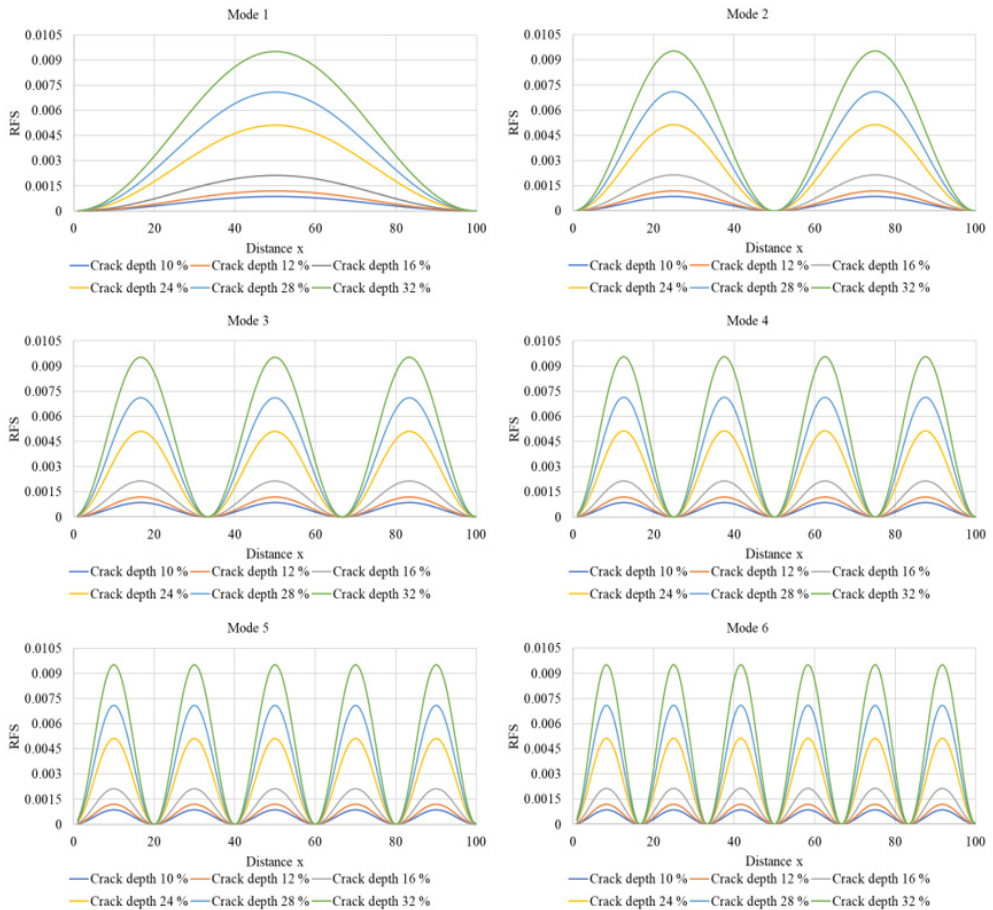


Figure 2. Plotted RFS curves for the defined damage scenarios

3. Training the ANN model

After the RFS values are calculated for the first six modes of transverse vibration, they are imported into a MATLAB database and used to train a Feedforward Backpropagation Neural Network with six inputs. As the target value for the ANN we introduce the position of the crack and the corresponding severity value which is equated with the percentage depth of the transverse crack. For the given training and output data we have considered a network architecture of one hidden layer with the number of neurons $N_h=25$ according to relation (4):

$$N_h = \frac{N_s}{\alpha \cdot (N_i + N_t)} \quad (4)$$

where:

N_s – number of scenarios; $N_s=600$; α – coefficient dependent of the ANN's complexity; $\alpha=3$; N_i – number of inputs; $N_i=8$; N_t – number of targets; $N_t=2$.

The network is trained by applying the Bayesian Regularization algorithm [13] and considering 70% of the data for training, 15% for validation and 15% for testing. The architecture of the ANN is presented in Figure 3, where the input layer contains 6 neurons representing the 6 RFS values, the hidden layers contain 25 neurons according to Eq. (4) and the output layers contain 2 neurons for predicting two parameters i.e., crack location and depth. The terms w and b represent the considered weights and bias values used in each iteration for defining the activation function of the network [14].

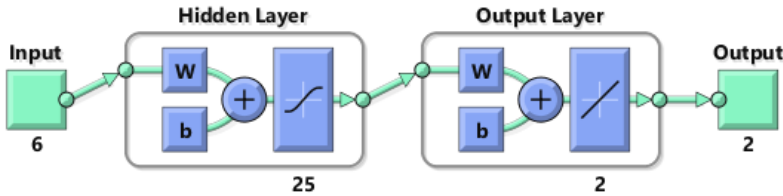


Figure 3. Developed ANN architecture

The performance of the ANN is evaluated based on the 15% test data directly from the MATLAB interface by plotting the regression curves, as shown in Figure 4.

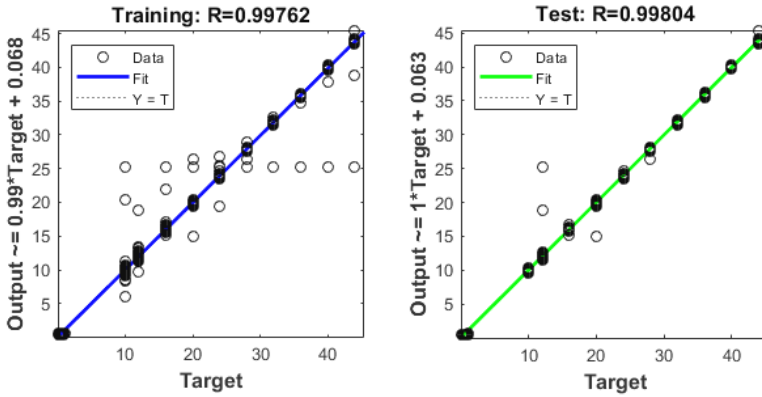


Figure 4. ANN plotted performance

4. Evaluating the accuracy of the ANN model

To test the accuracy of the ANN developed using MATLAB, we performed FEM modal simulations considering several damage scenarios to extract the natural frequency values for the simply supported steel beam of a constant section, both in an undamaged and damaged state, with the dimensions presented in Figure 1 and physical-mechanical properties of the Plain carbon steel material chosen from the SolidWorks library presented in Table 2.

Table 2. Physical-mechanical properties of the material

| Physical-mechanical properties of the material | | | | | |
|--|---|-----------------------------|------------------------------|----------------------------|---------------|
| Density [kg/m ³] | Young modulus [N/m ²] | Poisson criterion [-] | Tensile strength [MPa] | Yield strength [MPa] | Elong. [%] |
| 7800 | $2 \cdot 10^{11}$ | 0.3 | 470-630 | 355 | 20 |

The beam and crack geometry were generated also using SolidWorks. The crack is generated by removing material, with its width being defined as a maximum of 0.04 mm, and its location as the distance from the left end of the beam to the damage. Fine meshing was calculated for all cases, applying elements with a maximum edge size of 3 mm. After meshing, the healthy beam consists of 44587 elements and 241639 nodes. For the damaged beam, due to the crack, a larger number of elements is required. The simulation configuration as well as the vibration analysis is shown in Figure 5 for the case where a 1 mm crack is present at position $x=250$ mm. To achieve the required boundary conditions for the simply supported beam, we have considered the bottom edge of the left face as fixed, al-

lowing only the rotation along its transverse axis (axis y) and for the right face of the beam we have constrained the bottom edge by fixing the translation along the y and z axis, allowing only the rotation along the y axis and translation along the x axis.

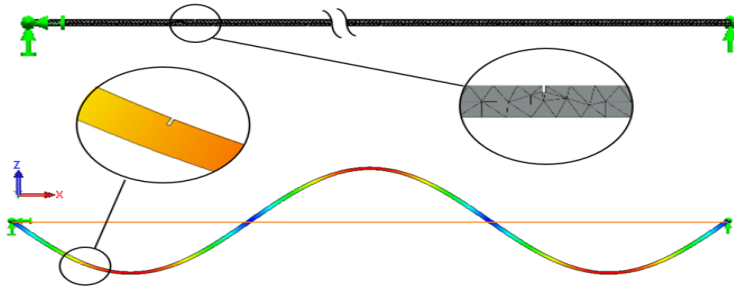


Figure 5. FEM frequency simulation for the simply supported beam

After the results are acquired, the RFS's are calculated and introduced as test data into the developed ANN. The damage scenarios as well as the prediction errors obtained from the neural network are presented in Table 3. Because of the symmetry of the mode shapes caused by the boundary conditions, FEM tests were performed for damage scenarios considering the crack position in the interval from 0 to 500 mm.

Table 3. Defined damage scenarios and obtained results

| Defined simulation values | | | Predicted values | | | |
|---------------------------|---------------------|-----------------|---------------------|--------------------|-----------------|--------------------|
| Damage scen. | Crack position [mm] | Crack depth [%] | Crack Position [mm] | Position error [%] | Crack depth [%] | Severity error [%] |
| 1 | 50 | 12 | 43.00 | 0.70% | 12.33 | 0.33% |
| 2 | 150 | 12 | 168.2 | 1.82% | 14.36 | 2.36% |
| 3 | 365 | 12 | 350.6 | 1.44% | 13.85 | 1.85% |
| 4 | 458 | 12 | 462.0 | 0.40% | 12.35 | 0.35% |
| 5 | 50 | 20 | 56.50 | 0.65% | 20.00 | 0.00% |
| 6 | 150 | 20 | 143.4 | 0.66% | 22.71 | 2.71% |
| 7 | 365 | 20 | 377.4 | 1.24% | 23.54 | 3.54% |
| 8 | 458 | 20 | 470.2 | 1.22% | 23.095 | 3.10% |
| 9 | 50 | 28 | 50.10 | 0.01% | 28.00 | 0.00% |
| 10 | 150 | 28 | 150.6 | 0.06% | 28.38 | 0.38% |
| 11 | 365 | 28 | 364.2 | 0.08% | 29.10 | 1.10% |
| 12 | 458 | 28 | 458.1 | 0.01% | 29.27 | 1.27% |

5. Conclusion

In the current research, we have tested the accuracy of a Feedforward Back-propagation ANN to locate and evaluate transverse cracks occurring in steel simply supported beams. The study demonstrates that by using the RFS determined analytically with the presented methods, one can train precise intelligent algorithms for damage identification and evaluation. The accuracy of the presented ANN can be furtherly enhanced by dividing the training data into sectors [8].

References

- [1] Choi S., Park S., Stubbs N., Nondestructive damage detection in structures using changes in compliance, *International Journal of Solids and Structures*, 2005, 42(15), 2005, pp. 4494-4513.
- [2] Wahab M.A., De Roeck G., Damage detection in bridges using modal curvatures: Application to a real damage scenario, *Journal of Sound and Vibration*, 226, 1999, pp. 217-235.
- [3] Kenley R.M., Dodds C.J., *West Sole we platform: detection of damage by structural response measurements*, 12th Annual Offshore Tech. Conf., 1980, pp. 111–118.
- [4] Sharma U., *Damage Detection in a Steel Beam using Vibration Response*, Youngstown State University, Aug., 2020.
- [5] Pooya S.M.H., Massumi A., A novel and efficient method for damage detection in beam-like structures solely based on damaged structure data and using mode shape curvature estimation, *Applied Mathematical Modelling*, 91, 2021, pp. 670-694.
- [6] Kumar G.S., Das S., Damage detection in a cantilever beam using noisy mode shapes with an application of artificial neural network-based improved mode shape curvature technique, *Asian Journal of Civil Engineering*, 22, 2021, pp.1671-1693.
- [7] Tran-Ngoc H., Khatir S., Le-Xuan T., Tran-Viet H., De Roeck G., Bui-Tien T., Wahab M.A., Damage assessment in structures using artificial neural network working and a hybrid stochastic optimization, *Sci Rep.*, 23:12(1):4958, 2022.

- [8] Gillich N., Tufisi C., Sacarea C., Rusu C., Gillich G.R., Praisach Z.I., Ardeljan M., Beam Damage Assessment Using Natural Frequency Shift and Machine Learning, *Sensors*, 22, 1118, 2022.
- [9] Gillich, G.R., Praisach, Z.I., Robust method to identify damages in beams based on frequency shift analysis, *Health Monit. Struct. Biol. Syst.*, 2012, 8348, 83481D.
- [10] Gillich N., Tufisi C., Vasile O., Gillich G.R., Statistical Method for Damage Severity and Frequency Drop Estimation for a Cracked Beam using Static Test Data, *Rom. J. Acoust. Vib.*, 16, 2019, pp. 47–51.
- [11] Gillich G.R., Tufoi M., Korca Z.I., Stanciu E., Petrica A., The relations between deflection, stored energy, and natural frequencies, with application in damage detection, *Rom. J. Acoust. Vib.*, 13, 2016, pp. 87–93.
- [12] Praisach Z.I., Gillich G.R., Protocsil C., Muntean F., *Evaluation of crack depth in beams for known damage location based on vibration modes analysis*, Applied Mechanics and Materials, 430, 2013, pp. 90-94.
- [13] <https://www.mathworks.com/help/deeplearning/ref/trainbr.html;jsessionid=b6ad10a78b987242c7c285ce1596> – accesed 12.10.2022.
- [14] Fauselt L., *Fundamentals of Neural Networks, Architectures, algorithms and applications*, Prentice-Hall, Inc.Division of Simon and Schuster One Lake Street Upper Saddle River, NJ United States.

Addresses:

- PhD. Stud. Eng. Alexandra-Teodora Aman, Babeş-Bolyai University, Faculty of Engineering, Piața Traian Vuia, nr. 1-4, 320085, Reșița, Romania, aman.alexandra@yahoo.com
- Lect. Dr. Eng. Cristian Tufisi, Babeş-Bolyai University, Faculty of Engineering, Piața Traian Vuia, nr. 1-4, 320085, Reșița, Romania cristian.tufisi@ubbcluj.ro
(*corresponding author)
- Prof. Dr. Eng. Gilbert-Rainer Gillich, Babeş-Bolyai University, Faculty of Engineering, Piața Traian Vuia, nr. 1-4, 320085, Reșița, Romania gilbert.gillich@ubbcluj.ro

Analysis of the quality of the sales forecast

Olga-Ioana Amariei, Codruța-Oana Hamat*, Daniel-Mihai Amariei

Abstract. *This paper presents how to solve the forecasting problems in the conversational system using WinQSB and QM computer products. The study is carried out using three forecasting methods (moving average, single exponential smoothing, linear regression with time) based on sales in the last 12 weeks.*

Keywords: *forecast, moving average, single exponential smoothing, linear regression with time*

1. Introduction

Maximizing profits is the major concern of industrial decision-makers. Obviously, one of the most important factors in the amount of profit is the volume of production, along with the unit selling price, cost structure, etc. [8] Depending on the possibility of the decision maker/researcher to act on the factors in the organization's environment and to influence their evolution, internal and external factors can be identified [6]. Trying to take these factors into account (whether controllable or not) leads to the use of different prediction-US methods [8][6]:

- methods of judgment – Delphi method, expert opinion, historical analogues, etc.;
- causal methods – multiple regression analysis, correlation analysis;
- methods based on time series (dynamic) – moving average method, adjustment method, decompositional methods, etc.;
- econometric methods.

A forecasting system must ensure a significant reaction to a rapid variation of one of the elements that make up the demand and also stabilize and mitigate variations that are purely random [3].

All companies that rely on sales forecasting confirm that the most important aspect of forecasting is how the forecasting activities, the information system, and the people who produce and use the forecasts interact [2].



There are several effective measures of forecast accuracy, namely: mean error (Bias), mean absolute error, sum of squared errors and mean squared error (MSE), as well as measures of accuracy relative to a perfect forecast: percent error, mean absolute percent error (MAPE), year-to-date mean absolute percent error [4].

2. Input data

An industrial enterprise wants to estimate sales for the next periods, with the evolution over the last 12 weeks at its disposal and taking into account that the sales dynamics are not seasonal.

| Week | Sales (p.u.) | Week | Historical Data |
|------|--------------|------|-----------------|
| 1 | 85 | 1 | 85 |
| 2 | 130 | 2 | 130 |
| 3 | 180 | 3 | 180 |
| 4 | 145 | 4 | 145 |
| 5 | 250 | 5 | 250 |
| 6 | 200 | 6 | 200 |
| 7 | 285 | 7 | 285 |
| 8 | 190 | 8 | 190 |
| 9 | 275 | 9 | 275 |
| 10 | 250 | 10 | 250 |
| 11 | 300 | 11 | 300 |
| 12 | 340 | 12 | 340 |

Figure 1. Problem input data in matrix form (in QM and WINQSB programs)

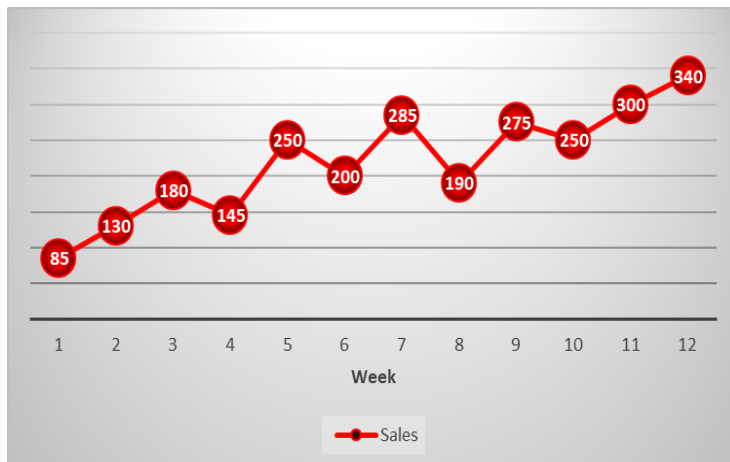


Figure 2. The input data of the problem in graphical form

Based on these data (Figure 1 and Figure 2), the following methods are used:

1. Moving average (MA)
2. Single exponential smoothing (SES)
3. Linear regression with time (LR)

With WinQSB and QM software, the following errors will be determined and analyzed:

- Mean Absolute Deviation (MAD) – with WinQSB and QM
- Cumulative Forecast Error (CFE) – with WinQSB
- Mean Square Error (MSE) – with WinQSB and QM
- Mean Absolute Percent Error (MAPE) – with WinQSB and QM
- Mean Error (Bias) – with QM

3. Problem solving in the conversational system

The following aspects shall be considered:

a) the determination of the forecast shall be made using the values recorded for the first 8 weeks;

b) forecast errors will be calculated over the last 4 weeks (actual sales values are known).

Following the application of the methods mentioned in section 2, the errors obtained will be analyzed and the method will be determined which is more accurate, and we will consider those data as those forecast for the coming weeks.

| 09-20-2022 Week | Actual Data | Forecast by 8-MA | Forecast Error | CFE | MAD | MSE | MAPE (%) | Tracking Signal | R-square |
|--------------------|----------------|---------------------|-------------------|----------|---------|-----------|----------|--------------------|----------|
| 1 | 85.0000 | | | | | | | | |
| 2 | 130.0000 | | | | | | | | |
| 3 | 180.0000 | | | | | | | | |
| 4 | 145.0000 | | | | | | | | |
| 5 | 250.0000 | | | | | | | | |
| 6 | 200.0000 | | | | | | | | |
| 7 | 285.0000 | | | | | | | | |
| 8 | 190.0000 | | | | | | | | |
| 9 | 275.0000 | 183.1250 | 91.8750 | 91.8750 | 91.8750 | 8441.0160 | 33.4091 | 1.0000 | |
| 10 | 250.0000 | 206.8750 | 43.1250 | 135.0000 | 67.5000 | 5150.3910 | 25.3295 | 2.0000 | |
| 11 | 300.0000 | 221.8750 | 78.1250 | 213.1250 | 71.0417 | 5468.0990 | 25.5669 | 3.0000 | |
| 12 | 340.0000 | 236.8750 | 103.1250 | 316.2500 | 79.0625 | 6759.7660 | 26.7579 | 4.0000 | |
| 13 | | 261.2500 | | | | | | | |
| 14 | | 261.2500 | | | | | | | |
| 15 | | 261.2500 | | | | | | | |
| 16 | | 261.2500 | | | | | | | |
| CFE | | 316.2500 | | | | | | | |
| MAD | | 79.0625 | | | | | | | |
| MSE | | 6759.7660 | | | | | | | |
| MAPE | | 26.7579 | | | | | | | |
| Trk.Signal | | 4.0000 | | | | | | | |
| R-square | | | | | | | | | |
| | | m=8 | | | | | | | |

Figure 3. Detailed solution offered by WinQSB –Moving average (MA) method

The first method applied in this study is the moving average (MA) method, and the results are shown in Figure 3 (WinQSB program) and Figure 4 (QM program).

In the case of applying the Single exponential smoothing (SES) method with the WinQSB program, first of all the work mode is chosen, i.e.:

- the method of estimating parameters is selected:
 - Assign Values
 - Search for Best
- the input data is entered
 - number of periods for forecast
 - smoothing constant alpha (α)
 - initial value F(0) if it is known

| | Sales (p.u.) | Forecast | Error | Error | Error^2 | Pct Error |
|----------------------|--------------|----------|---------|---------|----------|-----------|
| 1 | 85 | | | | | |
| 2 | 130 | | | | | |
| 3 | 180 | | | | | |
| 4 | 145 | | | | | |
| 5 | 250 | | | | | |
| 6 | 200 | | | | | |
| 7 | 285 | | | | | |
| 8 | 190 | | | | | |
| 9 | 275 | | | | | |
| 10 | 250 | 193,333 | 56,667 | 56,667 | 3211,112 | 22,667% |
| 11 | 300 | 211,667 | 88,333 | 88,333 | 7802,777 | 29,444% |
| 12 | 340 | 230,556 | 109,444 | 109,444 | 11978,09 | 32,19% |
| TOTALS | 2630 | | 254,444 | 254,444 | 22991,97 | 84,301% |
| AVERAGE | 219,167 | | 84,815 | 84,815 | 7663,992 | 28,1% |
| Next period forecast | | 248,333 | (Bias) | (MAD) | (MSE) | (MAPE) |
| | | | | Std err | 151,631 | |

Figure 4. Detailed solution offered by QM –Moving average (MA) method

The *Forecasting* module in WinQSB has built in the α coefficient simulation routine [7]. *Search the best* it is selected and then the comparison criterion (MAD, CFE, MSE or MAP), according to Figure 5, for finding of the best value.

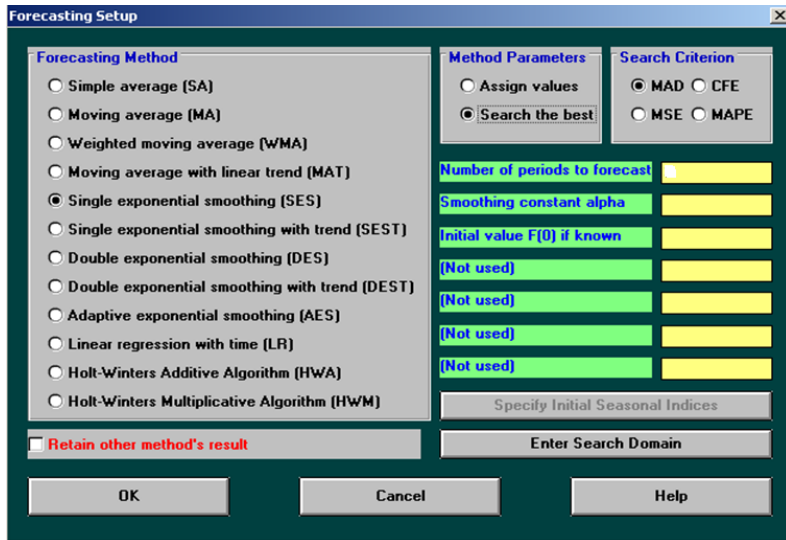


Figure 5. Forecasting Setup dialog window

| US-2U-2UZZ Week | Actual Data | Forecast by SES | Forecast Error | CFE | MAD | MSE | MAPE [%] | Tracking Signal | H-square |
|--------------------|----------------|--------------------|-------------------|----------|---------|-----------|----------|--------------------|----------|
| 1 | 85.0000 | | | | | | | | |
| 2 | 130.0000 | 85.0000 | 45.0000 | 45.0000 | 45.0000 | 2025.0000 | 34.6154 | 1.0000 | |
| 3 | 180.0000 | 108.8500 | 71.1500 | 116.1500 | 58.0750 | 3543.6620 | 37.0716 | 2.0000 | |
| 4 | 145.0000 | 146.5595 | -1.5595 | 114.5905 | 39.2365 | 2363.2520 | 25.0729 | 2.9205 | |
| 5 | 250.0000 | 145.7330 | 104.2670 | 218.8576 | 55.4941 | 4490.3430 | 29.2314 | 3.9438 | |
| 6 | 200.0000 | 200.9945 | -0.9945 | 217.8631 | 44.5942 | 3592.4720 | 23.4845 | 4.8855 | |
| 7 | 285.0000 | 200.4674 | 84.5326 | 302.3957 | 51.2506 | 4184.6870 | 24.5139 | 5.9003 | |
| 8 | 190.0000 | 245.2697 | -55.2697 | 247.1261 | 51.8247 | 4023.2650 | 25.1675 | 4.7685 | |
| 9 | 275.0000 | 215.9767 | 59.0233 | 306.1493 | 52.7246 | 3955.8250 | 24.7044 | 5.8066 | |
| 10 | 250.0000 | 247.2591 | 2.7409 | 308.8903 | 47.1708 | 3517.1240 | 22.0813 | 6.5483 | |
| 11 | 300.0000 | 248.7118 | 51.2882 | 360.1785 | 47.5826 | 3428.4600 | 21.5828 | 7.5695 | |
| 12 | 340.0000 | 275.8945 | 64.1055 | 424.2840 | 49.0847 | 3490.3740 | 21.3348 | 8.6439 | |
| 13 | | 309.8704 | | | | | | | |
| 14 | | 309.8704 | | | | | | | |
| 15 | | 309.8704 | | | | | | | |
| 16 | | 309.8704 | | | | | | | |
| CFE | | 424.2840 | | | | | | | |
| MAD | | 49.0847 | | | | | | | |
| MSE | | 3490.3740 | | | | | | | |
| MAPE | | 21.3348 | | | | | | | |
| Trk.Signal | | 8.6439 | | | | | | | |
| R-square | | | | | | | | | |
| | | Alpha=0.53 | | | | | | | |
| | | F(0)=85 | | | | | | | |

Figure 6. Detailed solution offered by WinQSB – Single exponential smoothing (SES) method –MAD criteria

| 09-20-2022 Week | Actual Data | Forecast by SES | Forecast Error | CFE | MAD | MSE | MAPE (%) | Tracking Signal | R-square |
|--------------------|----------------|--------------------|-------------------|----------|---------|-----------|----------|--------------------|----------|
| 1 | 85.0000 | | | | | | | | |
| 2 | 130.0000 | 85.0000 | 45.0000 | 45.0000 | 45.0000 | 2025.0000 | 34.6154 | 1.0000 | |
| 3 | 180.0000 | 130.0000 | 50.0000 | 95.0000 | 47.5000 | 2262.5020 | 31.1966 | 2.0000 | |
| 4 | 145.0000 | 180.0000 | -35.0000 | 60.0001 | 43.3333 | 1916.6670 | 28.8437 | 1.3846 | |
| 5 | 250.0000 | 145.0000 | 105.0000 | 165.0000 | 58.7500 | 4193.7490 | 32.1328 | 2.8085 | |
| 6 | 200.0000 | 249.9999 | -49.9999 | 115.0001 | 57.0000 | 3854.9970 | 30.7062 | 2.0175 | |
| 7 | 285.0000 | 200.0000 | 85.0000 | 200.0001 | 61.6666 | 4416.6640 | 30.5593 | 3.2432 | |
| 8 | 190.0000 | 284.9999 | -94.9999 | 105.0001 | 66.4285 | 5074.9960 | 33.3365 | 1.5806 | |
| 9 | 275.0000 | 190.0001 | 84.9999 | 190.0001 | 68.7500 | 5343.7450 | 33.0331 | 2.7636 | |
| 10 | 250.0000 | 274.9999 | -24.9999 | 165.0001 | 63.8889 | 4819.4400 | 30.4738 | 2.5826 | |
| 11 | 300.0000 | 250.0000 | 50.0000 | 215.0001 | 62.5000 | 4587.4960 | 29.0931 | 3.4400 | |
| 12 | 340.0000 | 300.0000 | 40.0000 | 255.0002 | 60.4545 | 4315.9050 | 27.5178 | 4.2180 | |
| 13 | | 340.0000 | | | | | | | |
| 14 | | 340.0000 | | | | | | | |
| 15 | | 340.0000 | | | | | | | |
| 16 | | 340.0000 | | | | | | | |
| CFE | | 255.0002 | | | | | | | |
| MAD | | 60.4545 | | | | | | | |
| MSE | | 4315.9050 | | | | | | | |
| MAPE | | 27.5178 | | | | | | | |
| Trk.Signal | | 4.2180 | | | | | | | |
| R-square | | | | | | | | | |
| | | Alpha=1 | | | | | | | |
| | | F(0)=85 | | | | | | | |

Figure 7. Detailed solution offered by WinQSB –
Single exponential smoothing (SES) method –CFE criteria

| 09-20-2022 Week | Actual Data | Forecast by SES | Forecast Error | CFE | MAD | MSE | MAPE (%) | Tracking Signal | R-square |
|--------------------|----------------|--------------------|-------------------|----------|---------|-----------|----------|--------------------|----------|
| 1 | 85.0000 | | | | | | | | |
| 2 | 130.0000 | 85.0000 | 45.0000 | 45.0000 | 45.0000 | 2025.0000 | 34.6154 | 1.0000 | |
| 3 | 180.0000 | 113.8000 | 66.2000 | 111.2000 | 55.6000 | 3203.7210 | 35.6966 | 2.0000 | |
| 4 | 145.0000 | 156.1680 | -11.1680 | 100.0320 | 40.7893 | 2177.3880 | 26.3651 | 2.4524 | |
| 5 | 250.0000 | 149.0205 | 100.9795 | 201.0116 | 55.8369 | 4182.2570 | 29.8718 | 3.6000 | |
| 6 | 200.0000 | 213.6473 | -13.6473 | 187.3642 | 47.3990 | 3383.0560 | 25.2621 | 3.9529 | |
| 7 | 285.0000 | 204.9130 | 80.0870 | 267.4512 | 52.8470 | 3888.2000 | 25.7352 | 5.0609 | |
| 8 | 190.0000 | 256.1687 | -66.1687 | 201.2825 | 54.7501 | 3958.2130 | 27.0339 | 3.6764 | |
| 9 | 275.0000 | 213.8207 | 61.1793 | 262.4618 | 55.5537 | 3931.2990 | 26.4355 | 4.7245 | |
| 10 | 250.0000 | 252.9754 | -2.9754 | 259.4863 | 49.7117 | 3495.4720 | 23.6305 | 5.2198 | |
| 11 | 300.0000 | 251.0712 | 48.9288 | 308.4152 | 49.6334 | 3385.3280 | 22.8984 | 6.2139 | |
| 12 | 340.0000 | 282.3856 | 57.6144 | 366.0296 | 50.3589 | 3379.3360 | 22.3572 | 7.2684 | |
| 13 | | 319.2588 | | | | | | | |
| 14 | | 319.2588 | | | | | | | |
| 15 | | 319.2588 | | | | | | | |
| 16 | | 319.2588 | | | | | | | |
| CFE | | 366.0296 | | | | | | | |
| MAD | | 50.3589 | | | | | | | |
| MSE | | 3379.3360 | | | | | | | |
| MAPE | | 22.3572 | | | | | | | |
| Trk.Signal | | 7.2684 | | | | | | | |
| R-square | | | | | | | | | |
| | | Alpha=0.64 | | | | | | | |
| | | F(0)=85 | | | | | | | |

Figure 8. Detailed solution offered by WinQSB –
Single exponential smoothing (SES) method –MSE criteria

| 09-20-2022 Week | Actual Data | Forecast by SES | Forecast Error | CFE | MAD | MSE | MAPE (%) | Tracking Signal | R-square |
|--------------------|----------------|--------------------|-------------------|----------|---------|-----------|----------|--------------------|----------|
| 1 | 85.0000 | | | | | | | | |
| 2 | 130.0000 | 85.0000 | 45.0000 | 45.0000 | 45.0000 | 2025.0000 | 34.6154 | 1.0000 | |
| 3 | 180.0000 | 108.4000 | 71.6000 | 116.6000 | 58.3000 | 3575.7810 | 37.1966 | 2.0000 | |
| 4 | 145.0000 | 145.6320 | -0.6320 | 115.9680 | 39.0773 | 2383.9870 | 24.9430 | 2.9677 | |
| 5 | 250.0000 | 145.3034 | 104.6966 | 220.6647 | 55.4822 | 4528.3370 | 29.1769 | 3.9772 | |
| 6 | 200.0000 | 199.7456 | 0.2544 | 220.9191 | 44.4366 | 3622.6820 | 23.3670 | 4.9716 | |
| 7 | 285.0000 | 199.8779 | 85.1221 | 306.0412 | 51.2175 | 4226.5310 | 24.4504 | 5.9753 | |
| 8 | 190.0000 | 244.1414 | -54.1414 | 251.8998 | 51.6352 | 4041.4960 | 25.0282 | 4.8784 | |
| 9 | 275.0000 | 215.9879 | 59.0121 | 310.9120 | 52.5573 | 3971.6130 | 24.5821 | 5.9157 | |
| 10 | 250.0000 | 246.6742 | 3.3258 | 314.2378 | 47.0872 | 3531.5520 | 21.9986 | 6.6735 | |
| 11 | 300.0000 | 248.4036 | 51.5964 | 365.8342 | 47.5381 | 3444.6160 | 21.5186 | 7.6956 | |
| 12 | 340.0000 | 275.2337 | 64.7663 | 430.6005 | 49.1043 | 3512.8030 | 21.2941 | 8.7691 | |
| 13 | | 308.9122 | | | | | | | |
| 14 | | 308.9122 | | | | | | | |
| 15 | | 308.9122 | | | | | | | |
| 16 | | 308.9122 | | | | | | | |
| CFE | | 430.6005 | | | | | | | |
| MAD | | 49.1043 | | | | | | | |
| MSE | | 3512.8030 | | | | | | | |
| MAPE | | 21.2941 | | | | | | | |
| Trk.Signal | | 8.7691 | | | | | | | |
| R-square | | | | | | | | | |
| | | Alpha=0.52 | | | | | | | |
| | | F(0)=85 | | | | | | | |

Figure 9. Detailed solution offered by WinQSB – Single exponential smoothing (SES) method – MAPE criteria

Using the QM program, we obtained the following results by choosing four different values for α (Figure 10).

| Measure | Value |
|------------------------------------|----------|
| Error Measures | |
| Bias (Mean Error) | 39.145 |
| MAD (Mean Absolute Deviation) | 49.104 |
| MSE (Mean Squared Error) | 3512.802 |
| Standard Error (denom=n-2=9) | 65.524 |
| MAPE (Mean Absolute Percent Error) | 21.294% |
| Forecast | |
| next period | 308.912 |
| 0.52 | |

| Measure | Value |
|------------------------------------|----------|
| Error Measures | |
| Bias (Mean Error) | 38.571 |
| MAD (Mean Absolute Deviation) | 49.085 |
| MSE (Mean Squared Error) | 3490.374 |
| Standard Error (denom=n-2=9) | 65.315 |
| MAPE (Mean Absolute Percent Error) | 21.335% |
| Forecast | |
| next period | 309.87 |
| 0.53 | |

| Measure | Value |
|------------------------------------|----------|
| Error Measures | |
| Bias (Mean Error) | 33.275 |
| MAD (Mean Absolute Deviation) | 50.359 |
| MSE (Mean Squared Error) | 3379.336 |
| Standard Error (denom=n-2=9) | 64.267 |
| MAPE (Mean Absolute Percent Error) | 22.357% |
| Forecast | |
| next period | 319.259 |
| 0.64 | |

| Measure | Value |
|------------------------------------|----------|
| Error Measures | |
| Bias (Mean Error) | 23.182 |
| MAD (Mean Absolute Deviation) | 60.455 |
| MSE (Mean Squared Error) | 4315.909 |
| Standard Error (denom=n-2=9) | 72.629 |
| MAPE (Mean Absolute Percent Error) | 27.518% |
| Forecast | |
| next period | 340 |
| 1.00 | |

Figure 10. The solution offered by QM – Single exponential smoothing (SES) method

The last method to be applied is Linear regression with time (LR). The results obtained with WinQSB are shown in Figure 11, and those with QM in Figure 12, in matrix form, and in Figure 13, in graphic form.

| 09-20-2022 Week | Actual Data | Forecast by LR | Forecast Error | CFE | MAD | MSE | MAPE (%) | Tracking Signal | R-square |
|-----------------|-------------|---------------------|----------------|----------|---------|-----------|----------|-----------------|----------|
| 1 | 85.0000 | 115.7052 | -30.7052 | -30.7052 | 30.7052 | 942.8065 | 36.1237 | -1.0000 | |
| 2 | 130.0000 | 134.5163 | -4.5163 | -35.2215 | 17.6107 | 481.6019 | 19.7989 | -2.0000 | 0.7874 |
| 3 | 180.0000 | 153.3275 | 26.6725 | -8.5490 | 20.6313 | 558.2082 | 18.1386 | -0.4144 | 0.1621 |
| 4 | 145.0000 | 172.1387 | -27.1387 | -35.6877 | 22.2582 | 602.7834 | 18.2831 | -1.6034 | 0.4490 |
| 5 | 250.0000 | 190.9499 | 59.0501 | 23.3624 | 29.6166 | 1179.6100 | 19.3504 | 0.7888 | 0.2395 |
| 6 | 200.0000 | 209.7611 | -9.7611 | 13.6013 | 26.3073 | 998.8879 | 16.9388 | 0.5170 | 0.3727 |
| 7 | 285.0000 | 228.5723 | 56.4277 | 70.0290 | 30.6102 | 1311.0600 | 17.3474 | 2.2878 | 0.3653 |
| 8 | 190.0000 | 247.3835 | -57.3835 | 12.6456 | 33.9569 | 1558.7850 | 18.9542 | 0.3724 | 0.5115 |
| 9 | 275.0000 | 266.1946 | 8.8054 | 21.4509 | 31.1623 | 1394.2010 | 17.2040 | 0.6884 | 0.5815 |
| 10 | 250.0000 | 285.0058 | -35.0058 | -13.5549 | 31.5466 | 1377.3220 | 16.8838 | -0.4297 | 0.7397 |
| 11 | 300.0000 | 303.8170 | -3.8170 | -17.3719 | 29.0257 | 1253.4350 | 15.4646 | -0.5985 | 0.7988 |
| 12 | 340.0000 | 322.6282 | 17.3718 | -0.0001 | 28.0546 | 1174.1310 | 14.6016 | 0.0000 | 0.7822 |
| 13 | | 341.4394 | | | | | | | |
| 14 | | 360.2506 | | | | | | | |
| 15 | | 379.0618 | | | | | | | |
| 16 | | 397.8729 | | | | | | | |
| CFE | | -0.0001 | | | | | | | |
| MAD | | 28.0546 | | | | | | | |
| MSE | | 1174.1310 | | | | | | | |
| MAPE | | 14.6016 | | | | | | | |
| Trk. Signal | | 0.0000 | | | | | | | |
| R-square | | 0.7822 | | | | | | | |
| | | Y-intercept=96.8940 | | | | | | | |
| | | Slope=18.8112 | | | | | | | |

Figure 11. Detailed solution offered by WinQSB – Linear regression with time (LR) method

| Details and Error Analysis | | | | | | | | | | |
|----------------------------|--------------|------|----------------|-------|----------|---------|---------|-----------------------|-----------|--|
| Amariei Olga Solution | | | | | | | | | | |
| | Sales (p.u.) | Time | x ² | x * y | Forecast | Error | Error | (E-Ebar) ² | Pct Error | |
| 1 | 85 | 1 | 1 | 85 | 115,705 | -30,705 | 30,705 | 942,807 | 36,124% | |
| 2 | 130 | 2 | 4 | 260 | 134,516 | -4,516 | 4,516 | 20,397 | 3,474% | |
| 3 | 180 | 3 | 9 | 540 | 153,328 | 26,672 | 26,672 | 711,421 | 14,818% | |
| 4 | 145 | 4 | 16 | 580 | 172,139 | -27,139 | 27,139 | 736,509 | 18,716% | |
| 5 | 250 | 5 | 25 | 1250 | 190,95 | 59,05 | 59,05 | 3486,916 | 23,62% | |
| 6 | 200 | 6 | 36 | 1200 | 209,761 | -9,761 | 9,761 | 95,279 | 4,881% | |
| 7 | 285 | 7 | 49 | 1995 | 228,572 | 56,428 | 56,428 | 3184,089 | 19,799% | |
| 8 | 190 | 8 | 64 | 1520 | 247,384 | -57,383 | 57,383 | 3292,861 | 30,202% | |
| 9 | 275 | 9 | 81 | 2475 | 266,195 | 8,805 | 8,805 | 77,534 | 3,202% | |
| 10 | 250 | 10 | 100 | 2500 | 285,006 | -35,006 | 35,006 | 1225,408 | 14,002% | |
| 11 | 300 | 11 | 121 | 3300 | 303,817 | -3,817 | 3,817 | 14,57 | 1,272% | |
| 12 | 340 | 12 | 144 | 4080 | 322,628 | 17,372 | 17,372 | 301,78 | 5,109% | |
| TOTALS | 2630 | 78 | 650 | 19785 | | 0 | 336,655 | 14089,57 | 175,22% | |
| AVERAGE | 219,167 | 6,5 | | | | 0 | 28,055 | 1174,131 | 14,602% | |
| Next period forecast | | | | | 341,439 | (Bias) | (MAD) | (MSE) | (MAPE) | |
| Intercept | 96,894 | | | | | | Std err | 37,536 | | |
| Slope | 18,811 | | | | | | | | | |

Figure 12. Detailed solution offered by QM – Linear regression with time (LR) method

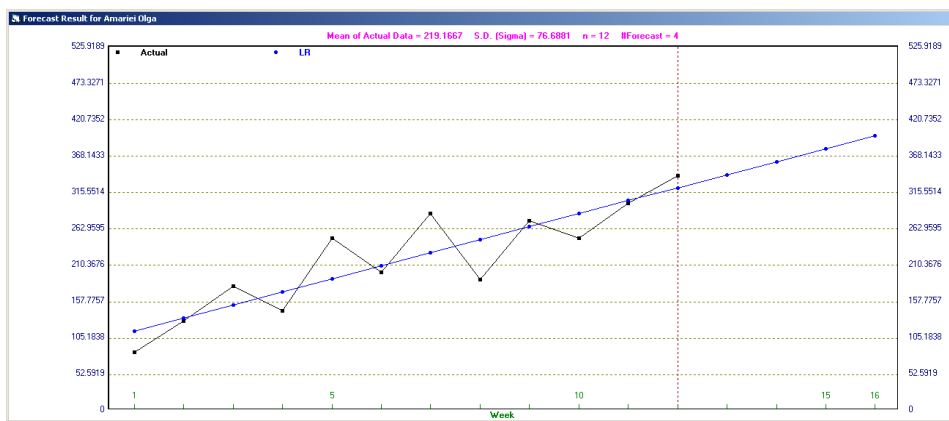


Figure 13. Results in graphic form (WinQSB)

In Table 1, the results obtained with the two programs are centralized, which, in fact, was observed during the work that they are identical. The error analysis in Table 1 is carried out for each type of error.

- Mean Error (Bias) – the highest value was obtained with the MA method and the lowest for LR method, namely: 0. There is no difference between results and forecasts.
- Mean Absolute Deviation (MAD) – the highest value was obtained in the same way as in the case of Bias, for the MA method: 79,063, and the lowest was recorded in the case of the LR method (28,054).
- Cumulative Forecast Error (CFE) – the highest value of 430,60 was obtained with the SES method ($\alpha=0,52$) and the lowest with the LR method (0).

Table 1. Centralized results

| Method used | | Forecast value for weeks | | | | Errors in forecasting | | | | |
|-------------|---------------|--------------------------|--------|--------|--------|-----------------------|---------------|----------|----------------|--------------|
| | | 9 | 10 | 11 | 12 | Bias | MAD | CFE | MSE | MAPE |
| MA | | 183,13 | 206,88 | 221,88 | 236,88 | 79,063 | 79,063 | 316,25 | 6759,77 | 26,76 |
| SES | $\alpha=0,52$ | 215,99 | 246,67 | 248,40 | 275,23 | 39,145 | 49,104 | 430,60 | 3512,80 | 21,29 |
| | $\alpha=0,53$ | 215,98 | 247,26 | 248,71 | 275,89 | 38,571 | 49,08 | 424,28 | 3490,37 | 21,33 |
| | $\alpha=0,64$ | 213,82 | 252,98 | 251,07 | 282,39 | 33,275 | 50,36 | 366,03 | 3379,34 | 22,36 |
| | $\alpha=1$ | 190,00 | 274,99 | 250,00 | 300,00 | 23,182 | 60,45 | 255,00 | 4315,90 | 27,52 |
| LR | | 266,19 | 285,00 | 303,82 | 322,63 | 0 | 28,054 | 0 | 1174,13 | 14,60 |

- Mean Square Error (MSE) – the highest value was obtained in the case of the MA method, and the lowest value, equal to 1174,13, was recorded as in all cases analyzed, in the LR method.
- Mean Absolute Percent Error (MAPE) – The highest value was also obtained with the SES method ($\alpha=1$) and the lowest value was obtained with the LR method (14,60%). The lower this value, the higher the accuracy of the forecast [9]. A superior accuracy for the forecast based on the linear regression function shall be observed.

| Measure | Value | Future Period | Forecast |
|--|----------|---------------|----------|
| Error Measures | | 13 | 341,439 |
| Bias (Mean Error) | 0 | 14 | 360,251 |
| MAD (Mean Absolute Deviation) | 28,055 | 15 | 379,062 |
| MSE (Mean Squared Error) | 1174,131 | 16 | 397,873 |
| Standard Error (denom=n-2=10) | 37,536 | 17 | 416,684 |
| MAPE (Mean Absolute Percent Error) | 14,602% | 18 | 435,495 |
| Regression line | | 19 | 454,307 |
| Sales (p.u.) = 96,894 | | 20 | 473,118 |
| + 18,811 * Time | | 21 | 491,929 |
| Statistics | | 22 | 510,74 |
| Correlation coefficient | ,884 | 23 | 529,551 |
| Coefficient of determination (r ²) | ,782 | 24 | 548,362 |
| Forecast | | 25 | 567,174 |
| x = 1 | 115,7052 | 26 | 585,985 |

Figure 14. 13-26 week forecast

The study revealed that the errors were lowest when applying the simple linear regression method. The forecasting was carried out using this method and obtaining the results shown in Figure 14.

5. Conclusion

In the present paper, it was possible to observe the use of the WinQSB and QM programs in order to make sales forecasts. The study was carried out with the help of these programs, using three forecasting methods, namely: moving average, single exponential smoothing and linear regression with time.

Analyzing in the end, each type of error separately, it was found that in absolutely all cases the lowest error values were obtained in the case of applying the simple linear regression method.

References

- [1] Amariei O.I., *Aplicații ale programului WinQSB în simularea sistemele de producție*, Editura Eftimie Murgu, Reșița, 2009.
- [2] Fildes R., Bretschneider S., Collopy F., Lawrence M., Researching Sales Forecasting Practice, *International Journal of Forecasting* 19, 2003, pp. 27-42
- [3] Jaba O., *Gestiunea producției și operațiunilor. Metode și tehnici ale managementului operațional al producției*, Editura Economică, București, 2002.
- [4] Mentzer J., Moon M., *Sales Forecasting Management: A Demand Management Approach*, University of Tennessee, SAGE Publication, Inc. Thousand Oaks, California, 2005.
- [5] Pant N., Starbuck W., Innocents in the Forest: Forecasting and Research Methods, *Journal de Management*, 16(2), 1990, pp. 433-460.
- [6] Rațiu-Suciu C., Luban F., Hîncu D., Ciocoiu N., *Modelare economică*. Ediția a doua, Editura ASE București, 2009.
- [7] Rațiu-Suciu C., *Modelarea & simularea proceselor economice. Teorie și practică*, Ediția a treia, Editura Economică, București, 2003.
- [8] Rațiu-Suciu C., Luban F., Hîncu D., Ene N., *Modelare economică aplicată. 50 Studii de caz. 525 Teste*, Editura Economică, București, 2002.
- [9] Ștefănescu R., Dumitriu R., *Smoothing of financial time series, Part 1*, Dunărea de jos University of Galați, MPRA, Paper No. 78329, 2018.
- [10] <https://www.proiecte.ro/mecanica/>
Nițu E. (coordonator), Planificarea producției pentru realizarea familiei de produse cablaj portieră spate în cadrul firmei SC Lear Corporation România SRL

Addresses:

- Ș. I. Dr. Eng. Olga-Ioana Amariei, Babeș-Bolyai University, Faculty of Engineering, Piața Traian Vuia, nr. 1-4, 320085, Reșița, Romania
olga.amariei@ubbcluj.ro
- Prof. Dr. Eng. Codruța-Oana Hamat, Babeș-Bolyai University, Faculty of Engineering, Piața Traian Vuia, nr. 1-4, 320085, Reșița, Romania
codruta.hamat@ubbcluj.ro
(*corresponding author)
- Prof. Daniel-Mihai Amariei, Reșița Student Culture House, Piața Traian Vuia, nr. 1-4, 320085, Reșița, Romania
amarieidaniel@yahoo.com

Analysis of the optimal location of new facilities within a production section

Olga-Ioana Amariei, Andrea-Amalia Minda*, Daniel-Mihai Amariei

Abstract. *In this paper the location of the warehouse of finished products and technical inspection post in the new space of a section for an industrial enterprise, intended for the processing of new products is proposed. This will be done according to several conditions imposed by the company's management. This was done using the Facility Location and Layout module of the WinQSB program, using two problem types: Facility Location and Functional Layout. The first type of problem was used for the location of the two new production units, and the second for the verification, using the CRAFT method, of the spatial location of the production units.*

Keywords: *optimisation, rectilinear distance, Euclidean distance, objective function, initial emplacement*

1. Introduction

Today, in order to face global competition, the industry needs to focus on computer science and technology. In this regard, industrial firms that focus on shortening the production cycle and also on the quality of the manufactured products will face the challenges of the market, adapting quickly to the needs and expectations of customers. To do this, however, he must respond promptly to rapid changes in technology, to turn to high-performance production systems, which lead to an increase in productivity and an improvement in quality, and at the same time to a significant decrease in costs [1]. Based on these considerations, in this paper we will analyse the problem of siting new production units.

Localization problems form a broad class of mathematical optimization problems [9]. The location decision is strategic, long-term and non-repetitive. For this reason, this type of decision must be taken with great care, as the lack of good and thorough site planning from the outset leads to ongoing operational problems in the future and can be a constant source of higher costs [5].



In this paper the location of the warehouse of finished products (WFP) and technical inspection post (TIP) in the new space in a section of an industrial enterprise, intended for the processing of new products is proposed and the optimal solution has been obtained.

Two essential conditions imposed by the management of the company are set out [1]:

- The new location is aimed at the decommissioning of a space in a production station, where there are the necessary facilities to ensure the energy supply of the machines.

- In the new location will be used existing equipment (noted U1-U22), coming from the decommissioning of two production halls within the company.

The working regime of the workshop is 5 days/week, 2 shifts/day, 8 hours/shift.

Table 1 shows the main products to be made in the refurbished section.

Table 1. Manufacturing schedule

| No. crt. | Product name | Volume production [pieces/year] |
|----------|----------------------------------|---------------------------------|
| 1. | Threaded bolt 1 | 352 |
| 2. | Threaded bolt 2 | 2304 |
| 3. | Threaded bolt | 128 |
| 4. | Bolt | 128 |
| 5. | Fitting 1 | 2200 |
| 6. | Fitting 2 | 2200 |
| 7. | Nozzle | 4400 |
| 8. | Nut | 4400 |
| 9. | Fixing bush | 24960 |
| 10. | Buffer | 24960 |
| 11. | Coupling GS type A PN 160 PN 160 | 2200 |
| 12. | Coupling GS type B PN 160 PN 160 | 2200 |

The organization of a production line for these parts must be carried out using the machines available from two production sites of the enterprise, due to the restriction of the previous manufacturing profile.

Following the design of the production system, it was concluded that it is composed of three manufacturing cells and that it was dimensioned using the method based on the detailed layout of machinery, furniture and workplaces developed in Autodesk inventor (Figure 1), observing the normalized location distances and the normalized width of the traffic lanes (Figure 2).

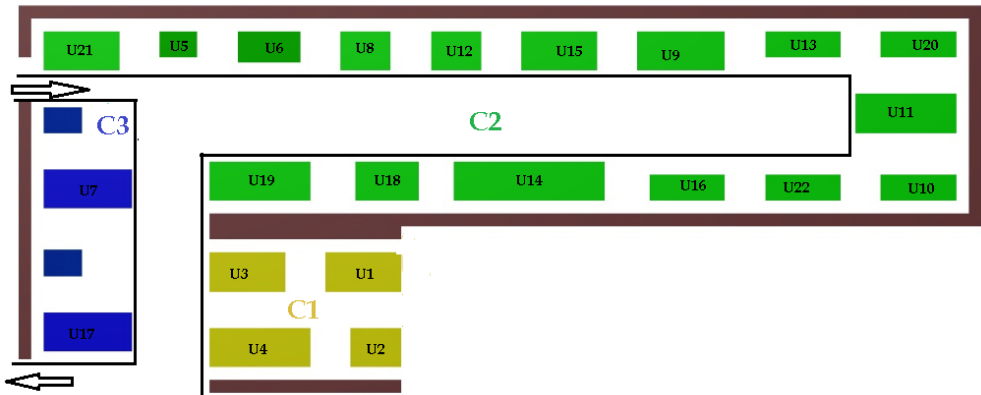


Figure 1. 2D Placement
Source: [1], pg.218

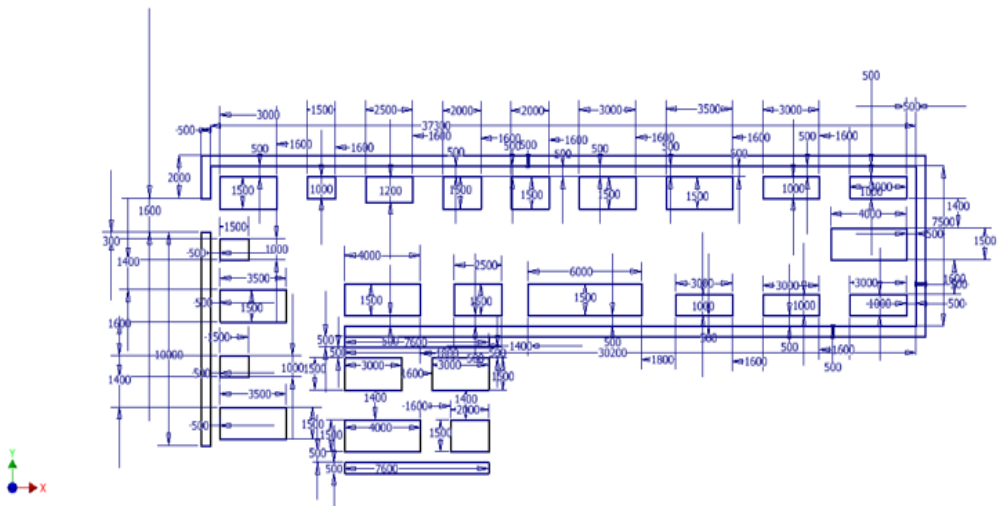


Figure 2. Detailed 2D location
Source: [1], pg. 260

2. Input data

Based on the known data of the study, namely:

1. workshop working regime;
2. the time rules of each product;
3. volume of production;
4. distribution of parts per production cells;
5. the location of the three manufacturing cells;
6. possible locations for WFP and TIP,

we calculate the amount of products executed by each manufacturing cell per day. This brings us to the following results:

- Cell C1, parts are manufactured: Threaded bolt 1, threaded bolt 2, threaded bolt and bolt – 12 pcs/day, toward the TIP post, then WFP;
- Cell C2, the following marks are executed: fitting 1, fitting 2, nozzle, nut, fixing bush and buffer – 265 pcs/day, of which 56 (fitting 1, fitting 2, nozzle and nut) go to cell C3, and 209 (fixing bush and buffer) to station TIP, then WFP;
- Cell C3 – 18 pcs/day (coupling GS type A PN 160 and coupling GS type B PN 160), to TIP post, then WFP.

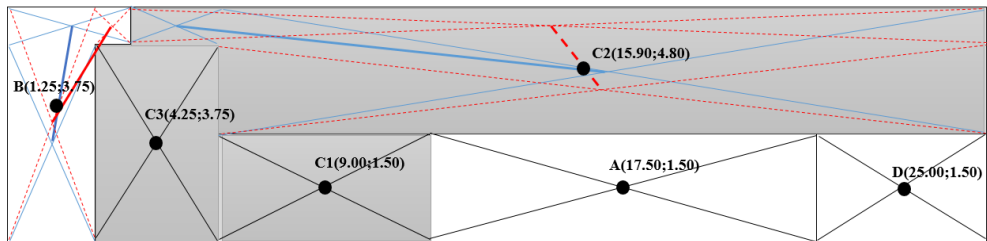


Figure 3. Possible locations for WFP and TIP

There are two possible locations: A(17.50; 1.50) and B(1.25; 3.75), and for TIP – B(1.25; 3.75) and D(25.00; 1.50). Starting from the data presented above, we determine the coordinates of the point in the hall where we need to place the WFP.

3. Results

Changing the location of the production units must take into account the fact that the total area of the redeveloped section cannot be changed, but the way the units are located relative to one another can be changed [3].

The QSB program package uses three types of distance measurement models, namely: Rectilinear, Euclidean and squared Euclidean.

| 09-13-2022 | New Facility | X Axis | Y Axis | New Facility | X Axis | Y Axis |
|------------|--------------|--------------|----------|--------------|--------------|----------|
| 1 | WFP | 15.90 | 4.80 | WFP | 15.89 | 4.80 |
| Total | Flow to&from | New Location | = 239 | Flow to&from | New Location | = 239 |
| Total | Cost to&from | New Location | = 373.50 | Cost to&from | New Location | = 307.36 |
| (by | Rectilinear | Distance) | | Euclidian | Distance) | |

Figure 4. The optimal solution offered by WinQSB for rectilinear and Euclidean distance

It is noted in fig.4. that WFP and production cell C2 have the same location.

| Summary of Optimal Location for Amariei O | | | |
|---|--------------|--------------|------------|
| 09-13-2022 | New Facility | X Axis | Y Axis |
| 1 | WFP | 14.68 | 4.46 |
| Total | Flow to&from | New Location | = 239 |
| Total | Cost to&from | New Location | = 2,854.80 |
| (by | Squared | Euclidian | Distance) |

Figure 5. The optimal solution offered by WinQSB for the squared Euclidean distance

Nor is the optimal solution for the squared Euclidean distance (Figure 5) better than the other solutions found. For this reason we take into account the two possible locations for WFP, namely points A(17.50; 1.50) and B(1.25; 3.75), and the results are shown in Figures 6 and 7.

| 09-13-2022 | New Facility | X Axis | Y Axis | New Facility | X Axis | Y Axis | New Facility | X Axis | Y Axis |
|------------|--------------|--------------|------------|--------------|--------------|------------|--------------|--------------|------------|
| 1 | WFP | 17.50 | 1.50 | WFP | 17.50 | 1.50 | WFP | 17.50 | 1.50 |
| Total | Flow to&from | New Location | = 239 | Flow to&from | New Location | = 239 | Flow to&from | New Location | = 239 |
| Total | Cost to&from | New Location | = 1,382.60 | Cost to&from | New Location | = 1,107.67 | Cost to&from | New Location | = 6,856.18 |
| (by | Rectilinear | Distance) | | Euclidian | Distance) | | Squared | Euclidian | Distance) |

Figure 6. Results related to point A, in synthetic form

| 09-13-2022 | New Facility | X Axis | Y Axis | New Facility | X Axis | Y Axis | New Facility | X Axis | Y Axis |
|------------|--------------|--------------|------------|--------------|--------------|------------|--------------|--------------|-------------|
| 1 | WFP | 1.25 | 3.75 | WFP | 1.25 | 3.75 | WFP | 1.25 | 3.75 |
| Total | Flow to&from | New Location | = 239 | Flow to&from | New Location | = 239 | Flow to&from | New Location | = 239 |
| Total | Cost to&from | New Location | = 3,477.80 | Cost to&from | New Location | = 3,225.04 | Cost to&from | New Location | = 46,058.14 |
| (by | Rectilinear | Distance) | | Euclidian | Distance) | | Squared | Euclidian | Distance) |

Figure 7. Results related to point B, in synthetic form

From the solution provided by the WinQSB software (Figure 6 and Figure 7), the total costs are different depending on the model used for measuring distances.

As the total cost of transport is lower in the Euclidean model than in the rectilinear model, this is considered the optimal solution in the case of location in point A.

Table 2. Results obtained at both possible WFP locations

| Model for measuring distance | Coordinate | | Total cost | Point |
|------------------------------|--------------|-------------|----------------|-------|
| | x | y | | |
| Rectilinear | 17.50 | 1.50 | 1382.60 | A |
| Euclidean | 17.50 | 1.50 | 1107.67 | |
| Squared euclidean | 17.50 | 1.50 | 6856.18 | |
| Rectilinear | 1.25 | 3.75 | 3477.80 | B |
| Euclidean | 1.25 | 3.75 | 3225.04 | |
| Squared euclidean | 1.25 | 3.75 | 46058.14 | |

Then proceed with the location of the technical inspection post (TIP), taking into account the results previously obtained, i.e. the location of the WFP at point A(17.50, 1.50). The first possible location for TIP is at point B(1.25; 3.75) and the results obtained are given in Figure 8 and the second possible location is at point D(25.00; 1.50), with the results shown in Figure 9.

| 09-13-2022 | New Facility | X Axis | Y Axis | 09-13-2022 | New Facility | X Axis | Y Axis |
|------------|--------------|--------------|------------|------------|--------------|--------------|------------|
| 1 | WFP | 17.50 | 1.50 | 1 | WFP | 17.50 | 1.50 |
| 2 | TIP | 1.25 | 3.75 | 2 | TIP | 1.25 | 3.75 |
| Total | Flow to&from | New Location | = 534 | Total | Flow to&from | New Location | = 534 |
| Total | Cost to&from | New Location | = 6,683.30 | Total | Cost to&from | New Location | = 5,850.98 |
| (by | Rectilinear | Distance) | | (by | Euclidian | Distance) | |

Figure 8. Results in synthetic form for points A (for WFP) and B (for TIP)

| 09-13-2022 | New Facility | X Axis | Y Axis | 09-13-2022 | New Facility | X Axis | Y Axis |
|------------|--------------|--------------|------------|------------|--------------|--------------|------------|
| 1 | WFP | 17.50 | 1.50 | 1 | WFP | 17.50 | 1.50 |
| 2 | TIP | 25 | 1.50 | 2 | TIP | 25 | 1.50 |
| Total | Flow to&from | New Location | = 534 | Total | Flow to&from | New Location | = 534 |
| Total | Cost to&from | New Location | = 3,869.50 | Total | Cost to&from | New Location | = 3,442.24 |
| (by | Rectilinear | Distance) | | (by | Euclidian | Distance) | |

Figure 9. Results in synthetic form for points A (for WFP) and D (for TIP)

It can be seen from the results obtained and summarized in Tables 2 and 3 that the optimal location of the WFP is at point A(17.50; 1.50), and for TIP, for the point D(25.00; 1.50). The graphical representation of the optimal solution is shown in Figure 10.

Table 3. The results obtained at both possible points of placement of the TIP post

| Model for measuring distance | Coordinate for TIP | | Coordinate for WFP | | Total cost |
|------------------------------|--------------------|------|--------------------|------|------------|
| | x | y | x | y | |
| Rectilinear | 1.25 | 3.75 | 17.50 | 1.50 | 6683.30 |
| Euclidean | 1.25 | 3.75 | 17.50 | 1.50 | 5850.98 |
| Rectilinear | 25.00 | 1.50 | 17.50 | 1.50 | 3869.50 |
| Euclidean | 25.00 | 1.50 | 17.50 | 1.50 | 3442.24 |

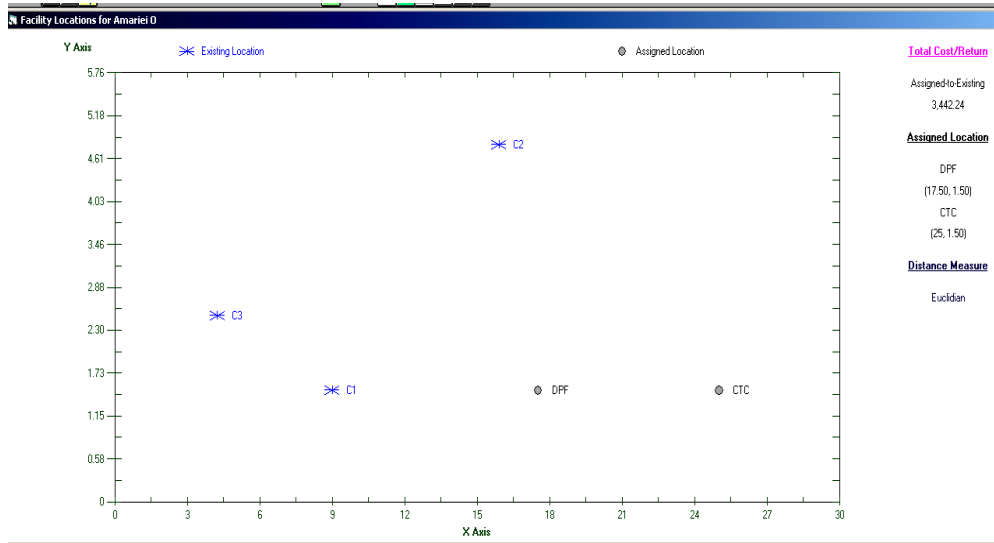


Figure 10. Results in graphic form

4. Verification of the obtained solution

Further we check whether the solution obtained is optimal or can be improved. For this purpose we have several options for problem solving, namely [6]: improvement by exchanging 2 departments, improvement by exchanging 3 departments, improvement by exchanging 2 then 3 departments, improvement by exchanging 3 then 2 departments, evaluation the initial layout only.

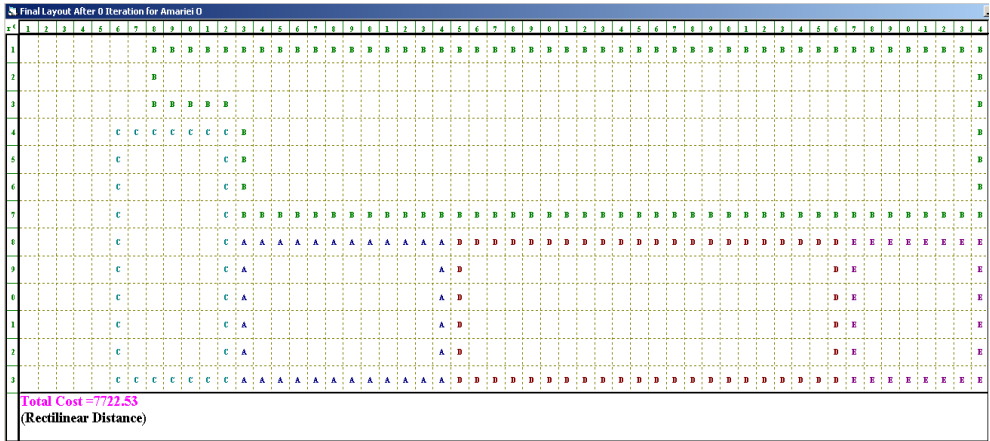


Figure 13. “Improvement by exchanging 3 departments” option

The location obtained from the permutation of two units (fig.13) is identical to the solution we started from (fig.11) and also the other three options are identical, but with a lower objective function value of 3414,84 (actual cost - 1707.42), which denotes an improvement in the previous location.

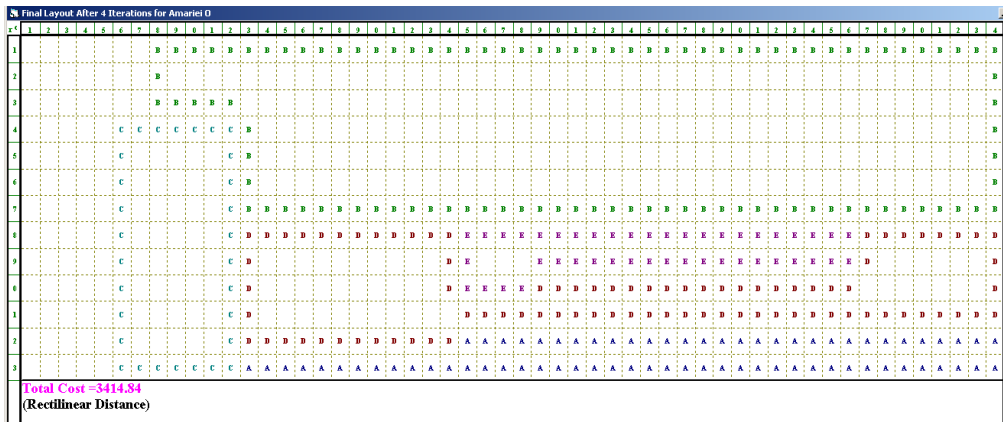


Figure 14. “Improvement by exchanging 2 then 3 departments” option

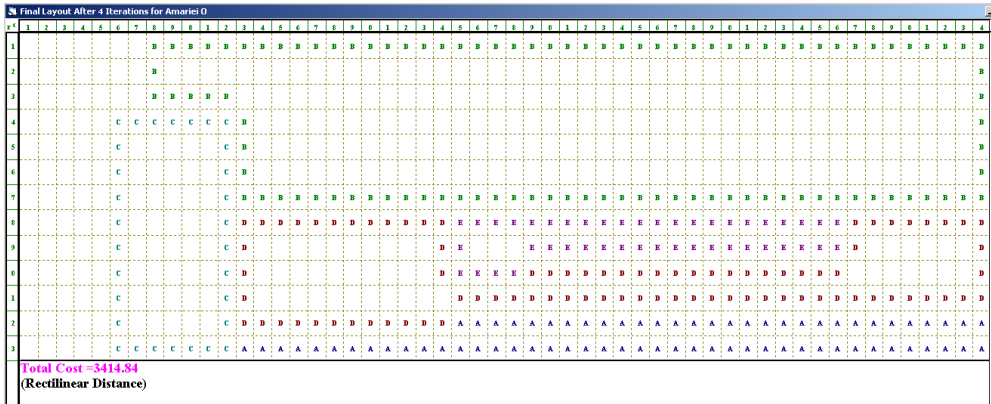


Figure 15. “Improvement by exchanging 3 then 2 departments” option

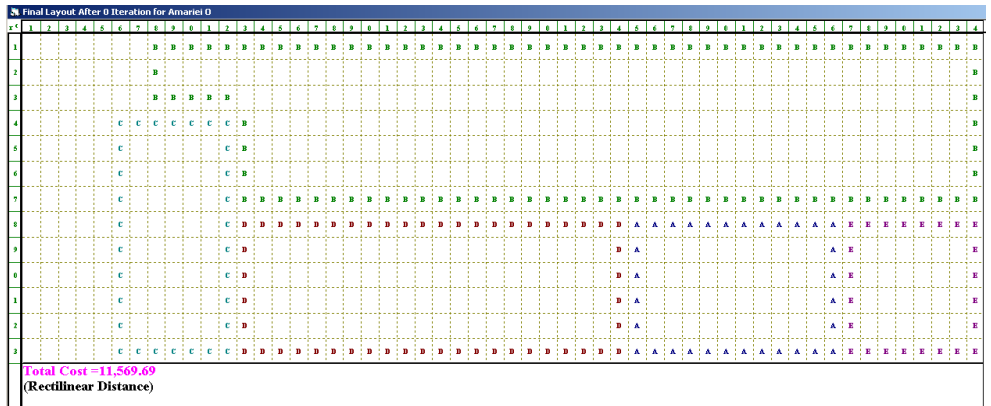


Figure 16. Adjusted location 1

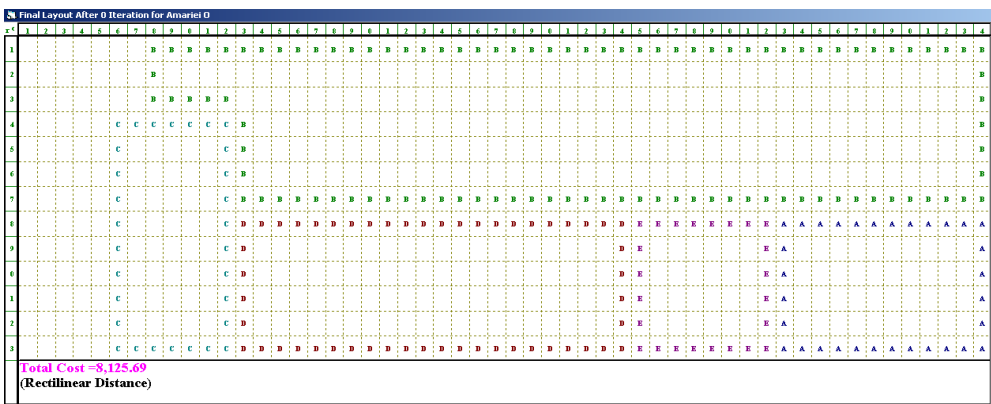


Figure 17. Adjusted location 2

5. Conclusion

The WinQSB program cannot take into account a predefined form of the units to be placed, but it allocates a certain area to them [1]. These sites generated by the program shall be harmonized with the form of the units to be located. These theoretical sites (fig.12, fig.14-15) are the basis of the final site. If C1 units with WFP and TIP are swapped, but provided that the shape of each unit is taken into account, we obtain locations with much higher objective function values (fig.16-17) than in the case of the initial location.

References

- [1] Amariei O.I., *Contribuții privind modelarea, simularea și optimizarea fluxurilor de producție utilizând programe dedicate*, Teze de doctorat ale UPT, Editura Politehnica, Timișoara 8(62), 2014.
- [2] Amariei O.I., Hamat C.O., Amariei D.M., Models for measuring distances used to obtain optimal locations, *Analele Universitatii „Eftimie Murgu“ Resita, Fascicula de Inginerie*, 26(1), 2019, pp. 9-16
- [3] Amariei O.I., Fourmaux D., Marta C., The way of establishing a relative position for some production units, *Analele Universitatii „Eftimie Murgu“ Resita, Fascicula de Inginerie*, 17(2), 2010, pp. 17-22
- [4] Amos N.B., Dogo E.B., *Facility Location (Linear Assignment Model)*, Part of the book: Operations Management, 2022.
- [5] Anucha, W., Phichit, K., Patcharee, D., Wisitsree, N., Analysis Plant Layout Design for Effective Production, *International MultiConference of Engineers and Computer Scientists* 2011. Vol. II, Hong Kong, IMECS 2011.
- [6] Blăjină O.A., *Decizii optime în management cu WinQSB 2.0. Vol.1.*, Editura Albastră, Cluj-Napoca, 2011
- [7] Lekan O.K., Kayode O.I., Morenikeji A.A., Analysis of Plant Layout Design for Operational Efficiency with Craft Algorithms, *Acta Universitatis Danubius. Oeconomica*, 13(4), Galați, 2017, pp.15-27.
- [8] Neagu C., Nițu E., Melnic L., Catană M., *Ingineria și managementul producției. Bazele teoretice*; Editura Didactică și Pedagogică București, 2006.
- [9] Saidani N., Chu F., Chen H., Competitive facility location and design with reactions of competitors already in the market, *European Journal of Operational Reserch*, 219(1), pp.9-17, 2012.

Addresses:

- Ş.l. Dr. Eng. Olga-Ioana Amariei, Babeş-Bolyai University, Faculty of Engineering, Piaţa Traian Vuia, nr. 1-4, 320085, Reşiţa, Romania
olga.amariei@ubbcluj.ro
- Lect. Dr. Andrea-Amalia Minda, Babeş-Bolyai University, Faculty of Engineering, Piaţa Traian Vuia, nr. 1-4, 320085, Reşiţa, Romania
andrea.minda@ubbcluj.ro
(* *corresponding author*)
- Prof. Daniel-Mihai Amariei, Reşiţa Student Culture House, Piaţa Traian Vuia, nr. 1-4, 320085, Reşiţa, Romania
amarieidaniel@yahoo.com

Sensitivity analysis on the vertical motion of heavy machine due to changing tires characteristics

Carmen Nicoleta Debeleac

Abstract. *In this paper the author presents some aspects about the motion of a heavy machine with tires in moving on the irregular roads. Based on the spatial 3-DOF model of machine it was evaluated all eigen pulsations and simulated the tire-road interaction only for the vertical motion of a wheel loader. The influence of the tire characteristics to the dynamic behavior of the loader was studied.*

Keywords: *heavy machine, tire, irregular terrain, dynamics, simulation*

1. Introduction

The operational capability of heavy machine to ensure technological and functional performance is significantly influenced by perturbator actions that may occur during the working process [1]. For example, the wheel loaders are a type of heavy machinery used all over the world in construction for various tasks, such as: scooping, digging, dumping and carrying. They have sturdy tires equipping for better handling, traction and maneuverability that allow deliver the specific tasks under inappropriate roads. In this regard, a wheel loader moving on the uneven road, specific for construction site conditions, was proposed for studying its dynamic behavior under random perturbations induced by the terrain profile.

2. Theoretical considerations

The paper is focused on the aspect of the wheel-terrain interaction process for a loader modeled as a rigid body system (representing by the mass m), supported on four tires, having spatial motion characterized by three degrees of freedom. Is assumed that each tire has linear viscoelastic behavior (k_i , c_i), with identical characteristics and, preponderant elasticity on vertical direction.



The dynamic response of the machine, when it travels with speed v on uneven terrain, consists in analysis of vibrations generated by the all movements refers to the $Oxyz$ coordinate (with origin in the mass center of the machine). Thus, it is interesting to know how to influence the viscoelastic characteristics of the tire over the angular oscillations about the x-axis (denoted by coordinate θ_2) and y-axis (denoted by coordinate θ_1), and, respectively, over the vertical translation motion (denoted by coordinate z) along the Oz axis, for the model described in Figure 1.

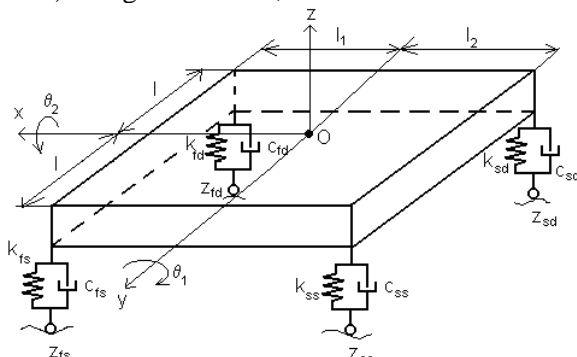


Figure 1. Dynamic model with 3-DOF for wheel-ground contact evaluation.

Many different roughness have been developed to parameterize terrain surfaces [2,3]. Usually, the uneven terrain profile (subjected to each tire i of heavy machine) can be modeled as following mathematic function:

$$z_i = A \sin(\omega t + i\varphi / 12), i = \overline{1,4}. \quad (1)$$

where A denotes profile magnitude, ω and φ are pulsation and phase of terrain irregularities, and index i indicates the effective tire - terrain interaction point.

The evaluation of vibrations that act to the wheel loader, modeled as a rigid body, is based on Lagrange equation of the second kind, so that, in advance will be required to express the kinetic and potential energies, respectively the dissipation functions of the rigid body [4].

The relative displacements of the machine wheels have following expressions:

$$\begin{aligned} \delta_{fd} &= z + \theta_2 l + \theta_1 l_1 - z_{fd}, \delta_{sd} = z + \theta_2 l - \theta_1 l_1 - z_{sd}. \\ \delta_{fs} &= z - \theta_2 l + \theta_1 l_1 - z_{fs}, \delta_{ss} = z - \theta_2 l - \theta_1 l_1 - z_{ss}. \end{aligned} \quad (2)$$

The total kinetic energy of the system is

$$E = \frac{1}{2} m(\dot{z})^2 + \frac{1}{2} J_1 \dot{\theta}_1^2 + \frac{1}{2} J_2 \dot{\theta}_2^2, \quad (3)$$

where J_1 is the moment of inertia of the rigid body about the y-axis, and J_2 the moment of inertia about the x-axis.

The potential energy of the system is

$$V = \frac{I}{2}k\delta_{fd}^2 + \frac{I}{2}k\delta_{fs}^2 + \frac{I}{2}k\delta_{sd}^2 + \frac{I}{2}k\delta_{ss}^2. \quad (4)$$

The dissipation function of the system is

$$D = \frac{I}{2}c\dot{\delta}_{fd}^2 + \frac{I}{2}c\dot{\delta}_{fs}^2 + \frac{I}{2}c\dot{\delta}_{sd}^2 + \frac{I}{2}c\dot{\delta}_{ss}^2. \quad (5)$$

After deriving the parameters involved in Lagrange equation, the second-order ordinary differential equations of motion result by the form:

$$\begin{cases} m\ddot{z} + 16\dot{z}c + 16zk - 8c\dot{\theta}_1(l_1 - l_2) - 8k\theta_1(l_1 - l_2) = 4c(\dot{z}_{fd} + \dot{z}_{fs} + \dot{z}_{sd} + \dot{z}_{ss}) + 4k(z_{fd} + z_{fs} + z_{sd} + z_{ss}) \\ -8\dot{z}c(l_1 - l_2) - 8zk(l_1 - l_2) + J_1\ddot{\theta}_1 + 8\dot{\theta}_1c(l_1^2 + l_2^2) + 8\theta_1k(l_1^2 + l_2^2) = \\ = 4k[l_1(z_{fd} + z_{fs}) - l_2(z_{sd} + z_{ss})] + 4c[l_1(\dot{z}_{fd} + \dot{z}_{fs}) + l_2(\dot{z}_{sd} + \dot{z}_{ss})] \\ J_2\ddot{\theta}_2 + 16\dot{\theta}_2cl^2 + 16\theta_2kl^2 = 4kl(z_{fd} + z_{fs} + z_{sd} + z_{ss}) + 4cl(\dot{z}_{fd} + \dot{z}_{fs} + \dot{z}_{sd} + \dot{z}_{ss}) \end{cases} \quad (6)$$

For similar characteristics of the tires, in the absence of damping and of the disturbing factors caused by the irregularities of the terrain, the eigenfrequencies of the system can be determined from the equation

$$\mathbf{M} \cdot \{\ddot{q}\} + \mathbf{C} \cdot \{\dot{q}\} + \mathbf{K} \cdot \{q\} = 0, \quad (7)$$

where

$$\{q\} = \begin{Bmatrix} z(t) \\ \theta_1(t) \\ \theta_2(t) \end{Bmatrix}, \quad \mathbf{M} = \begin{bmatrix} m & 0 & 0 \\ 0 & J_1 & 0 \\ 0 & 0 & J_2 \end{bmatrix}, \quad \mathbf{C} = \begin{bmatrix} 16c & -8(l_1 - l_2)c & 0 \\ -8(l_1 - l_2)c & 8(l_1^2 + l_2^2)c & 0 \\ 0 & 0 & 16cl^2 \end{bmatrix}, \quad \mathbf{K} = \begin{bmatrix} 16k & -8(l_1 - l_2)k & 0 \\ -8(l_1 - l_2)k & 8(l_1^2 + l_2^2)k & 0 \\ 0 & 0 & 16kl^2 \end{bmatrix}.$$

Thus, solving the equation (7) with the following solutions $q_i = A_i \sin(pt + \theta)$, we obtain the algebraic equations system

$$\begin{cases} (-mp^2 + 16k)z - 8k(l_1 - l_2)\theta_1 = 0 \\ -8k(l_1 - l_2)z + [-J_1p^2 + 8k(l_1^2 + l_2^2)]\theta_1 = 0 \\ (-p^2J_2 + 16kl^2)\theta_2 = 0 \end{cases}, \quad (8)$$

from where result the three natural eigenfrequencies (in term of $p_z, p_{\theta_1}, p_{\theta_2}$), corresponding with the 3-DOF of motions of mechanical system associated to heavy machine. The periodically wheel-road impacts generate higher amplitude of vertical vibrations if the resonance phenomena appear, and frequency analysis is required for avoid appearance of this situation, considering redesigning of the machine and repositioning the mass center [5].

3. Study case

The machine travelling with a constant velocity ($v = 20$ km/h), stressed by the road bumps that meets along its route in the areas of contact between tire and road profile, generates perturbations within the machine motion [6,7]. Finally, the numerical simulations have focused on the evaluation of dynamic loads transmitted to the machine by the terrain. Thus, it can evaluate the dynamic load coefficient, as a ratio between the dynamic load F_d and the static load G :

$$DLC = F_d/G = k(z-\delta)/mg. \quad (9)$$

The main parameters of the wheel loader (MMT 45, Romania) used for dynamic simulation are: heavy machine mass $m=4000$ kg, moments of inertia of the machine $J_1=J_2=1000$ kgm², vertical tire stiffness $k=25 \times 10^5$ N/m, tire damping $c=800$ Ns/m, constructive dimensions $l_1=l_2=2$ m. Thus, for the initial conditions $z_0 = \theta_{10} = \theta_{20} = 0$, $\dot{z}_0 = 0.1$ m/s, $\dot{\theta}_{10} = 0.1$ rad/s, $\dot{\theta}_{20} = 0.1$ rad/s, results the free vibrations of the mechanical system, as temporal evolutions of z , θ_1 , θ_2 (see Figure 2).

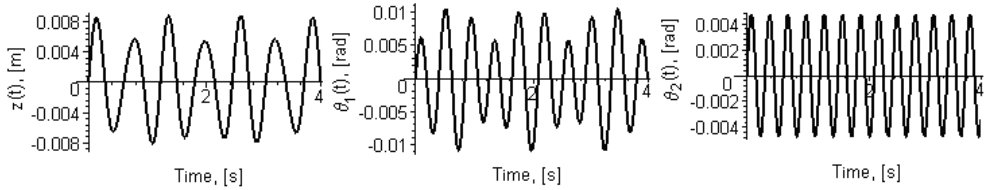


Figure 2. Wheel loader motion for each supposed 3-DOF

The equations of motion are implemented in the Matlab/Simulink environment. Thus, it was evaluating the natural frequencies (p_z , p_{θ_1} , p_{θ_2}) and the laws of motion corresponding to undamped vibrations of the machine (shown in fig.2).

4. Sensitivity analysis

When moving the machine on uneven roads, the tires have supplementary role of mitigating the vibrations that propagate to its structure. If only the vertical motion of the machine is important to study, then we assumed that a bump with the surface generated by expression $z_i = 0.2 \sin(5,5t)$ encounters the front-axle wheels. In this way, the vertical motion of the mass center along z axis can be highlighted for low frequency excitations of ground surface. The sensitivity analysis of viscoelastic characteristics of tires gives a general view over the dynamic behavior of the heavy machine, as can be seen in Figures 3 and 4.

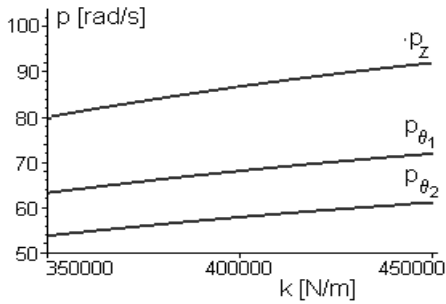


Figure 3. Variation of eigenpulsations versus stiffness tires

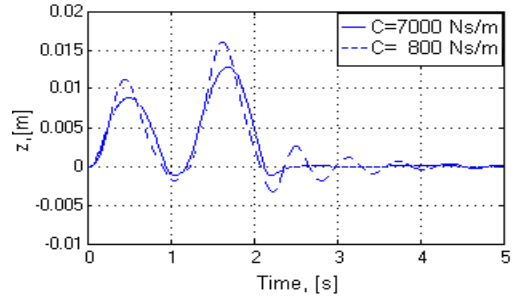


Figure 4. Vertical oscillations of machine versus damping tires

Thus, the tire stiffness range was varied between $3,5 \times 10^5$ - $4,5 \times 10^5$ N/m and the damping coefficient between 800 – 7000 Ns/m. All machine eigen pulsations have approximatively the same proportional variation in respect to stiffness tire increment. In addition, as the inflation pressure increases, the diagram shows higher amplitude of the vertical oscillation of the machine.

If the damping increases by more than eight times, the amplitude of motion decreases by only 128%. This fact highlights the nonlinear relationship between the vertical oscillation peaks and tires damping. In addition, for $c=800$ Ns/m results the dynamic loads coefficient $DLC=1.6$, which demonstrates the existence of overloads when machine traveling on uneven surface.

Next, for four simulation scenarios, in Figure 5 has been represented the vertical acceleration response of the proposed model to a singular terrain excitation, with the frequency increased twice, and defined as: $z_i = 0.2 \sin(11t)$.

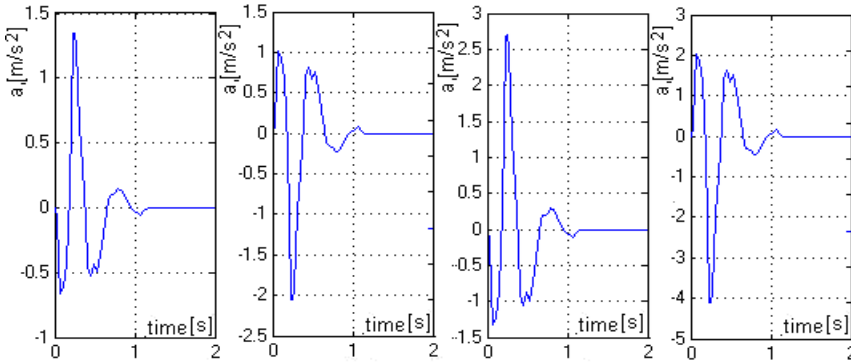


Figure 5. Vertical acceleration of the center of mass for motion over the bump with: a) front-right wheel; b) rear-right wheel; c) front-axle wheels; d) rear-axle wheels.

All kinematic excitations have inducing vertical oscillations into the machine frame, with different values of the peak amplitude depending on the position of the contact point between the wheel and the bump road.

5. Conclusion

Study of motion of a heavy machine, when this moves on irregular roads profiles, was approached in this paper. It was analyzed a free undamped (natural) vibration for a model assimilated with a 3-DOF mechanical system. The proposed mathematical model shows that the equation of rotation of the machine along the longitudinal axis Ox is decoupled from the other equations of motion.

Therefore, the influence of tire characteristics on the vertical movement of the machine, in the imposed road conditions, was highlighted in conditions of low frequency excitations generated by the terrain surface. Hereby, equipping with tires characterized by the high damping has the effect of reducing the amplitude of vibrations that are transmitted to the machine, a useful aspect both for the life of the structure and for the ride comfort of operator.

Possible directions for future work: finding technical solutions to reduce the vibrations caused by moving on irregular terrain through implementation of a device for controlling active suspensions.

References

- [1] Debeleac C., Oproescu Gh., About phenomenon which appear at driving earthmoving machine on the irregular surface, *Romanian Journal of Acoustics and Vibration-RJAV*, V(2), 2008, pp. 51-56.
- [2] Emam, M. A. A., Shaaban, S., El-Demerdash, S., El-Zomor, H., A tyre-terrain interaction model for off-road vehicles, *Journal of Mechanical Engineering Research*, V3(7), 2011, pp. 226-238.
- [3] Tengler, S. and Warwas, K., An Effective Algorithm of Uneven Road Surface Modeling and Calculating Reaction Forces for a Vehicle Dynamics Simulation, *Coatings*, V(11), 2021, pp. 535-552.
- [4] Debeleac C., Axinti, G., *Synthesis of Newtonian mechanics with applications. Vol. III. Dynamics*, Galati University Press, 2015.
- [5] Melcer, J., Vehicle-road interaction, analysis in a frequency domain, *Slovak Journal of Civil Engineering*, V(3), 2006, pp. 48–52.
- [6] Debeleac, C., On modelling of bucket oscillations for a wheel loader, *Romanian Journal of Acoustics and Vibration-RJAV*, (XI)2, 2014, pp.146-149.
- [7] Agostinacchio, M, Ciampa, D, Olita, S., The vibrations induced by surface irregularities in road pavements – a Matlab® approach, *European Transport Research Review*, V(6), 2014, pp. 267–275.

Address:

- Prof. Dr. Eng. Carmen Nicoleta Debeleac, Universitatea “Dunărea de Jos” din Galați, Facultatea de Inginerie și Agronomie din Brăila, Călărășilor, no. 29, Brăila
carmen.debeleac@ugal.ro

Analysis of the energy security of the Republic of Moldova in the context of accession and integration to the European Union

Nicolae Daniel Fita*, Liliana Samoila, Dragos Pasculescu,
Emilia Grigorie, Raluca Grigorie

***Abstract.** Energy security, which is defined by the availability at all times of energy in all its forms, in sufficient quantities and at affordable prices, without unacceptable or irreversible environmental impact, must be the central pillar of the strategic analysis of the national security of the Republic of Moldova, in the context of accession and integration to the European Union. Easy access to energy resources is an essential condition for the security and well-being of Moldovan individuals, businesses and communities. Given the status of the Republic of Moldova as an acceding state to the European Union, which is at the forefront of defense of the entire Euro-Atlantic space against the offensive of the hostile interests of the Russian Federation, the region has become the hottest geopolitical, geoeconomic and geostrategic space for direct confrontation of the interests of the West and East, with a huge potential for escalation to a military conflict. Against this background, the preferred means of threat of the Russian Federation proves to be the energy weapon, used both for the promotion of major economic interests, as well as as an instrument of influence and political blackmail. Therefore, energy is no longer only a factor of the equation of economic power of the Moldovan state, but also an element of political influence and control, with reflections in the military capabilities. The authors want to analyze the state of energy security regarding the state of energy resources and electricity.*

Keywords: Energy security, Energy resources, Energy weapon.

1. Introduction

The Republic of Moldova is a state located in South-Eastern Europe and has the following neighbors, according to Figure 1:



- North, East and South – Ukraine;
- West – Romania.

The Republic of Moldova is a parliamentary Republic with a president as head of state and a prime minister as head of government and is a Member of the United Nations, the Council of Europe, the Partnership for Peace, and other international organizations, and is a candidate state for membership in the European Union.

The Republic of Moldova is a state with no direct sea exit, but it has a 430-meter stretch of Danube at its southern extremity, through which it has potential access to the Black Sea as well.

The main cities:

- Chisinau (capital);
- Balti;
- Tiraspol;
- Tighina;
- Ribnita;
- Ungheni;
- Cahul;
- Soroca;
- Dubasari;
- Straseni, etc.

The main rivers:

- Nistru;
- Prut;
- Răut;
- Botna, etc.

Since 1990, the territory of the Republic of Moldova located on the eastern bank of the Dniester (Nistru) River is under de facto control of the separatist regime in Transnistria (controlled and/or supported by Russia).

Mineral resources:

- Limestone;
- Chalk;
- Gypsum;
- Sand;
- Sandstone;
- Bentonite;
- Tripoli;
- Diatomite.

Non-metallic mineral resources:

- Graphite;
- Phosphorite;
- Zeolite;
- Fluorite;
- Bariite;
- Iodine;
- Bromine;
- Iron;
- Lead;
- Zinc;
- Cooper.

Energy resources (very small amounts):

- Lignite;
- Oil;
- Natural gas. [6]



Figure 1. Map of Republic of Moldova

2. The state of energy security of the Republic of Moldova

2.1. Security of natural energy resources

Currently, the Republic of Moldova does not have its own natural energy resources (oil, natural gas, coal, uranium, etc.), except for small amounts of oil and natural gas present in the south of the country.

Because of this, Republic of Moldova is heavily dependent on imported natural energy resources, and the current level of harnessing the potential of renewable energy sources does not cover consumption needs.

The energy resources used to produce electricity and heat are [1] [2]:

- Natural gas: 91,1 %;
- Biofuels and waste: 4,6%;
- Oil products: 2,5%;
- Electricity: 1,3%;
- Coal: 0,5%.

Imports of energy resources and electricity are:

- Electricity: 80%;
- Oil products: 99%;
- Natural gas: 100%;
- Coal: 100%.

2.2. Security of electricity supply

The power system of the Republic of Moldova works in sync with the power system of Ukraine, which is part of the Integrated / Unified Energy System (IPS / UPS) of the Russian Federation, at a voltage of 330 kV with the following countries: Belarus, Ukraine, Kazakhstan, Georgia, Mongolia, Kyrgyzstan, Azerbaijan, Tajikistan.

The 330 kV voltage is atypical for the European ENTSO-E power system, which operates at the transmission voltage of 400 kV, and for this reason dependence on the Russian IPS/UPS power system is generated. [3]

A. Power supply and transport

The power supply and transport of electricity is carried out through the National Power Grid belonging to the Moldelectrica company, with the following infrastructure, according to Figure 2 [3] [5] [9]:

- 1 (one) 400 kV overhead line for cross-border interconnection with Romania (stability and reliability of the power system):
 - *Vulcănești – Isaccea*;

- 1 (one) 400 kV national overhead line (stability and reliability of the power system):
 - *Vulcănești – CERS Moldova.*
- 7 (seven) 330 kV overhead lines of cross-border interconnection with Ukraine (stability and reliability of the energy system):
 - *CERS Moldova – Novoodeska;*
 - *CERS Moldova – Usatove;*
 - *CERS Moldova – Podilska;*
 - *CERS Moldova – Artsyz;*
 - *Răbnița – Podilska (circuit 1);*
 - *Răbnița – Podilska (circuit 2);*
 - *Bălți – Dnistrovska HPP.*
- 3 (three) national air overhed lines of 330 kV (stability and reliability of the energy system):
 - *CERS Moldova – Chișinău (double circuit);*
 - *Chișinău – Strășeni;*
 - *Strășeni – Bălți.*
- 15 (fifteen) 110 kV overhead lines of cross-border interconnection with Ukraine (trade):
 - *Etulija – Budzhak;*
 - *Vulcănești – Reni;*
 - *Vulcănești – Kosa;*
 - *Vulcănești – Bolgrad (circuit 1);*
 - *Vulcănești – Bolgrad (circuit 2);*
 - *Vulcănești – Bolgrad (circuit 3);*
 - *CERS Moldova – Belyaevka;*
 - *CERS Moldova – Rozdil;*
 - *CERS Moldova – Starokazachye;*
 - *Vasilevik – Kr. Okni;*
 - *Brich – Dnistrovska HPP;*
 - *Otaci – Namiya;*
 - *Ocnița – Shahta;*
 - *Soroca – Poroghi;*
 - *Larga – Nelypivtsy.*
- 4 (four) 110 kV overhead lines for cross-border interconnection with Romania (trade):
 - *Cioara – Huși;*
 - *Ungheni – Țuțora;*
 - *Gotești – Fălciu;*
 - *Costești – Stâncă.*



Figure 2. National Power Grid

B. Electricity generation

The generation of electricity shall be carried out by means of the following power stations (plants): [5]

- CERS Moldova (Cuciurgan) – 2520 MW:
 - *the largest methane-based thermal power plant in the Republic of Moldova;*
 - *the only natural gas distributor is the Russian company SAD Gazprom (generates total dependence on Russia);*
 - *natural gas supplier is the daughter company of Moldovagaz – Tiraspoltransgaz.*
- CET 1 Chișinău – 66 MW;
- CET 2 Chișinău – 240 MW;
- CET Bălți – 24 MW;
- CHE Costești – 16 MW;
- CHE Dubăsari – 46 MW;
- Other generation sources – 87 MW.

C. Buyers of electricity

The following actors are present in the electricity market:

- Gas Natural Fenosa Energy supply – universal service provider;
- Electricity Supply North – provider of universal service;
- Red Union Fenosa – operator of the distribution system;
- Moldelectrica – transmission and system operator;
- Red Nord – operator of the distribution system.

2.3. Security of natural gas supply

The natural gas system of the Republic of Moldova is connected to the Unified Gas Supply System of Russia, which generates total dependence on this system.

The largest natural gas actor in the Republic of Moldova is Moldovagaz, which is a Moldovan-Russian joint stock company with the following share distribution: [1] [2]

- SAD Gazprom holds 50,0% + 1;
- SAD Gazprom controls another 13,44% of the Management Committee of the property of Transnistria (handed over to the management of SAD Gazprom);
- The Government of the Republic of Moldova holds 35,33%;
- different individuals and legal entities holds 0,23%.

Moldovagaz provides the following services:

- purchase of natural gas from the mother company SAD Gazprom;
- natural gas transport and transit through:
 - *Moldovatransgaz*;
 - *Tiraspoltransgaz (in the transnistrian region)*;
 - *Vestmoldtransgaz (interconnector operationalization Iasi – Ungheni – Chisinau)*;
- natural gas distribution through the 12 distribution companies;
- gas transit through the TransBalkan pipelines to:
 - *Romania*;
 - *Bulgaria*;
 - *Greece*;
 - *Turkey*.

The supply, transport and transit of natural gas shall be carried out through the Natural Gas Transmission Network, which shall have the following infrastructure, as shown in figures 3 and 4: [10]

- supply (Ukraine):
 - Gas Pipeline 1: Ananiev – Cernăuți – Bogorodceni (ACB);
 - Gas Pipeline 2: Ananiev – Tiraspol – Ismail (ATI);
 - Gas Pipeline 3: Șebelinka – Dnepropetrovsk – Krivoi – Rog – Ismail (DKRI);
 - Gas Pipeline 4: Tiraspol – Odesa (TO3).
- supply (Romania):
 - Gas Pipeline 5: Iași – Ungheni – Chișinău (IUC).
- transport:
 - 656,307 km. main pipe;
 - 903,478 km. pipe connection;
 - 3 gas compression stations;
 - 1 gas measuring station;
 - 81 gas transfer measuring stations;
 - 221 cathodic protection stations.

System of import and transit of natural gas, as shown in Figure 3:

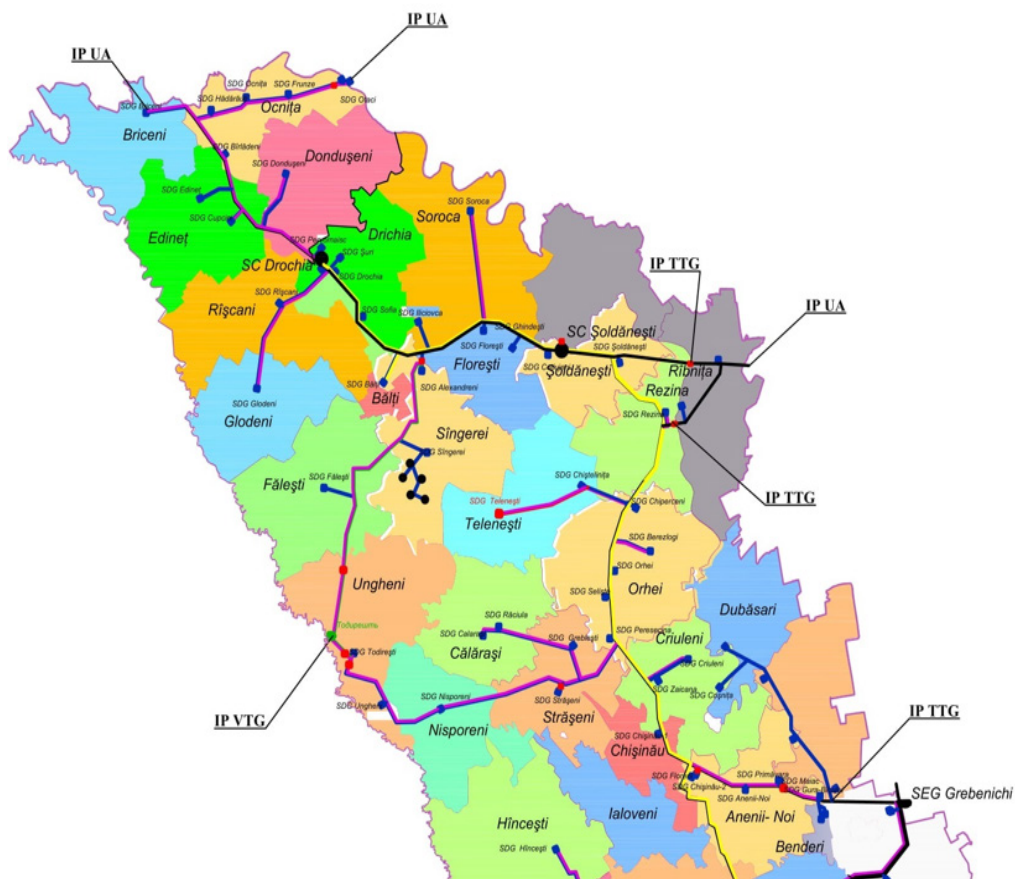


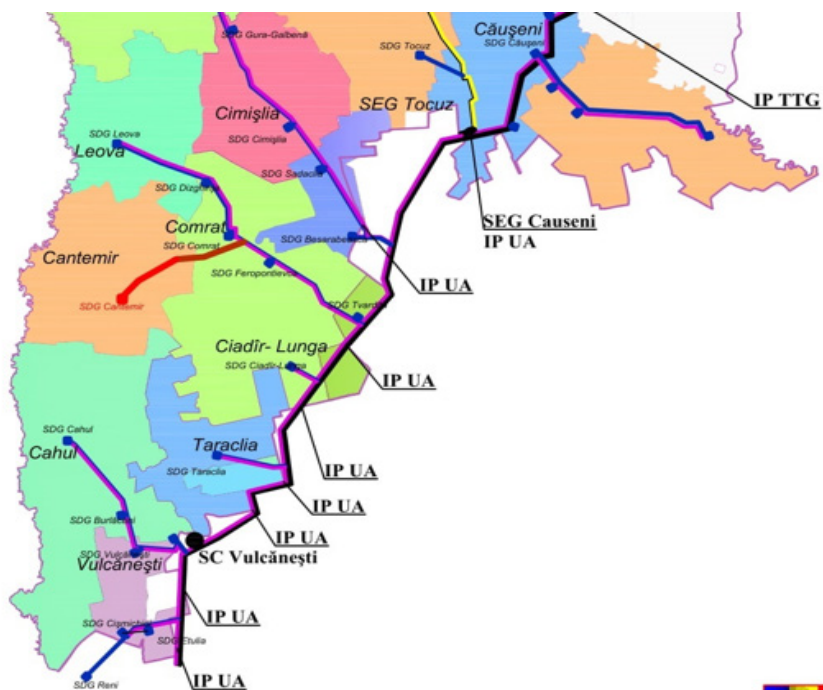
Figure 3. Import and transit of natural gas

The main gas crossing entry points are shown in table 1.

Table 1. Import of natural gas (crossing entry points)

| CROSSING ENTRY POINTS | | STATUS |
|-----------------------|---|--------------------|
| 1 | Olekseevka (Ukraine – Moldova Republic) | operațional |
| 2 | Ungheni (Romania – Moldova Republic) | under construction |
| 3 | Grebenichi (Ukraine – Moldova Republic) | operațional |
| 4 | Căușeni (Ukraine – Moldova Republic) | operațional |
| 5 | Isaccea (Romania – Moldova Republic) | operațional |











-  **Conducte magistrale de transport**
-  **Conducte de derivație**
-  **Rețea de cablu fibră optică**
-  **SDG- Stații de distribuție a gazelor**
-  **SEG- Stație de evidență și consum al gazelor**
-  **SC- Stație de compesare a gazelor**
- IP** **Punct de interconectare**
- TTG** **SRL "Tiraspoltransgaz"**
- VTG** **SRL "Vestmoldtransgaz"**

Figure 4. Natural gas transport infrastructure

Major consumers of natural gas of the Republic of Moldova:

- Thermal Power Plant CERS Moldova;
- Moldovan Metallurgical Factory;
- Moldavkabel company;
- Cement Factory Râbnita;
- Electromas company;
- Tirotext company;
- Kvint company.

3. Identify vulnerabilities

Vulnerabilities identified:

- a) The lack of own natural energy resources (oil, natural gas, coal, etc.), except for small amounts of oil and natural gas present in the south of the country;
- b) fully dependent on imported natural energy resources (oil, natural gas, coal, etc.);
- c) massive imports of energy resources and electricity;
- d) atypical electricity transmission voltage (330 kV);
- e) the impossibility of interconnection with the European electricity system ENTSO-E, only with major investments in power infrastructure;
- f) dependence on the Russian power system IPS / UPS;
- g) economic insecurity, through excessive and unilateral dependence of domestic systems of foreign monopolistic electricity and natural gas;
- h) lack of storage deposits of natural gas;
- i) there is no access to liquefied natural gas (LNG).

4. Conclusion

Since Moldova does not have its own natural energy resources (oil, natural gas, coal, uranium, etc.), it is strongly dependent on imported natural energy resources, and the current level of harnessing the potential of renewable energy sources does not cover the consumption needs.

As is probably known, the largest electricity producer in the Republic of Moldova is CERS Moldova, which is a natural gas-based power plant located on the left bank of the Dniester and belongs to the Russian company SAD "inter RAO UES".

Natural gas is distributed by SAD Gazprom from Russia and supplied by Tiraspoltransgaz, a company that is part of the Moldovagaz giant.

If natural gas is imported only through the TransBalkan gas pipeline, which does not cover the country's natural gas needs, then a real threat to the National Power System will be generated.

The debt of almost \$7 billion to the Russian distributor SAD Gazprom is putting energy security at risk by creating total dependence.

In this context of energy, economic and national insecurity, caused by total energy dependence, the Republic of Moldova must invest massively in the construction of critical power infrastructures (power substations and overhead lines operating at 400 kV, power plants, gas pipelines and natural gas stations, etc.), in the context of the security of supply and supply of electricity and natural gas from the European ENTSO-E (electricity) and ENTSO-G (gas) systems.

References

- [1] Avornic C., *Security of natural gas supply in the Republic of Moldova – challenges and perspectives*, Soros Foundation Moldova, Chisinau, 2021.
- [2] Borosan C-tin., *Study of Public Policies - Energy Security of the Republic of Moldova in the context of the functioning of the competitive market*, Soros Foundation Moldova, Chisinau, 2019
- [3] Fiță N.D., Radu M.S., Păculescu D., *Ensuring, controlling and stability of energy security in the context of increasing industrial and national security – Academic compendium*, Universitas Petroșani Publishing House, 2021.
- [4] Gheorghe A., Mureșan L., *Energy Security*, Springer Publishing House, Dordrecht, The Netherlands, 2010.
- [5] Fiță N.D., Păculescu D., Popescu F.G., Slusariuc R., Herbei R., Pupăza C., Visan R.N., *National Energy Security in European context*, Universitas Publishing House, Petroșani, 2022.
- [6] www.moldova.md
- [7] www.moldelectrica.md
- [8] www.moldovagaz.md
- [9] www.entsoe.eu
- [10] www.entsog.eu

Addresses:

- Lect. Ph.D. Eng. Nicolae Daniel Fita, University of Petrosani, Strategic Studies of Energy Security, University street, nr. 20, Petrosani district, Hunedoara county, Romania
daniel.fita@yahoo.com
(*corresponding author)

- Assoc. Prof. Ph.D. Eng. Liliana Samoila, University of Petrosani, Strategic Studies of Energy Security, University street, nr. 20, Petrosani district, Hunedoara county, Romania
branaliliana@gmail.com
- Assoc. Prof. Ph.D. Eng. Dragos Pasculescu, University of Petrosani, Strategic Studies of Energy Security, University street, nr. 20, Petrosani district, Hunedoara county, Romania
pdragos_74@yahoo.com
- Ph.D Stud. Eng. Emilia Grigorie, University of Petrosani, Strategic Studies of Energy Security, University street, nr. 20, Petrosani district, Hunedoara county, Romania
emilia_grigorie@yahoo.com
- Stud. Raluca Grigorie, University of Petrosani, Mining Faculty, University street, nr. 20, Petrosani district, Hunedoara county, Romania
grigorie_raluca@yahoo.com

Analysis of power system of the Republic of Moldova in the context of the interconnection to ENTSO-E and accession to European Union

Nicolae Daniel Fita*, Mihai Sorin Radu, Dragos Pasculescu,
Florin Mureșan, Danut Mircea Pinte

Abstract. *The need to analyze the Moldovan power system comes in the context in which the Republic of Moldova has become a serious candidate for accession to the European Union, and one of the conditions of accession is the interconnection to electricity European networks – ENTSO-E, which is the network of the 39 transmission system operators from 35 countries in the European Union. Against the background of military instability following the war between Russia and Ukraine and dependence on the Russian power system, interconnection with other States within the European Union becomes a strategic objective of ensuring energy security and implicitly national and European. Since Romania is the only credible potential strategic energy partner, all possibilities for cross-border interconnection must be considered. In order to have a safe and secure cross-border interconnection with Romania and implicitly with the European Union, the Moldovan power system must meet some criteria recommended by ENTSO-E: consumption coverage; primary power regulation; secondary frequency-power regulation; voltage regulation; operation safety at criterion (N-1) elements; anti-damage measures. Because a power system can be vulnerable to various threats, risks or internal or external dangers, the authors aim to critically analyze the Moldovan power system, as it generates critical infrastructures that ensure the energy and national security of the Republic of Moldova.*

Keywords: *Power system, ENTSO-E, Energy security.*

1. General information on ENTSO-E

ENTSO-E (European Networks of Transmission System Operators for Electricity) is the European network of 39 electricity transmission system operators from 35 countries in the European Union and extends beyond borders, as shown in Figure 1.



ENTSO-E was established and received legal mandates under the EU's third Internal Energy market Package in 2009, which aims to further liberalize gas and electricity markets in the EU. On 27 June 2008, 36 European electricity transmission system operators signed in Prague a declaration of intent to create ENTSO-E, which was established in Brussels on 19 December 2008 and became operational on 1 July 2009, and the former UCTE associations, ATSOI, UKTSOA, NORDEL and BALTSO have become part of ENTSO-E, while providing data by their predecessors in the public interest.

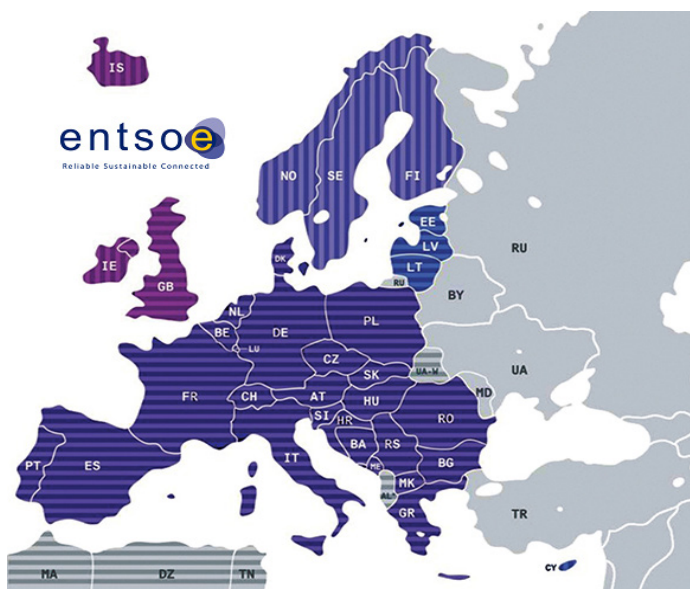


Figure 1. Map of ENTSO-E

ENTSO-E Member States: *Austria, Albania, Bosnia and Herzegovina, Belgium, Bulgaria, Switzerland, Cyprus, Czech Republic, Germany, Denmark, Estonia, Spain, Finland, France, Greece, Croatia, Hungary, Ireland, Iceland, Italy, Lithuania, Luxembourg, Latvia, Montenegro, Northern Ireland, North Macedonia, Netherlands, Norway, Poland, Portugal, Romania, Serbia, Sweden, Slovenia, Slovakia, Ukraine (observer Member).*

The interconnection of an power system is the main way to increase its reliability and security without affecting energy independence and provides emergency aid without the need to install and maintain a hot reserve of important power and the criteria for participation in interconnected operation (The ENTSO-E recommendations concern 6 major aspects of the operation of an energy system:

consumption coverage; primary power regulation; secondary frequency-power; voltage regulation; safety of operation under criterion (N-1) elements; anti-damage measures) [1].

In order to ensure the energy security of the Republic of Moldova and in the context of accession to the European Union, the synchronous connection to the ENTSO-E European electricity system is necessary and mandatory.

In this regard, in 2006, the joint request of the Republic of Moldova and Ukraine for a synchronous connection to the ENTSO-E system was submitted through a single block. Over several years, specialists of the Moldelectrica of the Republic of Moldova, Ukrenergo of Ukraine and Transelectrica of Romania, carried out the necessary documents preparation works.

At the moment, the technical and economic analysis on the possibility of carrying out the given project is carried out, the necessary steps are analyzed and processed, which must be taken by the Power System of the Republic of Moldova and the Power System of Ukraine for the possibility to enter ENTSO-E.

2. Power System – a system that generated critical infrastructures

In order to ensure the well-being and security of citizens, the Moldovan state has to provide a number of facilities for them, such as: Access to drinking water, sewerage, natural gas, electricity, medical care, to lead a normal and decent life, that society be happy.

These extremely important facilities are provided by certain infrastructures, which fall into three broad categories [9] :

- *ordinary infrastructure* – is a framework structure that ensures the construction and operation of a system;
- *special infrastructures* – with a consistent role in the functioning of systems and processes and a high degree of stability and security in the overall mechanisms of economic and social life of regional interest;
- *critical infrastructures* – are usually determinants of instability, security and security of systems and processes, playing an important role in the economic, social, political and military processes.

The vulnerability of these infrastructures creates a number of risks and threats to them, thus endangering societal life, creating malfunctions and causing extreme harm to society. Critical infrastructures thus become indispensable to society, without which the State and its mechanisms cannot function and ensure societal well-being, and their protection and/or security becomes a major national and European objective, determining the representatives of the Member States of the European Union to take action to identify and manage any risk or threat that could endanger the well-being of European citizens.

In this context, the Ministry of Infrastructure and Regional Development, through the Moldelectrica, must designate all the national and European critical infrastructures within the National Power System and have *Security Plans at the Operator* for each critical infrastructure, and these plans must be drawn up by the *Security Liaison Officers* [3].

In the Republic of Moldova the activity of electricity transmission, management and dispatching of the National Power System is carried out through the enterprise Moldelectrica, which is also the system operator.

The Power System of the Republic of Moldova works in sync with the Power System of Ukraine [2].

Energy infrastructure (power plants):

- *Gas-based thermoelectric plants – installed power: 2383,4 MW;*
- *Coal-fired thermal power plants – installed power: 1600 MW;*
- *Fuel oil-based thermoelectric plants – installed power: 2778 MW;*
- *Hydroelectric power plants – installed power: 64 MW;*
- *Renewable energy plants – installed power: 4 MW;*
- *main power plants:*
 - CET 1 Chişinău – installed power: 66 MW;
 - CET 2 Chişinău – installed power: 240 MW;
 - CET Bălţi – installed power: 24 MW;
 - CHE Costeşti – installed power: 16 MW;
 - CHE Dubăsari – installed power: 46 MW;
 - CERS Moldova (Cuciurgan) – installed power: 2520 MW;
 - Other generating sources – installed power: 87 MW.

Power infrastructure (power substations and overhead lines), as shown in Figure 2:

- *2 (two) 400 kV power substations (strategically important):*
 - Vulcăneşti;
 - CERS Moldova.
- *5 (five) 330 kV power substations (strategically important):*
 - CERS Moldova;
 - Răbniţa;
 - Chişinău;
 - Străşeni;
 - Bălţi.
- *9 (nine) 110 kV power substations for interconnection with Ukraine (commercial exchanges):*
 - Etulija;
 - Vulcăneşti;

- CERS Moldova;
 - Valilevik;
 - Soroca;
 - Otaci;
 - Ocnîța;
 - Brich;
 - Larga.
- 4 (four) 110 kV power substations for interconnection with Romania (commercial exchanges):
- Cioara;
 - Ungheni;
 - Gotești;
 - Costești.
- 1 (one) 400 kV overhead line for cross-border interconnection with Romania (stability and reliability of the power system):
- Vulcănești – Isaccea;
- 1 (one) 400 kV national overhead line (stability and reliability of the power system):
- Vulcănești – CERS Moldova.
- 7 (seven) 330 kV overhead line for cross-border interconnection with Ukraine (stability and reliability of the power system):
- CERS Moldova – Novoodeska;
 - CERS Moldova – Usatove;
 - CERS Moldova – Podilska;
 - CERS Moldova – Artsyz;
 - Răbnița – Podilska (circuit 1);
 - Răbnița – Podilska (circuit 2);
 - Bălți – Dnistrovska HPP.
- 3 (three) 330 kV national overhead line (stability and reliability of the power system):
- CERS Moldova – Chișinău (double circuit);
 - Chișinău – Strășeni;
 - Strășeni – Bălți.
- 15 (fifteen) 110 kV overhead line for cross-border interconnection with Ukraine (commercial exchanges):
- Etulija – Budzhak;
 - Vulcănești – Reni;
 - Vulcănești – Kosa;
 - Vulcănești – Bolgrad (circuit 1);

- Vulcănești – Bolgrad (circuit 2);
 - Vulcănești – Bolgrad (circuit 3);
 - CERS Moldova – Belyaevka;
 - CERS Moldova – Rozdil;
 - CERS Moldova Starokazachye;
 - Vasilevik – Kr. Okni;
 - Brich – Dnistrovska HPP;
 - Otaci – Namiya;
 - Ocnîța – Shahta;
 - Soroca – Poroghi;
 - Larga – Nelypivtsy.
- 4 (four) 110 kV overhead line for cross-border interconnection with Romania (commercial exchanges):
- Cioara – Huși;
 - Ungheni – Țuțora;
 - Gotești – Fălciu;
 - Costești – Stâncă.



Figure 2. National Power Grid

3. Analysis of the Power System

3.1. Identification of critical infrastructures

Table 1 lists the identified critical infrastructures within the Power System

Table 1. Critical Power Infrastructures

| Operator | Name of Critical Power Infrastructures | Type |
|--------------------------------|--|----------|
| Moldelctrica | Power substation 400 kV Vulcănești | European |
| | Power substation 400 330 kV CERS Moldova | European |
| | Power substation 330 kV Răbnița | European |
| | Power substation 330 kV Bălți | European |
| | Power substation 330 kV Chișinău | National |
| | Power substation 330 kV Strășeni | National |
| | OHL 400 kV Vulcănești – Isaccea | European |
| | OHL 400 kV Vulcănești – CERS Moldova | National |
| | OHL 330 kV CERS Moldova – Novoodeska | European |
| | OHL 330 kV CERS Moldova – Usatove | European |
| | OHL 330 kV CERS Moldova – Podilska | European |
| | OHL 330 kV CERS Moldova – Artsyz | European |
| | OHL 330 kV Răbnița – Podilska (circuit 1) | European |
| | OHL 330 kV Răbnița – Podilska (circuit 2) | European |
| | OHL 330 kV Bălți – Dnistrovska HPP | European |
| | OHL 330 kV CERS Moldova – Chișinău (1) | National |
| | OHL 330 kV CERS Moldova – Chișinău (2) | National |
| OHL 330 kV Chișinău – Strășeni | National | |
| OHL 330 kV Strășeni – Bălți | National | |

3.2. Identifying vulnerabilities

Table 2 lists the identified vulnerabilities within the Power System.

Table 2. Identifying vulnerabilities

| No. | Identifying vulnerabilities |
|-----|---|
| 1. | Dependence on IPS/UPS, the Power System of the Russian Federation, with the following component countries: Belarus, Ukraine, Kazakhstan, Georgia, Mongolia, Kyrgyzstan, Azerbaijan, Tajikistan → <i>Using electricity as a possible energy weapon or pressure instrument for the purpose of profitability or blackmail.</i> |

| No. | Identifying vulnerabilities |
|-----|---|
| 2. | Electricity transmission voltage at 330 kV (atypical European Union), which is specific only to IPS/UPS, which creates dependence on this power system and makes it almost impossible to connect to another power system (ex. ENTSO-E) → <i>Using atypical energy transmission voltage as a possible energy weapon or pressure instrument for profitability or blackmail.</i> |
| 3. | Radial distribution of the only energy main line (power grid) at 330 kV CERS Moldova – Chisinau – Straseni – Balti → <i>Possibility of power interruption in case of a terrorist attack or natural disaster on a critical infrastructure in this power chain (power substation or overhead line).</i> |
| 4. | Lack of critical power infrastructure (power substations and overhead lines) at 400 kV [exception: 400 kV Vulcanesti and CERS Moldova power substations and 400 kV Isaccea (Romania) – Vulcanesti and Vulcanesti – CERS Moldova overhead lines] → <i>Impossibility of interconnector to ENTSO-E.</i> |
| 5. | No international interconnection at 400 kV voltage in the north and center area with the European ENTSO-E system (Romania) → <i>Impossibility of interconnection to the European ENTSO-E.</i> |

4. Proposed measures in the context of interconnection to ENTSO - E and ensuring energy security and national security

1. Appointment of a Security Liaison Officer for each critical infrastructure and elaboration of the Security Plan to the critical infrastructure operator.

Argument: Mandatory transposition of the provisions of Council Directive 2008/114/EC of 8 December 2008 on the identification and designation of European critical infrastructures and the assessment of the need to improve their protection; [4]

2. The resilience of the power system in the event of terrorist attack, natural disaster or major technical failure, an important factor in ensuring energy and national security.

Argument: Resilience has become an indicator of the European Union's security policy, and in this regard the European Commission has developed the Action Plan for resilience in crisis countries 2013-2020, thus: a new approach has been reached to the societal dimension of national and european security, focusing on the citizen, community and population of a state or region;

3. Construction of national critical infrastructure:

Table 3. Construction of natural critical infrastructures

| Infrastructure | Argument |
|---|--|
| a. construction of OHL 400 kV Vulcanesti – Chisinau. | Power supply security at 400 kV voltage. |
| b. transition of OHL 330 kV CERS Moldova – Chisinau to a voltage of 400 kV. | Power supply security at 400 kV voltage. Possibility of multiple international connection with ENTSO-E. |
| c. transition of OHL 330 kV Chişinău – Străşeni to a voltage of 400 kV. | |
| d. transition of OHL 330 kV Străşeni – Bălţi to a voltage of 400 kV. | |
| e. construction of OHL 400 kV Străşeni – Răbniţa. | Closing the 400 kV ring in the area of Răbniţa, Straseneni, Balti → security in the power supply at the voltage of 400 kV. |
| f. construction of OHL 400 kV Bălţi – Răbniţa. | |

4. Construction of european critical infrastructure:

Table 4. Construction of european critical infrastructures

| Infrastructure | Argument |
|---|--|
| a. construction of OHL 400 kV Vulcanesti – Smârdan (Romania). | Closing the 400 kV ring in the area of Vulcanesti, Isaccea (Romania), Smârdan (Romania) → Security in the power supply at the voltage of 400 kV. 400 kV system stability – ENTSO-E. |
| b. construction of OHL 400 kV Chisinau – Iaşi Fai (Romania) under the condition OHL 220 kV Suceava – Iaşi Fai pass to the voltage of 400 kV, or construction of OHL 400 kV Chisinau – Roman Nord. | Security in the power supply at the voltage of 400 kV. Possibility of interconnection at 400 kV voltage to ENTSO-E. |
| c. construction of OHL 400 kV Balti – Suceava (Romania) under the condition of construction OHL 400 kV Suceava (Romania) – Gădălin (Romania). | Security in the power supply at the voltage of 400 kV. Possibility of interconnection at 400 kV voltage to ENTSO-E. |

| Infrastructure | Argument |
|---|--|
| d. passing OHL 330 kV Rabnita – Podilska (Ukraine) at the voltage of 400 kV. | Possibility of interconnection at 400 kV voltage of Ukrainian power system. System stability of 400 kV. |
| e. passing OHL 330 kV CERS Moldova – Podilska (Ukraine) at voltage of 400 kV. | Possibility of interconnection at 400 kV voltage of Ukrainian power system. Closing of the 400 kV ring in the area of CERS Moldova, Chisinau, Straseni, Rabnita, Podilska (Ukraine), CERS Moldova → Security in electricity supply at 400 kV between the Republic of Moldova and Ukraine. |
| f. passing OHL 330 kV Bălți – Dnistrovska HPP (Ukraine) at voltage of 400 kV. | Possibility of interconnection at 400 kV voltage of Ukrainian power system. Closing of the 400 kV ring in Balti area, Suceava (Romania), Dnistrovska HPP (Ukraine) → Security in electricity supply at 400 kV voltage between the Republic of Moldova and Ukraine. |

5. Construction of power plants:

Table 5. Construction of power plants

| Infrastructure | Argument |
|--|-----------------------|
| a. construction of hydroelectric power plants on the Prut River | energy independence. |
| b. construction of hydroelectric power plants on the Nistru River | energy stability. |
| c. construction of nuclear power plants | trade in electricity. |
| d. construction of power plants based on renewable energy sources, biomass, or other energy sources. | energy security. |

5. Conclusion

Considering that there are strong cooperation relations between Romania and the Republic of Moldova, we must be integrated into the same power system and especially have the same solid principles regarding the area energy security, where the Black Sea plays an increasingly crucial and strategic role. In this context, Romania provides governmental aid on the integration of the Republic of Moldova into the European Union and consistent support on the interconnection to the ENTSO-E energy system. In this paper, the authors came up with a series of proposals on different ways of interconnection to ENTSO-E and ensuring the stability and security of the Moldovan energy system. These proposals for measures consist mainly of major investments in energy infrastructure, such as:

- construction of hydroelectric power plants on the Prut and Nistru rivers, nuclear power plants, power plants based on renewable energy sources, or other energy sources, which will ensure the electricity needs for the Republic of Moldova to become an energy independent state;
- the construction of power substations at 400 kV voltage which will ensure the transit of electricity and its transformation to different voltages of household, industrial and especially critical consumers;
- the construction of overhead lines at a voltage of 400 kV which will ensure the interconnections between the Moldovan energy system and ENTSO-E.

The investments are major because Moldova is dependent on the Russian power system operating at the atypical voltage of 330 kV, and this can be easily used as an energy weapon or pressure instrument. Following these investments, of course with the help of Romania and the European Union, Moldova will become a credible, strategic and energy-secure partner state of the European Union.

References

- [1] ENTSO-E, www.entsoe.eu
- [2] Moldelectrica, www.moldelectrica.md
- [3] Fiță N.D., Radu S.M., Păsculescu D., Gregory E., Ranf D.E., Bucovetchi O.M.C., Badea D., (Coordinators), *Sustainability Management and managerial sustainability between classical and modern paradigms, chapter: Addressing national critical energy infrastructures correlated with societal resilience and sustainability*, "Nicolae Bălcescu" Academy of Land Forces Publishing House, Sibiu, 2021, p.p. 37 – 58.
- [4] Council Directive 2008/114/EC of 8 December 2008 on the identification and designation of European critical infrastructures and the assessment of the need to improve their protection.

- [5] Government of the Republic of Moldova, Decision no. HG701/2018 of 11.07.2018, for the approval of the Regulation on the anti-terrorist protection of critical infrastructure.
- [6] Fiță N.D., Radu S.M., Păsculescu D., *Ensuring, controlling and stability of energy security in the context of increasing industrial and national security*, Universitas Publishing House, Petrosani. 2021.
- [7] Fiță N.D., *Identifying the vulnerabilities of critical infrastructures within the national electricity system in the context of increasing energy security*, Universitas Publishing House, Petrosani, 2019.
- [8] Fiță N.D., Păsculescu D., Pupăza C., Gregory E., *Methodology for identification, designation, analysis, evaluation, protection and resilience of critical electroenergy infrastructures. In resilience Management in Contemporary society*, Bucovetchi O.M.C., Ranf D.E., (Coordinators): „Nicolae Bălcescu” Academy of Land Forces Publishing House, Sibiu, 2022, pp. 180-201.
- [9] Romanian Intelligence Service, www.sri.ro

Addresses:

- Lect. Ph.D. Eng. Nicolae Daniel Fita, University of Petrosani, Strategic Studies of Energy Security, University street, nr. 20, Petrosani district, Hunedoara county, Romania
daniel.fita@yahoo.com
(* corresponding author)
- Prof. Ph.D. Eng. Mihai Sorin Radu, University of Petrosani, Strategic Studies of Energy Security, University street, nr. 20, Petrosani district, Hunedoara county, Romania
sorin_mihai_radu@yahoo.com
- Assoc. Prof. Ph.D. Eng. Dragos Pasculescu, University of Petrosani, Strategic Studies of Energy Security, University street, nr. 20, Petrosani district, Hunedoara county, Romania
pdragos_74@yahoo.com
- Ph.D. Stud. Eng. Florin Muresan, University of Petrosani, Strategic Studies of Energy Security, University street, nr. 20, Petrosani district, Hunedoara county, Romania
flomavon2002@yahoo.com
- Stud. Danut Mircea Pintea, University of Petrosani, Mechanical and Electrical Engineering Faculty, University street, nr. 20, Petrosani district, Hunedoara county, Romania
mdm.pintea_prest@yahoo.com

The Electromagnetic Mapping of the City of Beiuș

Marius Lolea, Andrea Amalia Minda*, Eva Barla,
Andrei Sărăcuț–Ardelean, Emeric Szabo

Abstract. *The paper presents a method of the electromagnetic mapping for a locality - City of Beiuș from Bihor County. For this activity, it is first necessary to identify the public electromagnetic field sources. Then the measuring devices must be chosen and made the measurements. Finally, the values obtained for the electric and magnetic field sizes are integrated into a digital map that will be available to those interested. The authors have also taken photos of the sources for easier identification on in the city territory.*

Keywords: *electric field, magnetic field, characteristic quantities*

1. Introduction

The electromagnetic field (ELMF), as a form of existence of matter, exists both in natural form (coming from the Earth's own geomagnetic and electrical field, extraterrestrial radiation - radioactive particles and cosmic electromagnetic waves) and in anthropogenic form (generated by electromagnetic devices developed by man). From the structural point of view the electromagnetic field has two components: the electric field and the magnetic field

The propagation by space of the electromagnetic field, is done through the waves or electromagnetic radiation or in the form of particles. Because it is invisible to humans, the electromagnetic field is evaluated, by its components, through its effects using characteristic quantities (CQ-ELMF) [3, 8].

With the large-scale development and spreading of anthropogenic sources of electromagnetic field, certain influences on the exposure of living organisms in the new artificially created environment have also been found. Thus, exposure of the biological to the electromagnetic field has been shown to have beneficial and harmful effects. Depending on the effects on the atoms the electromagnetic waves are ionizing and non-ionizing. The negative effects of ionizing radiation that can cause



damage to living cells are easier to demonstrate. In medical therapies, these radiations have useful effects by destroying tumour cells in cancerous diseases. The non-ionizing radiations that are the object of the study in the paper have negative effects that are harder to prove and the results in this regard are controversial. [9]. A need to Long-term studies and state-of-the-art technologies to demonstrate the negative effects on humans of electrical and magnetic exposure. However, among the negative effects on health in the dedicate literature [2, 7, 9] is mentioned: insomnia, vertigo, anxiety, reducing fertility, lack of concentration, slowing metabolism or chronic conditions (tumors, leukemia and other forms of cancers etc). Beyond controversies, certain allowable threshold values of CQ-ELMF have been taken into account and regulated, which should not be exceeded in order not to be dangerous to health and which should be taken into account when avoiding exposure. These are correlated with amplification of effects, with other characteristics of ELMF sources and exposure such as proximity to sources or duration of exposure.

In norms(Romanian and international), for the characterization of the harmful effects of exposure, are given the threshold admissible values of CQ(in general for E, B, S – power density of ELMF or electromagnetic wave strength[W/m²], SAR – specific absorption rate[W/kg]), for general population and employees that work in electrical installations, on frequency ranges of ELMF[10, - 16]. Generally, threshold admissible values for workers are bigger like those for population, because this are protected by equipment against radiation (by variable ELMF and/or static electric and magnetic fields) or has means of access control in areas with intense fields. When in the natural environment, the values of CQ - ELMF are exceeded, is talk about the concept of electromagnetic pollution [7]. So, electromagnetic pollution also affects both technical and biological systems as it results from the results of various studies published by researchers.

The purpose of the paper is to experimentally determine the values of CQ and comparing them with the normed ones, for highlighting the level of electromagnetic pollution given by the sources distributed in the municipality of Beiuş. The admissible values of the CQ-ELMF considered in the paper come from the Romanian regulations or ICNIRP recommendations [11, 12, 16].

2. Public sources of ELMF

In this chapter, are described the public sources of ELMF along with some of their general characteristics. The data obtained together with the site are used by the authors for the elaboration of a digital electromagnetic map with the distribution of sources throughout the city. The ELMF sources investigated experimentally are: power stations (PS), power substations (power transformations points), overhead electricity lines(OEL or OPL) and mobile telecommunications base stations with antennas, noted SB-GSM(GSM sites).

2.1. Public energy sources in Beiuș

The City of Beiuș is located in the south of Bihor County, on the road that connects Oradea to Deva – național way DN 76 integrated into the European route E79 (at 62 km distance by the county seat - Oradea). The population of the city, which also includes the village of Delani, according to the 2011 census is 10667 inhabitants with a density of 494 inhab/km². As a relief area, the municipality is located in the Beiuș Depression known in the past as “Beiuș Country” (is also known as the Crișului Negru Depression, after the river that runs through the area). In Beiuș Depression, the average thermal values are around 10°C, they gradually decrease towards contact with the mountain regions. Thus, at Beiuș, located at the altitude of 191 m above sea level, the average multiannual temperature is 10,5°C, coldest month of the year, namely January, is characterized by the value of 1,5°C, and the hottest month, July, by the value of 21,2°C [4]. In Figure 1 is presented a panoramic image of the city.



Figure 1. Panoramic view of Beiuș



Figure 2. PS of Beiuș

Heat power supply of large consumers (blocks of flats, administrative institutions, hospitals, schools but also private houses) is made in centralized system by geothermal energy. The geothermal water is extracted through two production wells and re-injected through a third well. There are also individual consumers or small consumers who hold for heating and the production of domestic hot water, stoves and biomass or little electric power stations. Electricity is obtained from power station (PS) Beiuș, connected to the electricity system (PWS) Bihor through an OPL by 110 kV which has links with electric stations in Oradea, Sudrișiu, Ștei and Vașcău. A photograph of PS Beiuș can be seen in figure 2. The city is connected at a PS from Salonta town through a power line (PL) by 20 kV. A portion of the Oradea - Beiuș - Vașcău OPL is shown in figure 3.

The distribution of electricity is made through aerial and underground medium voltage lines, power substations (MT/JT) and low voltage lines. On the city territory are installed (to moment of study) about 5 km HV OPL, approximately 27 km of electricity lines (EL) by MV and 18 transformation points (PSS). From the city's electric station starting more EL by MV for supplying the rural localities in the vicinity.

Terrestrial surface of the municipality is of 21,593 km². On this territory, for the cover of signal level, are placed five GSM sites. With the exception of the flats block with eight floors from the centre of the city, which is tallest building and is shown in figure 4, other three antennas mounts are upon separated pillars or on water reservoir tower.

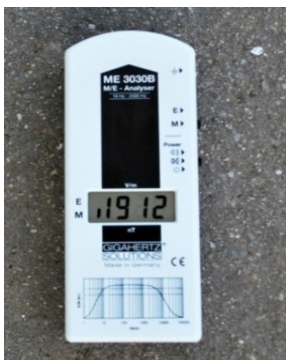


Figure 3 .110 kV OPL Beiuș - Vașcău **Figure 4**. Building with GSM antennas

The distribution and supply of electricity in the public system is made by the Bihorean department (local branch) of the company S.C. Electrica SA Transilvania North, with the headquarters in the city of Cluj-Napoca. For the supply of heat and domestic hot water in centralized system, on the territory of the Beiuș municipality operates the Company Transgex, from Oradea. Mobile telecommunication services are provided by operators who also operate on the international market: Orange, Vodafone, Telekom and Digi (RDS&RCS).

2.2. Electromagnetic field sources distribution on the territory of Beiuș

Images of the detectors devices of ELMF is shown in the figure 5 –a, for E and B of low frequency, respectively 5 – b, for high frequency.



a.



b.

Figure 5. ELMF devices

The device EMF Tester ME3030 B (fig.5.a) for frequency range 16 Hz÷100 kHz, produced by Gigahertz Solution - Germany, measures both the electric field and the magnetic field, has domains of measurement of 1÷ 5000 V/m and respectively 1÷1999 nT. The device Tenmars TM-195(fig.5.b) made in U.K.(Seeit/ RS Components Ltd), measures in the frequency range of 50 MHz ÷ 3,5 GHz , having recording time by 2,5 values/sec and resolution of 0,001 $\mu\text{W}/\text{m}^2$.

For additional checks and determining deviations between measured sizes, have also used the device Spectran 5035, made by Aaronia Company from Germany. The distances to the sources were measured with the BOSCH PLR 50 laser telemeter. Temperature, atmospheric pressure and humidity, were recorded with a TFA Faktum type (Germany) portable weather micro-station with external sensor.

3. Schemes and measuring devices. Experimental results

This chapter briefly describes the measurement schemes adopted and the devices used. It is the experimental part of the work that determined the CQ-ELMF values. In the period of measurements, the weather was sunny, with outdoor ambient temperatures in range of 3÷7 °C, during month of February.

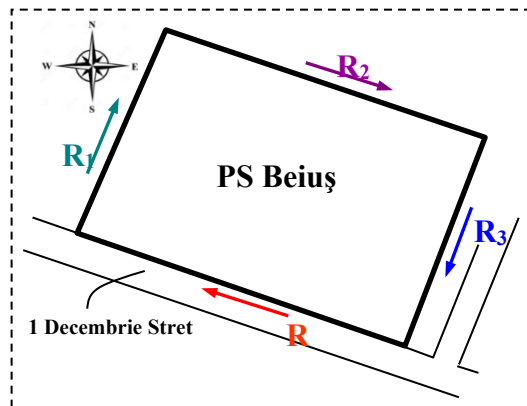


Figure 6. Measure scheme for Beiuș PS

For PS by distribution of electricity, which is the only from Beiuș, is considered a measure scheme with four routes outside the fence ($R_1\div R_4$), according to the figure 6. On each way are allocated 10 measure points at the quotas (heights to the ground) $h_1=1\text{m}$ și $h_2=1,7\text{ m}$, located at a distance $d = 1\text{ m}$ from the fence. There will be 20 measurements for each route and 80 values for the entire perimeter of the station. The results are given in table 1. For the Power transformers points (noted PSS), which are low power transformer stations on MT / JT voltage levels and rela-

tive symmetrical constructive structures, the adopted measurement scheme is shown in Figure 7. Are adopted the same quotas like in case of PS. The distances and the results of measurements are given in table 2 and table3. With the measured values, classifications of the sources can be prepared according to the electromagnetic pollution produced in the public space. For example, in the figures 8÷11 is presented in graphic form, a synthesis of the results obtained for five PSS and five OPL – MV.

Table 1. Measured values of E, for PS. Measured values of B, for PS Beiuş

| Heights T ₁ | Values of E[V/m] on route 1 Measure points P ₁ →P ₅ | | | | |
|------------------------|---|-----|-----|------|-----|
| h ₁ = 1 m | 210 | 230 | 245 | 260 | 310 |
| h ₂ = 1,7 m | 320 | 410 | 430 | 460 | 370 |
| Heights T ₂ | Values of E[V/m] on route 1 Measure points P ₆ →P ₁₀ | | | | |
| h ₁ = 1 m | 300 | 295 | 225 | 210 | 200 |
| h ₂ = 1,7 m | 340 | 325 | 260 | 250 | 220 |
| Heights T ₃ | Values of E[V/m] on route 2 Measure points P ₁₁ →P ₁₅ | | | | |
| h ₁ = 1 m | 110 | 130 | 145 | 160 | 110 |
| h ₂ = 1,7 m | 220 | 210 | 230 | 260 | 270 |
| Heights T ₃ | Values of E[V/m] on route 2 Measure points P ₁₆ →P ₂₀ | | | | |
| h ₁ = 1 m | 200 | 195 | 125 | 110 | 110 |
| h ₂ = 1,7 m | 240 | 225 | 160 | 150 | 150 |
| Heights T ₃ | Values of E[V/m] on route 3 Measure points P ₂₁ →P ₂₅ | | | | |
| h ₁ = 1 m | 510 | 630 | 845 | 960 | 850 |
| h ₂ = 1,7 m | 620 | 710 | 930 | 1060 | 980 |
| Heights T ₃ | Values of E[V/m] on route 3 Measure points P ₂₆ →P ₃₀ | | | | |
| h ₁ = 1 m | 810 | 695 | 525 | 410 | 300 |
| h ₂ = 1,7 m | 950 | 725 | 670 | 540 | 410 |
| Heights T ₄ | Values of E[V/m] on pentru route 4 Measure points P ₃₁ →P ₃₅ | | | | |
| h ₁ = 1 m | 520 | 630 | 740 | 550 | 420 |
| h ₂ = 1,7 m | 610 | 710 | 850 | 670 | 560 |
| Heights T ₄ | Values of E[V/m] on route 4 Measure points P ₃₆ →P ₄₀ | | | | |
| h ₁ = 1 m | 320 | 255 | 205 | 220 | 210 |
| h ₂ = 1,7 m | 380 | 330 | 250 | 240 | 230 |

| Heights T ₁ | Values of B[μT] on route 11 Measure points P ₁ →P ₅ | | | | |
|------------------------|---|-------|-------|-------|-------|
| h ₁ = 1 m | 2,15 | 3,15 | 3,20 | 3,30 | 4,20 |
| h ₂ = 1,7 m | 2,65 | 3,45 | 3,55 | 3,60 | 4,50 |
| Heights T ₁ | Values of B[μT] on route 1 Measure points P ₆ →P ₁₀ | | | | |
| h ₁ = 1 m | 3,10 | 2,60 | 3,30 | 3,15 | 3,10 |
| h ₂ = 1,7 m | 3,25 | 2,75 | 3,40 | 3,25 | 3,15 |
| Heights T ₂ | Values of B[μT] on route 2 Measure points P ₁₁ →P ₁₅ | | | | |
| h ₁ = 1 m | 2,25 | 3,35 | 3,25 | 3,40 | 4,20 |
| h ₂ = 1,7 m | 2,75 | 3,55 | 3,55 | 3,65 | 4,40 |
| Heights T ₂ | Values of B[μT] on route 2 Measure points P ₁₆ →P ₂₀ | | | | |
| h ₁ = 1 m | 3,20 | 2,50 | 3,35 | 3,10 | 3,05 |
| h ₂ = 1,7 m | 3,35 | 2,60 | 3,45 | 3,20 | 3,10 |
| Heights T ₃ | Values of B[μT] on route 3 Measure points P ₂₁ →P ₂₅ | | | | |
| h ₁ = 1 m | 9,15 | 9,15 | 9,20 | 8,30 | 9,20 |
| h ₂ = 1,7 m | 11,65 | 12,45 | 10,55 | 9,60 | 10,50 |
| Heights T ₃ | Values of B[μT] on route 3 Measure points P ₂₆ →P ₃₀ | | | | |
| h ₁ = 1 m | 7,10 | 6,60 | 5,30 | 4,15 | 3,80 |
| h ₂ = 1,7 m | 8,25 | 7,75 | 6,40 | 5,25 | 4,15 |
| Heights T ₄ | Values of B[μT] on route 4 Measure points P ₃₁ →P ₃₅ | | | | |
| h ₁ = 1 m | 10,15 | 13,15 | 13,20 | 12,40 | 11,20 |
| h ₂ = 1,7 m | 12,65 | 14,45 | 14,55 | 13,50 | 12,55 |
| Heights T ₄ | Values of B[μT] on route 4 Measure points P ₃₆ →P ₄₀ | | | | |
| h ₁ = 1 m | 10,10 | 9,40 | 7,30 | 5,15 | 4,20 |
| h ₂ = 1,7 m | 11,15 | 9,75 | 8,45 | 6,20 | 4,85 |

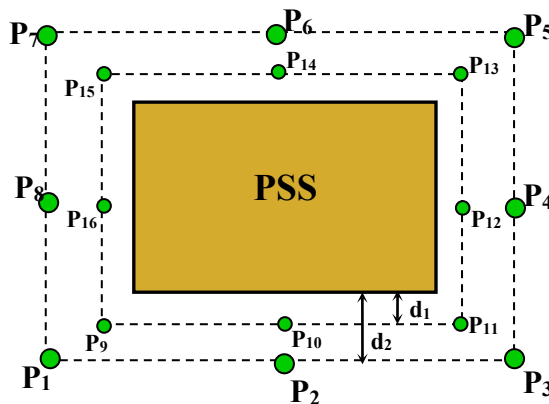


Figure 7. Measurement scheme for PSS

There are given minimum and maximum values obtained directly by measurements and calculated average values for all measurement points in the vicinity of the sources and with reference to the magnetic induction and the intensity of the electric field. That five PSS are named after the streets on which they are located and the power lines, depending on the interconnection points.

The graphs above refer to the distribution of PSS on the streets: PTA Habitat (PSS1), PTZ Pandurilor(PSS2), PTab Bihorului(PSS3), PTZ Ciordaş(PSS4) and PTZ Independenței(PSS5).

Table 2. Values of E for PSSb Pandurilor

| Distances | Values of E[V/m]for measure points (E _i P _j , i=j) | | | |
|-----------------------|--|-------------------------------------|-------------------------------------|-------------------------------------|
| d ₁ =0,5 m | E ₁ P ₁ =120 | E ₂ P ₂ =110 | E ₃ P ₃ =135 | E ₄ P ₄ =120 |
| d ₂ = 1 m | E ₉ P ₉ =90 | E ₁₀ P ₁₀ =85 | E ₁₁ P ₁₁ =95 | E ₁₂ P ₁₂ =90 |
| d ₁ =0,5 m | E ₅ P ₅ =115 | E ₆ P ₆ =125 | E ₇ P ₇ =110 | E ₈ P ₈ =115 |
| d ₂ = 1 m | E ₁₃ P ₁₃ =90 | E ₁₄ P ₁₄ =95 | E ₁₅ P ₁₅ =80 | E ₁₆ P ₁₆ =85 |

Table 3. Values of B for PSSb Pandurilor

| Distances | Values of B[μT]for measure points (E _i P _j , i=j) | | | |
|-----------------------|---|---------------------------------------|---------------------------------------|---------------------------------------|
| d ₁ =0,5 m | B ₁ P ₁ =0,25 | B ₂ P ₂ =0,22 | B ₃ P ₃ =0,33 | B ₄ P ₄ =0,45 |
| d ₂ = 1 m | B ₉ P ₉ =0,10 | B ₁₀ P ₁₀ =0,09 | B ₁₁ P ₁₁ =0,06 | B ₁₂ P ₁₂ =0,07 |
| d ₁ =0,5 m | B ₅ P ₅ =0,15 | B ₆ P ₆ =0,25 | B ₇ P ₇ =0,14 | B ₈ P ₈ =0,15 |
| d ₂ = 1 m | B ₁₃ P ₁₃ =0,04 | B ₁₄ P ₁₄ =0,11 | B ₁₅ P ₁₅ =0,03 | B ₁₆ P ₁₆ =0,05 |

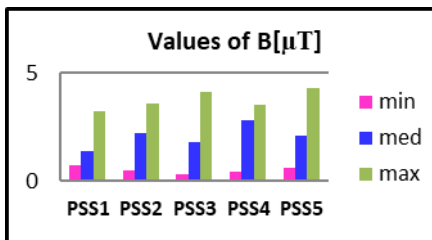


Figure 8. Variation of B for PSS

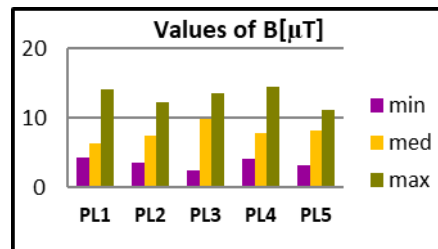


Figure 9. Variation of B for OPL (MV)

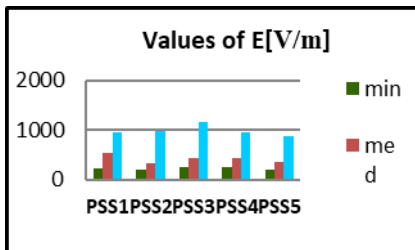


Figure 10. Variation of E for PSS

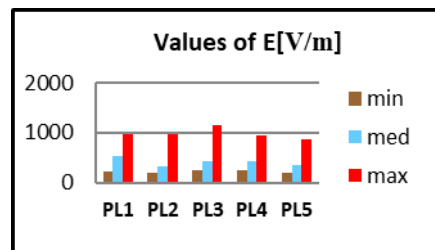


Figure 11. Variation of E for OPL (MV)

The results from figures 9 and 11 include the overhead MV lines: Beiuș-Drăgănești (PL1), Beiuș – Remetea (PL2), Beiuș – Nimăești (PL3), Beiuș – Târcaia (PL4) and Beiuș – Pocola (PL5). In figure 12, through the side view and in figure 13, through the image from above, is presented the measurement scheme for the overhead power lines (OPL), for both high and medium voltage. The first and last measuring points in the center of the line are in the axis of the pillars at the end of each aperture. It is considered three measurement paths, under each conductor of the three-phase line at heights above soil level $h_1 = 1,7$ m (considered at head level of the human by medium height), respective $h_2 = 1$ m. On each opening is considered 10 measurement points, the total number being 60 measurements between two consecutive pillars.

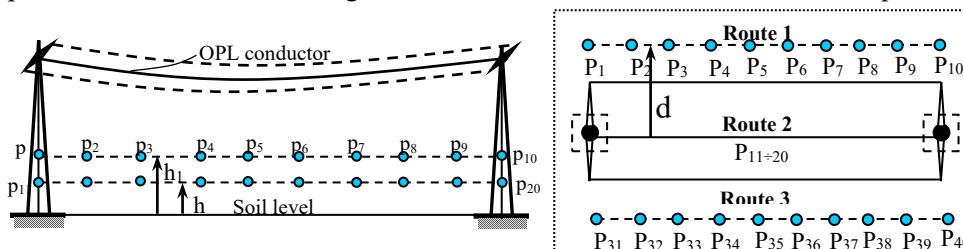


Figure 12. Measure scheme for OPL – size view(a) from above(b)

The measuring process results of E și B, in case of aperture no. 2 of OPL by 110 kV (started from PS Beiuș), are given under graphic form, in figures 13 .

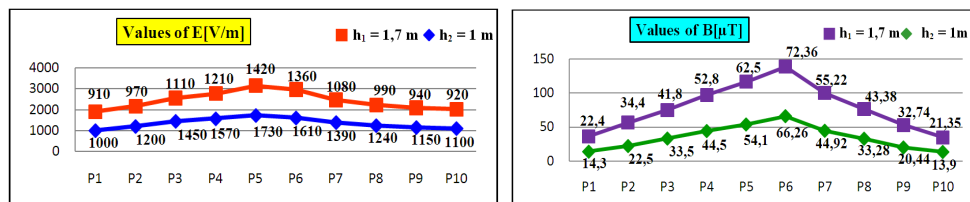


Figure 13. Results of E, B measurements for 110 kV OPL

In the case of telecommunications systems, for the measurement schemes were considered two situations, such us the antennas with additional facilities are mounted on buildings or pillars.



Figure 14. Places of measurements for GSM case

In the only case of placement on a block, the registration points were integrated into (inside) four flats located to the last floor, under BS-GSM. Also, in this case, measurements were made and in four points located on the building, over considered apartments. In the second situation, the measurements were made in four directions (N, W, S, E) in rooms from the buildings closest to the pillars.

For each cardinal point two maximum values identified in the two measuring rooms were taken and for scoring the results were used indexes, thus: position 11,12 → North point; position 21,22 → West point; position 31, 32 → South point; position 41,42 → East point; finally, 8 cases were obtained. For the apartments from the vicinity of a GSM pillar placed inside of the public institution yard, the measuring points (MP), are indicated with red arrows in figure 14. The results of measurements are presented in table 4.

Table 4. Results of measurements near GSM sites

| GSM places | Values of Power density [mW/cm ²] (averaged over 30 min) | | | | | | | |
|------------|--|----------------|----------------|----------------|----------------|----------------|----------------|----------------|
| | Measure points | | | | | | | |
| | P ₁ | P ₂ | P ₃ | P ₄ | P ₅ | P ₆ | P ₇ | P ₈ |
| Case 11 | 2,2 | 1,3 | 2,4 | 1,8 | 3,8 | 2,7 | 2,5 | 1,6 |
| Case 12 | 1,4 | 1,2 | 1,5 | 1,7 | 4,2 | 1,7 | 2,6 | 1,4 |
| Case 21 | 3,3 | 3,2 | 1,3 | 2,1 | 2,2 | 2,5 | 3,5 | 2,6 |
| Case 22 | 1,5 | 1,3 | 1,4 | 2,7 | 3,2 | 3,7 | 1,5 | 3,6 |
| Case 31 | 1,2 | 2,3 | 1,6 | 2,3 | 3,5 | 3,2 | 2,5 | 4,3 |
| Case 32 | 3,1 | 1,5 | 2,2 | 3,4 | 2,6 | 2,7 | 3,1 | 1,1 |
| Case 41 | 1,6 | 1,6 | 2,5 | 4,7 | 4,2 | 3,7 | 2,4 | 1,8 |
| Case 42 | 1,7 | 2,3 | 1,7 | 2,7 | 3,2 | 2,8 | 2,6 | 2,1 |

To highlight the territorial distribution of ELMF sources, the authors created a map called “Beiuș Electromagnetic Map” (abbreviated: M - ELMF Beiuș).

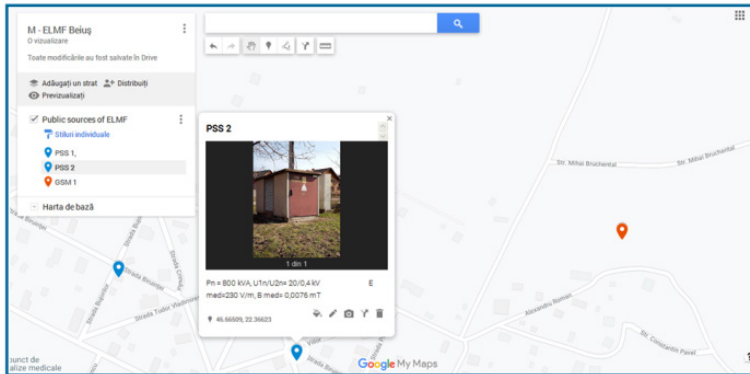


Figure 15. ELMF Map of Beiuș

The map was developed using the Google Maps software utility. On the map, in addition to marking the position of the sources, the following facilities are also offered: spotting GPS coordinates of sources and of the distance between them,

technical features, average values of CQ- ELMF obtained experimentally, images of the sources. From the map you can easily identify the neighborhoods and streets where the objects of interest are located. The map is useful especially for employees in energy and telecommunications service companies (for those who do not know the area) which in case of damage or other incidents can be oriented and reach the required location more easily. A sector from M - ELMF Beiuș can be observed in figure 15.

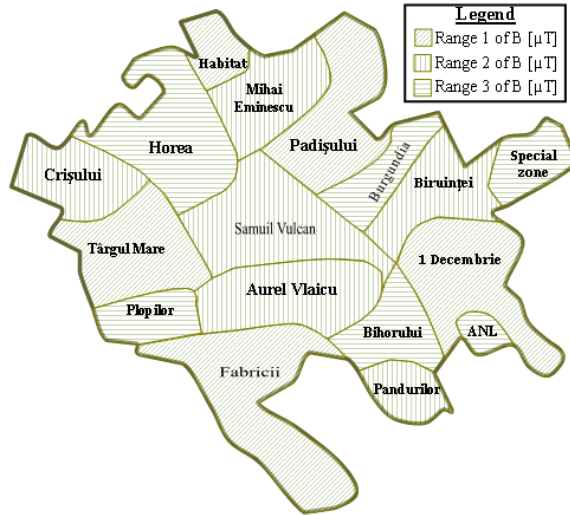


Figure 16. Neighbourhoods B ranking map

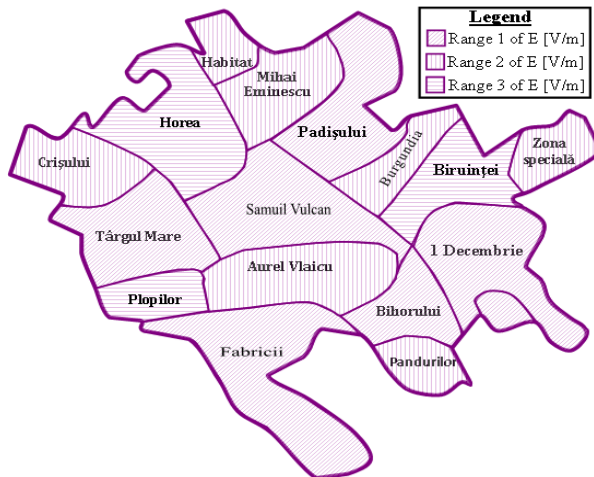


Figure 17. Neighbourhoods E ranking map

Urbanistic, the territory of the city has divided in 15 districts with a total streets number of 93. There were also created two graphic maps, represented in the figures 16(with B values) and 17(with E values), with the framing of neighbourhoods by value domains (average values) of CQ - ELMF. The establishment of these domains (ranges) was done as follows: a).in case of B values. Range 1: $0 \div 1,50$ [μT]; Range 2: $1,51 \div 10,5$ [μT]; Range3: $> 10,5$ [μT], b). In case of E values. Range 1: $0 \div 120$ [V/m]; Range 2: $121 \div 600$ [V/m]; - Range 3: > 600 [V/m].

For comparison and testing of electromagnetic pollution, the allowable values of CQ – ELMF extracted from the literature [1,11,12,16], are:

- For general public (index 1):
 - $E_{adm1} = 5000$ [V/m], low frequency (50 Hz);
 - $B_{adm1} = 100$ [μT], low frequency (50 Hz);
 - $S_{adm1} = f/200(10)$ [mW/cm^2], high frequency (Rf);
 - $SAR_{adm1} = 0,08$ [W/kg], high frequency (Rf)/whole body; 2 [W/kg]/head level.
- For occupational (index 2):
 - $E_{adm2} = 10000$ [V/m], low frequency (50 Hz);
 - $B_{adm2} = 500$ [μT], low frequency (50 Hz);
 - $S_{adm2} = f/40(50)$ [mW/cm^2], high frequency (RF);
 - $SAR_{adm2} = 0,4$ [W/kg], high frequency (RF)/ whole body; 10 [W/kg]/head level.

If only the experimental values obtained for population testing are taken into account, it can be stated that none of the CQ-ELMF exceeds the normed limit values and therefore the electromagnetic pollution in the investigated areas is reduced. From the statistical analysis of the electromagnetic map, on the whole of the districts (neighbourhoods), results the weight of the ranges of values of the field quantities (fig. 18).

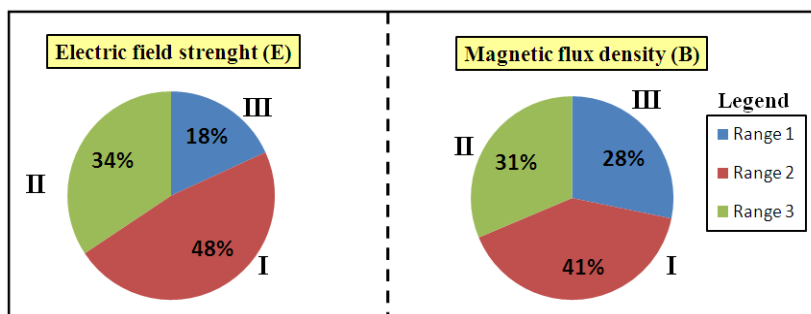


Figure 18. CQ-ELMF ranges percentage

Figure 18 shows the classification of the districts (the top three in the ranking) according to the number of ELMF sources.

The hierarchy presented in figure 19, includes each category of ELMF sources and their sum. Knowing the intensity of the electromagnetic field by the public can lead to decisions to avoid those areas, even if the value limits of the CQ indicating the exposure harmfulness are not exceeded. It is possible that some people are more sensitive to the action of the ELMF [2].

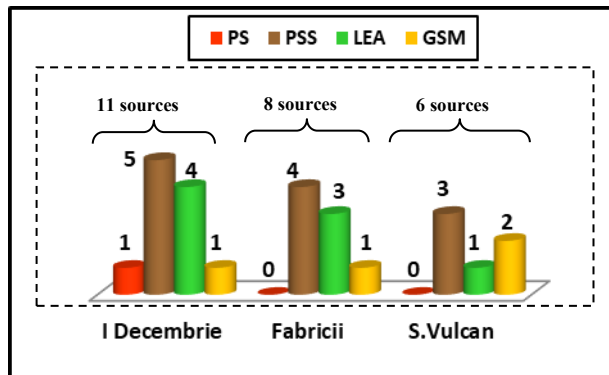


Figure 19. Neighbourhoods ranking by sources number

4. Discussion

The sources of high frequency electromagnetic field are considered most dangerous. Perhaps the fact that alarmist articles which appear regularly in the mass media about the harmful effects of telecommunication antennas leads to a higher interest of them. There have even been public calls signed by scientists, specialists and researchers from several fields, against wireless data transmission systems. It is the case of International Appeal against 5G technology [17], named: "Stop 5G on Earth and in Space", which had 231,326 online signatories from 214 nations and territories (in April 11th, 2020). In the case of the GSM telecommunication installations investigated, the highest values of the intensity of the electromagnetic waves were recorded in the places inside the cone (cylinder) or the emission bulb of the antennas (in the direct visibility of the antennas). From the specific measurement conditions mentioned in [6], it follows that the power density of GSM 900 signals coming from the sectoral antennas of the base stations (at the frequency of 947.5 MHz,) at a certain source distance, changes their cylindrical character of radiation and turns into a spherical one. The importance of the spectral analyzer settings in accurately reproducing the radiation levels must be appreciated [6]. The pointed and momentary values of the CQ-ELMF, recorded in the paper, are not relevant enough in the assessment of the electromagnetic pollution, considering the alternative and dynamic character of the electromagnetic field generated by sources. Thus, as in [1], the monitoring of the electromagnetic field (in radio frequency) must be

done with the input of fixed monitoring systems, which will collect data for a longer period of time. The monitoring of the electromagnetic field for three consecutive months for sources distributed on the territory of the city of Iași, showed that the highest value recorded for the intensity of the electric field represented a percentage of less than 40% of the imposed limit [1]. Even if the current Romanian regulations do not provide in some situations, measurements of the power density of electromagnetic waves but just of SAR (and also E or H), as are the cases of the changes from [10] compared to [11] and [12], we did not want to determine the pathological effects of the exposure but only the situation of possible electromagnetic pollution. That's why we determined the values of S for GSM frequencies.

5. Conclusions

The measurement schemes initiated by the authors are original and the values obtained are difficult to compare exactly with results from other researchers. However, on a larger scale, by extrapolation, these can be confirmed, but the operating conditions of the sources, which are alternating current, vary in time. Although they are of great importance in generating electromagnetic pollution (when exceeding the allowable values of CQ-ELMF) and they are present in greater number on the territory of cities, the sources by high power within the electrical grids do not arouse among the population the same interest as the mobile telecommunications systems.

In the measuring areas, the admissible values of CQ-ELMF were not exceeded. This thing does not exclude the possibility that, at certain distances from the sources, the threshold values are exceeded. In addition to the installations investigated in the paper, both the public and the workers from various domains of activity, use other devices that are sources of ELMF. These include electro-technical, electronic and office equipment or energy-technology systems: PCs, printers, faxes, electric hobs, refrigerators, televisions, automation systems, electrolysis installations, generators and electric motors, induction and microwave ovens etc. Certain economic entities grant salary increases to employees working in spaces with outdated values of CQ-ELMF. As general recommendations for protection and limitation of exposure we have identified: keeping an optimal distance from sources, limiting access in spaces with intense fields, signalling the presence in areas with ELMF, using protective equipment against static or variable electric and magnetic fields, using of electromagnetic shields, limiting the duration of exposure. From the data analysis, results a density of 0,26 ELMF sources per m^2 on the surface of the city. For the population number, results an allocation of 0,12 sources / inhabitant. The total number of ELMF sources is 55(identified at the study time). Measurements for GSM sites were performed in only four cases, because a pillar and the base station were located outside of the city and far from buildings. Created maps

with CQ-ELMF values and implicitly with the distribution of sources, can be integrated into a specialized web-site and thus will become public and useful to those interested. In apartments or other enclosures where there are active ELMF sources, must be stopped during measurements process because they further disturb the environment and is difficult to appreciate the frequency range or the direction of the electromagnetic waves, due to overlaps that appear. Therefore, is need high-performance field analyzers that measure on 3 axes (with isotropic probes) or spectrometers that will be tuned (make the selection) to the frequency of the ELMF sources if this is known.

References

- [1]. Bejenaru O., *Cercetări privind expunerea umană la câmpurile electromagnetice generate de sisteme de comunicații*, Teză de doctorat, Univ. Tehnică „Gheorghe Asachi”, Iași, 2019.
- [2]. Drăgulescu A., *Idolii fără fir*, Editura Cristhiana, București, 2010.
- [3]. Goiceanu C., Calotă V., ș.a., *Ghid practic pentru evaluarea conformității cu normele naționale de expunere a lucrătorilor la câmpuri electromagnetice*, Publicat prin Programul Național de Monitorizare a Factorilor Determinanți din Mediul de Viață și Muncă susținut de Ministerul Sănătății prin Institutul Național de Sănătate Publică, București, 2018.
- [4]. Indrieș C.A., Indrieș A.A., *Zona geografică Beiuș*, Editura Primus, Oradea, 2015.
- [5]. Miclaus S., Demeter S. ș.a., Modelarea absorbției campului de radiofrecventa in structuri biologice omogene si eterogene folosind metode analitice si numerice, *Buletinul Stiintific al Academiei Fortelor Terestre*, 2(18), 2004.
- [6]. Miclaus S., *Determinarea nivelelor de câmp electromagnetic de radiofrecvență exogen și dozarea energetică endogenă pentru evaluarea impactului bio-electromagnetic al expunerii ambientale și profesionale*, Teză de abilitare, UT din Cluj Nappoca, 2017.
- [7]. Milham S., *Dirty Electricity, Electrification and the Diseases of Civilization*, Publisher: Universe Star, New York, U.S.A, 2012.
- [8]. Mocanu C, *Teoria câmpului electromagnetic*, Ed.DP Bucuresti, 1981;
- [9]. Morega M, *Bioelectromagnetism*, Editura MatrixRom, 1999.
- [10].*** Hotărâre Nr. 520/2016 din 20 iulie 2016 privind cerințele minime de securitate și sănătate referitoare la expunerea lucrătorilor la riscuri generate de câmpuri electromagnetice, Emisă de Guvernul României și publicată în MO nr. 576 din 28 iulie 2016.

- [11].*** Hotărârea Guvernului României Nr. 1193 din 29.09.2006 privind limitarea expunerii populației generale la câmpuri electromagnetice de la 0 la 300 GHz.
- [12].*** Hotărârea Guvernului României Nr. 1136 din 30.08.2006 privind cerințele minime de securitate și sănătate referitoare la expunerea lucrătorilor la riscuri generate de câmpuri electromagnetice.
- [13].*** ICNIRP - *Exposure to Static and Low Frequency Electromagnetic Fields, Biological Effects and Health Consequences (0-100 kHz)*, Review of the Scientific Evidence and Health Consequences, Static and Low Frequency, 2003.
- [14].*** ICNIRP – *Guidelines on limits of exposure to static magnetic fields*, Published in: Health Physics 96(4):504-514, 2009.
- [15].*** ICNIRP – *Guidelines for limiting exposure to time-varying electric and magnetic fields (1 Hz – 100 kHz)*, Published in Health Physics 99(6), pp. 818-836, 2010.
- [16].***ICNIRP - *Guidelines for limiting exposure to electromagnetic fields (100 kHz to 300 GHz)*, Published in Health Physics 118(5): 483–524, 2020.
- [17].*** www.5gspaceappeal.org/the-appeal

Addresses:

- Dr. Eng. Lolea M., MAs, University of Oradea, str. Universității, nr.1, 410087, Oradea, Romania
mlolea@yahoo.com
- Lect. Dr. Minda A.A, Babeș-Bolyai University, Faculty of Engineering, Piața Traian Vuia, nr. 1-4, 320085, Reșița, Romania
andrea.minda@ubbcluj.ro
(* *corresponding author*)
- Dr. Barla E., University of Oradea, str. Universității, nr. 1, 410087, Oradea, Romania
ebarla@uoradea.ro
- Eng. Sărăcuț-Ardelean A., University of Oradea, nr.1, 410087, Oradea, Romania
saracut_alm@yahoo.com
- Eng. Szabo E., University of Oradea, str. Universității, nr.1, 410087, Oradea, Romania
emericremus@gmail.com

Analysis of heat flows in the eddy current wind generator

Octavian Mangos

Abstract. *In the paper are presented the results of the analysis of heat flows in the wind generator with permanent magnets and. SOLIDWORKS Flow Simulation software was used to determine the circulation and heat transfer and determine the quantitative relations of heat exchange through the thermogenerator at the variation of the heat transfer liquid flow rate from 10 to 3500 l/h. The obtained results will serve for the design of new thermal generators with permanent magnets for domestic hot water preparation systems using wind energy.*

Keywords: *thermogenerator with permanent magnets, heat transfer, convective heat flow, simulation; SOLIDWORKS Flow Simulation*

1. Introduction

The permanent magnet thermogenerator is a thermal generator for the direct conversion of mechanical energy generated by a wind turbine into thermal energy using eddy currents [1].

The basic purpose of the study is to analyze the heat flows in the eddy current wind generator to produce thermal energy by direct conversion of wind energy.

For this purpose, various constructive models of the thermogenerator with permanent magnets were developed to study the heat transfer fluid flow through the thermogenerator sleeves and, consequently, to determine a constructive model that is more thermally efficient. Simulations were performed using SOLIDWORKS Flow Simulation software for an ongoing analysis of heat flows through the thermogenerator, to understand the circulation and transmission of heat and to determine the quantitative relationships of heat exchange through the thermogenerator.

The study, development and implementation of these technologies would contribute to improve of the state in the rural sector in terms of hot water supply but would also lead to the achievement of the objectives of the Republic of Moldova on the use of renewable energies [2].



2. Simulation and analysis of heat flows in the thermogenerator

Heat flow is a quantity that characterizes the intensity of heat transfer. The heat transfer in the permanent magnet thermogenerator is mostly by convection, less by conduction. Convective heat transfer has the highest rate of thermal flows through the thermogenerator.

Convection is the process of heat transfer between the surface a solid body and a fluid, in the presence of a temperature gradient and which is due to the movement of fluid. Convection has two elements:

- Energy transfer due to random molecular motion (diffusion);
- Energy transfer by bulk or macroscopic motion of the fluid (advection).

The mechanism of convection can be explained as follows: as the layer of the fluid adjacent to the hot surface becomes warmer, its density decreases (at constant pressure, density is inversely proportional to the temperature) and becomes buoyant. A cooler (heavier) fluid near the surface replaces the warmer fluid and a pattern of circulation forms, figure 1 [4].

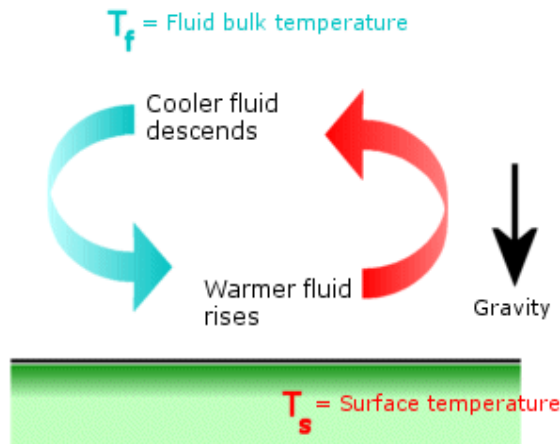


Figure 1. Convective heat transfer [4]

The rate of heat exchange between a fluid of temperature T_f and a face of a solid of area A at temperature T_s , can be written as [4]:

$$Q_{\text{convection}} = \alpha \cdot A \cdot (T_s - T_f) \quad (1)$$

where α is the convection heat transfer coefficient. The units of α are $W/m^2 \cdot ^\circ C$. The convection heat transfer coefficient depends on fluid motion, geometry, and thermodynamic and physical properties.

The analysis of heat flows through the heat generator were developed in SOLIDWORKS Flow Simulation software for the following input conditions: liquid temperature in the inlet pipe $T_1=11\text{ }^\circ\text{C}$, the sleeves imposed temperature $T_0=60\text{ }^\circ\text{C}$, ambient temperature $T_a=20\text{ }^\circ\text{C}$, the negligible heat losses $P_{th}=0$ and the liquid flow variation through the thermogenerator sleeves from 10 to 3500 l/h.

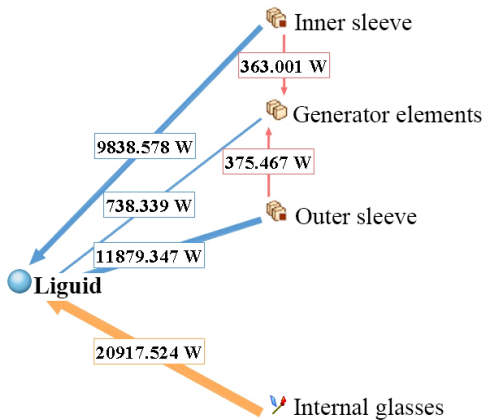


Figure 2. Heat flow in the direct inlet thermogenerator and the sleeves connected in series, $T_0=60\text{ }^\circ\text{C}$

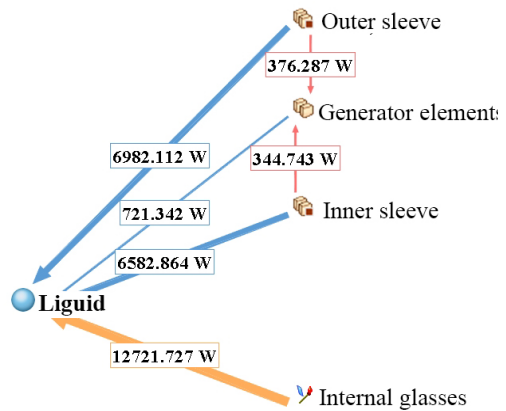


Figure 3. Heat flow in the direct inlet thermogenerator and the sleeves connected in parallel, $T_0=60\text{ }^\circ\text{C}$

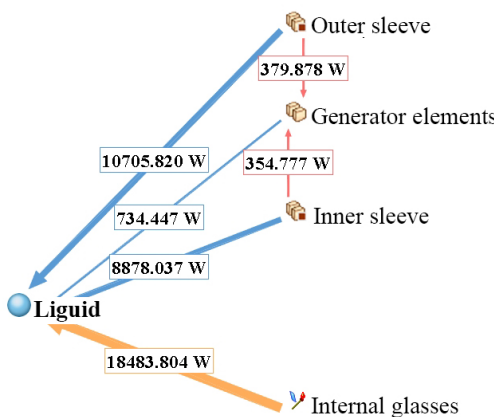


Figure 4. Heat flow in thermogenerator with direct inlet through internal pipe with sleeves connected in series, $T_0=60\text{ }^\circ\text{C}$

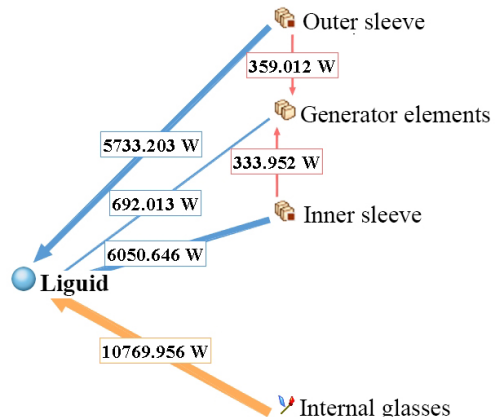


Figure 5. Heat flow in thermogenerator with direct inlet through internal pipe with sleeves connected in parallel, $T_0=60\text{ }^\circ\text{C}$

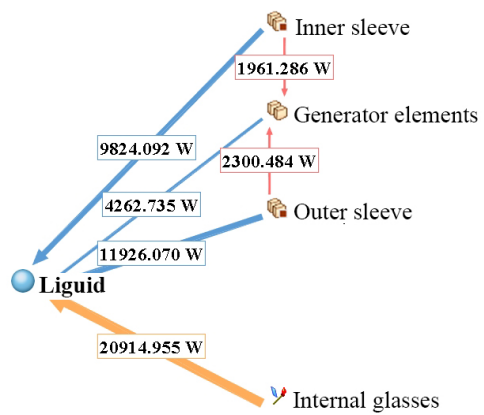
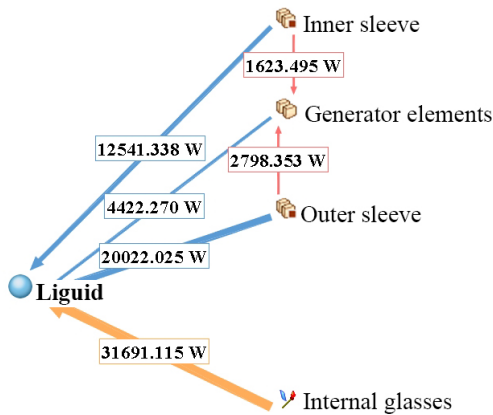


Figure 6. Heat flow in the thermogenerator with directioned inlet and sleeves connected in series, $T_0 = 60\text{ }^\circ\text{C}$ **Figure 7.** Heat flow in the thermogenerator with directioned inlet and sleeves connected in parallel, $T_0 = 60\text{ }^\circ\text{C}$

In the figures 2 – 7 are presented the conductive and convective thermal flows through the thermogenerator, at the flow rate of 1000 l/h, for each constructive model at the imposed temperature of sleeves $T_0=60\text{ }^\circ\text{C}$.

Conductive heat flows occur between the glasses of inner and outer sleeves and all elements adjacent to them, in the figures are shown with red arrows. In any case, the heat from these elements is subsequently transmitted to heat transfer fluid by convection, in simulation conditions where thermal losses are negligible, $P_{th}=0$.

In turn, convective heat flows occur between the entire surface of the flow channel and the moving heat transfer fluid, in the figures they are shown with blue arrows. There are three major convective heat fluxes: from the outer sleeve, from the inner sleeve and from the other generator elements.

Separately, the convective heat flow only from the internal cups, which initially have a respective imposed temperature, is shown with orange arrows.

The internal glasses, mentioned above, with the imposed temperature of $60\text{ }^\circ\text{C}$, which are constructively part of the generator sleeves, are the outer glass in the inner sleeve and the inner glass in the outer sleeve, see [1, 3].

In accordance with the simulation conditions of heat flows, it should be mentioned that, initially, all elements of the generator, without the internal glasses, have a temperature equal to the ambient temperature $T_a=20\text{ }^\circ\text{C}$.

Hydraulic losses or fluid energy losses, which are compensated by increasing fluid pressure to maintain a constant flow rate, are finally converted into heat energy.

These factors together influence of the liquid temperature in discharge pipe, possibly influencing the distribution of thermal flows through the thermogenerator and, as a result, the useful thermal flow of the thermogenerator.

3. The variation of useful heat flow in the thermogenerator depending on the flow rate

In the Table 1 are presented the results of simulations, regarding the variation of useful heat flow depending on the flow rate, for the imposed temperature of internal and external sleeves equal to $T_0=60$ °C, the liquid temperature in inlet pipe - $T_1 = 11$ °C, ambient temperature $T_a=20$ °C, negligible thermal energy losses $P_{th}=0$ and variation of liquid flow rate through the thermogenerator sleeves from 10 l/h to 3500 l/h.

The characteristic quantity for the heat transfer intensity is the heat flux absorbed by the heat transfer liquid, quantity denoted by \dot{Q} . In the given case, for the thermogenerator, the useful heat flow can be calculated using the expression:

$$\dot{Q}_{ut} = \dot{M} \cdot c_p \cdot (T_2 - T_1) \quad (2)$$

where:

\dot{M} - mass flow, in *kg/s*;

c_p - specific heat of the heat transfer liquid, in *kJ/kg · °C*;

T_2 - temperature of the liquid in the discharge pipe, in *°C*;

T_1 - temperature of the liquid in the inlet pipe, in *°C*.

According to the simulation results, variation of the useful heat flow for all constructive models, when sleeves is connected the in series and parallel, has the same shape of the curve, which can be characterized as follows: with increase in the flow rate of liquid through the thermogenerator, the value of useful heat flow also increases, figure 8.

This happens due to the fact that at a higher flow rate, the mass flow rate is also higher, respectively, in a unit of time, a larger volume of liquid passes through the thermogenerator sleeves and a larger amount of heat is absorbed, respectively.

The following were found:

1. In the constructive models with the sleeves connected in series, the useful thermal flow has a higher value compared to the same models but with the sleeves connected in parallel, figure 8. This is explained by the fact that when connected in series, the temperature difference ($T_2 - T_1$), is higher than when the connection is in parallel, see [3].
2. It is observed that in the constructive model with directed intake, when connecting the jackets in series, the useful thermal flow presents the highest values, followed by the same model, only with the jackets connected in parallel. This is because in these constructive models, the total surface area of the flow channel is greater compared to the other models. The surface area of contact of the liquid with the surface of the flow channel is larger because inside the jackets metal sheet spirals are mounted to direct the flow of heat transfer liquid.

Table 1. The variation of useful heat flow depending on the flow rate $\dot{Q}_{ut}(Q)$, $T_0=60\text{ }^\circ\text{C}$

| Useful heat flow depending on the flow rate, for $T_a=20\text{ }^\circ\text{C}$; $T_0=60\text{ }^\circ\text{C}$; $T_i=11\text{ }^\circ\text{C}$ and $P_{th}=0$ | | | | | | |
|---|--|---|---------------------|--|---|---------------------|
| Flow rate, l/h | Useful heat flow \dot{Q}_{ut} , kW | | | | | |
| | Model with sleeves connected in series | | | Model with sleeves connected in parallel | | |
| | with direct inlet | with direct inlet through internal pipe | with directed inlet | with direct inlet | with direct inlet through internal pipe | with directed inlet |
| 10 | 0,55 | 0,55 | 0,57 | 0,55 | 0,55 | 0,57 |
| 50 | 2,33 | 2,28 | 2,82 | 2,05 | 1,99 | 2,80 |
| 100 | 4,00 | 3,84 | 5,46 | 3,36 | 3,19 | 5,32 |
| 500 | 11,98 | 11,18 | 21,44 | 8,28 | 7,99 | 14,76 |
| 1000 | 19,17 | 19,17 | 39,32 | 14,00 | 12,38 | 26,09 |
| 1500 | 25,59 | 27,48 | 56,34 | 18,87 | 16,63 | 35,82 |
| 2000 | 32,76 | 35,83 | 72,76 | 24,89 | 21,32 | 45,04 |
| 2500 | 38,71 | 44,05 | 88,76 | 31,23 | 25,84 | 53,97 |
| 3000 | 45,24 | 52,02 | 104,48 | 36,24 | 30,09 | 62,62 |
| 3500 | 52,49 | 60,12 | 120,07 | 41,72 | 34,88 | 71,01 |

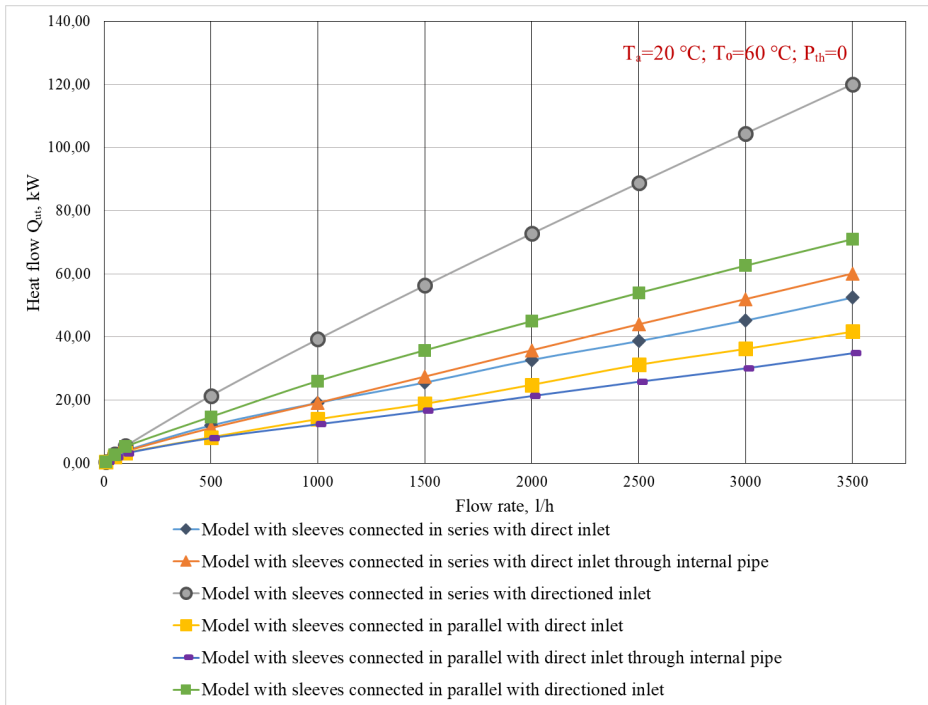


Figure 8. The variation of useful heat flow as function of the flow rate $\dot{Q}_{uH}(Q)$, $T_0=60\text{ }^\circ\text{C}$

4. Conclusion

Were performed simulations to determine the circulation and heat transfer and to determine the quantitative relations of heat exchange through the thermogenerator depending on the flow rate, to variation through the thermogenerator sleeves from 10 to 3500 l/h.

From the point of view of heat transfer efficiency, according to the results shown in table 1 and the heat flux variation characteristic, figure 8, the constructive model with directioned inlet with sleeves connected in series, has a higher heat transfer efficiency the heat flow values being significantly higher compared to the other models due to the fact that in this constructive model the total surface area of the flow channel is larger compared to the other models.

A positive effect on the thermal characteristics of the thermogenerator is attested because of mounting sheet metal spirals in the thermogenerator sleeves to directing the flow of heat transfer liquid. Both values of the temperature of heat transfer liquid in the discharge pipe and the values of the useful heat flows are twice as high compared to the other cases.

Acknowledgment. This work was supported by the project 20.80009.7007.10 „Studying the wind and solar energy potential of the Republic of Moldova and developing conversion systems for dispersed consumers”.

References

- [1] Mangos O., Ciupercă R., Sobor I., *Generator termic eolian cu curenți turbionari*. Brevet de invenție 4815(13) B1, F03D 9/00; H05B 6/02; F24H 1/10. Universitatea Tehnică a Moldovei, 2022.
- [2] Mangos O., *Evaluarea consumului de energie în gospodării pentru încălzirea apei calde menajere*, Conferința tehnico-științifică a studenților, masteranzilor și doctoranzilor, 23-25 Mar 2021, Universitatea Tehnică a Moldovei, Chișinău, Tehnica-UTM, Vol. I, pp.146-149.
- [3] Mangos O., *Study of the Circulation of Heat Transfer Fluid in the Permanent Magnets Thermogenerator*. 13th International Conference on Electro-mechanical and Energy Systems SIELMEN-2021. 7-8 Oct. 2021 Iași-Chișinău, pp. 538-542.
- [4] Convection Heat Coefficient. [online], 2022, [accesat 12.06.2022]. https://help.solidworks.com/2019/english/SolidWorks/cworks/c_Convection.htm?verRedirect=1.
- [5] Mangos O., Sobor I., Cazac V., Burduniuc M., *Study of the pressure and distribution of heat transfer fluid in the thermogenerator with permanent magnets and eddy currents*. Conferința Națională de Acționări Electrice CNAE-2022. 12-13 May 2022, Timișoara. ANNALS of Faculty Engineering Hunedoara – International Journal of Engineering..
- [6] Sobor I., Chiciuc A., Ciupercă R., Rachier V., *Conversion of the wind energy into heat*, 9th International Conference on Electromechanical and Power Systems SIELMEN 2013, Oct. 2013, Chisinau.
- [7] Sobor I., Rachier V., Chiciuc A., Ciupercă R., Small wind energy system with permanent magnet eddy current heater, *Bulletin of the polytechnic institute of Iasi*, Tome LIX (LXIII), Fasc. 4, 2013.

Address:

- PhD. stud. Octavian Mangos, Technical University of Moldova, Faculty of Energetics and Electrical Engineering, Department of Electrical Engineering, Chisinau, Republic of Moldova.
octavian.mangos@ie.utm.md

On the Milling Process Simulation of an Injection Mold Part

Calin-Octavian Miclosina, Alexandru-Stefan Filip,
Vasile Cojocaru, Daniel-Gheorghe Vela*

Abstract. *The paper presents the 3-phases milling process simulation of a surface of a polystyrene injection mold, by using CATIA software. The cutting regime parameters are computed and are used, together with other data, as inputs for the simulation process. On the basis of milling process simulation, the software generates the manufacturing program for the NC machine tool.*

Keywords: *milling, simulation, die casting, mold, CATIA.*

1. Introduction

Injection molding is a current method to obtain polystyrene components of various shapes and sizes. Research on proper operation of this manufacturing process is accomplished, for example regarding the detection of interference elements and release directions [8], the coating of cavities [9], or the process simulation [1], [13].

Usually, a mold is composed of a fixed part and a mobile one. The mold parts are frequently obtained by milling on numerical control (NC) machine tools. The NC program can be entered manually by the machine tool operator, or it can be provided by a specialized software, as a result of the milling simulation process. The *NC Manufacturing* module, a component of CATIA software, offers this possibility [3], [4], [6], [10]. The 3D model of the part to be milled is necessary, and it can be obtained by using the *Part Design* module [5], [7], [11] of CATIA software, or another software [2] - and then imported in CATIA.

The paper presents the manner of 3-phases milling process simulation of the concave side of a fixed mold part, by using CATIA *NC Manufacturing* module.

2. The 3D models of the Mold Part and of the Semi-Finished Part

The 3D models are achieved by using CATIA *Part Design* module and are presented in fig. 1.



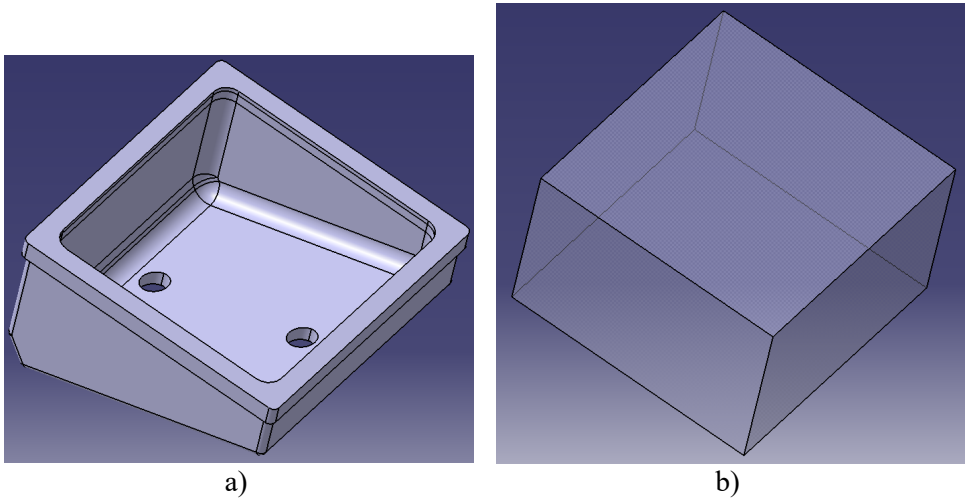


Figure 1. The 3D models of the fixed mold part (a) and of the semi-finished part (b).

In order to simulate the milling process, the 3D model of the *mold part - semi-finished part* assembly is necessary. This assembly is achieved by using CATIA *Assembly Design* module and is presented in fig. 2.

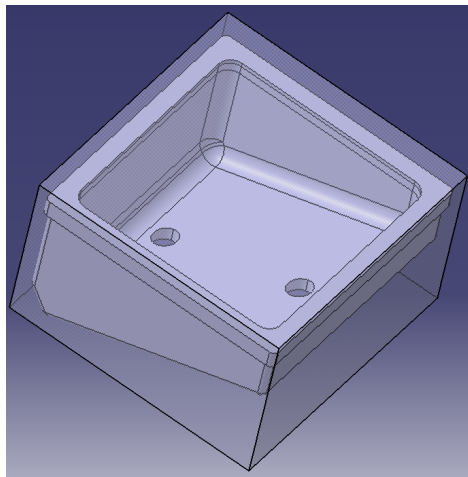


Figure 2. The 3D model of the *mold part - semi-finished part* assembly.

3. The Cutting Regime Parameters

The parameters of the cutting regime are computed for the roughing and finishing phases [3], [4], based on the relations from [12].

Thus, the computed cutting regime parameters used as input data in the simulation settings are as follows [3], [4]:

1. For the rough milling with the Ø50 mill,
- the spindle speed chosen for the machine tool is:

$$n_{mt} = 750 \text{ [turn/min]}, \quad (1)$$

based on the computed spindle speed:

$$n = \frac{1000 \cdot v_c}{\pi \cdot D_c} = \frac{1000 \cdot 119}{\pi \cdot 50} = 757.578 \text{ [turn/min]}, \quad (2)$$

where: $v_c = 119$ [m/min] – the cutting speed, computed in [2], [3];
 $D_c = 50$ [mm] is the mill diameter.

- the feed rate:

$$v_f = n_{mt} \cdot z \cdot f_z = 750 \cdot 5 \cdot 0.067 = 251,25 \text{ [mm/min]}, \quad (3)$$

where: $z = 5$ [tooth] – the number of the mill's teeth;

$f_z = 0.067$ [mm/tooth] is the feed per tooth, computed in [2], [3].

2. For the finish milling with the Ø25 mill,
- the spindle speed chosen for the machine tool is:

$$n_{mt} = 1500 \text{ [turn/min]}, \quad (4)$$

based on the computed spindle speed:

$$n = \frac{1000 \cdot v_c}{\pi \cdot D_c} = \frac{1000 \cdot 119}{\pi \cdot 25} = 1515.155 \text{ [turn/min]}, \quad (5)$$

where: $v_c = 119$ [m/min] – the cutting speed, computed in [2], [3];
 $D_c = 25$ [mm] is the mill diameter.

- the feed rate:

$$v_f = n_{mt} \cdot z \cdot f_z = 1500 \cdot 4 \cdot 0.067 = 402 \text{ [mm/min]}, \quad (6)$$

where: $z = 4$ [tooth] – the number of the mill's teeth;

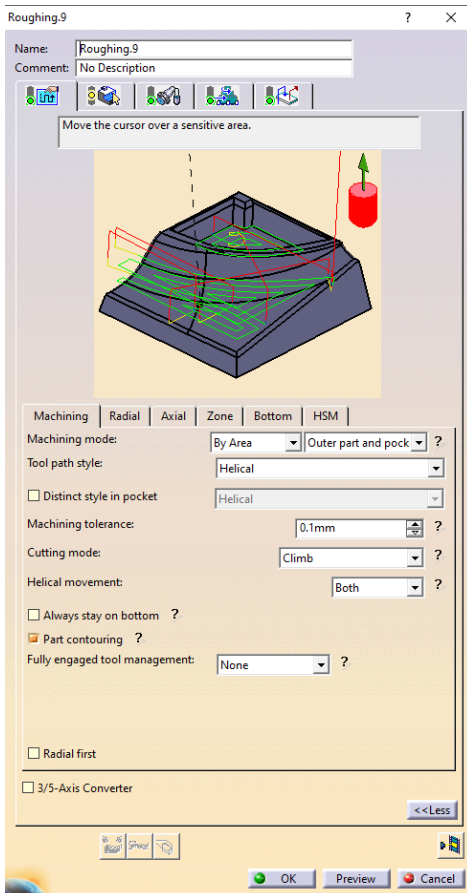
$f_z = 0.067$ [mm/tooth] is the feed per tooth, computed in [2], [3].

4. Simulation of the Milling Process

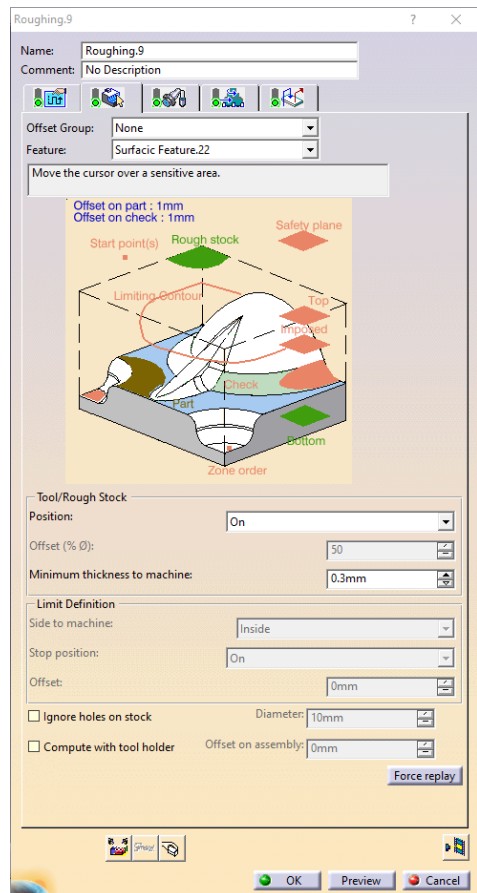
The simulation of the milling Process is accomplished for 1 roughing and 2 finishing phases of the concave side of the fixed mold part by using CATIA *Advanced Machining* module, as below.

4.1. Simulation of the Rough Milling Phase of the Concave Side

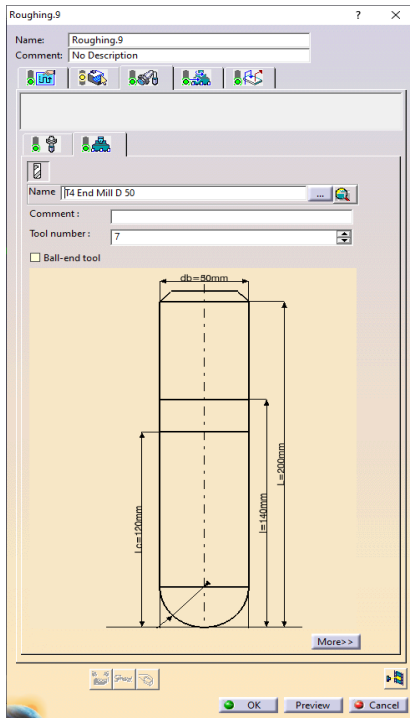
For this simulation, *Roughing* option is used. The setting of parameters for the rough milling phase is shown in fig. 3.



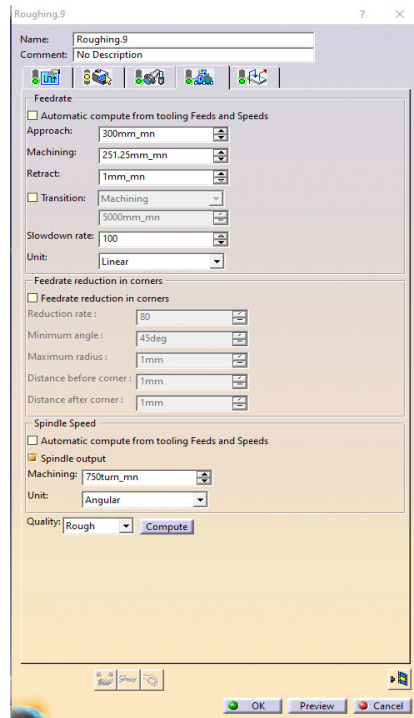
a) The work strategy.



b) The surfaces.



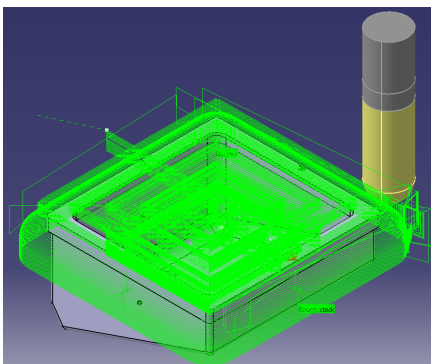
c) Shape and dimensions of the mill.



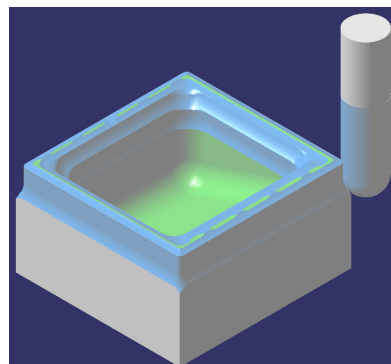
d) The values of the milling regime parameters

Figure 3. Setting the parameters for the rough milling phase.

In fig. 4 there are presented screen captures taken during the simulation of rough milling phase.



a) *Tool Path Replay* mode.



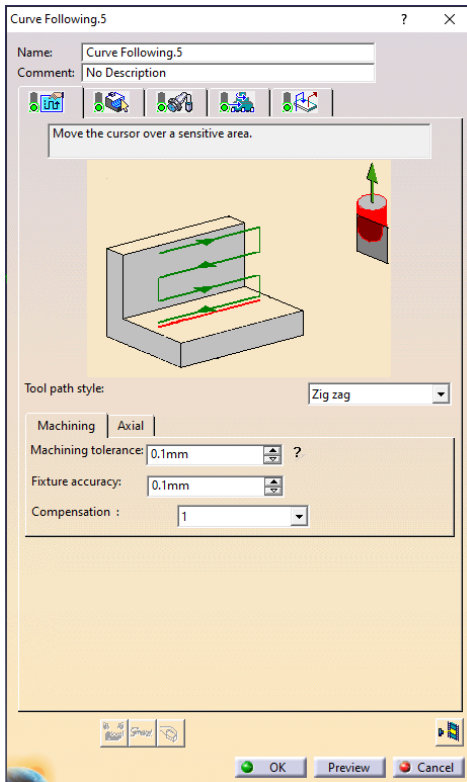
b) *Video* mode.

Figure 4. Screen captures during the simulation of rough milling phase.

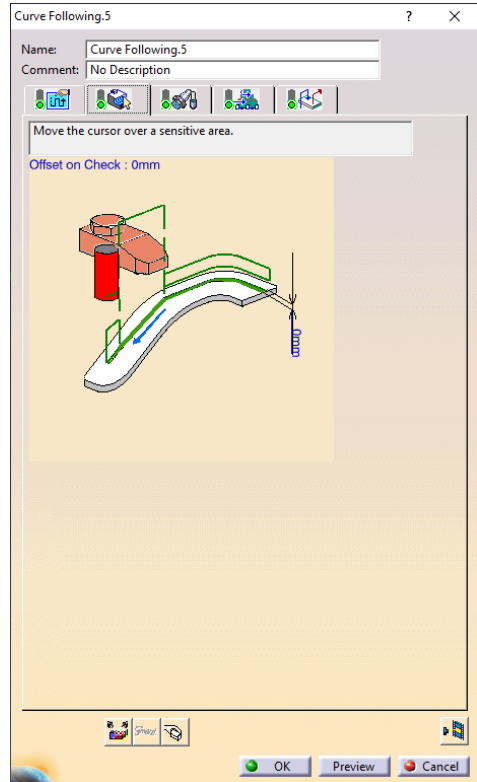
In fig. 4, a), the trajectory of the mill tip can be observed in the *Tool Path Replay* mode, while in fig. 4, b), a more realistic visualization of the process is accomplished in *Video* mode.

4.2. Simulation of the Finish Milling Phase of the Upper Side

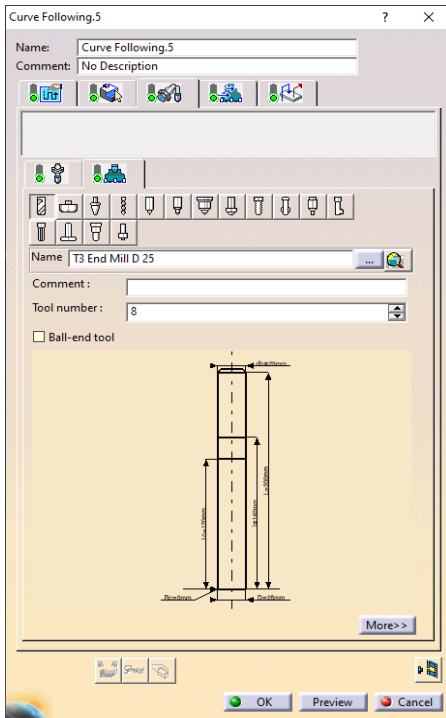
For this simulation, *Curve Following* option is used. The setting of parameters for the finish milling phase of the upper side is presented in fig. 5.



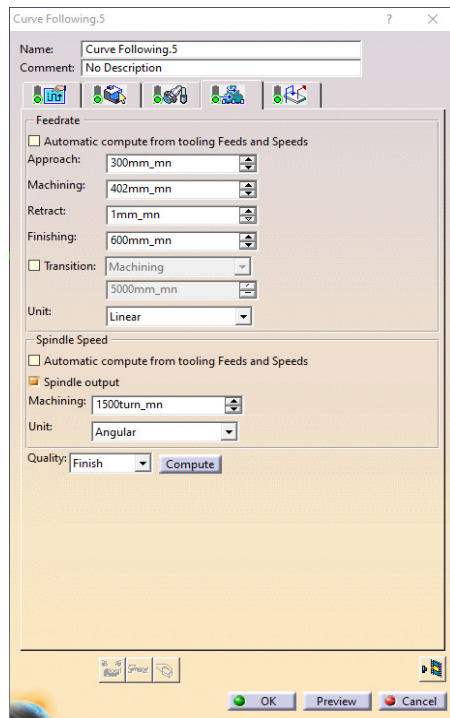
a) The work strategy.



b) The surfaces.



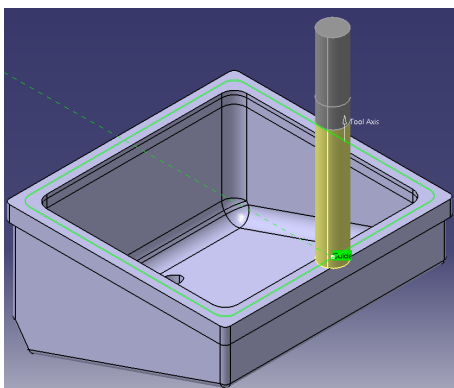
c) Shape and dimensions of the mill.



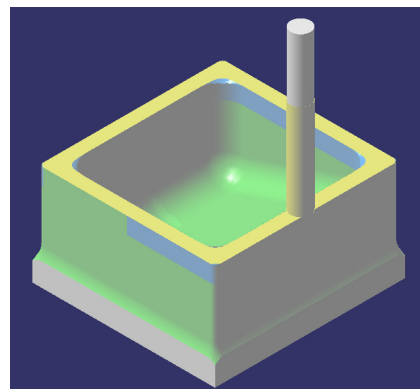
d) The values of the milling regime parameters.

Figure 5. Setting the parameters for the finish milling phase of the upper side.

In fig. 6 there are presented screen captures taken during the simulation of finish milling of the upper side. The plane face of the tool sweeps the processing surface.



a) *Tool Path Replay* mode.

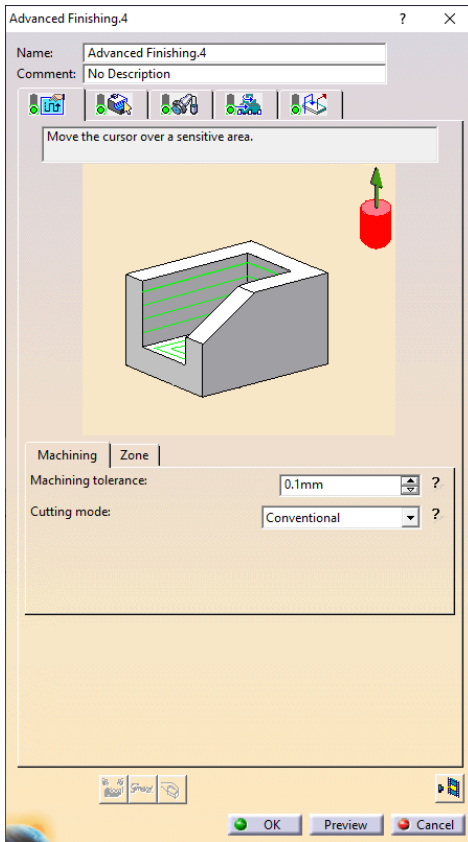


b) *Video* mode.

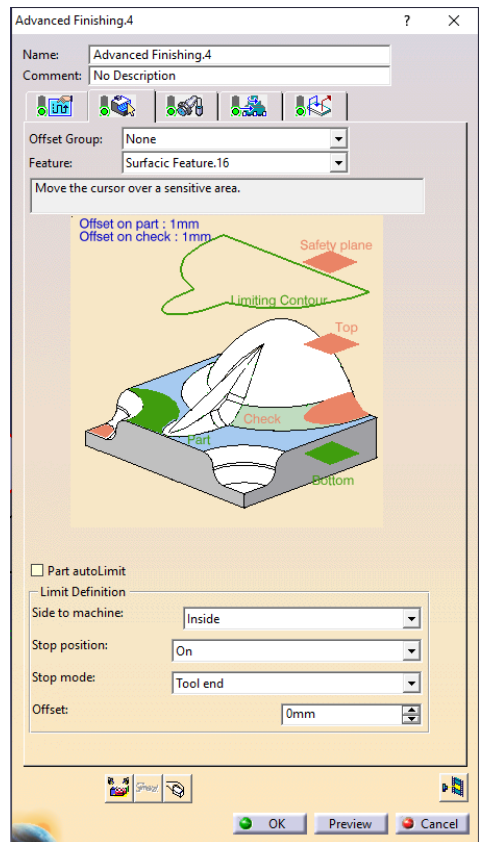
Figure 6. Screen captures during the simulation of finish milling of the upper side.

4.3. Simulation of the Finish Milling Phase of the Concave Side

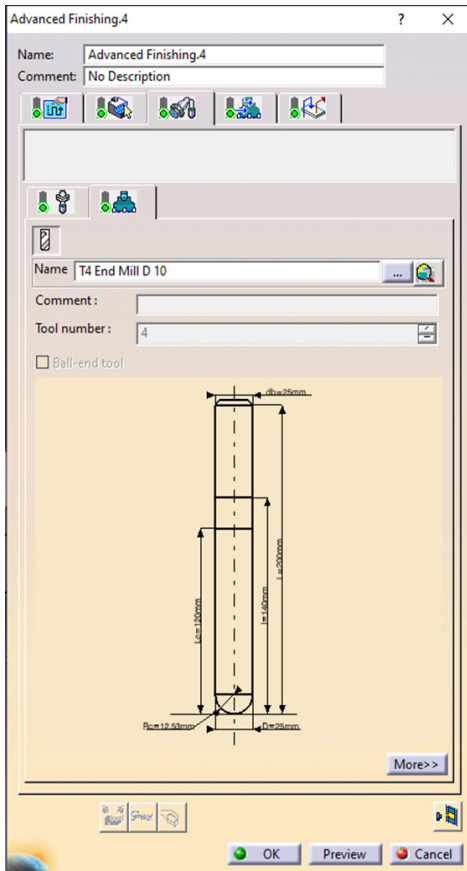
For this simulation, *Advanced Finishing* option is used. The setting of parameters for the finish milling phase is presented in fig. 7.



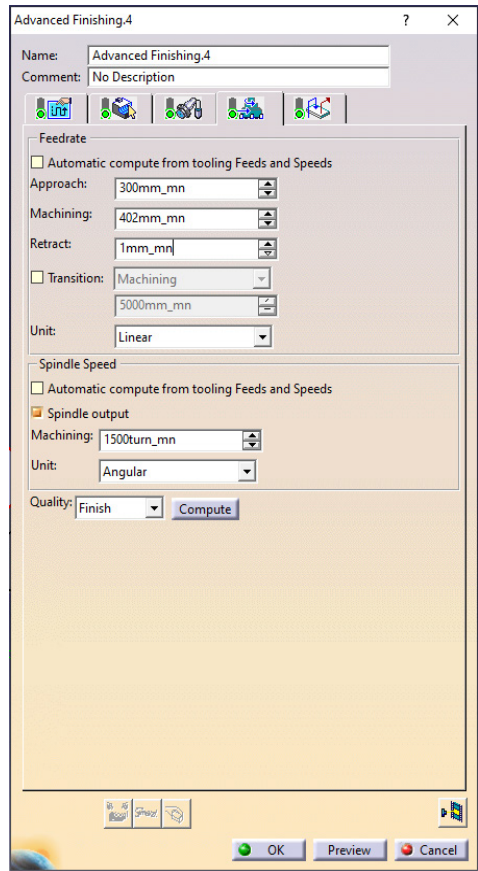
a) The work strategy.



b) The surfaces.



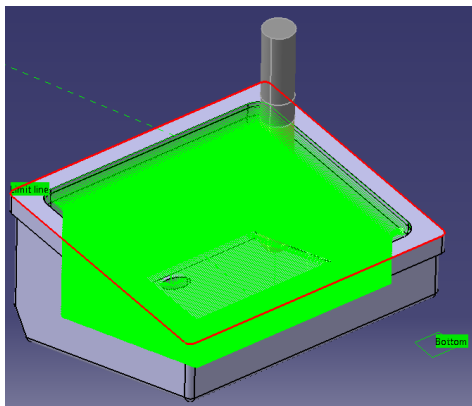
c) Shape and dimensions of the mill.



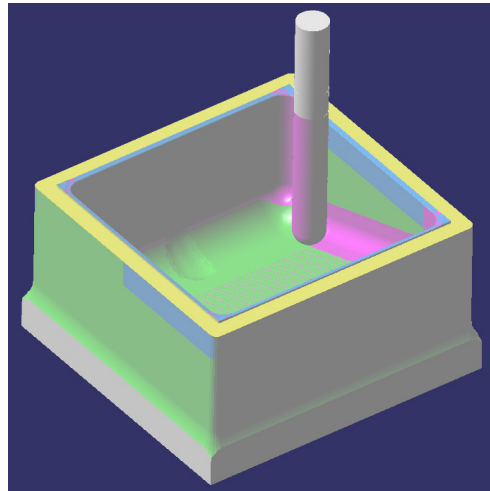
d) The values of the milling regime parameters.

Figure 7. Setting the parameters for the finish milling phase of the concave side.

In fig. 8 there are presented screen captures taken during the simulation of finish milling of the concave side.



a) *Tool Path Replay* mode.



b) *Video* mode.

Figure 8. Screen captures during the simulation of finish milling of the concave side.

In this finishing phase the tool sweeps all the concavity in order to obtain a high quality surface.

4. Conclusions

The simulation of the milling process, including the roughing and finishing phases, of the injection mold part is accomplished. On the basis of this simulation, CATIA software can generate the program, in NC or APT format, for manufacturing on NC machine tool. The post-processor has to be chosen, depending on the type and model of the machine tool.

The same manner of simulation can be used for other types of manufacturing processes, like drilling or turning.

References

- [1] Bress T.J., Dowling D.R., Simulations and measurements of in-mold melt flow during the injection molding of polystyrene, *Polymer Engineering and Science*, 53(4), 2013, pp. 770-779.

- [2] Cojocaru V., Nedelcu D., Miclosina C.-O., The Parametrical Design of the Parts from the Same Technological Family, *Analele Universității "Eftimie Murgu" Reșița, Fascicula de Inginerie*, 15(1), 2008, pp. 113-118.
- [3] Filip A.-S., *Simularea operației de frezare utilizând mediul CATIA / Simulation of the Milling Operation by Using the CATIA Environment*, EMING 2022 Student Scientific Symposium, May 04-07, 2022, Resita.
- [4] Filip A.-S., *Contribuții la proiectarea tehnologică asistată și la fabricația pe MUCN a unei matrițe pentru turnarea prin injecție a maselor plastice / Contributions to the aided technological design and to the manufacturing on CNMT of a mold for injection molding of plastics*, Master Thesis, Babeș-Bolyai University, Faculty of Engineering, 2022.
- [5] Ghionea I.G., *Proiectare asistată în Catia V5. Elemente teoretice și aplicații*. Editura Bren, Bucuresti, 2007.
- [6] Ghionea I.G., *CATIA V5. Aplicații în inginerie mecanică*, Editura Bren, Bucuresti, 2009.
- [7] Ghionea I.G., Tarbă C.I., Čuković S., *CATIA V5. Aplicații de proiectare parametrică și programare*, Bren Publishing House, Bucuresti, 2021.
- [8] Lu H.Y., Lee W.B., Detection of interference elements and release directions in die-cast and injection-moulded components, *Proceedings of the Institution of Mechanical Engineers Part B-Journal of Engineering Manufacture*, 214(6), 2000, pp. 431-441.
- [9] Masato D., Sorgato M., Babenko M., Whiteside B., Lucchetta G., Thin-wall injection molding of polystyrene parts with coated and uncoated cavities, *Materials & Design*, 141, 2018, pp. 286-295.
- [10] Miclosina C.-O., Korca Z.I., Cojocaru V., *Some Aspects on Technological Design of a Cam Type Workpiece Using CATIA Software*, *Analele Universității "Eftimie Murgu" Reșița, Fascicula de Inginerie*, 20(2), 2013, pp. 33-38.
- [11] Miclosina C.-O., *Bazele proiectării asistate de calculator*, Eftimie Murgu Publishing House, Resita, 2018.
- [12] Popovici G., *Tehnologia Construcțiilor de Mașini. Proiectarea tehnologică / Editura Didactica si Pedagogica*, Bucuresti, 2010.
- [13] Sonmez D., Eker A.A., *Numerical Simulation and Process Optimization of a 3D Thin-Walled Polymeric Part Using Injection Compression Molding*, *International Polymer Processing*, 36(4), 2021, pp. 459-467.

Addresses:

- Assoc. Prof. Dr. Eng. Calin-Octavian Miclosina, Babeş-Bolyai University, Faculty of Engineering, Department of Engineering Science, Traian Vuia Square, no. 1-4, 320085 Reşiţa, Romania
calin.miclosina@ubbcluj.ro
- Eng. Alexandru-Ştefan Filip, BOWEDI IMPEX S.R.L. Reşiţa, Furnalelor Str., no. 26, 320034, Reşiţa, Romania
alexfilip16@yahoo.com
- Lect. Dr. Eng. Vasile Cojocaru, Babeş-Bolyai University, Faculty of Engineering, Department of Engineering Science, Traian Vuia Square, no. 1-4, 320085 Reşiţa, Romania
vasile.cojocaru@ubbcluj.ro
- Lect. Dr. Eng. Daniel-Gheorghe Vela, Babeş-Bolyai University, Faculty of Engineering, Department of Engineering Science, Traian Vuia Square, no. 1-4, 320085 Reşiţa, Romania
daniel.vela@ubbcluj.ro
(* *corresponding author*)

Sine Wave Electromagnetic Generation Using H-Bridge and Microcontroller

Ion - Cornel Mituletu*, Alexandru Predica, Ionut Voina

Abstract. *The paper presents a way of accomplishing a non-contact excitation by electromagnetic waves generated from a system that includes WiFi microcontroller, H-Bridge and coil. The ESP 32 microcontroller software achieves PWM signal, which follows a sinusoidal shape of variable frequency. The PWM signal drives the H-bridge resulting in a more powerful electric signal that also drives the coil, accomplishing in this way the pseudo-sine electromagnetic wave. The source code from microcontroller provides variable frequency and working period as well. The main features of the system are 0.5 to 3000 Hz, working periods between 0.1 and 10 seconds, the possibility to achieve more than one working period with standby periods in between.*

Keywords: *sine electromagnetic wave, WiFi microcontroller, H-bridge, software PWM, vibration based modal analysis.*

1. Introduction

Structural Integrity Monitoring (SIM) is a multidisciplinary field that represents the development and implementation of techniques that are used in monitoring and maintenance of structures [1,2,3].

One of the most used techniques is Vibration Based Detection (VBD). Method used to obtain the vibration that is applied to the analyzed structure can vary from methods of contact (e.g. using vibration or impact hammers) to non-contact methods (by using an electromagnetic system) [4,5].

To obtain information about the general condition of structures and to detect and locate hidden defects, VBD SIM systems are made using accelerometers with micro electromechanical system (ASME). These accelerometers are used to measure linear acceleration, vibrations and orientation of an object in space [6].

This system is based on platforms and applications from the Internet of Things sphere (IoT). The data obtained by the sensors is sent via wireless communication.



The main feature of the system is to produce a sine electromagnetic wave and by testing to determine if the impact of a smooth wave has better results on the cantilever beam than the square pulses.

2. Mathematical background

Electromagnetic excitation scenario gives the mathematical structure of the resulting source code, establishing the limit conditions and experimental evaluation structure. Excitation scenario supposes excitation periods, assumed as working periods, and no-excitation periods, in order for the cantilever to slow down/in order to slow down the cantilever beam. Also, the working period can be at a constant frequency value, or the frequency can be swept between a small and a big value and reversal. Sweep scenario supposes an average value of the frequency in the sweeping interval, which is the same with the constant value of the frequency. In both cases, that frequency is performed by a carrier-frequency, or switching frequency, which is 20 times bigger.

Figure 1 shows the main parameters that contribute to the achieving of the desired signal at a certain frequency. For the source code analysis more important is the period than the frequency, therefore both will be provided from now on. At a certain moment, the sweeping frequency (SF) corresponds to a period (SP). The period includes 20 or more switching periods (SWP), each one having a duty cycle (DC) that follows a sinusoidal evolution.

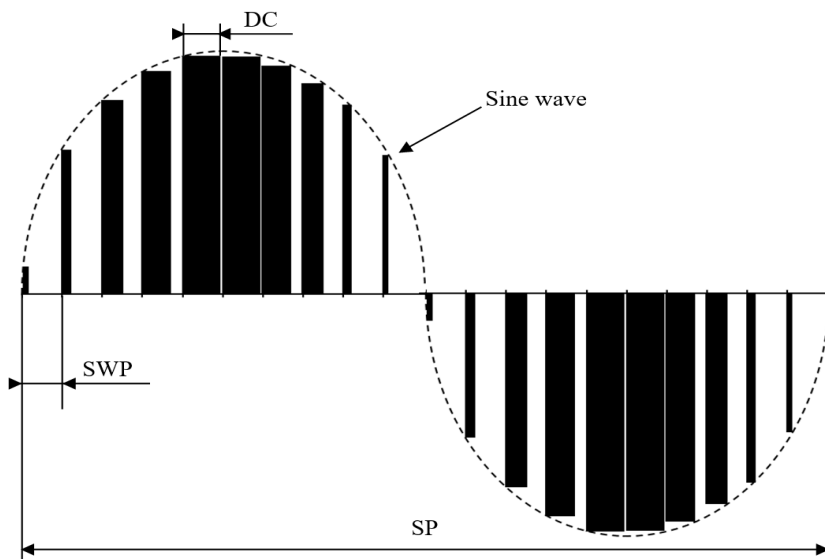


Figure 1. A certain period sampled by the switching period and the evolution of the duty cycle to achieve a sine evolution.

The first thing is to establish the limits of the excitation/working period.
Working time:

$$WT \in [0; 10] \text{ (s)} \quad (1)$$

Stopping / standby time:

$$ST \in [0, 180] \text{ (s)} \quad (2)$$

Sweeping frequency and period:

$$SF \in [0.5, 3000] \text{ (Hz)} \quad (3)$$

$$SP \in [2, 0.3 \cdot 10^{-3}] \text{ (s)} \quad (4)$$

If the end frequency and period are bigger than the star ones, the sweeping will be performed in the reverse direction.

For the sweeping case, firstly a medium frequency/period value is determined:

$$MP = \left\lfloor \frac{SP+EP}{2} \right\rfloor \text{ (s)} \quad (5)$$

Afterwards, the number of cycles:

$$NC = \frac{WT^{(R)}}{MP} \text{ (s)} \quad (6)$$

(R) - round down;

After that, the exact working time is calculated:

$$EWT = 9 \cdot NC + NC \cdot MP = NC(MP + 9) \quad (7)$$

9 – microcontroller’s clock cycles need to setup the timer.

Added value to each frequency and period shift:

$$AP = \left\lfloor \frac{SP+EP}{NC} \right\rfloor + 9 \cdot NC \quad (8)$$

Switching frequency and period:

$$SWF = 60 \text{ (kHz)} \quad (9)$$

$$SWP = 1.67 \cdot 10^{-5} \text{ (s)} \quad (10)$$

For a certain frequency:

$$f_k \in [SF; EF] \quad (11)$$

$$P_k \in [SP; EP] \quad (12)$$

The number of switches:

$$NS = \frac{P_k}{SWP} \text{ (s)} \quad (13)$$

Added period value to shift the duty cycle (DC):

$$DCP = \frac{P_k}{NS} \text{ (s)} \quad (14)$$

DC value is:

$$DC = \sin(2 \cdot \pi \cdot f_k \cdot n) \quad (15)$$

where:

$$n \in [1, NS] \quad (16)$$

The source code was written in order to meet these mathematical structure. The hardware main condition was to choose a development board able to generate PWM at least 60 kHz.

3. System design and testing

Figure 2 presents the functional block structure of the sine wave electromagnetic generator, which consists of two subsystems: excitation subsystem and data acquisition subsystem.

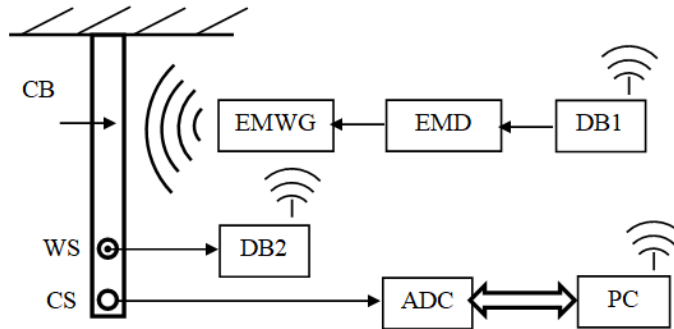


Figure 2. Functional block structure of the sine wave electromagnetic generator.

The non-contact excitation subsystem consists of the Development Board 1 (ESP 32), the Electromagnetic Driver (EMD) and the Electromagnetic Wave Generator (EMWG).

The data acquisition subsystem is made using an accelerometer wireless sensor and the Development Board 2 (ESP 32). This subsystem detects the vibrations of the excited cantilever beam and sends the data wirelessly to the P.C.

Figure 3. a) depicts the connection diagram of the sine wave electromagnetic generator in two image. The first image details the electronic links between the DB1 and the H-bridge (HB), which is based on the IC L298N. H-bridge includes the sine wave driver (SW) and the force bridge based on the T1 – T4 MOSFET transistors. Development board DB1 drives the H-bridge by two digital outputs (D5 and D7). Image b) simply shows the connection strategy between the wireless vibration sensor (WS) and the second development board (DB2).

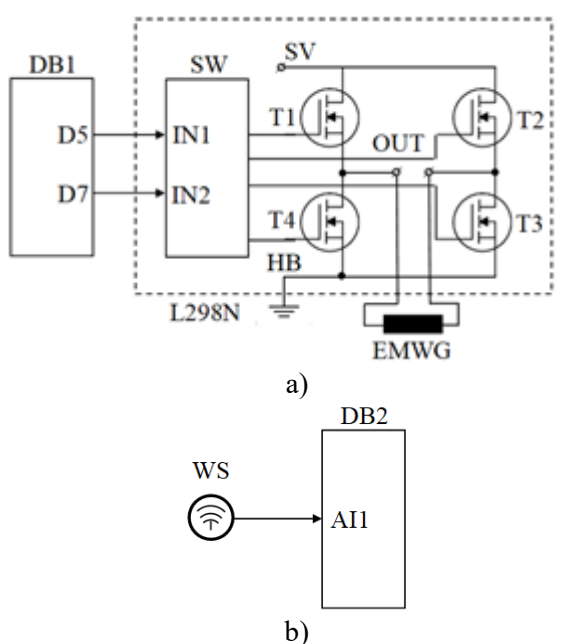


Figure 3. Connection diagram of the sine wave electromagnetic generator a), and vibration acquisition b).

The ESP-WROOM-32 module has the following features [6]:

- Xtensa processor with frequency between 160 and 240 MHz;
- RAM memory 320 kB;
- ROM memory 448 kB;
- Wi-Fi: 802.11 b/g/n;

- 34 programmable general purpose ports;
- 18 12-bit analog-to-digital converters;
- 2 8-bit digital-to-analog converters;
- 4 SPI interfaces;
- 2 I2C interfaces;
- 3 UART interfaces;

L298N is a high voltage, high current dual full-bridge driver. It has the following features [7]:

- Operating supply voltage up to 46 V;
- Over temperature protection;
- Current up to 4A.

The experimental setup is presented in figure 4.

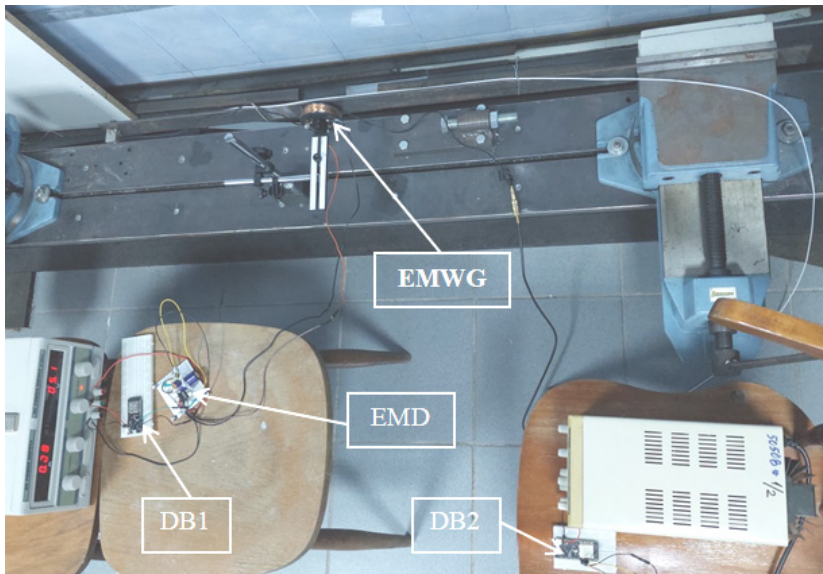


Figure 4. Experimental setup

A number of five parameters are required to achieve the excitation:

- working time (WT);
- stopping time (ST);
- excitation period (PE);
- Start frequency and period: SF and SP;
- Number of cycles: NC.

These parameters are transmitted from an Internet browser interface configured by the first development module when the mobile device is first connected to it.

After the excitation cycle is executed and the acquired data is sent from DB2 to P.C. in the form of a .csv format file, the data is processed using the Lab View program and the obtained signal indicates that the frequency for any mode of vibration can be easily achieved. An example of the excitation process in time is shown in figure 5 for the first vibration mode in the up-side image.

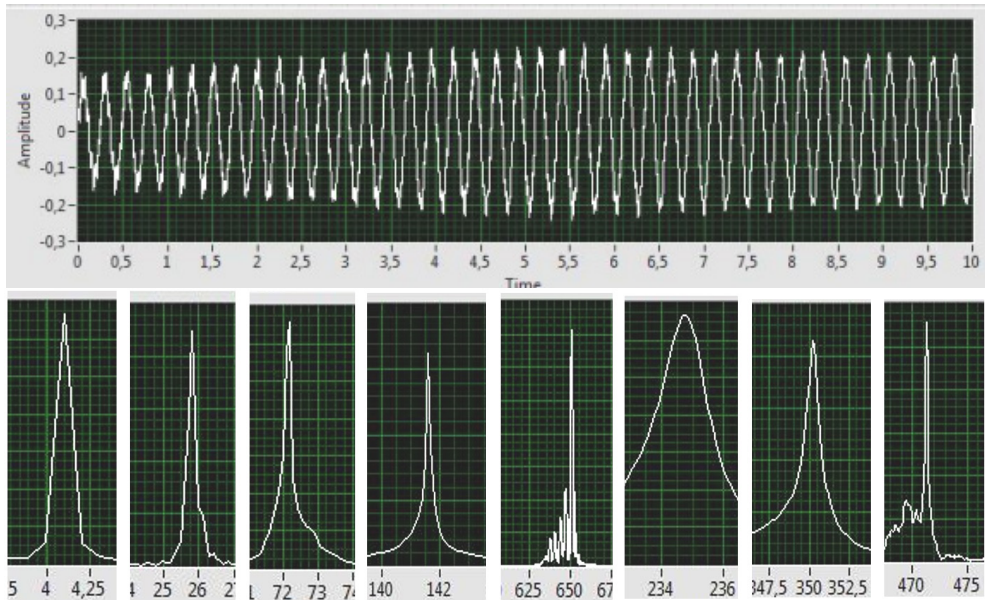


Figure 4. Time vibration for the first vibration mode, and the resulted frequency values for the first 8 vibration modes.

Down-side image of figure 5 presents the resulted values of the frequency for the first 8 vibration modes after the sweep excitation. As can be seen, the amplitude of the frequencies at the modes values is very high and easy to read.

4. Conclusion

Pseudo-sine electromagnetic wave generation system based on microcontroller, H-bridge and coil produces a well-shaped sinusoidal wave at a variable frequency 0.5 to 300 hertz on a certain working time period and sweep feature. Thus, this system can excite magnetic and ferromagnetic mechanical structures with a constant or variable frequency.

The sine electromagnetic waves are preferred to simple square pulses because of smooth evolution in time, which achieve light impact to the mechanical structures.

Also, it should be specified that ferromagnetic mechanical structures oscillates at double of the excitation frequency and the magnetic structures at the excitation value. That is due to the phenomenological behavior of these structures, ferromagnetic materials forms no magnetic poles, but the magnetic materials have already formed poles that interact with the direction of the electromagnetic field.

References

- [1] Zhou Z., Wegner L.D., Bruce F., Sparling Data quality indicators for vibration-based damage detection and localization, *Engineering Structures*, 230(1), March, 2021.
- [2] Pereira S., Magalhaesa F., Gomes J.P., Cunha A., Lemo J.V., Vibration-based damage detection of a concrete arch dam, *Engineering Structures*. 235(1), May, 2021
- [3] Zhu S., Zhang Q., Zhai W., Yuan Z., Cai C., Sensor deploying for damage identification of vibration isolator in floating-slab track using deep residual network, *Measurement*, 183, Oct., 2021.
- [4] Firrone C.M., Berruti T., An Electromagnetic System for the Non-Contact Excitation of Bladed Disks, *Experimental Mechanics*, 2012.
- [5] Xu K., Yan X., Du D., Sun W., Vibration response prediction of coated blisks under multi-point non-contact excitations using mistuning identification data, *Thin-Walled Structures*, 159, Febr. 2021.
- [6] ESP 32 datasheet:
https://espressif.com/sites/default/files/documentation/esp32_datasheet_en.pdf
- [7] L298N datasheet:
<https://eu.mouser.com/datasheet/2/389/1298-1849437.pdf>

Addresses:

- Lect. Dr. Eng. Ion-Cornel Mituletu, Babeş-Bolyai University, Faculty of Engineering, Piața Traian Vuia, nr. 1-4, 320085, Reșița, Romania
ion.mituletu@ubbcluj.ro
(*corresponding author)
- Eng. Alexandru Predica, Babeş-Bolyai University, Faculty of Engineering, Piața Traian Vuia, nr. 1-4, 320085, Reșița, Romania
alexandru.predica@stud.ubbcluj.ro
- Eng. Ionut Voina, Babeş-Bolyai University, Faculty of Engineering, Piața Traian Vuia, nr. 1-4, 320085, Reșița, Romania
ionut.voina@stud.ubbcluj.ro

About the availability of hydro-energy units from the Iad–Drăgan Hydropower Subsystem

Daniela Negrea, Cornelia-Victoria Anghel - Drugărin*,
Marius Lolea, Emeric Szabo

Abstract. *The paper presents possibilities to determine the factors that influence the availability of hydro aggregates. The case study presented in the paper is focused on the hydro-energy units from the Remeți and Munteni hydroelectric power plants belonging to Bihor Power System. The analyzed performance indicators refer to the specific activities of electricity production, respectively the management and exploitation of hydro aggregates at the maximum allowed capacity, as well as the specific activities of the system service, respectively the coordination of operation to meet the demand of National Power System. The purpose is to determine, respectively analyze, the availability coefficient (POF) respectively unavailability (UOF) and the cost of maintenance over a certain period of time.*

Keywords: *hydro-energy units, availability, cost-maintenance*

1. Introduction

The method of obtaining hydroelectric energy is due to the operation of hydro aggregates (hydro-energy units). Hydro aggregates are the most robust, reliable and durable structures that facilitate lifetime repairs, without major modernizations for optimal operation [6]. Due to the robustness, all energy generation equipment suffers irreversibly by reducing performance, reliability and availability, which lead over time to total unavailability, re-engineering, withdrawal from operation for a certain period of time and modernization. The availability of any technical system, including hydro aggregates, can be quantified by three specific indicators [3]: availability, average availability and the availability coefficient. Each of these indicators has a particular practical importance, as they characterize locally or on an interval the state of the system. The results recorded over a period of time indicate the cost for planned and accidental works.



The share of unavailability of hydro aggregates increased from year to year, both for planned and accidental works. Efficiency in operation by reducing the time of unavailability and maintenance costs is the basis of a refurbishment program, a catalog that is applied according to Romanian Government Decision no. 2139 of November 30, 2004 and also includes the classification and normal operating durations of fixed assets [8]. Following a re-engineering, the downtime is reduced, after the expiration of the guarantees for the works, the application of preventive maintenance is considered [1][2].

The hydroelectric plants (HPP) on which the study was carried out in the paper are Remeți HPP and CHE Munteni I HPP. They are located on the Crisuri hydropower development in the upper basin of the River of Crișul Repede. They are under the management of the Cluj branch of Hidroelectrica SA, being managed through the Oradea Hydroelectric Plan [9]. They have the installed power of 100 MW (Remeți) and 50 MW (Munteni I). They are equipped with Francis-type turbines, respectively vertically arranged synchronous electric generators, with a power of 50 MW per unit in the case of the Remeți HPP and 25 MW/unit for the Munteni HPP.

2. Iad-Drăgan Hydropower Subsystem

The Iad - Drăgan hydropower subsystem is part of the Romanian National Power System (NPS) and is included in the Crișuri hydrographic basin. It is distributed on the territory of Cluj and Bihor counties. The location of the subsystem with its territorial delimitation is shown in figure 1.

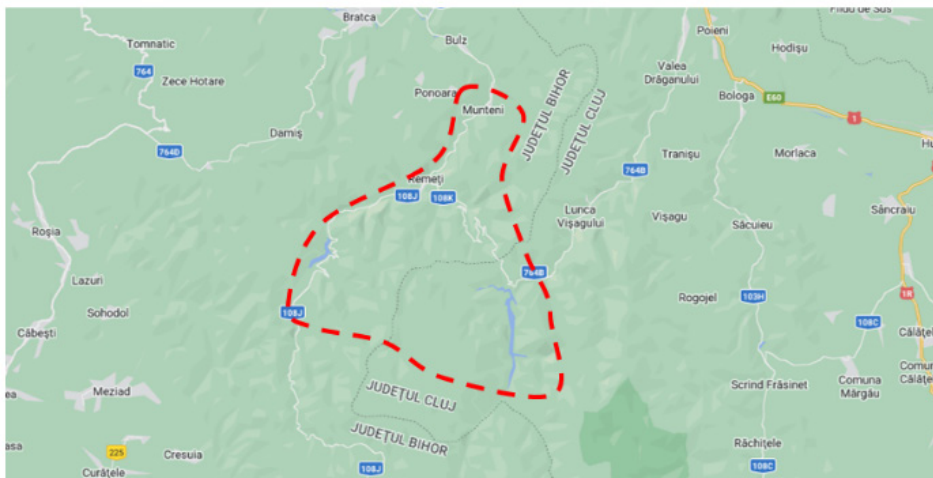


Figure 1. Location of Iad-Drăgan hydropower subsystem

As a hydraulic development, it consists of two reservoirs Drăgan and Leșu and for electricity production it includes two hydropower plants (HPP), Remeți and Munteni I and two microhydropower plants (μ HPP), Leșu and Munteni 2. Two of these hydropower projects are presented in figure 2.

Located on the course of the Drăgan River, with a height of 120 meters and a canopy opening of 424 meters, with a double-arch concrete construction, the Drăgan Dam is the largest of its kind in the country. The reservoir formed behind the dam has a total volume of 112 million m^3 of water, allowing the annual regulation of a flow of 8,7 m/s, the production of electricity, the water supply of complex uses as well as the mitigation of torrents and floods.

The Remeți Hydroelectric Power Plant, located on “Valea Bisericii”, is the largest power station within the Oradea branch, being a semi-buried station, the average energy supplied is 200 GWh/year, the nominal flow rate $Q = 40 m^3/s$, the drop height $H = 335 m$.



a.
b
Figure 2. Dam&lake of Drăgan(a) and Munteni I HPP(b)

The Leșu microhydropower plant is located at the foot of the Leșu dam (a dam belonging to the Crișuri – Oradea Water Directorate) and discharges the water, after processing, into the main intake Munteni I, through an 8.1 km long secondary intake gallery Energy produced is $E = 10 GWh/ year$, nominal flow rate $Q = 9,3 m^3/s$ at a drop height H of 53,5 m.

The Munteni I Hydroelectric Power Plant, located on the right bank of the Iad Valley, is an underground plant on the derivation, being equipped with two vertical turbines of the Francis type, it processes the turbine water at the Remeți HPP and the Leșu μ HPP. The average electrical energy produced is $E = 120 GWh/year$, flow rate $Q. = 49 m^3/s$, height $H = 146m$. A Munteni II microhydropower plant was commissioned in 1992 in the Munteni I HHP premises, which is equipped with a

0,63 MW Francis type horizontal turbine, processing the water from the difference in the basin of the river Iad, between the Leșu μHPP and the Munteni I HPP. The energy produced by the Munteni II microhydropower plant is about 2 GWh/year at a flow rate Q of $2 \text{ m}^3/\text{s}$ and the drop height $H = 45 \text{ m}$.

The functional schemes with the location of the hydropower units (HA) for the Remeti and Munteni I hydropower plants are presented in figure 3.

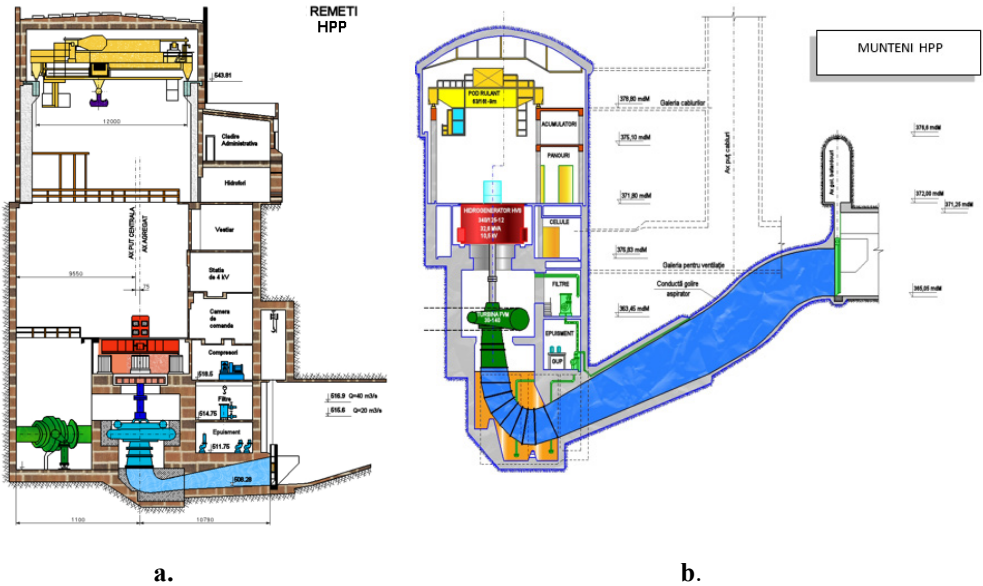


Figure 3. Functional diagrams with location of HAs into Remeti HPP(a) and Munteni I HPP(b)

3. A few calculating models for the availability of hydro aggregates

To determine the availability of hydropower aggregates, specific coefficients are determined [3], [4], [5], the applied mathematical model indicating their degree of reliability.

Availability(D), represents the ability of a system (equipment) to fulfill its specified function under the combined aspects of reliability, maintainability and management of maintenance actions, at a given moment, or in a specified time interval[3]:

$$D(t) = R(t) + F(t) \cdot M(t) \quad (1)$$

Along with the term that specifies the maintainability or degree of maintenance of the hydroaggregate $M(t)$, in relation (1) appear the terms $R(t)$ and $F(t)$ which will be defined as follows:

- The probability of good operation $R(t)$ is itself the "quantitative concept of reliability", it represents the probability that a product (device, system, etc.) will fulfill its specified function, under given conditions and over a given duration, namely [4] :

$$R(t) = \text{Prob}(t \geq T) \quad (2)$$

whete : t – time variable(time of mission);

- The failure probability $F(t)$ is complementary to the function $R(t)$ and it has the relation [3]:

$$F(t) = \text{Prob}(t < T) \quad (3)$$

If the equipment can only be in one of two states (operational, malfunctioning), then write:

$$R(t) + F(t) = 1 \quad (4)$$

The occurrence of defects can be characterized by the frequency function or the distribution density $f(t)$ which expresses the relative frequency of falls (Δn_i) in a period of time Δt_i , namely [3]:

$$\left\{ \begin{array}{l} \Delta n_i = N(t_i) - N(t_i + \Delta t_i) \\ \hat{f}(t_i) = \frac{\Delta n_i}{\Delta t_i \cdot N_0} \end{array} \right. \quad (5)$$

In which: $N = N_0 - n$ – the number of hydro units in operation at the time (t_i), $\Delta n_i = f_i$ – the absolute frequency; $\Delta t_i \cdot N_0 = T_i$ - the total number of test hours in the considered interval.

Between indicators $R(t)$, $F(t)$ și $f(t)$ exist the following relations:

$$F(t) = \int_0^t f(t) dt, \quad R(t) = 1 - F(t) = \int_t^{\infty} f(t) dt \quad (6)$$

For the failure record can be considered the indicator called Rate (intensity) of falls (defects) $Z(t)$ which is defined by the relationship [3]:

$$Z(t) = \frac{f(t)}{R(t)} \quad (7)$$

If we accept the exponential distribution for the operation and recovery times, the indicator called "availability coefficient" can be expressed as follows:

$$K_D = \frac{MTBF}{MTBF + MTR} = \frac{\mu}{\lambda + \mu} \quad (8)$$

Similarly, the following coefficients are defined:

- the unavailability coefficient (the proportion of inactive time):

$$K_I = \frac{MTR}{MTBF + MTR} = \frac{\lambda}{\lambda + \mu} \quad (9)$$

- the coefficient (proportion) of use:

$$K_U = \frac{MTBF}{T_A} \quad (10)$$

Where MTR is the mean time to repair and MTBF is the mean time to good operation. The term T_A represents the duration of the analysis, including actual use times, maintenance times, stagnation times.

In this paper for the calculation of the two specific indicators, the following relationships were applied[3]:

- POF (Planned Outage Factor) - which represents a component of the time unavailability coefficient corresponding to the planned shutdowns:

$$POF = \frac{100 \times TP}{T} \quad [\%] \quad (11)$$

Where TP: the total duration of planned stops in the reference period T[hours] and respectively:

- UOF(Unplanned Outage Factor) – which represents a component of the unavailability coefficient over time (UF) corresponding to unplanned stops:

$$UOF = \frac{100 \times TN}{T} \quad [\%] \quad (12)$$

Where, TN : the total duration of unplanned shutdown states in the reference period T [hours].

4. Evaluation of the availability indicators for the considered hydro-energy units

From the power plants analyzed, the evaluation of the coefficients of interest was carried out for the two hydro aggregates from Remeti HPP and the respective two from Munteni HPP. These hydro aggregates are marked HA₁ and HA₂ and the results obtained are presented graphically in color code. The analysis period was 9 years, respectively from 2013 to 2021. The reduced availability requires thorough technical

analyzes to determine the factors that contributed to it. Depending on their nature, measures for maintenance, modernization or replacement of a hydro unit can be established. Thus the technical aspects are linked with the economic and financial ones. The allocation of expenses for increasing the availability of hydro aggregates can be done on the basis of the cost-benefit analysis that includes several economic criteria [7]. For example, this method of analysis and evaluation of expenses may represent an attempt to measure the costs and gains from the operation of a hydropower plant as a result of the development of the programs established on the hydro-energy units.

The results of the financial analysis according to the cost-maintenance criterion, in order to make production more efficient and to reduce major expenses in the case of the UOF and POF indicators, of the unavailability time are mentioned in figures 4 and 5.

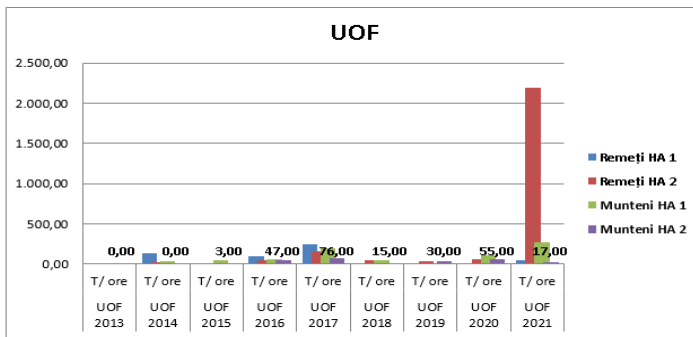


Figure 4. Values of UOF

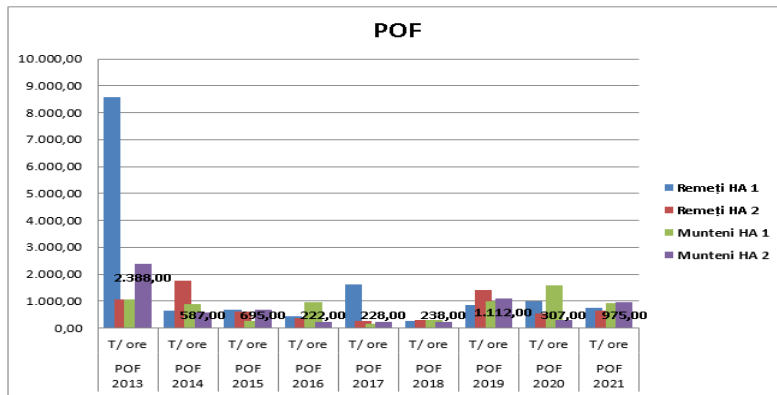


Figure 5. Values of POF

From the comparison of the continuity indicators recorded in the mentioned period, it can be seen that for planned interruptions (POF) they recorded degradations, and for unplanned interruptions (UOF) they recorded decreases. Also, it can be seen from the recording of the values for the case of the accidental unavailability index, an average of 5% over the analyzed time interval, the causes that can explain this situation can be taken into account, namely, the state of all assemblies and installations that complete the operation process of the hydro unit (planning and carrying out preventive maintenance, to reduce long-term unavailability).

The results obtained for the calculation of the energy availability coefficient are presented in figure 6.

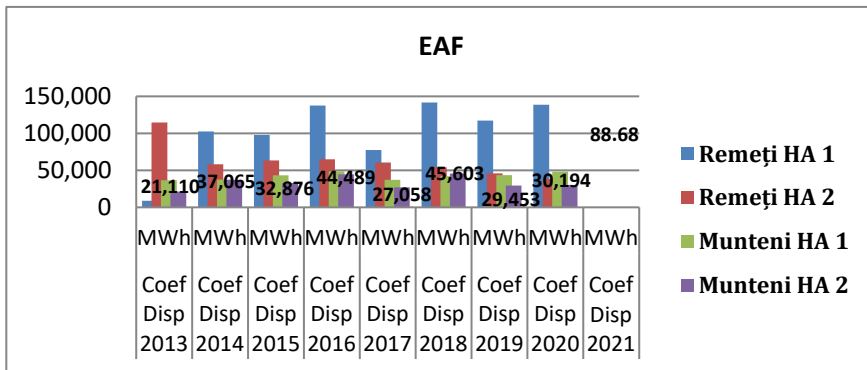


Figure 6. Values of Energy Availability Factor (EAF)

4.1. Availability of Remeți HPP

The calculation results obtained for the availability coefficient of Remeți HPP, for the analysis period, are graphically highlighted in figure 7.

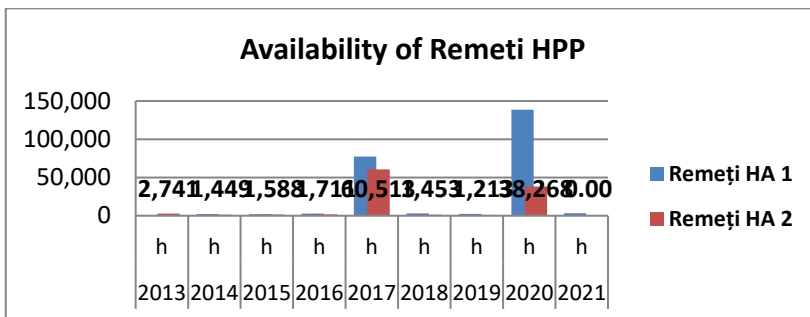


Figure 7. Availability coefficient of Remeți HPP, from 2013 to 2021

4.2. Availability of Munteni HPP

The calculation results obtained for the availability coefficient of Remeți HPP, for the analysis period, are highlighted graphically in figure 8. For comparison, the availability coefficients for a Munteni II μ HPP and Leșu μ HPP were also evaluated. The latter was stopped in 2012. The results obtained in this case are presented in figure 9.

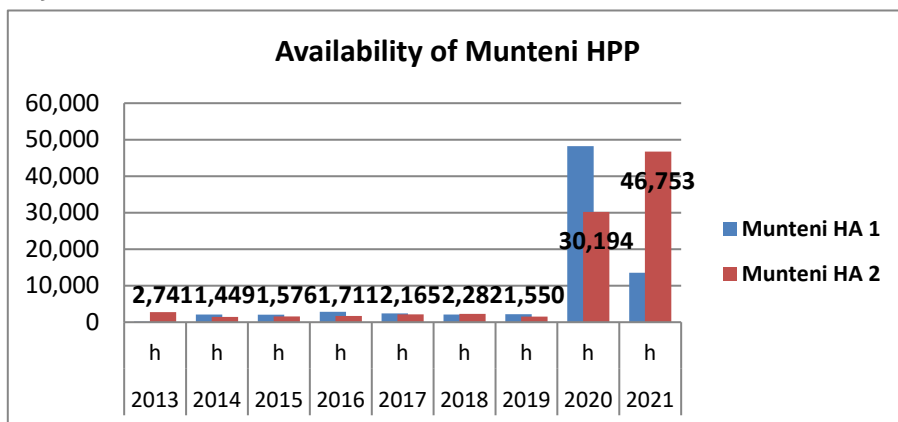


Figure 8. Availability coefficient of Munteni HPP, from 2013 to 2021

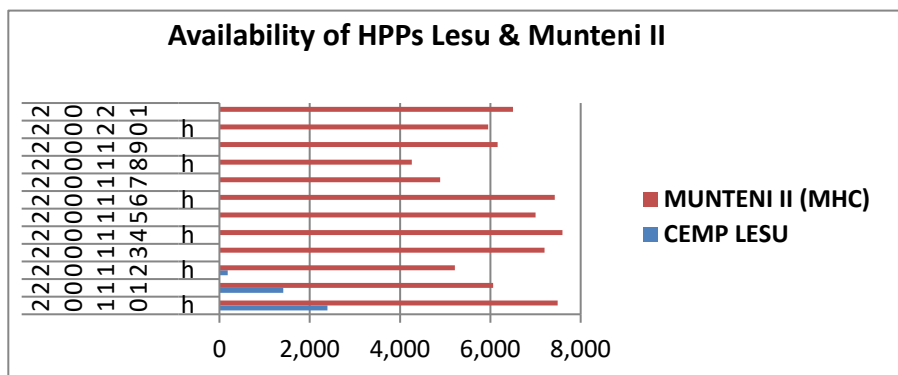


Figure 9. Availability coefficients of Leșu - Munteni II μ HPP from 2010 to 2021

5. Conclusions

In the elaboration of the paper, two directions were followed as an approach: a theoretical one in which the studied theme and mathematical modeling are presented, issues included in chapters 1, 2 and 3, and an applied one, in chapter 4, in which based

on experimental measurements and records of given in the centrals, the indicators of interest were calculated. At the end of the paper, are presented the conclusions resulting from the study.

The maximum powers at which the hydro-energy units can operate are 47,86 MW for HA₁ and respectively 37,43 MW for HA₂ due to the operating restrictions resulting from the operation of the generators, the maximum powers given by the producer for each hydro-energy unit, being 50 MW. With reference to HA₁ and HA₂ of Munteni I HPP is to conclude following the monitoring that the maximum achieved powers at which the hydro-energy units operate are 20,34 MW for HA₁ and respectively 19,83 MW for HA₂. These are lower than the maximum powers given by the manufacturer, which have a value of 29 MW for each hydro aggregate. Based on the measurements and analysis performed, the minimum operating power for both hydro aggregates can be $P = 5$ MW.

Following the results obtained and represented graphically in chapter 4 of the paper, the following specific conclusions can be formulated:

- the factor of energy availability has the highest values in the years 2018 and 2019 respectively for the hydro unit HA1 of the Remeți HPP;
- the availability coefficient of Munteni II μ HPP is much higher than that of Lesu μ HPP. The availability of MHC Munteni II was the highest in 2014 when the availability coefficient reached the maximum value of 7245 hours/year;
- the availability coefficient for Munteni HPP was the highest in 2020 for HA₁. For HA₂, this coefficient reached its maximum value in 2021;
- for CHE Remeți, the highest values of availability were recorded in the case of HA1, the first maximum being equivalent to 2017 and the second for 2020.

Finally, we can highlight the observation that the hydro aggregates cannot be exploited at the maximum capacity given by the manufacturer, due to wear and tear in operation.

The original contributions of the authors were focused in particular on: experimental measurements and investigations of databases from the archives of hydropower plants, the calculation of availability indicators, the selection, processing and statistical analysis of the data of interest or the synthesis of the results with their presentation in a logical form.

References

- [1] Amaya E.J., Alvares A.J., Gudwin R.R., *Open system architecture for condition based maintenance applied to a hydroelectric power plant*, 8th Latin-American Congress on Electricity Generation and Transmission, Proceedings. CLAGTEE 2009, Ubatuba, SP, Brazil, 2009.

- [2] Cocioran A., Bucur D.M, *Soluții tehnice aplicate în retehnologizarea și modernizarea hidrocentrelor de pe râul Olt inferior*, A șasea conferință a hidroenergeticienilor “Dorin Pavel”, Sebeș, mai 2010, pp.355-366.
- [3] Felea I., *Ingineria fiabilității în electroenergetică*, Editura Didactică și Pedagogică, București, 1996.
- [4] Felea I., Coroiu N., *Fiabilitatea și mentenanța echipamentelor electrice*, Editura Tehnica, București, 2001.
- [5] Hora C., *Fiabilitatea echipamentelor din centralele hidroelectrice*, Editura Universitatii din Oradea, 2007.
- [6] Pavel D., Zarea S., *Turbine hidraulice și echipamente hidroenergetice*, Editura Didactică și Pedagogică, Bucuresti. 1965.
- [7] Platon V., Antonescu D., Constantinescu A., *Preliminary methodology Cost benefit analysis for river basins*. In Munich Personal RePEc Archive Papers, No. 101293, 2015, <https://mpra.ub.uni-muenchen.de/101293/>
- [8] *** Hotărârea de Guvern nr.2139 din 30 noiembrie 2004 pentru aprobarea Catalogului privind clasificarea si duratele normale de functionare a mijloacelor fixe.
- [9] www.hidroelectrica.ro

Addresses:

- Ph.D. Stud. Eng. Daniela Negrea, University of Oradea, str. Universității, nr.1, 410087, Oradea, Romania
dana_negreal@yahoo.com
- Lect. Dr. Eng. Cornelia Anghel-Drugarin, Babeș-Bolyai University, Faculty of Engineering, Piața Traian Vuia, nr. 1-4, 320085, Reșița, Romania
cornelia.anghel@ubbcluj.ro
(*corresponding author)
- Dr. MAs. Marius Lolea, University of Oradea, str.Universității nr.1, 410087, Oradea, Romania
mlolea@yahoo.com
- Ph.D Stud., Eng. Emeric Szabo, University of Oradea, str. Universității, nr.1, 410087, Oradea, Romania
emericremus@gmail.com

A literature review of land title with the aim of maximising the benefits of Blockchain technology in the management of Land Title in Nigeria

Adeolu Seun Obamehinti*, Victor Eguavoen

Abstract. *Blockchain is a trending technology that has paved way to solving various challenges in different sectors. It has received much interest from researchers over the years, as it is known to be a transparent, secured, no third party and tamper-proof public records repository system for documents, contracts, properties and assets. Land title has been a major challenge in Nigeria due to the fact that existing system, digital archives, used to manage the sector is not effective, thus brought about issues such as, double spending, possibility of tampering, third party interference and non-transparency of operations. Hence the need for blockchain technology. Blockchain has characteristics, such as decentralization, security, immutability, smart contract, it is therefore expected to improve land title management. This paper applies a content-analysis based literature review blockchain technology and existing method of land title in Nigeria. This paper propose five benefits. Blockchain can help to improve proper land record keeping, information transparency, accountability, anonymity and avoidance of double spending.*

Keywords: *blockchain, land regulation, ethereum, smart contract*

1. Introduction.

The previous years have seen researchers pick interest in Bitcoin and Blockchain. Bitcoin is a cryptography type of currency which leans on the technology of Blockchain. The fact is, the original and most common application of Blockchain technologies is Cryptocurrency, in recent times further use cases have been proposed. The current trending and important Blockchain application which focuses on Ethereum and smart contract is explored.

The Blockchain is a novel disruptive technology based on cryptography. The Block Chain technology has been known to be the work of Nakamoto who defined Blockchain as a peer-to-peer network which is immutable, transparent, and secure



and needs no third party interference. Nakamoto S. (2008) explains how this technology can become the core component to support transactions of the digital currency (Bitcoin). With the introduction of Blockchain, many fields such as finance, accounting, and real estate will receive a positive impact using the benefits of this technology. One area in which Blockchain technology could play a vital role is the use of Blockchain technology to manage land titles.

Blockchain beyond currency, Ethereum and smart contracts. The main purpose of Bitcoin is to transfer currency, the highly immutability quality and openness of its Blockchain have given rise to the birth of new protocols, which uses Ethereum type of block chain where Ether is been spent and the smart contract code are written to permit transactions, beyond Cryptocurrency. Taking for instance, some protocols permit the certification of a document. The platform where smart contract is executed is written in a Turing complete language. The Consensus protocol of Ethereum makes sure all valid updates of the contract are recorded on the Blockchain, making sure of valid execution. These researches have provided some benefit in blockchain such as performing transaction on a secured network. Its efficiency, while there are also challenges including scalability and immature technology, this paper aims to fill the gap. The purpose of this paper is to explore how the current land title system in Nigeria operates and to propose using blockchain technology to address current restrictions. As a result, this paper responds to the following research topics.

1. Research question 1: what research has been carried out on existing method of land title in Nigeria?
2. Research Question 2: what research has been carried out on blockchain-related work?
3. Research Question 3: What is the importance of blockchain adoption to land title management in Nigeria?

To answer these questions and to achieve the aim of the study, a collective summary of related papers, for both the existing method of land management in Nigeria and existing method of blockchain technology are studied with literature review. The organization of the paper from section 2 provides blockchain overview, literature review on existing method of managing land title in Nigeria, literature review on blockchain related method, importance and challenges of blockchain technology and finally a conclusion is drawn to the research.

2. Blockchain overview

The core technology of this protocol, the Blockchain, is widely acknowledged as a major breakthrough in fault-tolerant distributed computing, after decades of research in this field. In overly concise terms, Deloitte (2016) we can define the Blockchain as a database that contains all the transactions ever executed in a peer-to-peer network. It consists of a permanent, distributed digital ledger, resistant to tampering and carried out collectively by all the nodes of the system.

The advancement presented by this innovation is that the system is open and members don't have to know or confide in one another to transact, the electronic exchanges, can be consequently confirmed and recorded by the hubs of the system through cryptographic calculations, without human interference, specialist or outsider (for example governments, banks, money related establishments or different associations). Regardless of whether a few hubs are problematic, unscrupulous or pernicious, the system can effectively confirm the exchanges and shield the record from altering through a scientific component called proof of work, which makes human interference or controlling specialist pointless. Sharples M. and Domingue j. (2015) Blockchain could therefore be regarded as a distributed ledger of records that is immutable to attack. The Ethereum V. Buterin, (2013) platform has been attracting attention for its good support to the execution of smart contracts, e.g. programs that are executed in a decentralized way. As an irreversible and tamper-proof public records repository for documents, contracts, properties, and assets, the Blockchain can be used to embed information and instructions, with a wide range of applications. These incorporate, for example: smart contracts, to be specific automated, self-executing activities in the assentation between two or different nodes; as against the old way of, multi-signature exchanges, which require the assent of numerous organization for their execution; smart properties, to be specific advanced responsibility for and elusive resources inserted to the Blockchain, which can be followed or traded on the Blockchain itself. In these cases, the benefit of the Blockchain is that there would not be need for a legal official, by authorizing the execution of directions by a cryptographic code, with insurance of members against dangers of extortion and a noteworthy decrease of the executives' overheads. On account of the exceptional preferences identified with computerization, straightforwardness, auditability and cost-adequacy, the Blockchain may in this way speak to a problematic advancement for some assortments of agreements and business exercises. Other critical uses of the Blockchain incorporate for instance Xu J (2016) the creation of decentralized domain name system resistant to top- level domains censorship (e.g. Name coin); (DAOs/DACs/DASSs), namely self-sufficient agents derived from artificial intelligence and capable to execute tasks without human involvement, for which the Blockchain can provide additional functionality.

The fields of application of the Blockchain are potentially countless since it allows the disintermediation of any digital transaction at global level. "Accordingly, all kinds of business and human activities are expected to be reconfigured, with pervasiveness similar to that of the Web" (Swan, 2015). For this very reason, the Blockchain has been described as fundamental for human progress as the Magna Charta or the Rosetta Stone (Swan, 2015), and it is often referred to as a "Black Swan" – namely an accident of major impact in history that cannot be anticipated, creates surprise to the observer and can only be rationalized by hindsight (Taleb, 2007).

3. Methodology

The method adopted for this research, is a content-analysis based literature review blockchain technology from Briner and Denyer (2012) in other to provide a transparent scientific literature review of blockchain application and Traditional system of managing land title Nigeria there are steps which are involved in this method approach:

Step 1: identify the related work of existing system and draw a comparison with blockchain technology, to ascertain the need for blockchain technology

Step 2: review blockchain related work and the research covered area to ascertain the proposed blockchain to land title is novelty.

Step 3: Identify and show the unique characteristics of blockchain in the reviewed literatures to provide an answer to the research questions

This section provides a brief review of the relevant concepts, including real estate as blockchain is yet to be explored for land title management this research paper therefore, set a precedence on land title in Nigeria. Blockchain, and traceability/ auditability, transparency, tamperproof to provide some background information as the basis for this study. For this section a review of existing method of land titling in Nigeria and a review of blockchain method is carried out.

3.1. Review on Land Title in Nigeria

A few studies have been carried out on land title in Nigeria, this section provide a literature review on land title in Nigeria. According to Ajoku et al (2003) and examination of how effective land administration in Lagos Nigeria with a consent of the government of right to certificate of occupancy within 30days interval, this at the time was introduced to improve the land title management and housing allocation in Lagos Nigeria. This study discovered, it has not brought about to significant improve has the reduction in the time for processing and issuing certificate of occupancy is yet to still give a smooth running of land title management.

According to babade (2003) findings of activities in Lagos Nigeria on land title allocation ministry in giving approval of Urban land in Nigeria. The author through its findings, who obtained data of land title record for this research and also administer questionnaire on the staff of the ministry to get their view, and other stakeholders in the land title management, the study indicated that there is no transparency in the allocation of land where the politicians and civil servants had greater access the this said urban land. Their by living the poor and the less bridge at the mercy of this few notables.

Omirin (2003) also state the challenges of land title in Lagos Nigeria. A non-empirical approach was devised by also stating related view from previous empirical studies, the research concluded on its findings and discovered that extant policy are not effective and our unproductive where they have produced barriers and bottleneck for private individuals to access land. The research also stated that the existing system of land titling is not effective as it is not equitable, sustainable, not transparent, brings about third party interference hence the need a proposed a new working technology.

In the study of how effective land title is on the less privilege people of Argentine, according to Galiani et al (2010), using survey data from 20003 to 2007, findings indicates that due to lack of land title to the poor masses it has barred them from getting access to decent housing and this is as a result of the lack of government to give access to improved credit system. Findings further stated if the citizen would have improved system of land title in Nigeria, this would improve the standard of living.

Nigeria land use act of 1978 according to, Ndukaku (2010) in Enugu Nigeria, emphasizing on land accessibility this law state that every land belong to the government. However the law has not been effective has it has become difficult for the common citizen to have access to land, researcher therefore propose, an amendment of law or a technology that could give a policy guidance to land title in Nigeria.

In Ondo Nigeria, an empirical study was carried out. According to ojo (2014) a survey on a hundred and eleven person was carried out by administering questionnaire, which was analyzed, findings show the dissatisfaction of respondent on how land title is managed in the state. Findings stated lack of transparency, time effectiveness and accessibility, accessibility. Also, there are possibilities that staff in the offices of the land ministry are tampering with the documents

Therefore stated the need for a new technology that would find solutions to the present limitations.

An examination of land reforms in Lagos Nigeria, was carried out with a respondent of 160, which includes the surveyors, legal practitioners, people and staff of land ministry. Thontteh et al (2015), discovered that the present system cannot effectively keep records of land title. Hence the ministry would need a new technology that can serve as public record of database which would effectively keep land title documents for proper accountability.

In a study carried by, Awolaja (2016) in Lagos Nigeria the researchers stated the importance of having a good technology to manage the land title, the researcher stated that it gives land guarantee, which in turn can be used to access loans for building or development of the said land however the researcher stated that the present system of land title hasn't given rise to this importance due to its challenges efficiency, improper storage of land documents, lack of proper documentation. The research therefore stated that a new technology should be look into to have a seamless process.

According to Udoka (2017) carried out a research on how effective land title registration is in Akwa Ibom Nigeria, a descriptive design was adopted by the researcher which he obtained is data from a secondary source. The research findings indicate that multiple people have access to the land title information which should be made private for every citizen who has a land title document in the ministry. I.e. every person's document should be private and not accessible to others. This has therefore lead to the double spending, where same land is sold to different parties and also there is no anonymity in this process.

The existing system reviewed above indicates that there are limitations in the present system use to manage land title hence the need for blockchain technology to manage land title effectively. The limitations of the existing system are;

1. Land title transparency
2. Third party interference
3. Land title tamperproof
4. Land title effective documentation
5. Land title double spending
6. Land title anonymity (privacy)

3.2. Review on Blockchain Technology

Blockchain has it was introduced to give override to primitive business process, where trusted parties are needed for transaction verification and it also run a centralized architecture. With blockchain technology, sectors can now run a decentralized system of transaction and no need for third part interference, with credible transactions. The unique characteristics of blockchain technology has provided security, tamperproof, transparent, database for proper public record keeping according to Devetsikiotis et al (2016) and Greenspan (2015).

Blockchain is regarded as a public ledger of database for public repository. According to Dasaklis, et al (2019) It was researched that blockchain can be used in banking sectors, where banks use same blockchain for customers transaction thereby providing transparency off transaction.

Blockchain is also seen to be used for auditing of transactions there it was proposed by Coinmarketcap (2017) for company to put resources together and invest in blockchain technology to used it to build a decentralized architecture thereby minimizing transaction cost as the technology also proffer safe, fast and transparent system.

Furthermore, it was stated by Tschorsch and Scheuermann (2016) that blockchain is being considered beyond cryptocurrency, with smart contract playing a pivotal role. Also according to Quintana et al (2015) considered smart contract has the next level of blockchain used as executable code for transaction policy.

Szabo (1994) define smart contract as an executable protocol that execute the terms of a specified contract. He also allows it to be translated into embedded code from the contractual clauses

It can therefore be said that smart contracts with the context of blockchain as embedded code run in a decentralized way used in the blockchain without the need of a centralized authority to operate the blockchain, according to Christidis et al (2016).

Blockchain system according to Zhao et al (2016) supports smart contract in other to accommodate complex transaction and interaction within the limitless application. This in a way has indicate another relevance of blockchain technology

In addition according to the research findings of IBM (2017) 33% of C-suite executives has shown interest in considering rather actively engages in blockchain.

Christidis et al (2016) pointed out developers are beginning to see the effectiveness and capabilities of blockchain technology and need to explore various application depending on sectors to adopt the technology.

Also according Zhao et al (2016) stated based on the audience there are three distinguished generations of blockchain which are: blockchain 1.0 this is the cryptocurrency digital transaction while Blockchain 2.0 includes smart contract, which provides a system beyond cryptocurrency and blockchain 3.0 involves the science, internet of things government and health sector.

Fully knowing that about the review of blockchain technology, Tama et al (2017) and another researcher known to be Brandao et al (2018) gave their basis of argument on the fact that blockchain technology enabled application has received limited attention.

It is also interesting to state that a researcher known as Zheng et al (2016) states that blockchain has not covered it full capabilities.

Another research was carried out by Conoscenti et al (2016) and Christidis et al (2016) on how blockchain and decentralized system can be used for internet of things and how it can also manage big data in a decentralized way this is according to Karafiloski et al (2017).

Table 1 shows the strength and weakness of the proposed blockchain for land management in Nigeria over the existing system.

Table 1.

| Blockchain related work | Research area covered |
|--------------------------------|--|
| Dasaklis (2019) | Proposed blockchain to bank sector |
| Karamitsos et al (2018) | Blockchain for real estate |
| Jonas Johansson et al (2018) | Proposed blockchain to use in sustainability of contractors in the construction industry |

| Blockchain related work | Research area covered |
|----------------------------------|--|
| Coinmarketcap (2017) | Proposed blockchain for Auditing transaction |
| Jonatan. H (2017) | Proposed blockchain technology as privacy-preserving tools in the medical sector |
| Karafiloski et al (2017) | Blockchain for big data transaction |
| Conoscenti et al (2016) | Blockchain for internet of things |
| Zheng et al (2016) | Research on blockchain hasn't gotten to its full potential |
| Christidis et al (2016) | Blockchain for decentralized application |
| Tschorsch and Scheuermann (2016) | Blockchain beyond cryptocurrency |
| Devetsikiotis et al (2016) | Research on the characteristics of blockchain |
| Jonas Johansson et al (2018) | Proposed blockchain to use in sustainability of contractors in the construction industry |

Karamitsos, I. (2018) researched that blockchain technology can be used in the real estate sector, for the purpose of tenant and landlord rent. It was clearly discussed in the research on how smart contract is written as executable rule for the purpose of the real estate sector so as to provide solution to the rental challenges and a secured platform for the said transaction.

However, owing to the review of the related works of blockchain stated none has seen to focus on land title management. It is therefore pertinent, to propose the use of blockchain technology to manage land title in other to solve the various challenges of existing method of land titling in Nigeria as stated in section 1. Table 2 indicates areas presently covered by blockchain research in related work

Table 2. Related work and researche covered

| Blockchain related work | Research area covered |
|--------------------------------|--|
| Dasaklis (2019) | Proposed blockchain to bank sector |
| Karamitsos et al (2018) | Blockchain for real estate |
| Jonas Johansson et al (2018) | Proposed blockchain to use in sustainability of contractors in the construction industry |
| Coinmarketcap (2017) | Proposed blockchain for Auditing transaction |
| Jonatan. H (2017) | Proposed blockchain technology as privacy-preserving tools in the medical sector |
| Karafiloski et al (2017) | Blockchain for big data transaction |
| Conoscenti et al (2016) | Blockchain for internet of things |

| Blockchain related work | Research area covered |
|----------------------------------|--|
| Zheng et al (2016) | Research on blockchain hasn't gotten to its full potential |
| Christidis et al (2016) | Blockchain for decentralized application |
| Tschorsch and Scheuermann (2016) | Blockchain beyond cryptocurrency |
| Devetsikiotis et al (2016) | Research on the characteristics of blockchain |
| Jonas Johansson et al (2018) | Proposed blockchain to use in sustainability of contractors in the construction industry |

This research as shown in table 2 gave a summary of literature review on the recent researches considered in blockchain. This has however not yet shown interest in land title management hence, necessitated this research to be carried out and propose the use of blockchain for land title.

4. Benefits of Blockchain for Land Title Management in NIGERIA

Blockchain has benefits that could be the solution to the challenges of land title in Nigeria if adopted. The following are the benefits of blockchain technology over the traditional system of land title in Nigeria

1. **Tamperproof:** according to Nakamoto, s. (2008), blockchain technology is tamperproof. A vital point that should be considered when transaction is being conducted is how tamperproof is the system that is being adopted. Blockchain system is known for its tamperproof quality and its best needed in conducting a land transaction through the blockchain as against the manual system where most times, documents are influenced or tampered with.
2. **Transparency and no double spending:** according to Tschorsch, F. and Scheuermann, B. (2016) discovered that blockchain system is highly transparent where nobody can influence any decision. It is a decentralized system that gives power to every participant and not just one person. That is why it has private and public key digital encryption, where the private key is own by the election team who declares the election process open and every citizen of age to vote/ participant has the public key to verify the land transaction.
3. **Secured:** an important part of an election system is for it to be secured. Blockchain in the voting system adoption, is highly secured everyone doesn't need to come out to perform land transaction just as it is done the manual way, all you need do is stay as you were and transact on a secured blockchain network. According to Walsh C, et al. (2016), discusses how secured blockchain transaction is secured. This in a way help to prevent every form.

4. No third party and Anonymous: according to Paul, G, et al. (2014), blockchain technology is anonymous and does not need a third party interference. One of the beauty of transaction is to make it completely anonymous in other to prevent victimization of land buyers as to who and why they bought from a particular individual. Blockchain system takes care of the anonymity aspect of the land transaction system. A unique Identity is generated for every participant of the blockchain that is not traceable to any participant. There is also no need for third party interference as the smart contract would serve as a guideline/ policy for every transaction initiated in the blockchain and with this two trustless individuals can perform transaction
5. Cost effective: there won't be need to bribe any officer of the ministry of land to fast track the process of land titling anymore. This would save the cost of spending on such frivolities. Also all that is need to do is to go on internet and log onto the application and make transaction this would also rule out the cost of travelling to the ministry of land title.
6. Accessible to everyone: blockchain technology as in this case for the purpose of this research is public blockchain which is a permissionless type of blockchain. This gives opportunity for every citizen of Nigeria to access the network system and transact land easily without dures.
7. Database for record keeping: Atzori, Marcella (2016), discusses blockchain as a ledger for keeping public records. Blockchain technology would serve as a database for keeping public record pertaining to land titles. This would make the records of land title in Nigeria secured and there would not be unnecessary loss of documents as the case use to be in the traditional way of land title in Nigeria.

5. Conclusion

For this research a literature review was carried out to show the strength and weakness of existing method of land titling in Nigeria and also a literature review was carried out on blockchain technology and the research areas covered in the previous years, and it was confirmed that blockchain for managing land title is novelty and such could be considered a precedent. The research questions as been answered with the result obtained in the course of undergoing this research.

1. Research question 1 is answered in section 3 and also with the table 1 therein. Related work to blockchain and existing work was study and a comparison is indicated to show the strength of the proposed blockchain technology over the existing, digital archives used to manage land title in Nigeria.

2. Research question 2 is answered in section 3 and also table 2, where the blockchain literature review was carried out and a comparison of research done so far identified to show that no research on blockchain on land title is yet to be carried out.
3. Research question 3 is answered section 4 Importance of blockchain and why it is needed to manage blockchain technology is stated.

References

- [1] Awolaja A.G., Land Registration in Nigeria: Issues and Challenges <http://convenantuniversity.edu.ng/content/download/33937/233886/file/Land+Registration+IN+NIGERIA> retrieved, April, 2016.
- [2] Atzori M., Blockchain-Based Architectures for the Internet of Things: A Survey Available at SSRN: <https://ssrn.com/abstract=2846810>, 2016
- [3] Babade T., Access to Urban Land in Nigeria; An Analysis of the Activities of Lagos State Land Use and Allocation Committee in Omirin, M.M., Nubi, T.O., and Fawehinwi, A. (Ed). *Land Management and Property Tax Reforms in Nigeria*. Lagos University of Lagos Press, 2003.
- [4] Buterin V., *On Public and Private Blockchain*. *Ethereum Blog*, Crypto Renaissance Salon. 7th August 2015.
- [5] Das M.L., Privacy and Security Challenges in Internet of Things, *Distributed Computing and Internet Technology*, 2015, pp. 33-48.
- [6] Galiani S., Scharagrodsky E., Property Rights for the Poor: Effects of Land Titling, *Journal of Public Economics*, 9, 2010, pp. 700-729.
- [7] Kosba A., Miller A., Shi E., Wen Z., Papamanthou C. 'Hawk: the Blockchain model of cryptography and privacy-preserving smart contracts', *Proceedings of IEEE Symposium on Security and Privacy (SP)*, San Jose, CA, USA, 2016, pp. 839–858.
- [8] Karamitsos I., Papadaki M., Al Barghuthi N.B., Design of the Blockchain Smart Contract: A Use Case for Real Estate, *Journal of Information Security*, 9, 2018, pp. 177-190.
- [9] Kraft D., Difficulty control for Blockchain-based consensus systems, *Peer-to-Peer Networking and Applications*, 9(2), 2016, pp.397–413.
- [10] Miorandi D., Sicari S., Pellegrini F.D., Chlamtac I., Internet of things: vision, applications and research challenges, *Ad Hoc Networks*, 10(7), 2012. pp.1497–1516.
- [11] Nakamoto S., Bitcoin: A Peer-to-Peer Electronic Cash System <https://bitcoin.org/bitcoin.pdf>, 2008

- [12] Noyes C. Bitav: Fast Anti-Malware by Distributed Blockchain Consensus and Feed forward, 2016a
- [13] Ndukaku L.I., *Critical Analysis of the Impact of the Land Use Act of 1978 on Property Development in Nigeria: A Case Study of Enugu Urban*. Unpublished M.Sc. Dissertation, University of Nigeria, Nsukka, 2012.
- [14] Omohundro S., 'Cryptocurrency, smart contracts, and artificial intelligence', *AI Matters*, 1(2), 2014, pp.19–21.
- [15] Ojo B., Evaluation of End-Users Satisfaction on Land Title Registration Process in Akure, Nigeria, *Covenant Journal of Research in the Built Environment*, 2(2), 2014, pp.176-194.
- [16] Omirin M.M., Issues in Land Accessibility in Nigeria in Omirin, M.M., Nubi, T.O. and Fawelinwi, a (Ed). *Land Management and Property Tax Reforms in Nigeria*. Lagos: University of Lagos Press, 2003.
- [17] Thontteh E.O., Omirin, M.M., Land Registration within the Framework of Land Administration Reform in Lagos State, *Proceedings of 21st Annual Pacific-Rim Real Estate Society Conference*, Malaysia, Jan. 2015, pp.18-21.

Addresses:

- Adeolu Seun Obamehinti, Wellspring University, Irhirhi road Benin city, Nigeria
lebiobamehinti@gmail.com
(*corresponding author)
- Victor Eguavo, Wellspring University, Irhirhi road Benin city, Nigeria

Street Guide Mapping of Auchi, Edo State, Nigeria

Michael Banji Olatunde*, Faith Ozofu Olatunde, Henry Eronmosele Oriakhi

Abstract. *This project is on the production of a Street Guide Map of Part of Auchi town in Etsako West Local Government Area of Edo State. The remote sensing method of map production was adopted for this project. Geo-referenced satellite imagery was downloaded in WGS84 datum and was saved in Geo-Tiff file format from Terra Incognita. The image was imported, and re-projected into Minna/UTM zone 32 and mosaicked in ArcGis 10.3 software environment, which was printed in A0 paper size and was used during ground-truthing. Garmin GPS60 was used to obtain the coordinates of well-located points which were identified on the printed satellite image and used to verify the accuracy of the georeferenced image. Layers were created and the features were digitized into their respective layers, some simple queries were carried out to test the database such as identification of hotels along the major road, the position of a particular school e.t.c. Map annotation and compilation were done, and at the end, a street guide map of part of Auchi Town was printed on A0 paper size at a scale of 1:10,000. In conclusion, the newly updated map can serve as a base map for other applications such as tourism navigation, urban planning, development traffic studies and control, crime monitoring, utility management, etc.*

Keywords: *GIS, Remote Sensing, Street Guide map, Satellite imagery, Auchi*

1. Introduction

A map is a model to scale part of the earth's surface showing the shape, political borders, natural features such as rivers and mountains, and artificial features such as roads and buildings (Abbas, Adama & Koje, 2010). Maps can perform several functions such as general inventories, planning of urban/rural development and administration, management of public properties and utilities, and execution of constructional works (Abbas et al., 2010). A map is produced to serve the purpose of giving direction, showing the extent covered by a certain feature, showing relief, and so on (Addai, Owusu, Poku-Gynanbibi, 2011). There are several types of maps



such as street guide, political, physical, topographical, climatic, economic, resource, thematic and population maps (Addai *et al.*, 2011). From the above types of maps mentioned, a street guide map can be defined as a graphic portrayal of a town or city, showing the positions and names of all the streets; major/minor highways and roads, railroads, tracks, and other points of interest and the general road network. According to (Idowu, Taofik Abayomi & Olayemi, 2016). A street guide map is a kind of map that focuses on the locations of streets and routes that links residential area in a civilized area such as towns, urban area, and city, etc. The following are the uses of a street guide map; it can be used as a guide for visitors and tourists for easy accessibility routing and information dissemination (Fasote, Haliu & Muibi, 2016). It provides tourists services information system. It provides information that will enhance map review. It provides an effective guide to rescuers in emergency situations e.g. Fire service, and police.

Also, the study area due to the settlement pattern, the majority of the social amenities such as health care facilities, financial institutions, educational institutions, hotels, recreational amenities, markets; petrol stations, and so on are located within the study area. Also, the presence of the institution within the periphery of the study area makes it one of the most visited places in the local government area by people who come to do business within the town. It is to note that majority of towns in Nigeria do not have street guide maps while others possess out-of-date of such maps despite their enormous importance.

Auchi is the administrative headquarters of Etasko West Local Government Area. Due to the settlement pattern of the local government area, the majority of the social amenities such as health care facilities, financial institutions, educational institutions, hotels, recreational amenities, markets; petrol stations, and so on are located within the headquarters. The presence of natural resources such as the vegetation, and rivers within the town makes Auchi one of the most visited towns in the local government area by people who came from different cities, towns, communities, and villages to do business within and outside the town. It is sad to note that majority of towns in Nigeria do not have street guide maps while others possess outdated maps, despite their enormous importance. Auchi, as it is with many towns in the country does not have an updated street guide map. For this reason, this project focuses on the production of a street guide map of the area using remote sensing and the GIS method.

2. Materials and Methods.

2.1. Study area

Auchi is the administrative headquarter of Etsako West Local Government Area of Edo state. Auchi community has a distance of 130km from Benin City t above sea level. The administrative headquarters of Etsako West Local Government Area,

Edo State. It is situated geographically between latitude $05^{\circ} 40' 42''\text{N}$ and longitude $06^{\circ} 23' 41''\text{E}$ to latitude $05^{\circ} 43' 18''\text{N}$ and longitude $06^{\circ} 26' 61''\text{E}$ of the Greenwich meridian. The map of the study area is shown in Fig.1. The state capital. The town itself is located on a terrain that is approximately 300m.

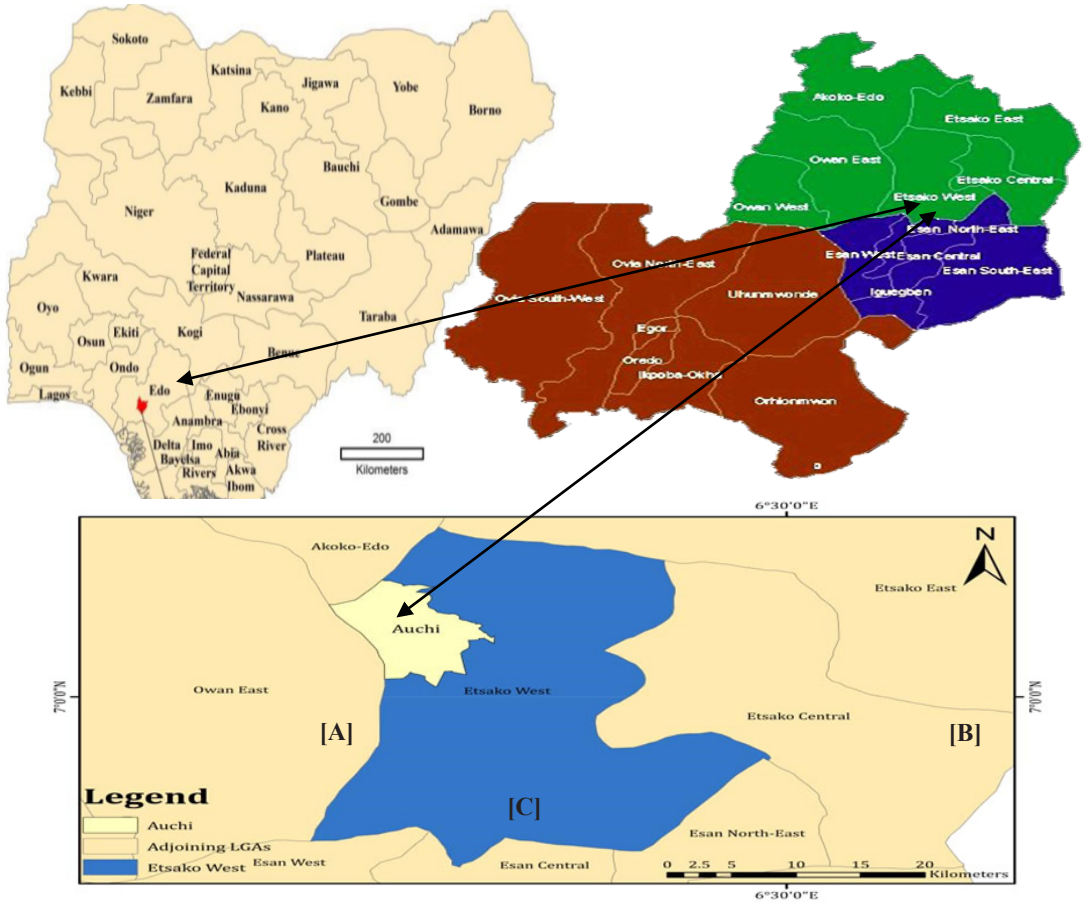


Figure 1. (a) Map of Nigeria showing Edo State; (b) Map of Edo North district; and (c) Map of Auchi indicating the experimental field at Auchi Polytechnic-Campus One. Source: Author’s Arcmap 10.1 Production, 2022.

2.2. Study Design and Planning

The method entails planning, choosing the required instrument needed for the study, and seeking data necessary for the production of a digital street map. After due consideration of the cost of executing the project and knowing that the primary

data was readily available and cheaper to be acquired from Google Earth via Terra incognita. The remote sensing method was adopted for the street guide map production. The area coverage was extracted from Google Earth via Terra Incognita. The area of interest could not be extracted as one scene, because the street could not be viewed at such resolution (Hajara, Garba, Vincent, Ojeh & Ayeni, 2018). The geo-referenced imagery of part of Auchi was downloaded in two tiles with the use of the terra incognita software at which each scene required was saved in Geo-Tiff image format which was then matched together (i.e. mosaicked) with ArcGIS 10.3 software (Hajara *et al.*, 2018). The mapping of the street guide was basically done by digitizing the road/streets within the study area. Primary data and secondary data were used for this work these include:

- i. Attribute data of marked features and street annotation of the study area;
- ii. Aerial images were taken; and
- iii. Land satellite is the longest method of a program in running an enterprise for the acquisition of satellite imagery of the earth.

Therefore, for the effective execution of the project, a workflow plan was designed for easy execution of each stage of the project, the study's flowchart is shown in Fig.2.

2.3. Reconnaissance Survey

This is a preliminary survey or the overview of a place to obtain information by visual observation or other detection methods. Reconnaissance for this study was done in two stages:

- i. Office Reconnaissance;
- ii. Field Reconnaissance.

2.3.1. Office and Field Reconnaissance

After due consideration of the cost of executing the project and knowing that the primary data was readily available and cheaper to be acquired from online Google Earth Imagery through Terra Incognita, it was decided that the remote sensing method will be adopted for the street guide map production. So, the area of coverage was extracted. The area of interest could not be extracted as one scene, due to the fact that the street could not be viewed at such resolution. So, it was downloaded in two tiles to a better viewing resolution at which each scene required was saved in Geo-Tiff image format which was then stitched together (i.e. mosaicked) saved in Geo-Tiff image format which was then stitched together (i.e. mosaicked) with ArcGis 10.3 software.

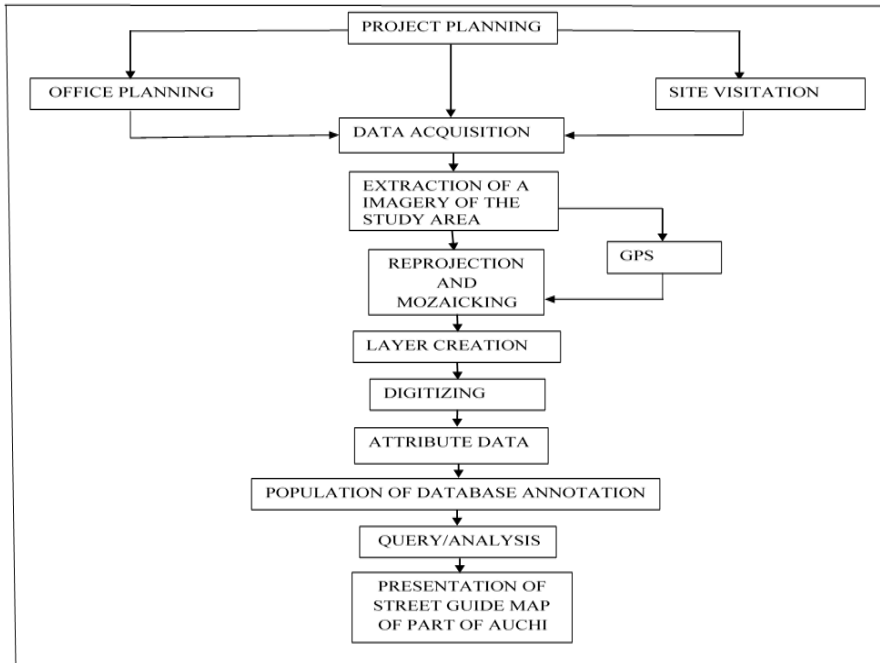


Figure 2. The work flow chart of street guild map of part of Auchi town.

2.4. Data search and Acquisition.

Data is a measure of quantity that when processed becomes information. In any project/research, the importance of data cannot be overlooked because it is the processed data that supply information upon which any research work depends. Satellite imagery of the area was obtained from Google Earth via Terra Incognita at a suitable resolution (12864×18064) and saved in Geo-TIF format, Spatial data (coordinates) of features were extracted from a satellite image of the area (Igbokwe, Itoro & Joel, 2008). The attribute data such as names of streets, roads, and so on were also obtained from field observation /social survey. The acquired satellite image was then imported into ArcGIS 10.3 software as a raster image as shown in Fig. 3.

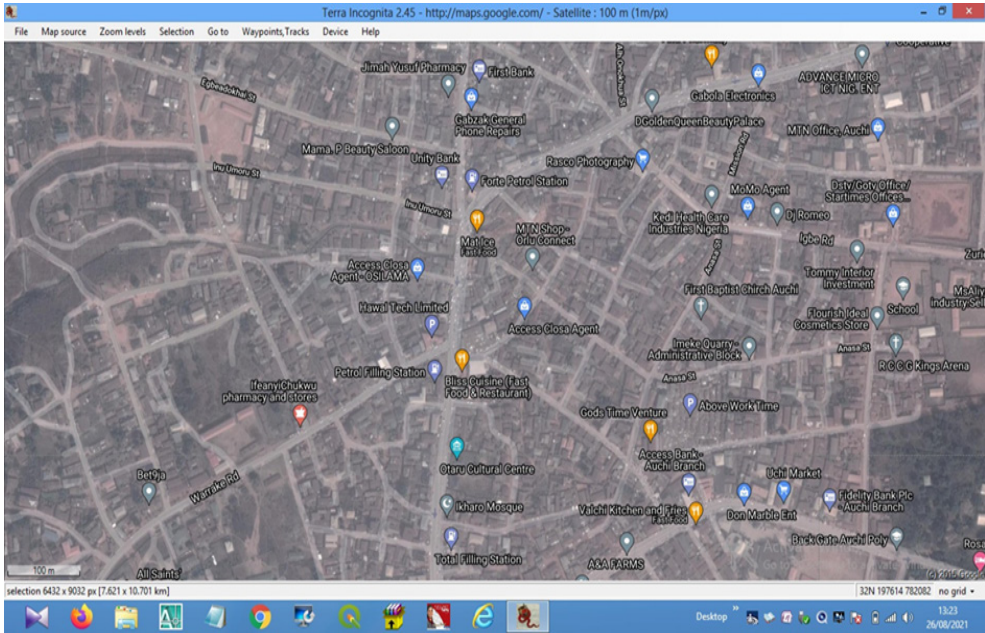


Figure 3. Google Earth Image via Terra Incognita of part of Auchi (Project Area), Etsako West LGA.

2.5. Field operation-ground truthing

This stage involved printing and taking the satellite image to the field for ground-truthing; many roads were captured within three classes of roads network namely, Major roads, Minor Road, and Street Road, prominent features such as Banks, Market, schools, and so on were obtained and written on the printed satellite imagery for verification. Table 2 presents extracted coordinates from the re-projected image whose coordinates were obtained from Google earth, coordinates of the same points were then taken to the field to confirm and verify the accuracy of the re-projected image, and points were obtained during ground-truthing. Table 2 shows the comparison of both coordinates, it is shown that the re-projected coordinates are of an acceptable standard. For capturing the geo-spatial data, we moved around all the roads in the town so as to be able to capture all the vital features (such as street names, schools, markets, banks, religious worship centres, palaces, and so on) with respect to their true ground position, this was made possible with the handheld GPS receiver and Satellite imagery. The data obtained were written on the printed satellite imagery for proper identification.

Table 2. Google Earth and GPS Field Coordinates for check

| Point ID | Google Earth Coordinates | | GPS Field Coordinate | | Difference | |
|----------------|--------------------------|--------------|----------------------|--------------|-------------|--------------|
| | Easting (m) | Northing (m) | Easting (m) | Northing (m) | Easting (m) | Northing (m) |
| FGP/ EDY073 | 199292.495 | 775546.359 | 199292.398 | 775546.305 | 0.097 | 0.054 |
| 2 | 193129.776 | 777082.225 | 193128.987 | 777081.999 | 0.789 | 0.226 |
| 3 | 192870.755 | 785199.117 | 192870.739 | 785199.114 | 0.016 | 0.003 |
| 4 | 199569.727 | 784157.626 | 199569.738 | 784157.627 | 0.011 | 0.001 |

3. Results and Discussion

3.1. Satellite Image Mosaicking

Due to the extent of the study location and the solution required to conveniently identify features on the ground, it was not possible to download a single scene satellite image covering the study area, so Google Earth satellite images were downloaded in tiles and saved in Geo-TIF file format as described by (Kolawole, Alaga & Oloko, 2016). The mosaicking of the image (or stitching) in the ArcGIS software environment as depicted in Fig 3a-e. Georeferencing could be understood as the process of conveying real coordinates to the spatial data. It assigns coordinates to the pixels of raster images. Common frames and coordinate systems are developed to define the positions within the information. It helps in determining how the areas in an image corresponding to the surface (Olatunde, Omoniyi & Olatunde, 2016).

The geo-referencing of spatial data can be done through two main methods. Firstly, by using 3D coordinates in which the center of the earth serves as the point of origin of all 3 axes.

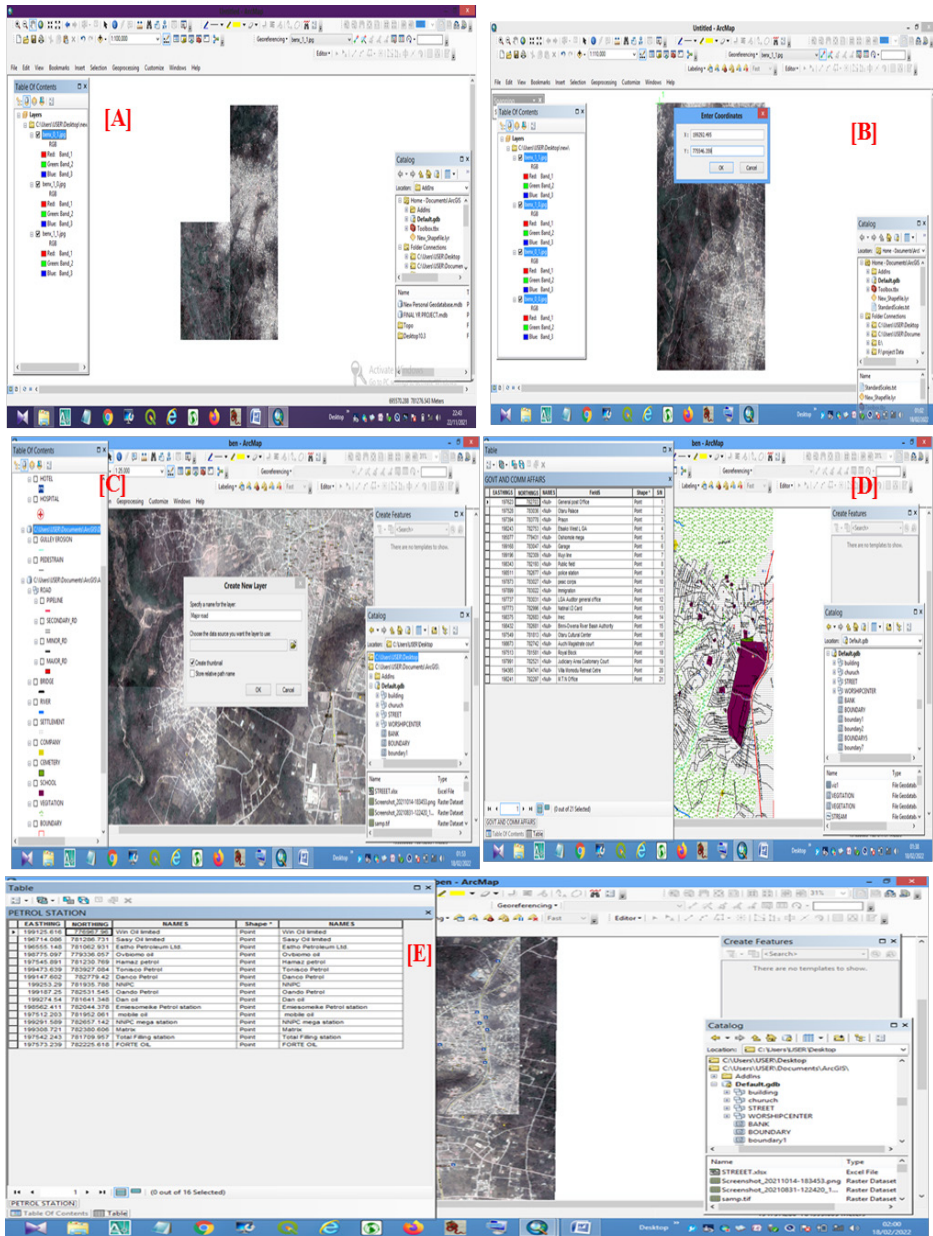


Figure 3. Mosaicking image of the study area (a), Geo-referencing of the imagery of the study area (b), Layers creation of the study area (c), Attribute table of government and community affair (d), and Attribute table of petrol station (e).

It is a popular method for scientific applications, but it is not considered feasible for applying to the points on the earth's surface. The second method is the projection of the points. In this method, 3D coordinates are expressed as a plane with some height above them. This technique helps in flattening the curved area of a small region into a flat surface for referencing purposes. The plane coordinates point towards a particular point within the projection. It is measured in terms of distances, north, and east from the origin (Raymon, Balogun & Clement, 2012).

3.2. Digitization and Vectorisation

The re-projected satellite image was digitized (vectorized) using the on-screen digitizing method. In achieving this task, layers were created for features on the image and appropriate properties were also created for them as in the studies of Raymon *et al.* (2012) and Sedi (2013). The features digitized for the purpose of this study include roads, prominent features such as schools, worship center market filling stations, government and community affairs, and financial institutions and hotels. The technique of layering is one very important facility. In this, particular features were placed in their own unique layer; for example, all major roads were placed in a major road layer. The software allows layers to be turned on or off as required by the users. This enabled to set up layers of details and allows only those of particular interest to be selected and digitized or plotted. This is easily achieved by turning off all unwanted layers and turning on all the required layers. The finding agrees with the studies of Udoh and Jude (2014) and Vicctor, Nnam, Bernard, Ekpete, Obinna & Anejionu (2012). In other to digitize the features on the satellite image, a manual method of on-screen digitizing was adopted. All the mentioned features on the image were manually vectorized as depicted in Fig. 4.

3.3. Map Compilation

Compilation of the map was done in ArcGIS 10.3 software where all necessary details were put together. Map elements such as frames, scale, legend, title, etc. were shown on the map at this stage of compilation. A printed copy of the street guide map was taken back to the field to ascertain and reconcile both features on the ground and that on paper which is commonly referred to as field completion.

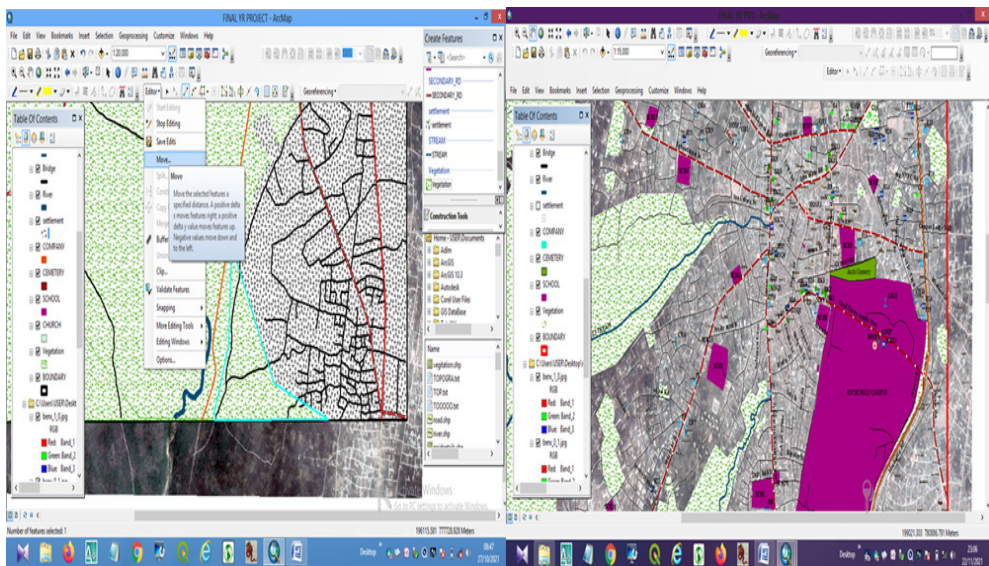


Figure 4. Vectorising and Vectorized Image of the Study Area

The information that was not found on the printed copy was updated and edited for the final finishing of the work. It is a query that has to do with how close an object is to another. In proximity query, the use of geometric distance to define the neighborhoods of one or more target locations. It has to do with the length between one object and another within an environment which in this case was 200m proximity between objects. This query is done or performed to determine the distance of petrol station located in this project area from the residential area, it was discovered that some of the petrol stations are located very close to a residential area. This query was performed to determine how many government and community facilities in the range of 50 meters from the major road from the Muyi line and Jattu garage as specified. With the simple query performed we discovered that Auchu is full of different denominations of church, a total of 15 different churches were captured with our project area, and most of the churches are within the range of 50 meters and below from the secondary and major roads respectively. Fig.5a-e shows the query outcomes over the study area.

The proximity query showed the hotels that are within a distance of 200 m to major roads. The result revealed that Hossana Resort and Suit, GNL Rental Hotel, Hotel De James, and Gabby Guest House are within the specified distance from the major road which was strategically and well located so as to serve the purpose of visitors that comes to the town, which gave easy access to a place for them to lodge if they need to pass the night.

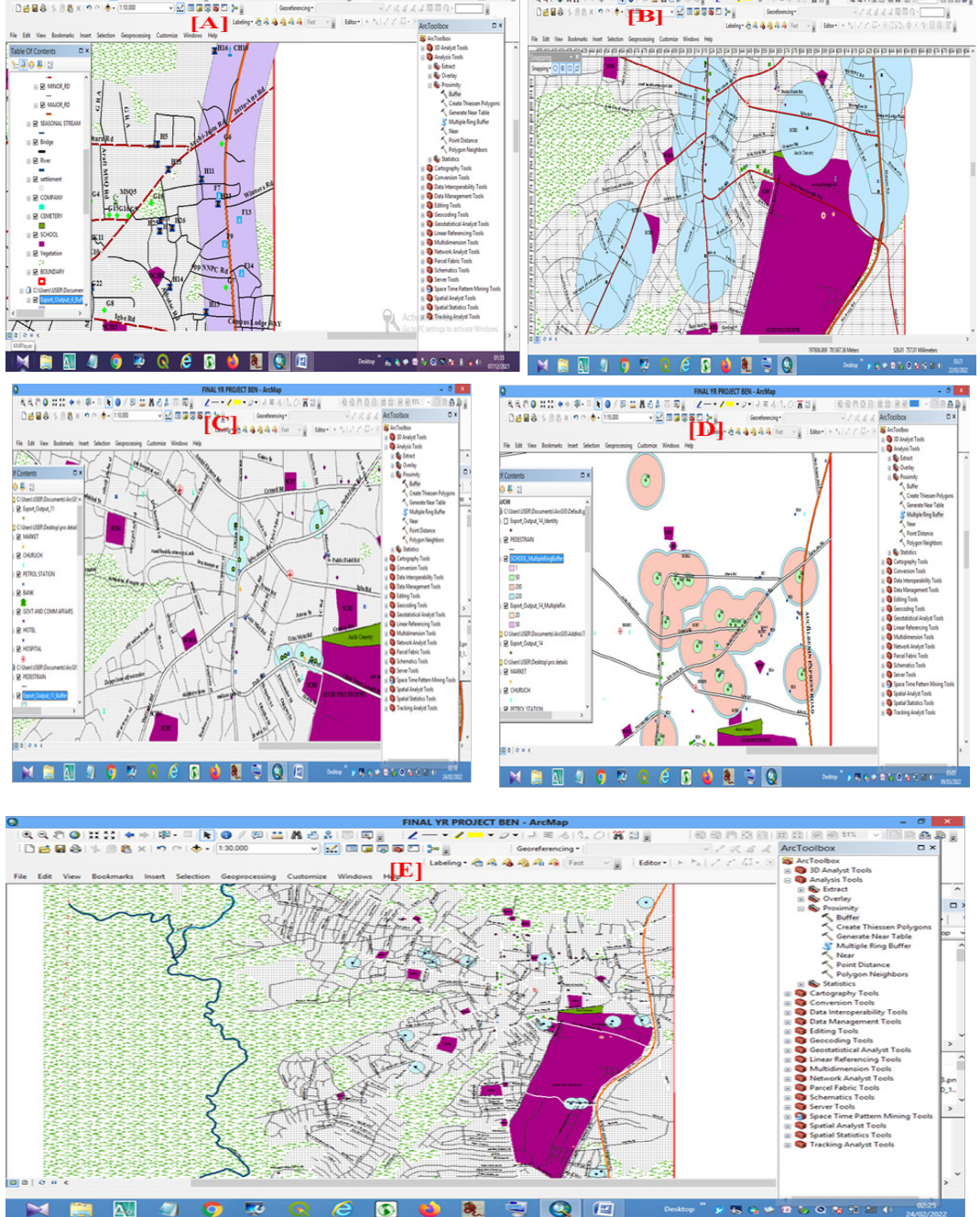


Figure 5. Proximity query of hotel within 200 metres away from major road (a), Query on petrol station in part of Auchi (b), Query of banks in Auchi (c), Query on government and community facility (d), and Query on church (e).

4. Conclusion

Concern with the idea of producing and up to date street guide map in Auchi and achieving it was indeed a huge success. This newly built map can serve as a base map for other applications such as navigation, urban planning, and development, traffic studies and control, crime monitoring, utility management, etc. With the simple query performed, the map can equally be used for business feasibility studies.

Acknowledgment. The authors equally contributed to this study. The also thank Engr.(Dr.) Olotu Yahaya for his technical contributions and review.

References

- [1] Abbas K., Adama U., Koje P., Street Mapping of Kaduna Metropolis, Using Remotely Sensed Data and GIS Technique, *International Journal of Engineering Research and Technology*, 3, 2010, pp. 1794-1799.
- [2] Addai O, Poku-Gynamfi, O., Gyanbibi L., Street guide map using GIS and Ghana Land Administration project (LAP), *International Journal of Geographic Information Systems*, 8, 2011, pp. 300-310.
- [3] Fastor, R., Adewoyi, W., Mohammed, O., Kolawole Y., Street guide map using Remote sensing data and geographic information system technique, *Greener Journal of Environmental Management and Public Safety*, 5(2). 2016, 033-040.
- [4] Fasote U., Halilu M., Carried out street guide map of Ijero-Ekiti State with an integrated and conceptualized approach consisting of digital image processing and Cartographic procedures, *Greener Journal of Environmental Management and Public Safety*, 5(2), 2016, 030-037.
- [5] Hajara A., Garba V.N., Ojeh E., Bishop E., Ayeni U., The Use of GIS and Google Earth Image for Mapping of Taraba State University Campus, *Asian Journal of Geographical Research*, 1(1) 2018, 1-16, Article no. AJGR.40306.
- [6] Idowu O., Taofik L., Ogunyemi, O., Oladimeje, K., Olayemi H., Street Mapping of Ife Metropolis, Osun State, Nigeria, *Journal of Geographic Information System*, 8, 2016, pp. 387-395.
- [7] Igbokwe P. Itoro U., Joel P., Application of GIS and Remote Sensing approach for analysis of Auchi Urban Street Network of Edo State Nigeria, *Asian Journal of Geographical Research*, 2008, pp. 1-16.
- [8] Kolawole C., Alaga P., Oloko A., Carried out a street guide map of Ile Ife metropolis the network intends to produce a street map that will ease navigation within the area, *Photogrammetric Engineering and Remote Sensing*, 53, 2016, pp. 1417-1421.

- [9] Olatunde M.B., Omoniye O., Olatude F.O., Production of street guide map of Igarra Township, Edo state, Nigeria, *Research Journal of Applied Sciences, Engineering and Technology*, 2, 2016, pp. 191-197.
- [10] Raymon G., Balogun Y., Clement P., Production of Street Guide Map of part of Kwale town in Nigeria West Local Government Area of Delta State. *Journal of Environmental Sciences and Resource Management*, 2, 2010, pp. 56-64.
- [11] Sedi P., Street Guide mapping of part of Ekpoma Esan –West Local Government Area, Edo state. *International Journal of Engineering Research and Technology*, 3, 2013, pp. 1792-1799.
- [12] Udoh P., Jude O., Production of Revised Street Map of Uyo Urban Area. Nigeria, *Research Journal of Applied Sciences, Engineering and Technology*, 2, 2014, pp. 191-197.
- [13] Nnam V.C., Ekpote B.O., Anejionu O.C.D., Improving Street Guide Mapping of Enugu South Urban Area through Computer Aided Cartography a Journal present at FIG Week 20, 612, Rome, Italy-10 May 2021.

Addresses:

- Michael Banji Olatunde, Auchi Polytechnic, Department of Surveying & Geoinformatics, Auchi, Edo State, Nigeria
banjiolatud@gmail.com
(*corresponding author)
- Faith Ozofu Olatunde, Auchi Polytechnic, Department of Surveying & Geoinformatics, Auchi, Edo State, Nigeria
- Henry Eronmosele Oriakhi, Edo State Polytechnic, Department of Surveying & Geoinformatics, Usen

Control Extension Using Global Navigation Satellite System Receivers in Auchi, Nigeria

Michael Banji Olatunde*, Faith Ozofu Olatunde,
Iyotor Thaddeus Eshiemokhai, Hussani Idris

Abstract. *Auchi is the headquarters of Etsako West Local Government Area of Edo State, which is opening up with many developments and diverse construction activities taking place. It was observed that there are limited numbers of reliable survey controls to check these activities; hence the study focuses on second order control (Class 1) extension along the New Auchi- Igarra road to the Polytechnic (Up Iyekhei) road through the Water Board. The controls serve as references for engineering, topographic, cadastral, and route survey projects in and around the project location. An in-situ check using point positioning technique revealed that they were in good condition for use (FGP/EDY072, FGP/EDY089, and FGP/EDY090) were used for extension, and an in-situ check using point positioning technique revealed that they were in good condition for A total of 15 points (AME 001 to AME 015) were observed in static mode with Hi Target GNSS dual frequency receivers and were post processed based on the Clark 1880 spheroid while the total length was 8.503km (8503m). The interval of the new controls ranged between 58.30m and 1569.76m; which is aimed at providing users within these routes a good proximity to at least three of the controls for effective usage. Not less than fifteen satellites were acquired by the GNSS receivers for every observation, and a time range of not less than 60 minutes (1 hour) was used for data acquisition at every station, with a Positional Dilution of Precision (PDOP) value that ranged between 1.1 and 1.5. The study was intended for horizontal control only, but the vertical control values were obtained as well. For easy future location of the new extended controls, a proper description of the controls was carried and recorded in appropriate field sheets. The entire survey was carried out according to specification and is fit to be used for subsequent lower order surveys within the project area.*

Keywords: *first order controls, in-situ check, control point, point positioning technique, static mode, GNSS dual frequency receivers, dilution of Precision (DOP), Auchi*



1. Introduction

Surveying has been an essential element in the development of the human environment since the beginning of recorded history (5000 years ago). It is required in the planning and execution of nearly every form of construction. Its most familiar modern use is in the fields of transportation, building and construction, communication, mapping, and the definition of legal boundaries for land ownership (as in cadastral surveying), etc. (Ghilani & Wolf, 2012). Surveying is defined as the art, science, and technology of measuring the relative position of natural and man-made features on, above, or below the earth's surface and the presentation of such processed data (information) graphically or numerically (Agor, 2012). Surveying could also be seen as the technique and science of accurately determining the terrestrial or three-dimensional positions of points, and the distances and angles between them. These points are usually on, above, or below the earth's surface, and they are used to establish land maps and boundaries, for individuals, corporate bodies, or for government purposes, as in the case of public and private surveys (Ajibade, 1997).

Uren and Price (2001) defined a control survey as the survey that provides a rigid framework of fixing points on which a detailed survey is based, or which are used as the reference points for setting out work. A control survey (on which this study is centered) is a class of survey that establishes the positions of points with a high degree of accuracy in order to support activities such as mapping and GIS, property boundary surveys, construction projects, etc. (Dashe 1987). Every survey depends on established frame networks or controls. An established control network is a network of monumented control points that can provide a unified coordinate base for survey and other related activities within a given area. These control points can also be referred to as coordinated and correlated horizontal and vertical position data, forming a framework whose surveys are adjusted. The purpose of control survey or control extension generally, is to establish a network of points on the ground that are sufficiently accurate to provide control for any survey project, including boundary, route, locative or construction, planimetry or photogrammetry (Ezeigbo, 1990).

These controls are classified into four orders: zero, first, second, and third (or tertiary). The second and third orders can be sub-divided into classes I and II, respectively. The second order controls are controls which are usually used to control precise engineering surveys, urban control, multi-purpose control densification, inter-cadastral densification in urban areas, and extension and supplementary controls (*Specifications for Geodetic Surveys in Nigeria, 2007*). Control surveys established precise horizontal and vertical positions of reference monuments (Ezeigbo, 1990). These serve as the basis for originating or checking subordinate surveys. Most of the time, these control points are not easily available for surveyors and engineers within a closer range (a distance within 10 km range) to enable them to carry out survey jobs. They are either destroyed by farmers or engineers during construction,

or they are not initially available, necessitating control extension. The various methods for control extension are triangulation, trilateration, traversing, and the Global Navigation Satellite System (GNSS) (Fasehun, 2014). The method adopted for any survey work is subject to the available instruments, time, and accuracy required.

The principle of the GNSS/Global Positioning System (GPS) is based on the fact that if the orbit of a satellite is accurately known, the position of a receiver on earth can be determined using satellite positions. A GPS receiver calculates distances to satellites as a function of the amount of time it takes for the satellite signals to reach the ground/receiver position. To calculate it, the receiver must be able to determine precisely when the signal was transmitted and when it was received. The satellites are equipped with extremely accurate automatic clocks, so the firmness of transmission is always known. GPS employs the principle of trilateration to calculate the coordinates of positions at or near the earth's surface. Trilateration is based on the trigonometric law that if the distances of all three sides of a triangle are known, then the interior angles can be calculated. As a result, this study employs the established controls for the second order (Class I) using GNSS instrumentation along Tonny Annenih road to Otaru road via Water Board and connects the new Auchi Igarra road, Auchi, Edo State.

2. Materials and Methods

This study used primary data sets which were obtained through observations from the DGPS instrument. To complement the observation, necessary information such as the location of the existing control points used and their coordinates (Northing, Easting, and Height) were obtained from the Ministry of Land and Survey, Benin City, as shown in Table 1.

Table 1. Coordinates and Locations of the control points used

| Pillar Number | Easting (m) | Northing (m) | Height(m) | Location |
|---------------|-------------|--------------|-----------|-------------------------------------|
| FGP/EDY/072 | 198513.794 | 782022.800 | 199.974 | Akpekpe Model Primary School, Auchi |
| FGP/EDY/089 | 205874.631 | 777157.276 | 96.922 | Iyerekhu Primary School, Iyerekhu |
| FGP/EDY/090 | 209318.674 | 772977.317 | 61.189 | Udame Primary Schoo |

Source: Ministry of Land and Survey, Benin-City, 2020

Also, the appropriate instrument was used for the observation pattern and the time to capture data per station was carefully taught out. Necessary arrangements were made concerning the molding of pillars (beacons) to be buried at each observation

station. Observations were planned to be made for at least one hour per station. A Hi-Target GNSS receiver instrument, which has the capability of tracking both GPS and GLONNAS data, was chosen. The following precautions were taken in deciding the most suitable positions for the stations:

- i. The site should be located such that local settlement along the project area has good proximity to any three controls for effective usage;
- ii. The ground's stability; and
- iii. Excellent horizon for GNSS observation

According to specifications, concrete beacons measuring 150cm in length and 40cm by 40cm in section were cast in-situ at each. The following instruments point as presented in Figure 1. After burying the pillars, they were numbered serially, starting from AME001 to AME015 (AME represents Auchi Mapping Extension).

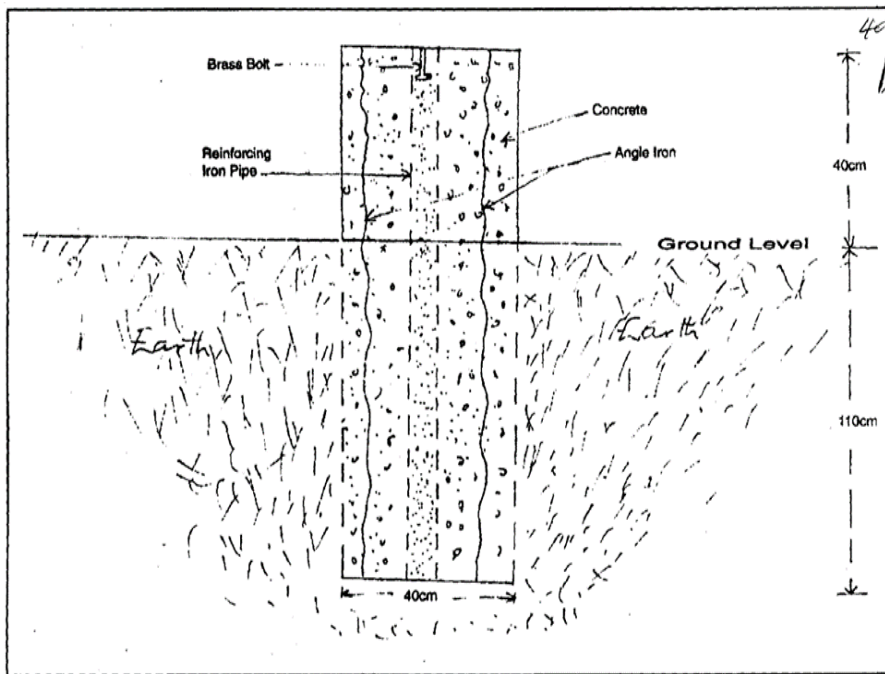


Figure 1. Specification for Secondary Control Beacon
Source: Specifications for Geodetic Surveys in Nigeria (SURCON, 2007)

2.1. Material selection

The following tools, materials and softwares applications were used to carry out the project:

- i. Hi Target Double Frequency Differential GPS (Master and Rover Receivers) and Accessories (H32 series GNSS RT1)
- ii. Tripod
- iii. Hammer,
- iv. Field Book
- v. Cutlasses
- vi. Iron rods
- vii. Toyota Highlander jeep
- viii. Shovel, trowel and beacon box
- ix. Hand held (Garmin GPS)
- x. Linen tape
- xi. Prismatic Compass

2.1.1. Selected software applications

The following softwares were selected:

- i. Hi-Target Geomatics Office (HGO) and
- ii. GEOCAL

2.1.2. Instrument Used (Hi-Target Receiver) Configuration

The instrument used, Hi-Target DGPS receiver was configured in such a way that is most appropriate for the project at hand. The configuration is listed below:

- | | |
|------------------------------------|-----------------------|
| i. Logging device- | Data-Logger (Qmini H) |
| ii. Antenna type- | Hi-Target H32 |
| iii. Survey mode- | Static |
| iv. Logging Interval- | Five seconds (5 sec) |
| v. Satellite cut of angle- | Fifteen degrees (15°) |
| vi. Antenna measurement reference- | Top of Antenna |
| vii. Time zone- | GMT + 1 Hour |

2.2. Data Acquisition using Static Relative Positioning

For the highest accuracy (geodetic control surveys), static GNSS procedures are used (Ghilani, 2008). The procedure is such that the base station remained continuously on a known station while the roving station was moved from one unknown

station to the other. The instrument, Hi-Target GNSS receiver, and its accessories and other items were taken to the base/reference station as described by Agor (2012), Ajibade (1997), and Dashe (1987). The receiver (reference) was centered and leveled properly (temporary adjustments) on the base station (FGP/EDY072). Then the slant height of the antennae was measured from the center of the bumper of the receiver to the top of the iron rod (which was 1.960m), which defines the center of the base station. Then the station ID (FGP/EDY072), instrument serial number, interval of record time (5 secs) and cut off angle (15^0) were inputted into the data logger. Then the instrument was turned on and was connected to the data logger via in-built bluetooth. It was observed that PDOP was 1.1 and the number of satellites available (GPS and GLONASS satellites) was 17. The instrument (rover) was configured in the same way and set up on AME001. At this station, the slant height was measured to be 1.80m. The instrument possessed the capacity to pick signals from L1, L2, Lc, Ln, Lw, and L1L2 frequencies. Typically, an observation session for a static method of positioning for a dual frequency receiver is to be about 20 min + 2 min/km (Ghilani, 2008). The distance from the base to the points to be positioned ranges between 666.483m and 3415.155m. But due to the capacity of the instrument (the number of channels includes L1, L2, L1L2, LC, Ln and Lw) and the ability to track both GPS and GLONASS satellites, therefore, for this study, the roving receiver was allowed to pick observational and navigational data for a minimum of one hour at an epoch rate of 5 seconds. These procedures were repeated for all the points to be coordinated (Fig 2). Due to the number of stations to be coordinated (15) and the time spent on each station (1 hour plus), the entire data acquisition exercise lasted for three days (14th to 16th of January 2022) and the above explained procedures were observed on all the points established.

Note: 1 hour or more is sufficient for GNSS data acquisition at respective stations since the longest vector line from the base station FGP/EDY 072 was 3415.155m, a minimum of 15 satellites was observed and there was increased strength in satellite geometry since PDOP varies from 1.1 to 1.5 during observation (PDOP less than 3 is ideal).

2.2.1. Precautions taken During Observation

Among the precautions taken to ensure successful data acquisition were the following:

- i. Slant heights of station above station mark was carefully measured before and after data collection at respective stations and recorded appropriately;
- ii. Antenna set up with tribrach on tripod were carefully centered and leveled over station mark before data collection at respective stations;
- iii. Time for observation on each unknown stations not less than 1 hour.



Figure 2. Hi-Target instrument set-up on one of the stations

3. Results and Discussion

3.1. Data Processing and Adjustment

Data downloading is the process of transferring the observed observational and navigational data (ON data) from the memory of the Hi-Target instrument into a computer (Laptop) for further preprocessing, processing, and data analysis. For efficient data management, a folder was created for each day's observation (the observation was done for three days (14th to 16th of January 2022)) and the raw data from each receiver was downloaded into separate folders and saved on the computer's desktop. The data was later sorted out by adding reference/base data with the rover's data for each day. Within Hi-Target Geomatics Office (HGO) software, there are provisions to import GNSS observation files. The observation files contained the phase and other observables, the broadcast ephemeris, and site data consisting of station identifiers and antenna height. Then, the software was launched, and, through the navigation field, a new project was created and okayed. The coordinates' parameters/properties for the new project were set through the navigation field, North Africa was selected, and then Nigeria was picked. Zone 32 was selected via the navigation field while WGS 84 was chosen as the reference ellipsoid. The target ellipsoid was selected as Clarke in 1880. Then the files containing the

GNSS raw data files in a folder on the desktop were selected, clicked and all files opened, and then the static observation file for the first day (14th) was selected and imported into the software (HGO) environment. The HGO software then automatically generated the baseline, but this was inverted to reflect that the observation was made from control point FGP/EDY072 to the unknown points. To process the observed data, the mask angle was increased from 150 to 250, and various frequency channels available in the instrument processing software, such as L1L2, L1, L2, LC, and others, were used until all of the data was processed and passed using the Process Baseline button in the navigation field (Fig. 3). At first, the data observed was edited by checking the data plot, and observations that were lost were filtered out before processing the data. This is the preprocessing stage.

The essence of this stage is to analyze the data observed for internal consistency and to eliminate possible blunders. After all the points were passed, the slant height of the antenna as measured on the field (2.0068) for the base was entered. Likewise, the corresponding heights for other points (1.9117) were equally entered. In order to carry out network adjustment, FGP/EDY072 (the control point used on the field) was edited by right clicking on it and the *Set as Control Point* item from a dialogue box was selected. The coordinates of the control point as observed by the receiver were then edited by inputting its register value (198513.794 mE, 782022.800mN) and also the height (199.974m). Adjust the report options in the navigation field so that text file format is selected. Thereafter, the data is post processed and adjusted, and the report is generated automatically. These processes were carried out on the data observed for the three days (14th to 16th), while the slant height of the antenna for base station and rover stations was inputted accordingly and reports were generated. The coordinates of the new control points were tabulated in geographic and rectangular systems. The coordinates of the newly established controls were later converted into Nigeria Transverse Mercator adopting Minna Datum using GEOCAL software (Table 2).

The issue of standards is of paramount importance to surveyors and, with the ever increasing advancement in technology, surveys have become faster and milestone successes have been achieved. Standards are clear statements of the requirements of acceptable surveys. Fortunately, there are various indicators for determining the quality of GNSS surveys and the processing software. Therefore, after network adjustment, the misclosure ratio for each baseline vector was computed in order to ascertain the accuracy of each baseline (Table 3). The misclosure ratios computed above imply the extremely high accuracies that are now possible with GNSS receivers. The misclosure also indicates that the result is within the acceptable limit (Second order Horizontal Controls Class 1 Accuracy is 1:50,000; *Specifications for Geodetic Surveys in Nigeria, SURCON, 2007*). Also, bearing and distance between the control points were computed as additional information for control location (Table 4).

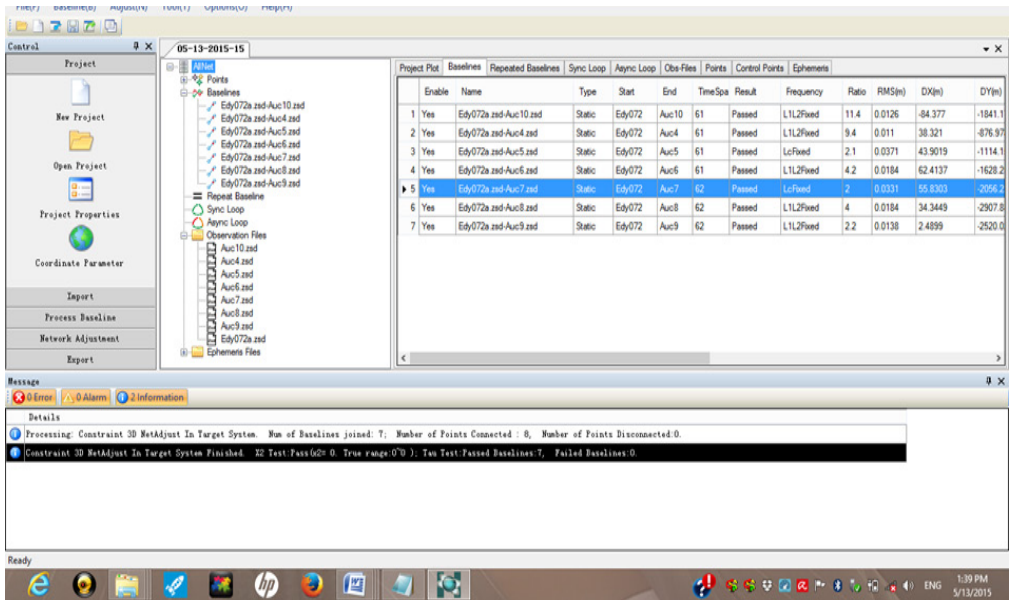


Figure 3. Processed Data for Day 2 before Adjustment (Result: Passed)

Table 2. Summary of the Processed Coordinates of the Newly Established Controls

| Station | UTM (m) | | NTM (m) | | Geodetic (Deg) | | Height (m) |
|---------|------------|------------|------------|------------|-----------------|-----------------|------------|
| | Easting | Northing | Easting | Northing | Longitude | Latitude | |
| AME001 | 198953.555 | 781448.493 | 424811.120 | 339006.190 | 06° 16' 32.61"E | 07° 03' 40.73"N | 230.093 |
| AME002 | 198909.103 | 781486.209 | 424766.637 | 339043.849 | 06° 16' 31.16"E | 07° 03' 41.95"N | 229.298 |
| AME003 | 198846.929 | 781481.335 | 424704.482 | 339038.910 | 06° 16' 29.13"E | 07° 03' 41.78"N | 228.301 |
| AME004 | 197639.963 | 782485.020 | 423496.706 | 340041.075 | 06° 15' 49.64"E | 07° 04' 14.20"N | 198.532 |
| AME005 | 197404.182 | 782614.411 | 423260.844 | 340170.170 | 06° 15' 41.94"E | 07° 04' 18.36"N | 193.921 |
| AME006 | 196892.982 | 782990.465 | 422749.357 | 340545.626 | 06° 15' 25.22"E | 07° 04' 30.50"N | 202.247 |

| Station | UTM (m) | | NTM (m) | | Geodetic (Deg) | | Height (m) |
|---------|------------|------------|------------|------------|-----------------|-----------------|------------|
| | Easting | Northing | Easting | Northing | Longitude | Latitude | |
| AME007 | 196469.811 | 783303.868 | 422325.459 | 340858.318 | 06°15' 11.37"E | 07°04' 40.61"N | 187.239 |
| AME008 | 195628.160 | 783849.361 | 421483.878 | 341402.948 | 06° 14' 43.87"E | 07° 04' 58.20"N | 139.397 |
| AME009 | 196017.628 | 783874.940 | 421873.251 | 341428.951 | 06° 14' 56.55"E | 07° 04' 59.10"N | 153.478 |
| AME010 | 196702.919 | 783962.497 | 422558.282 | 341517.208 | 06° 15' 18.85"E | 07° 05' 02.08"N | 152.330 |
| AME011 | 197608.403 | 784045.197 | 423463.472 | 341600.867 | 06° 15' 48.32"E | 07° 05' 04.95"N | 166.203 |
| AME012 | 198103.070 | 784109.626 | 341665.815 | 423957.959 | 06° 16' 04.41"E | 07° 05' 07.14"N | 183.786 |
| AME013 | 199348.363 | 784005.538 | 341563.093 | 425203.087 | 06° 16' 44.98"E | 07° 05' 03.99"N | 242.877 |
| AME014 | 199419.882 | 783785.003 | 341342.684 | 425274.828 | 06° 16' 47.35"E | 07° 04' 56.83"N | 246.204 |
| AME015 | 199448.609 | 783570.131 | 341127.891 | 425303.781 | 06° 16' 48.33"E | 07° 04' 49.84"N | 245.549 |

Table 3. Base Vector Analysis

| Base Vector | X Misclosure (sX) (m) | Y Misclosure (sY) (m) | Length (m) | Misclosure Ratio | Parts Per Million (ppm) |
|-----------------|-----------------------|-----------------------|------------|------------------|-------------------------|
| Edy072 – AME001 | 0.0022 | 0.0014 | 723.4647 | 1:277,000 | 4ppm |
| Edy072 – AME002 | 0.0021 | 0.0007 | 666.6664 | 1:301,000 | 3ppm |
| Edy072 – AME003 | 0.0017 | 0.0009 | 635.9253 | 1:331,000 | 3ppm |
| Edy072 – AME004 | 0.0013 | 0.0009 | 987.8608 | 1:625,000 | 2ppm |
| Edy072 – AME005 | 0.0057 | 0.0039 | 1256.6114 | 1:182,000 | 5ppm |
| Edy072 – AME006 | 0.005 | 0.0022 | 1886.3832 | 1:345,000 | 3ppm |
| Edy072 – AME007 | 0.0071 | 0.0034 | 2410.6013 | 1:306,000 | 4ppm |

| Base Vector | X Misclosure (sX) (m) | Y Misclosure (sY) (m) | Length (m) | Misclosure Ratio | Parts Per Million (ppm) |
|--------------------|----------------------------------|----------------------------------|-----------------------|-----------------------------|------------------------------------|
| Edy072 – AME008 | 0.0034 | 0.0026 | 3413.2613 | 1:797,000 | 1ppm |
| Edy072 – AME009 | 0.0029 | 0.0014 | 3106.4107 | 1:965,000 | 1ppm |
| Edy072 – AME010 | 0.0022 | 0.0009 | 2652.1795 | 1:1,116,000 | 0.9ppm |
| Edy072 – AME011 | 0.0057 | 0.0027 | 2214.5093 | 1:351,000 | 3ppm |
| Edy072 – AME012 | 0.0064 | 0.0046 | 2125.4335 | 1:270,000 | 4ppm |
| Edy072 – AME013 | 0.0101 | 0.0028 | 2817.1727 | 1:269,000 | 4ppm |
| Edy072 – AME014 | 0.0068 | 0.0049 | 1980.6783 | 1:236,000 | 4ppm |
| Edy072 – AME015 | 0.007 | 0.0044 | 1807.689 | 1:219,000 | 5ppm |
| Edy072 – Edy089 | 0.0034 | 0.0013 | 8818.2487 | 1:2,423,000 | 0.4ppm |

Source: Authors' field work, 2022

Table 4. Bearing and Distance between Control Points

| From Station | Bearing | | | Distance (m) | To Station |
|---------------------|----------------|----------|----------|---------------------|-------------------|
| | ° | ' | “ | | |
| AME 001 | 310 | 18 | 48 | 58.296 | AME 002 |
| AME 002 | 265 | 31 | 03 | 62.365 | AME 003 |
| AME 003 | 309 | 44 | 46 | 1569.761 | AME 004 |
| AME 004 | 298 | 45 | 25 | 268.951 | AME 005 |
| AME 005 | 306 | 20 | 22 | 634.620 | AME 006 |
| AME 006 | 306 | 31 | 26 | 526.588 | AME 007 |
| AME 007 | 302 | 56 | 53 | 1002.965 | AME 008 |
| AME 008 | 086 | 14 | 33 | 390.307 | AME 009 |
| AME 009 | 082 | 43 | 08 | 690.862 | AME 010 |

| From Station | Bearing | | | Distance (m) | To Station |
|--------------|---------|----|----|--------------|------------|
| | 0 | ' | “ | | |
| AME 010 | 084 | 46 | 53 | 909.253 | AME 011 |
| AME 011 | 082 | 31 | 03 | 498.734 | AME 012 |
| AME 012 | 094 | 42 | 58 | 1249.358 | AME 013 |
| AME 013 | 162 | 01 | 56 | 231.842 | AME 014 |
| AME 014 | 172 | 23 | 06 | 216.784 | AME 015 |

Source: Authors' field work, 2022

3. Conclusion

A total of 15 new stations were established, covering a total length of 8.503km. Observations from three (3) different stations over the course of three (3) days. Accuracy after adjustment ranges between 1:182,000 and 1: 1,115,780. The following recommendations are hereby suggested:

- i. Although the established control points can now be used as connections for other lower order survey work, more control points must be established around town to ensure completeness.
- ii. There is a need for public enlightenment on the usefulness of the controls for the safety of the newly established controls.
- iii. The National Horizontal Control Accuracy Standard as detailed in *SURCON Specifications for Geodetic Surveys in Nigeria (2007, pg 6)* needs to be reviewed in the light of modern high-accurate GNSS receivers as already done in some other countries.

Acknowledgment. The authors equally contributed to this study. The also thank Engr.(Dr.) Olotu Yahaya for his technical contributions and review.

References

- [1] Agor R., *Surveying and Levelling*. 11th Ed. Delhi, 2012.
- [2] Ajibade S.A., Horizontal and Vertical Controls for the Study and Monitoring of Structures. *32nd Annual General Meeting at Uyo, Akwa Ibom State*. 6–9 May, 1997, pp. 17–20.
- [3] Ghilani C.D., Wolf P.R., *Elementary Surveying: An Introduction to Geomatics*, USA, Pearson Education, Inc., Pearson Prentice Hall, 2012.

- [4] Ezeigbo C.U., *Nigerian Geodetic Network*, The Control Question in Map Maker, vol. 1, March 1990, pp. 83.
- [5] Fasehun O., (2014): Second Order GPS Control Densification within OyoMropolis. <https://academic.edu/31883391/secondordergpscontroldensificationwithinOyometropolis> (accessed 30th December. 2021).
- [6] SURCON, *Specifications for Geodetic Surveys in Nigeria*, Lagos, Nigeria, 2007.
- [7] Uren J., Price W.F., *Surveying and Mapping*, 3rd edition, Macmillan, 2001.

Addresses:

- Michael Banji Olatunde, Auchi Polytechnic, Department of Surveying & Geoinformatics, Auchi, Edo State, Nigeria
banjiolatud@gmail.com
(* corresponding author)
- Faith Ozofu Olatunde, Auchi Polytechnic, Department of Surveying & Geoinformatics, Auchi, Edo State, Nigeria
- Iyotor Thaddeus Eshiemokhai, Auchi Polytechnic, Department of Surveying & Geoinformatics, Auchi, Edo State, Nigeria
- Hussani Idris, Auchi Polytechnic, Auchi, Department of Surveying & Geoinformatics, Edo State, Nigeria

Re-calibration of an automatic evaporimeter

Yahaya Olotu*, Livinus Apebuamhe Izah, Moses Eromosele Eseigbe,
Reuben Ishiekwene, John Friday Ogbodo

Abstract. *A set of pre-programmed sensors and transducers, including 0.71 EAP, carbon resistor, semi-carbon conductor, IN4007, and lighting diode-4v, 60 mm amp, were used to develop and build an automatic evaporimeter for automating/self-recording evaporation rate. 10 ILP values, 8 FLP values, 150.4 and 12.3 refractive values, respectively, were used to design the evaporimeter's operating principle. The results of equipment calibration utilizing various statistical validations of voltage, calibration index, and refractive index values demonstrate high agreement with R^2 values of 0.999, 0.869, and 16.4 correspondingly. Every level (0.1 cm) of the instrument's time response to a step change in the water level caused by evaporation in the pan was calibrated. The voltage (v) was 225.6v, the highest evaporation value was 0.3 cm, and the refractive index was 15.0. With $R^2 = 0.9718$ and 0.9635, statistical validation shows that there was a significant correlation between the initial evaporation reading (IER) and the final evaporation reading (FER).*

Keywords: *Sensitivity, Water level, Calibration, Sensor, Evaporimeter*

1. Introduction

The rate of evaporation, a crucial component of climate, is influenced by the weather. Agro-meteorological research is crucial for agricultural, environmental, and water resource modeling and requires accurate measurements of environmental variables such as rainfall, runoff, soil moisture, evaporation rates, and minimum and maximum temperatures. There are now just a few techniques for calculating evaporation rates. Sadly, the three reliable direct measurement techniques weighing lysimeter, Bowen ratio, and eddy flux instrumentation are unreliable for routinely measuring evaporation at meteorological enclosures. The evaporation pan has been suggested as the standard instrument for calculating crop water use by the World Meteorological Organization (WMO). The "class A" evaporation pan and the "sunken Colorado pan" are the two pans that are most well-known (Stanhill and Cohen, 2001). By measuring the evaporation loss from a water source and using empirical coefficients to tie pan



evaporation to reference evapotranspiration (ET_o), the pan has successfully been used to estimate reference evapotranspiration (Stanhill and Cohen, 2001). However, insufficient coverage and inconsistent instrumentation continue to hamper routine evaporation monitoring in Nigeria.

It is demonstrated that in humid areas, measurements of "class A" pan evaporation were accurate estimates of evapotranspiration when soil water was not impeding plant growth (Parmele and McGuinness, 2004). Evaporation from water surfaces or water bodies is rarely directly observed due to its nature, with the exception of relatively brief periods of time (Jones, 1992). Most frequently, evaporation from water is calculated indirectly using one or more procedures. These include mass transfer, water balance, energy balance, pan coefficients determined via pan evaporation, and combinations of other approaches (Peterson *et al.*, 1995; Robock *et al.*, 2000). The availability of data, the type or size of the water body, and the needed precision of the projected evaporation all play significant roles in determining the "optimal" technique to utilize for a given computation.

Evaporation from a standard pan, such as the "class A" pan, is measured, and the evaporation is then multiplied by a co-efficient, which is the most widely used technique in the world for measuring evaporation from tiny, shallow bodies of water. Irrigation scheduling has recently seen considerable advancements thanks to precision agricultural technology, particularly in industrialized nations where equipment for continuous climate monitoring is now available to help farmers decide how much water to apply and when to apply it. Regular measurement of evaporation rates from an automated class A tool for scheduling irrigation, an evaporation pan can be used to calculate reference evapotranspiration (Stanhill and Cohen, 2001; Robock *et al.*, 2000; Phene, 1992).

However, given Africa's cash-strapped economic realities, investing in such pricey automated systems is riskier. As a result, in this region of the world, little to no attention has been paid to using electronic level sensors to automate pan evaporimeters (Africa). The goal of this research is to develop a system for measuring evaporation that is more precise and to improve estimates of agricultural water demand. A real-time irrigation scheduling option will be made possible by the availability of an automated system, which will reduce the likelihood of human mistake in the measurement of evaporation from the pan evaporimeter. As a result, the goal of this project is to design and calibrate a low-cost electronic water level measurement device for use with class "A" pans.

2. Materials and Methods

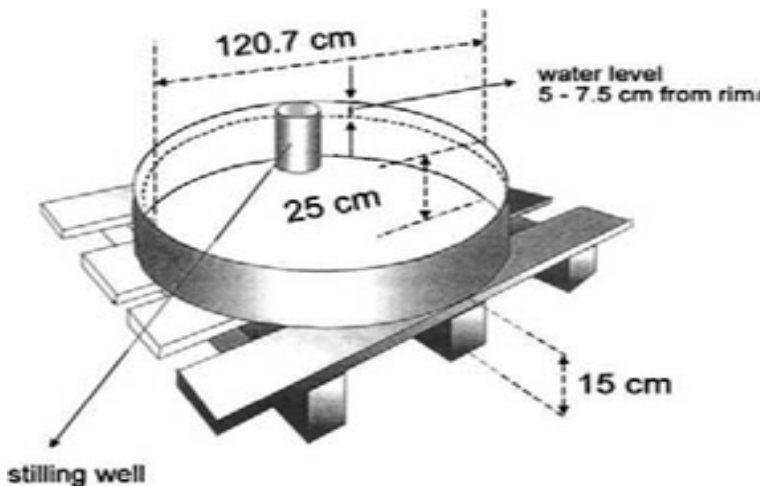
2.1. Description of class A pan

A Class A evaporation pan is cylindrical, measuring around 121 cm in diameter and 25 cm deep. The typical pan had a bottom that was 15 cm above the ground

and was constructed of twenty-two (22) gauged galvanized metal sheets put on an open frame (Peterson *et al.*, 1995; Plummer *et al.*, 1995). The cylindrical United States Class A pan measures 120.7 cm in diameter and 25.4 cm deep. In order to allow air to flow underneath the pan, maintain the bottom above the level of standing water during wet weather, and make it easier to inspect the base of the pan, the bottom of the pan is elevated 3 to 5 cm above the ground level on an open-frame wooden platform. The pan is typically left unpainted and is made of 0.8 mm of galvanized iron, copper, or metal. 5 cm of the pan's bottom are filled with liquid (which is known as the reference level) Fig. 2.

2.1.1. Description of developed automated Class A Evaporation Pan

The Class A evaporation pan has a diameter and depth of 101.1 cm and 20.5 cm, respectively, and is constructed from metallic sheet measuring 3 mm gauge. The Class A pan's volume was calculated to be 0.145 m³. The stilling well, which is positioned in the middle of the evaporation pan, has a diameter of 5.5 cm and a depth of 20.5 cm. The assembled pan was set on a wooden box with a smooth surface that measured 1.09 m² in surface area and 0.91 m in height. As seen in Fig. 1 and 2, an automatic water level sensor that monitors changes in the water level in the evaporation pan was mounted to the front edge of the pan.



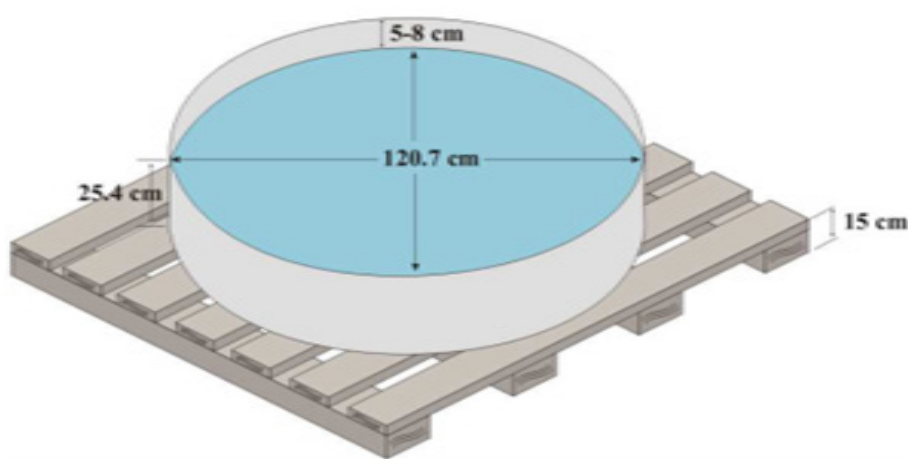


Figure 1. Class A evaporation pan

2.1.2. Instrumentation and calibration of Class A evaporation pan

The automatic evaporimeter utilizes an analog sensor that is made up of several probes (enament aluminum). The probes are in direct contact with the liquid, which causes them to change the physical variable (water) into an electrical variable when they make contact with it. The term "electrical" in this particular work refers to a change in resistance, or from 100 k Ω to infinity (Ohm), which is then utilized to activate the control line of the display unit. Each of the ten (10) units, or probes, which are made of aluminum-encased sensors, activates as soon as it touches the liquid (water). When the probe's end (a sensor or piece of aluminum) disengages from the physical variable and the control unit provides a signal to the physical variable, the process is reversed (water).

The control unit is made of:

- i. A carbon resistor (100 K Ω); and
- ii. A semi-carbon conductor diode (IN4007).

The light-emitting diodes used in the display unit (4v 60mini amp). The metallic conductor used for the sensor was particularly selected to prevent corrosion due to the aluminated conductor. One bulb turns on when the water level in the evaporating pan drops by 0.1 cm due to evaporation. The sensor has ten (10) graduations, or ten (10) metallic cables, with each one measuring 0.1 mm. Three lights illuminate in response to an evaporative reduction of 0.3 cm; each bulb has a refractive index value of 8.67 and is equivalent to 75.2 V. It has no dimensions, the index. The mechanism that lights up the bulb displays the outcome of the probe's contact with the physical factors at a specific time. The developed automatic evaporimeter is displayed on plate 1 in the feature (Class A pan).

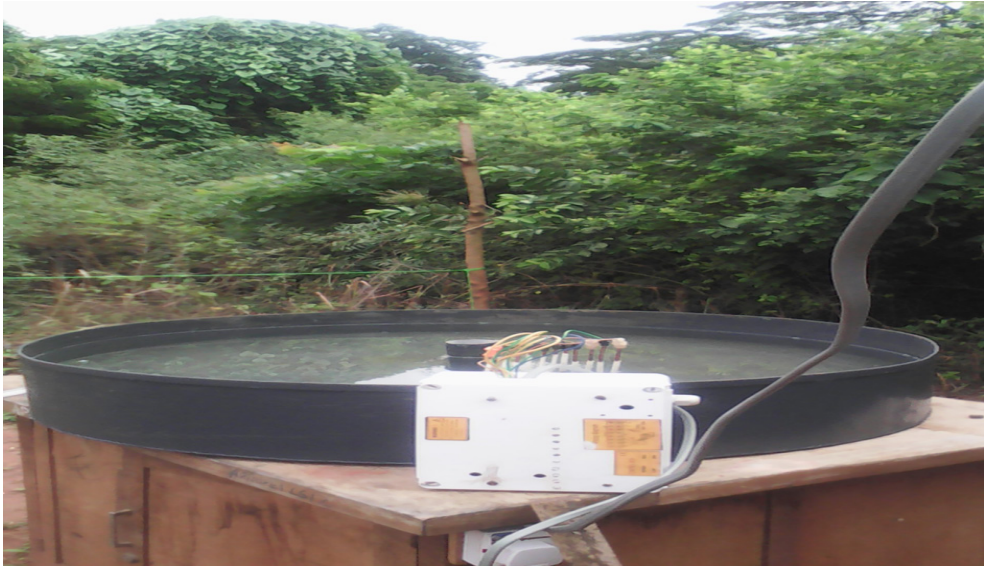


Figure 2. Developed automatic evaporimeter (Class A Evaporation pan).

2.1.3. Data analysis

The automated instrument was calibrated using the signal 1.0, power, and logarithmic components of the excel 2013 version and the generated evaporative data from the gauge and automated evaporimeters. Statistics for validation were calculated using the coefficient of determination. The estimation of the solar radiation R_s and evapotranspiration was performed using CROPWAT version 8.1. (ETo).

3. Results and Discussion

An automatic Class A evaporation pan was created and utilized to evaluate the rate of evaporation for 49 days. Voltage (v) and refractive index (RI) values were used to measure the rate of evaporation, as indicated in Table 1. As shown in Table 1, daily meteorological information including T_{max} and T_{min} , relative humidity, daylight hours, and wind speed were monitored and recorded. The maximum and minimum temperatures on the first day, June 13, 2015, were $24.5^{\circ}c$ and $34.2^{\circ}c$, respectively. These numbers were equivalent to IER, FER, and DER values of 0.2 cm at 20.9 cm and 20.7 cm, respectively. With 10 ILP, 8 FLP, 150.4, and 12.3 refractive value simulations, this analog notion of Class A evaporation was tested. The results of equipment calibration utilizing various statistical validations are displayed in Fig. 3. With $R^2 = 0.999$, 0.869, and 16.4 values of the calibration index, there was strong agreement with power and logarithm, demonstrating the instrument's sensi-

tivity to 0.1cm of evaporation. With R2 values of 0.9718 and 0.9635 for both linear and logarithmic trend analyses, respectively, statistical validation (R^2) in Fig. 4 demonstrates that there was a strong association between the initial evaporation reading (IER) and final evaporation reading (FER). It is discovered that other factors also affect evaporation rate, in addition to air temperature. On (27-06-2015), an evaporation rate of 0.3 cmday was observed at T_{min} and T_{max} temperatures of 24.50°C and 31.30°C, respectively, translating to a potential difference of 225.6V and a refractive index value of 15.0. T_{min} and T_{max} readings of 24.5 °C and 34.5°C were made on June 25, 2015, respectively. These values corresponded to an evaporation rate of 0.1 cmday, 75.2 v and a refractive value of 8.7. As a result, the accuracy of automatic Class A evaporation was determined to be ± 0.018 cm.

The crop, water, and soil model were ran using generated data from automatic evaporimeter and field meteorological measurements (CROPWAT version 8.1). The CROPWAT model's output showed that the supplied data was accurate and actual. The result in Table 1 presents that average solar radiation (Rs) and evapotranspiration (ETo) were produced. These values were 19.6MJ/m²/day and 4.12mm/day, respectively.

Note

T_{min} = Minimum temperature °C , T_{max} = Maximum temperature °C,
 $A_{ve}T$ = Average mean temperature °C ; IER= Initial evaporation value (cm),
 FER= Final evaporation value (cm), DER = Difference in evaporation values (cm);
 ILP = Initial lighting points; FLP = Final lighting points, V = Voltage output (v),
 (\sqrt{E}) = Refractive index, S.H = Sunshine hours, R.H = Relative humid

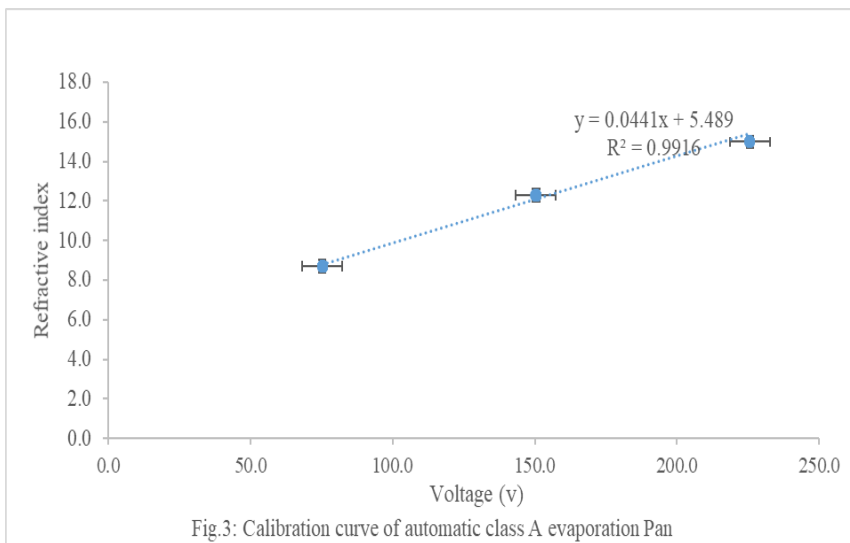


Fig.3: Calibration curve of automatic class A evaporation Pan

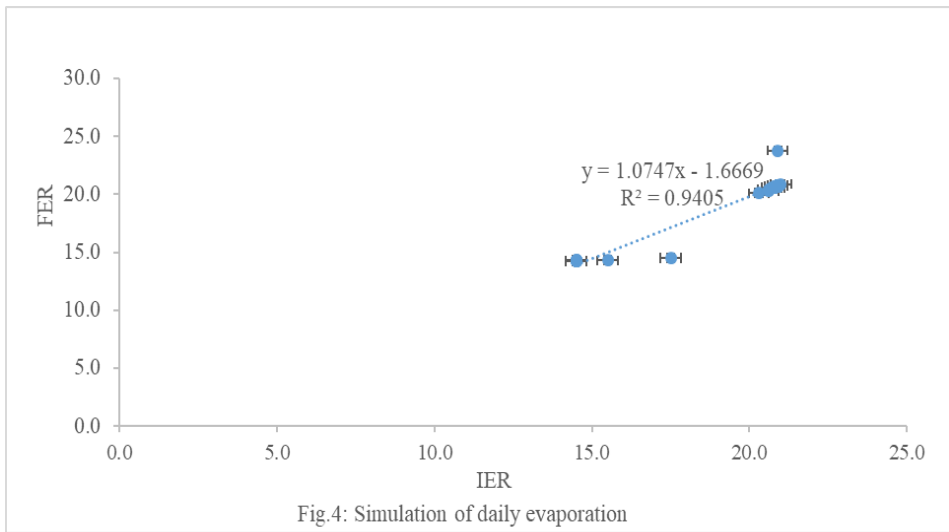


Table 1. Results of automatic Evaporimeter (Class A Pan)

| DATE | TMIN | TMAX | TMEAN | IER | FER | DER | ILP | FLP | V(v) | S.H | RH |
|----------|------|------|-------|------|------|-----|-----|-----|-------|------|------|
| 13\06\15 | 24.5 | 34.2 | 29.3 | 20.9 | 20.7 | 0.2 | 10 | 8 | 150.4 | 8 | 70.7 |
| 14\06\15 | 24.5 | 30.4 | 30.4 | 20.6 | 20.4 | 0.2 | 10 | 8 | 150.4 | 9 | 69.6 |
| 15\06\15 | 24.5 | 36.1 | 30.3 | 20.3 | 20.1 | 0.2 | 10 | 8 | 150.4 | 8 | 69.6 |
| 16\06\15 | 24.5 | 35.2 | 29.9 | 20.9 | 20.7 | 0.2 | 10 | 8 | 150.4 | 74.5 | 70.1 |
| 17\06\15 | 24.4 | 34.3 | 29.4 | 20.9 | 20.7 | 0.2 | 10 | 8 | 150.4 | 9 | 70.6 |
| 18\06\15 | 24.2 | 30.2 | 27.2 | 20.9 | 20.8 | 0.1 | 10 | 9 | 75.2 | 8.3 | 72.8 |
| 19\06\15 | 24.5 | 33.1 | 28.8 | 20.9 | 20.8 | 0.1 | 10 | 9 | 75.2 | 7 | 71.2 |
| 20\06\15 | 20.5 | 35.4 | 27.9 | 20.9 | 20.7 | 0.2 | 10 | 8 | 150.4 | 7 | 72.1 |
| 21\06\15 | 24.3 | 34.2 | 29.3 | 20.9 | 20.7 | 0.2 | 10 | 8 | 150.4 | 8 | 70.7 |
| 22\06\15 | 24.5 | 35.1 | 29.8 | 20.6 | 20.4 | 0.2 | 10 | 8 | 150.4 | 9 | 70.1 |
| 23\06\15 | 24.5 | 35.2 | 24.9 | 20.9 | 20.7 | 0.2 | 10 | 8 | 150.4 | 7.4 | 70.2 |
| 24\06\15 | 24.5 | 35 | 29.8 | 20.9 | 20.7 | 0.2 | 10 | 8 | 150.4 | 8.2 | 70.5 |
| 25\06\15 | 24.5 | 34.4 | 29.5 | 20.9 | 20.8 | 0.1 | 10 | 9 | 75.2 | 8.2 | 71.2 |
| 26\06\15 | 24.5 | 33.2 | 28.5 | 20.9 | 20.7 | 0.2 | 10 | 8 | 150.4 | 7.4 | 72.1 |
| 27\06\15 | 24.5 | 31.3 | 27.9 | 20.6 | 20.3 | 0.3 | 10 | 7 | 225.6 | 8 | 71.7 |
| 28\06\15 | 24.5 | 32.1 | 28.3 | 20.7 | 20.6 | 0.1 | 10 | 9 | 75.2 | 8.1 | 71.1 |
| 29\06\15 | 24.5 | 33.2 | 28.9 | 20.9 | 20.8 | 0.1 | 10 | 9 | 75.2 | 7.5 | 71.7 |
| 30\06\15 | 24.5 | 32.1 | 28.3 | 20.8 | 20.6 | 0.2 | 10 | 8 | 150.4 | 8.3 | 72.7 |
| 1\07\15 | 23.2 | 31.4 | 27.3 | 20.9 | 20.7 | 0.2 | 10 | 8 | 150.2 | 7.4 | 72.1 |

| DATE | TMIN | TMAX | TMEAN | IER | FER | DER | ILP | FLP | V(v) | S.H | RH |
|------------|------|------|-------|------|------|-----|-----|-----|-------|-----|------|
| 2\07\15 | 24.5 | 31.3 | 27.9 | 20.8 | 20.7 | 0.1 | 10 | 9 | 75.2 | 7.4 | 72.1 |
| 3\07\15 | 20.5 | 32.1 | 26.3 | 20.8 | 20.7 | 0.1 | 10 | 9 | 75.2 | 8 | 73.7 |
| 4\07\15 | 24.5 | 32.3 | 28.4 | 21.0 | 20.9 | 0.1 | 10 | 9 | 75.2 | 7.5 | 71.6 |
| 5\07\15 | 20.5 | 34.5 | 27.5 | 20.8 | 20.7 | 0.1 | 10 | 9 | 75.2 | 7.3 | 72.5 |
| 6\07\15 | 24.5 | 33 | 28.8 | 20.9 | 20.8 | 0.1 | 10 | 9 | 75.2 | 7.4 | 71.2 |
| 7\07\15 | 20.5 | 33.3 | 26.9 | 20.9 | 23.8 | 0.1 | 10 | 9 | 75.2 | 8.3 | 72.1 |
| 7\07\15 | 24.5 | 34.2 | 29.4 | 20.9 | 20.7 | 0.2 | 10 | 8 | 150.4 | 7.5 | 70.6 |
| 9\07\15 | 24.5 | 33.5 | 29 | 20.9 | 20.8 | 0.1 | 10 | 9 | 75.2 | 8 | 72.1 |
| 10\07\15 | 24.2 | 32.4 | 28.3 | 20.9 | 20.8 | 0.1 | 10 | 9 | 75.2 | 8.2 | 71.7 |
| 11\07\15 | 24.5 | 34.3 | 29.4 | 20.8 | 20.7 | 0.1 | 10 | 9 | 75.2 | 8.3 | 70.6 |
| 12\07\15 | 24.5 | 33.1 | 28.8 | 20.9 | 20.8 | 0.1 | 10 | 9 | 75.2 | 8.5 | 71.2 |
| 13\07\15 | 24.5 | 32.4 | 28.5 | 20.8 | 20.6 | 0.2 | 10 | 8 | 150.4 | 8 | 71.5 |
| 14\07\15 | 24.5 | 34.1 | 29.3 | 20.9 | 20.7 | 0.2 | 10 | 8 | 150.4 | 8.3 | 70.7 |
| 15\07\15 | 24.3 | 33 | 28.7 | 20.9 | 20.8 | 0.1 | 10 | 9 | 75.2 | 7.5 | 71.3 |
| 16/07/2015 | 24.2 | 33.2 | 28.9 | 20.9 | 20.8 | 0.1 | 10 | 9 | 75.2 | 8.5 | 71.1 |
| 17/07/2015 | 34.5 | 32.3 | 28.4 | 20.9 | 20.7 | 0.2 | 10 | 8 | 150.4 | 7.5 | 71.6 |
| 18/07/2015 | 24 | 33.3 | 28.2 | 20.9 | 20.8 | 0.1 | 10 | 9 | 75.2 | 7.4 | 71.8 |
| 19/07/2015 | 24.2 | 31.5 | 27.9 | 20.9 | 20.8 | 0.1 | 10 | 9 | 75.2 | 8.2 | 72.1 |
| 20/07/2015 | 23.5 | 30.2 | 26.9 | 20.9 | 20.7 | 0.2 | 10 | 8 | 150.4 | 8.2 | 73.1 |
| 21/07/2015 | 24.5 | 33.1 | 28.8 | 20.9 | 20.8 | 0.1 | 10 | 9 | 75.2 | 8.2 | 71.2 |
| 22/07/2015 | 24 | 32.3 | 28.2 | 20.9 | 20.7 | 0.2 | 10 | 8 | 150.4 | 7.5 | 71.8 |
| 23/07/2015 | 23.2 | 31.2 | 27.2 | 20.9 | 20.8 | 0.1 | 10 | 9 | 75.2 | 7.5 | 72.8 |
| 24/07/2015 | 20.2 | 35.2 | 27.7 | 17.5 | 14.5 | 2 | 10 | 8 | 150.4 | 8 | 72.3 |
| 25/07/2015 | 27 | 35.3 | 31.2 | 14.5 | 14.2 | 0.3 | 10 | 7 | 225.6 | 8.2 | 68.8 |
| 26/07/2015 | 20 | 35 | 27.5 | 14.5 | 14.2 | 0.3 | 10 | 7 | 225.6 | 8.1 | 72.5 |
| 27/07/2015 | 26 | 31 | 28.5 | 14.5 | 14.2 | 0.3 | 10 | 7 | 225.6 | 7 | 71.5 |
| 28/07/2015 | 24.2 | 31.3 | 27.8 | 14.5 | 14.3 | 0.2 | 10 | 7 | 225.6 | 7.2 | 72.2 |
| 29/07/2015 | 23.3 | 35.4 | 29.4 | 15.5 | 14.3 | 0.2 | 10 | 8 | 150.4 | 7.5 | 70.6 |
| 30/07/2015 | 24.5 | 25.2 | 29.9 | 14.5 | 14.3 | 0.2 | 10 | 8 | 150.4 | 7.2 | 70.1 |
| 31/07/2015 | 20.1 | 34.3 | 27.2 | 14.5 | 14.3 | 0.2 | 10 | 8 | 150.4 | 7.3 | 72.8 |

Source: Field study, 2015

4. Conclusion

Due to global climate change, the expensive and time-consuming direct measuring methods used to determine crop water use cannot be employed in a safe manner in the upcoming years. The methods for estimating evapotranspiration using meteorological data will be more and more crucial. In irrigation scheduling, water resource modeling, and management, the Pan evaporation method works well for obtaining findings quickly. Convectional evaporimeters must contend with problems including poor upkeep that causes inaccuracies because of leaks, the growth of algae in the water, an improper water level, and weed growth. The created automatic Class A evaporation pan measures the evaporation rate using enament aluminum probes and a self-recording system.

The measurement precision of the instrument is 0.018 cm, the evaporation depth is 0.1 cm, the voltage (V) value is 75.2 V, and the refractive index value is 8.7 V, respectively. A physics-deterministic model would be run using the instrument's exact and accurate readings/data to address issues with river flow regime, water and soil erosion management, and precision agriculture systems.

Acknowledgment. The authors equally contributed to this study. The also thank Engr.(Dr.) Olotu Yahaya for his technical contributions and review.

References

- [1] Purvis J.C., Pan evaporation records for the South Carolina, *Water International*, 19, 2006, pp. 30–34.
- [2] Stanhill G., Cohen S., Global dimming: a review of the evidence for a widespread and significant reduction in global radiation with discussion of its probable causes and possible agricultural consequences, *Agricultural and Forest Meteorology*, 107, 2001, pp. 255–278.
- [3] Linacre E.T., Estimating U.S. class A pan evaporation from few climate data, *Water International*, 19, 1993, pp. 5–14.
- [4] Jones C., Empirical method of estimating evapotranspiration, *Atmospheric Research*, 40, 1992, pp. 87–90.
- [5] Peterson T.C., Golubev V.S., Groisman P.Y., Evaporation losing its strength, *Nature*, 377, 1995, pp. 687–688.
- [6] Plummer N., Lin Z., Torok S. Trends in the diurnal temperature range, *Atmospheric Research*, 40, 1995, pp. 60–65.
- [7] Robock A., Konstantin V.Y., Srinivasan G., Entin J.K., Hollinger S.E., Spe-ranskaya N.A., Liu S.X., Namkhai A., The global soil moisture data bank, *Bulletin of the American Meteorological Society*, 81, 2000, pp. 1281–1299.

- [8] Parmele Y., McGuinness O., Comparison of measured and estimated daily potential evapotranspiration on humid region, *Atmospheric Research*, 40, 2004, pp. 77–84.
- [9] Phene C.J., Real-time irrigation scheduling of cotton with automated pan evaporation Australia since 1951, *Atmospheric Research*, 37, 1992, pp. 79–86. evaporation pans. 16: 61-67 Natural Resources, South Carolina State Climatology Office; Vol (3); pp. 10-17

Addresses:

- Dr. Engr. Yahaya Olotu, Auchi Polytechnic, Department of Agricultural & Bio-Environmental, Auchi, Edo State, Nigeria, olotu.abiodun@yahoo.com
(*corresponding author)
- Dr. Engr. Livinus Apebuamhe Izah, Auchi Polytechnic, Department of Mechanical Engineering, Auchi, Edo State, Nigeria
- Engr. Moses Eromosele Esegbe, Auchi Polytechnic, Department of Mechanical Engineering, Auchi, Edo State, Nigeria
- Engr. Reuben Ishiekwene, Delta State Polytechnic, Department of Electrical Engineering, Ogwashiku
- John Friday Ogbodo, Kogi State Polytechnic, Department of Metallurgy, Lokoja, Kogi State

Evaluation of the effects of non-revenue water on water security in Ondo State, Nigeria

Yahaya Olotu*, Edwin Omozuapo Oyathelemi, Shaka Momoh,
Olugbemiga Stephen Ifabiyi

Abstract. *The provision of safe drinking water is a crucial service that generates revenue for water utilities to fund their operations. The annual amount of water lost is a crucial indicator for evaluating how effectively water is supplied and distributed. According to the usage of a deterministic simulation model on public water supply variables, the volume of non-revenue water (NRW) and its cost consequences have further developed a complicated system for the availability, distribution, and affordability of the utility. Annual water accessed (AWA) was negatively impacted by the steady annual increase in public water supply (AWS) from $8.0 * 10^6 m^3$ to $13.4 * 10^6 m^3$, with $R^2 = 0.096$, and annual water loss (AWL) was significantly impacted with $R^2 = 0.99$. This result suggests that the public water supply plays a role in water loss, which primarily occurs through leaks and bursts. As a result, Akure's expected annual volume and revenue water costs (NRW) are 6 million m^3 and 15.6 million USD, respectively. A thorough investigation reveals that the annual money lost might be utilized to fund health and education programs for eight months. Therefore, it is predicted that the difficulty of determining safe drinking might be reduced by 30% if the rainwater is effectively harnessed in Ondo State, Nigeria*

Keywords: *Rainwater, Water, NRW, Simulation, Distribution, Resources, Public, Cost, Supply*



1. Introduction

The accessibility and even distribution of potable water is a serious global issue. Safe drinking water is limited, the population growth, industrial and social advancement have further complicated the already scarce utility through overstressing the provision of potable water and infrastructural mechanisms for water distribution such as reticulation pipeline networking system, reservoir construction, fitting of flowmeter e.t.c. Ensuring safe, adequate and affordable water supply is becoming an ever more pressing issue for government, water professionals and researcher across the globe. More than 75% of the drinking water infrastructure in Edo North has been in service for decades without replacing with integrated and efficient system this leads to significant source of water loss through leaks, cracks, expiration and damage (Idogho et al., 2013).

Gathering, converting and distribution of safe drinking water is a serious challenge in Nigeria and some other developing nations, these constraints occurred as water loss due to leakages in conveyance pipeline, wastages, theft, improper billing and metering systems (May,1994). The annual volume of water lost is an important indicator of water distribution efficiency, both in individual years, and as a trend over a period of years. High and increasing water losses are an indicator of ineffective planning and construction, and of low operational maintenance activities (Lambert, 1999). Water loss from a utility's distribution system is a serious constrain which is always associated with loss of revenue and production efforts. Water losses in the distribution system require more water to be treated, which requires additional energy and chemical usage, resulting in wasted resources and total loss of revenues (Mckenzie, 2001). Determining how much water is being lost and where losses are occurring in a distribution system can be a difficult task. Without consistent and accurate measurement, water losses cannot be reliably and consistently managed (Benser and Camper, 2011).

The confusion over inconsistent terms and calculations has led to the development of better tools and methods to track water losses from distribution systems. This scenario has an increasing effect on socio-economic development of entire region of Akure and its environs. Having considered the huge budgetary allocation for publication water supply and distribution, it is important to device technically based approaches of reducing water loss through physical or real and apparent water losses and also improves water quality at the end-point or delivery stage. Water loss reduction (WLR) often represents an efficient alternative to exploiting new resources, which frequently involves cost-intensive measures, such as new dams, deep wells, seawater desalination or even transferring water from one river basin to another. Therefore, water loss reduction and pressure management contribute to sustainable and integrated water resources management (IWRM). However, this research study is focused on the estimation and analysis of the effects of water losses on public water supply and distribution (PWSD) in relation to social-economic development and integration in Akure, Nigeria.

2. Materials and Methods

2.1. Study area

Akure is made up of 18 districts and located in the South-Southern Zone of Nigeria. Edo lies between longitudes 4°30' and 6° East of the Greenwich Meridian, 5° 45' and 8° 15' North of the Equator. This means that the city lies entirely in the tropics. It is bounded North by Ilara Mokin; in the East by Obanle; in the West by Ondo and Oda in the South. The total population of 763,000 comprising Male (56%) and Female (46%). The source of this estimate (OSMWR, 2005). The map of the city is shown in Fig. 1.

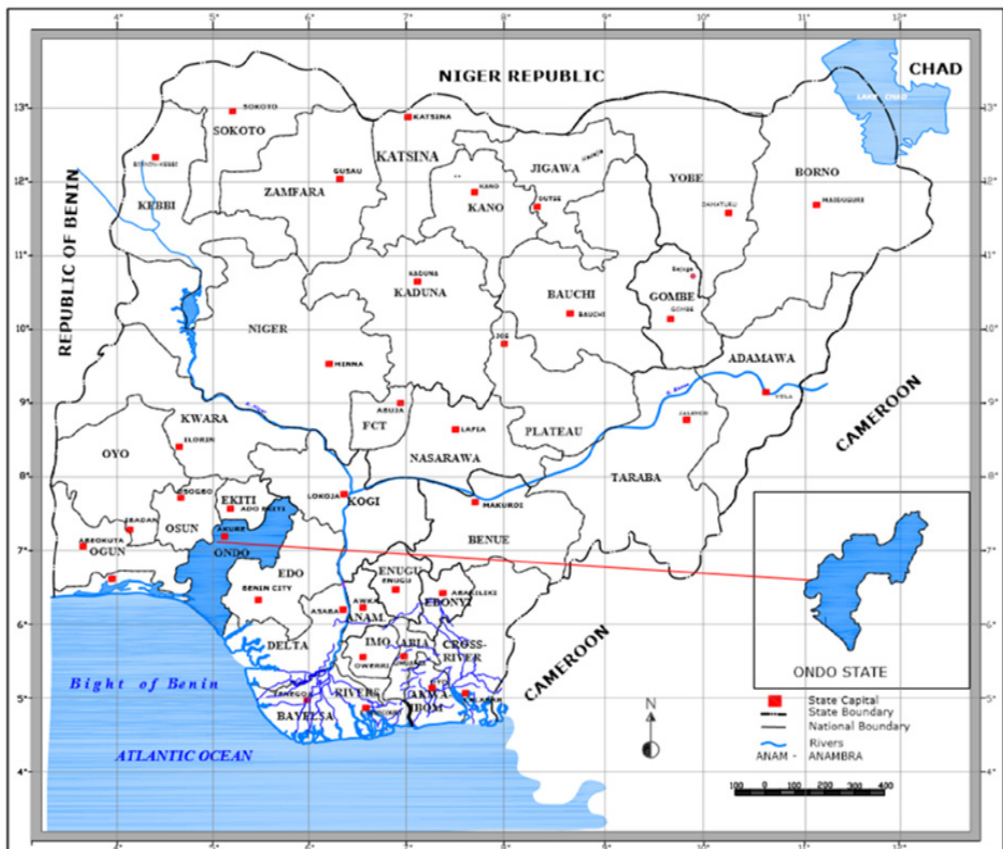


Figure 1. Map of Nigeria showing Ondo State
Source: Author's Arcmap 10.1 Production, 2022.

2.2. Water loss modelling

Many drinking water utilities around the world do not give instantaneous respond to leaks problems until the situation becomes complicated. Leaks can effectively be corrected using sensitive optimization modelling approaches which involves monitoring of real-time leaks problem, computerization of adequate pressure system, provision for eddy losses to prevent pipe burst (Fanner, 2009). However, soil conditions for example can have a great effect on the real losses as well as to the ability for them to be identified and located at the ground surface. Apparent and physical losses are computed as follows:

$$WL\epsilon = NRW\tau - KWS\beta \quad (1)$$

Where $NWR\tau$ is total Non- Revenue Water; $WL\rho$ is real Water Loss; and $WL\epsilon$ is apparent Water Loss (Idogho *et al.*, 2013).

2.2.1. Unavoidable Real Losses (URL)

Output of various studies conducted shown that it is impossible to eliminate real losses from a water distribution system. Therefore, Unavoidable Real Losses is therefore computed as follows:

$$URL = 18 \times Lm + Nc + 25 + Lp \times P \quad (2)$$

Where:

Lm = main length in km;

Nc = number of service connections;

Lp = total length in km; and

P = average pumping pressure.

Leak volume is the function of time (t) and flowrate (R); this development is therefore evaluated as:

$$Lv = t(W + L + P) * R \quad (3)$$

Where:

Lv = Leak volume (m^3);

t = Time (sec);

W = Awareness;

L = Location; and

P = Repairs.

2.3. Water supply and demand formation

Water resources involve simulating systems made up of many component parts that are interrelated. The system is driven by *hydrological variables* (i.e., precipitation, evaporation, demand) and involves uncertain processes, parameters, and events. The challenge when evaluating water supply and resource systems is to find an approach that can incorporate all the knowledge available to planners and management into a quantitative framework that can be used to simulate and predict the outcome of alternative approaches and policies (Butler, 2009). While developing a system, the starting point can also be some specific consumption that does not necessarily include leakage. In that case the leakage percentage has to be added in the following way:

$$Q_{ph} = \frac{Q_{av.day}}{f} (K_1 K_2 + \frac{1}{100-t}) \quad (4)$$

Factor, f , in the equation is a unit conversion factor while l represents the leakage percentage of the total quantity supplied to the system: is the quantity of water demand at the peak hour, while, $Q_{av.day}$ is the average quantity of water demanded daily. Therefore, annual average water supply is computed using the relationship on equation (5):

$$AWS = cP_i A_v N_d \quad (5)$$

Where:

- C = Coefficient of target population;
- P_i = Total population;
- A_v = Average total water volume;
- N_d = Number of water supplied days.

The volume of annual water supply that could finally be assessed by the targeted population is evaluated using the interconnectivity between annual water supply (AWS) and annual water loss (AWL) as related in equation (6):

$$AWA = AWS - AWL \quad (6)$$

Where:

AWA = Annual water assessed (m^3).

2.4. Water Cost Index Computation

It is very important and useful to calibrate the water supply-cost benefit ratio in order to monitor and improve on the service delivery of the utility (Idogho *et al.*, 2013). The Rickards Real Cost Water Index serves as a benchmark for helping measure

hundreds of critical projects on a like-for-like basis (Bond and Richard, 1997). Index values reflect estimated water production costs measured in US dollars per cubic meter for a variety of major global water infrastructure projects ranging from retail water utilities to wholesale water utilities. However, Water Cost index is calculated using Richard's relationship as follows:

$$WCI = \frac{T_p}{T_d} \quad (7)$$

Where:

T_p = Total cost of production is calculated as the sum of operating costs, capital costs, and identified subsidies; T_d = Total de-livered freshwater volume (in m³) is the amount the producer reports as delivered, and excludes water lost either due to system leakage, pilfering, or other forms of loss. This penalizes producers with a large fraction of production volume being lost due to system inefficiency:

WCI = Water Cost Index

2.5. Data analysis

Data on water loss variables were generated using a set of modelled relationships from the measured data. The generated outputs were subjected to *sensitivity* and dynamic simulation processes. Excel software and Sigma Plot were used for spread sheet calculations and graphical representations. Leakage from the burst pipeline is shown in Figure 2.



Figure 2. Leakage from the burst pipeline

3.1. Results and discussion

3.1.1. Calibration of Water supply

Many drinking water utilities around in Akure, Nigeria respond to leaks development only after receiving report of water erupting from a street or a complaint from a customer about a damp basement. Leakage control requires a proactive leakage management program that includes a means to identify hidden leaks, optimize repair functions, manage excessive water pressure levels, and upgrade piping infrastructure before its useful life ends. The result in Table. 1 shows the Public water supply system in Akure for a period of 10-year (2003-2012). The volume of annual water loss and accessed was simulated using the public water supply data obtained from the Ondo State Water Corporation. The result in Table 1 indicated that there is an increase in volume of water supply from year 2003 down to 2012. The output of simulation iteration shown that the increase in annual water supply (*AWS*) had negative effect on annual volume of water accessible (*AWA*) with $R^2 = 0.096$; and strong agreement exist between annual water supply (*AWA*) and annual water loss with the $R^2 = 0.999$ as shown in Fig. 3 and 4 respectively. In 2007, equilibrium exists among the public water supply variables; with the annual water supply (*AWS*) of value $10.8 * 10^6 m^3$; annual water loss (*AWL*) is $5.4 * 10^6 m^3$ and annual water accessed (*AWA*) is $5.4 * 10^6 m^3$ respectively. The implication of this development is that half of annual water supply is lost to leaks.

Table 1. Public water supply and loss

| Year | AWS | AWL | AWA |
|------|------|-----|-----|
| 2003 | 9 | 3.2 | 5.9 |
| 2004 | 9.6 | 3.8 | 5.8 |
| 2005 | 10 | 4.5 | 5.5 |
| 2006 | 10.3 | 4.8 | 5.5 |
| 2007 | 10.8 | 5.4 | 5.4 |
| 2008 | 11 | 5.7 | 5.3 |
| 2009 | 11.3 | 6.1 | 5.2 |
| 2010 | 11.8 | 6.7 | 5.1 |
| 2011 | 12.1 | 7.1 | 4.9 |
| 2012 | 14.4 | 8.6 | 5.8 |

Source: OSWC, 2013

Note: AWS = Annual water supply ($m^3 * 10^6$):

AWL = Annual water loss ($m^3 * 10^6$)

AWA = Annual water accessible ($m^3 * 10^6$)

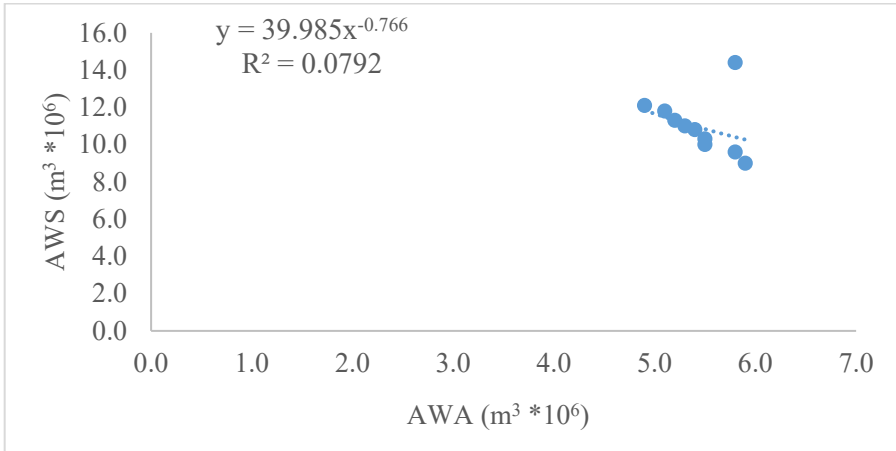


Figure 3. Calibration of water supply and accessibility

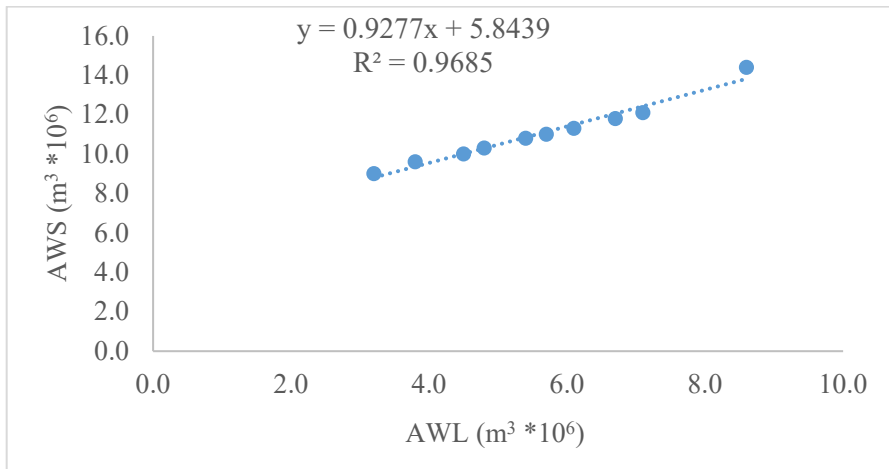


Figure 4. Calibration of water supply and loss

Most drinking water infrastructure in Akure, Nigeria has been in service for many years, and this could be a significant source of water loss through leaks. The pipelines got weak and usually burst if there is any pressure variation. Since pipelines were not properly marked, a lot of them could also be destroyed during road and construction of other infrastructure amenities. This type of water loss is referred to as Real/Physical loss. In addition to leaks, water could be “lost” through unauthorized consumption (theft), administrative errors, data handling errors, and metering inaccuracies or failure; and this is referred to as Apparent loss.

3.1.2. Water cost benefit estimates

It is important to establish sound relationship on water production cost, cost of water loss or Non- Revenue Water in order to monitor the degree of utility distribution and its impact on the end-user for possible optimization for better service delivery. Evaluation of water production varies from geographical location to another; and also depends on the hydrological formation of the region. The results in Fig.3 show the cost of water production; water loss and billed water (i.e water that finally reached the consumers). The true cost of water production in individual geographic areas, which includes operating, capital, and "hidden economic" costs. Highest cost of annual water loss of 30.1 million USD was estimated in 2012 compared 4.8 million USD in 2003. However, there was a progressive increase in the investment of water production from 13.5 million USD in 2003 to 50.4 million USD in 2012. Strong relationship exist between cost of annual supply of water (CAWS) and cost of annual water loss (CAWL) with $R^2=0.83$. Akure is estimated to have an annual Non-Revenue Water (NRW) (i.e mostly from real loss) volume of 6 million m^3 . This represents approximately 15.6 million USD in revenue that water utilities lose every year.

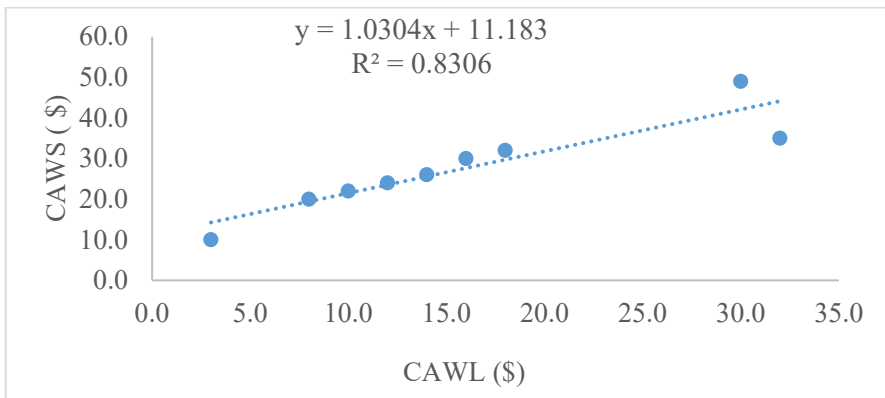


Figure 5. Cost benefit of public water supply-loss

4. Conclusion

Ensuring a safe, sufficient, and affordable water supply is becoming an ever more pressing issue for politicians and water professionals. This development has become a serious problem in most developing countries. An effective public water supply system is a productive function of many related variables, such as non-revenue water (NRW). Annual water loss, mainly through physical processes, is estimated to be a revenue loss of 15.6 million USD. This value fund could be applied to the 30% budgetary allocation for education and the agricultural section for the city. In addition, 60,623 people could

be provided with *safe drinking water* at a rate of 75 litres per person per day annually. An integrated water auditing model (IWAM) is a pivotal step in calibrating an effective water loss management program. Constructive application of the formulated model coupled with the introduction of automated metering devices, burst and leak detectors will produce a quantified understanding of the integrity of the distribution system and address sound plans to resolve water losses.

Acknowledgment: The authors equally contributed to this study. The authors thank the Ondo State Water Corporation for the provision of datasets.

References

- [1] Besner M.C., Camper A., Explaining the occurrence of coliforms in distribution systems, *Jour. AWWA*, 94(8), pp. 95-109.
- [2] Butler D., Leakage Detection and Management, *Palmer Environmental*, 6(3), 2009, pp. 50-67
- [3] Fanner P.V., Leakage Management Technologies, AWWARF Project Report 2928, 2009.
- [4] Lambert A., Brown T.G., Takizawa M., Weimer D., A review of performance indicators for real losses from water supply systems, *AQUA.*, Dec 1999.
- [5] May A., *International Benchmarking of Leakage from Water Reticulation Systems*, Proceedings of Leakage 2005 Conference, 2005.
- [6] Mckenzie R.S., *Development of a standardized approach to evaluate burst and background losses in potable water distribution systems*, SANFLOW User Guide. South African Water Research Commission, Report TT 109/99, 2001.
- [7] OSMWR, Ondo State Ministry of Works Reports on Census, Vol. 1, 2005, pp. 12-45
- [8] RMP, Guide on Road Map to Ondo-State Develop, 2003.

Addresses:

- Dr. Engr. Yahaya Olotu, Auchu Polytechnic, Department of Agricultural & Bio-Environmental Engineering, Auchu, Edo State, Nigeria, olotu.abiodun@yahoo.com
(* corresponding author)
- Engr. Edwin Omozuapo Oyathelemi, Auchu Polytechnic, Department of Mineral and Petroleum Resources Engineering, Auchu, Edo State, Nigeria
- TPL. Shaka Momoh, Auchu Polytechnic, Department of Urban & Regional Planning, Auchu, Edo State, Nigeria
- Engr Olugbemiga Stephen Ifabiyi, Auchu Polytechnic, Department of Civil Engineering, Auchu, Nigeria

Development and Evaluation of a Digital MPF5-Moisture Meter

Yahaya Olotu*, Reuben Ishiekwene, Mariam Abdul-Wajid Obomeghie,
Stephen Korede Abolaji, Ferdinand Aleonokhu Aigbodoh

Abstract. *An important advantage for applying the right amount of water to the fields is provided by the effective irrigation management techniques based on soil moisture monitoring. With a calibrated and exact resolution of $0.03\text{m}^3/\text{m}^3$ and 36 mV , the developed MPF5 moisture meter monitors soil moisture from a depth of 10 cm to 80 cm using a set of sensors, transducers, capacitors, resistors, and variable micro-switch. The response monitoring system compares the soil moisture to the user-specified target values and generates an alert if the soil moisture falls below the required level for particular crops. There were many similarities between the instrument's output and that of other automated soil moisture meters like the REOTEMP-MM17 moisture meter and the PR2 capacitance moisture meter. The device works very well for both mineral and organic soils to monitor soil moisture for reliable irrigation scheduling.*

Keywords: *Soil moisture, MPF5 moisture meter, Irrigation scheduling, Crop, Mineral and organic soil*

1. Introduction

The level of soil moisture is crucial to the survival of the plant. Through the process of transpiration, water is also necessary to control plant temperature (Gunnert, 2014). For agricultural applications, measuring soil moisture is crucial for better irrigation system management by farmers. Farmers are able to use less water overall by knowing the precise soil moisture conditions on their fields, but they are also able to boost crop yields and quality by better managing soil moisture during crucial plant growth stages. One important factor controlling the flow of energy between the ground and the atmosphere is soil moisture. The volumetric water content



of the soil is measured by soil moisture sensors (Gunneet, 2014). Soil moisture sensors measure the volumetric water content directly by using some other characteristic of the soil, such as electrical resistance, dielectric constant, or interaction with neutrons, as a proxy for the moisture content. Direct gravimetric measurement of free soil moisture requires the removal, drying, and weighting of a sample. It is necessary to calibrate the relationship between the measured property and soil moisture because it can change depending on the soil type, temperature, or electric conductivity (Bianca, 2014; Pulkit, 2013). Sensors that assess the volumetric water content are commonly referred to as soil moisture sensors. Water potential is a different type of soil moisture attribute that is measured by another class of sensors. Tensiometers and gypsum blocks are among the sensors, which are typically referred to as soil water potential sensors (Rishi, 2015; Zheng, 2011).

Soil moisture content is an essential component of the water balance equation. Hence, precise computation of changes in soil moisture storage is useful in estimating evapotranspiration (ET) for effective water management and irrigation scheduling. Additionally, this would aid in controlling the agricultural drought in northern Nigeria, which has grown to be a serious problem. To measure soil moisture, a variety of techniques and tools are employed, including Time Domain Reflectometry (TDR), tensiometers, and electrical resistance blocks (Rangem, 2010; Zheng *et al.*, 2010). At measurement depths of 10, 20, 30, 40, and 50 cm, the digital MPF5 moisture meter is anticipated to produce continuous and instantaneous moisture data in the form of m^3/m^3 , %vol, mm, and volts, respectively. The main objective of the study is to develop a simple, effective, and user-friendly digital moisture meter that measures soil moisture content in a range of climate change situations.

2. Materials and Methods

2.1. Development of a digital sensor for the MPF5 soil moisture meter

The soil between the probe wires was employed as a voltage divider along with a single sensor read wire (Arduino analog in) and a resistor. Depending on the chosen sensor and soil, various values for 57-100K resistors were used. The primary distinction is the usage of 100 logic pins to control the sensor (Arduino digital out). The 100 digital pins from the Arduino were used in this design to flip-flop the voltage (running the current forward, then reverse). Electrolysis is counteracted by this alternating current. But that doesn't mean that electrolysis does not happen. Simply put, the electrolysis-produced crust is disintegrated when the current is reversed. This would allow the soil moisture sensor to function efficiently for a longer duration. In this new configuration, the sensor reading differs slightly. Since the soil moisture sensor is simply a voltage divider, the relative voltage is switched when the current is reversed (Dingman, 1993; Farshad, 1997). This indicates that depending on the

sensor's direction, the sensor now provides two different readings. A two-probe pure nickel sensor was used to create the moisture sensor. Nickel was chosen because it has average conductivity and the durability to last a long time buried in the ground. In the earth, it would not easily corrode. Nickel probes measure 10.5 cm in length and 0.9 cm in breadth. The two probes are separated by 0.6 cm (d). Sensor probes include triangle-shaped tips that make it simple to bury them in the ground. Figures 1-3 depict the soil moisture sensor probes. The circuit diagrams for the instrument are shown in Figs. 4-6.



Figure 1. Setting of 100 cm probe sensors.



Figure 2. Testing of probe sensor electromagnetic flux at preset soil depth

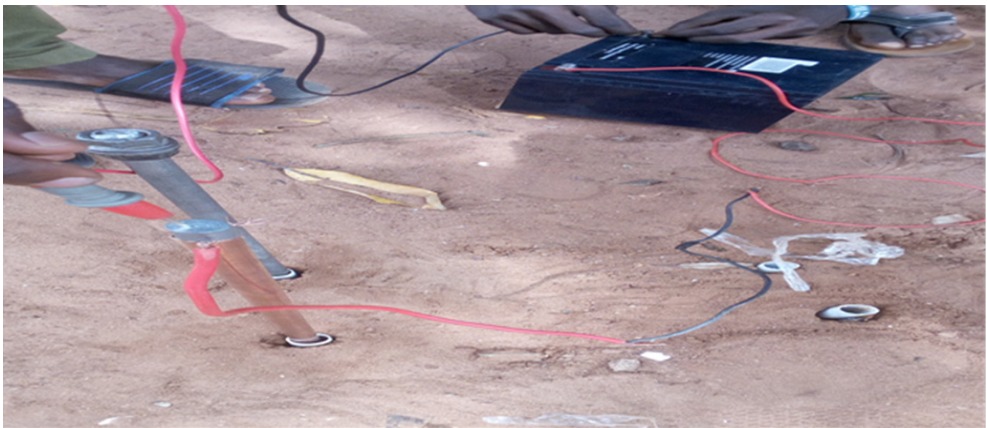


Figure 3. Probe sensor inserted in access tube for electromagnetic flux measurement at preset soil depth.

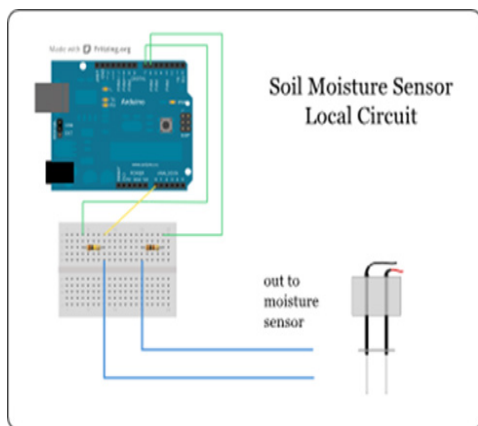


Figure 4. Local circuit breadboard

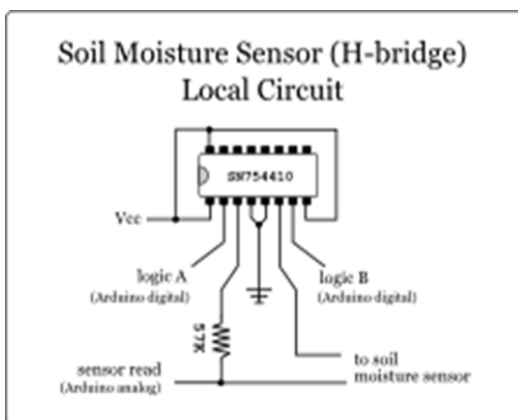


Figure 5. Local circuit – H-bridge, voltage sensor

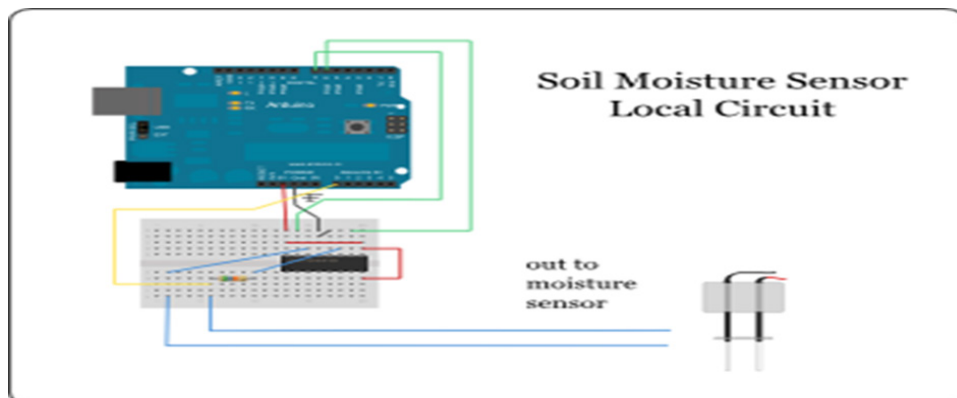


Figure 6. Local circuit - basic sensor (prone to electrolysis)

3. Results and Discussion

3.1. Calibration of MPF5 moisture meter

Using characteristics of the soil, such as the dielectric constant, electrical resistance, and electromagnetic induction, soil moisture transducers and sensors calculate the volumetric water content of the soil. Because using the gravimetric measuring strategy requires a lot of time and harms the soil layer, it is crucial to transition to integrated soil moisture solutions. The outcomes of the trial-testing on mineral and organic soils at varied measuring depths are shown in Tables 1 and 2. The soil moisture content was measured using the sensing probe at every depth at angles of

0°, 180°, and 360°, with corresponding voltage outputs of V_1 , V_2 , and V_3 , accordingly. The volumetric water content values at each measuring depth as determined by the gravimetric method were used to calibrate the findings of the measured soil parameters. The voltage values at each MP were measured with two replicates for the trial testing as described by Knight (1992) and Scott and Maitre (1998). The statistical metrics to analyze the results of duplicated trial tests are therefore shown in Tables 3 and 4.

Table 1. Calibration of MPF5 moisture meter using mineral soil

| N/S | MD (cm) | V_1 (volt) | V_2 (volt) | V_3 (volt) | Wet Weg (g) | Dry Weg. (g) | SMC (%) |
|-----|---------|--------------|--------------|--------------|-------------|--------------|---------|
| 1 | 20 | 6.0 | 6.2 | 6.3 | 3.2 | 2.8 | 14.3 |
| 2 | 40 | 5.5 | 5.6 | 5.7 | 5.1 | 4.1 | 23.0 |
| 3 | 60 | 6.3 | 6.4 | 6.5 | 5.5 | 5.0 | 10.0 |
| 4 | 80 | 7.5 | 7.3 | 7.2 | 3.0 | 2.9 | 8.4 |
| 5 | 100 | 8.2 | 8.3 | 8.4 | 3.4 | 3.3 | 3.2 |

The results in Table 3 show that there is a 10% (0.100) variation from the mean voltage value of 5.6 volts at the MP of 40 cm and 23% soil moisture content, whereas at MP of 60 cm and 100 cm, there is a 0.010 (1%) variation from the mean voltage values of 7.3 volts and 8.3 volts for 8.4% and 3.25% of SMC for mineral soil. It follows that it is evident that the deviation from the mean value rose significantly with high soil moisture content and fell with low SMC (Table 3).

Table 2. Calibration of MPF5 moisture meter using organic soil

| N/S | MD (cm) | V_1 (Volt) | V_2 (volt) | V_3 (volt) | Wet Weg (g) | Dry Weg. (g) | SMC (%) |
|-----|---------|--------------|--------------|--------------|-------------|--------------|---------|
| 1 | 20 | 12.3 | 12.1 | 12.0 | 5.0 | 4.0 | 22.7 |
| 2 | 40 | 14.5 | 14.2 | 14.4 | 4.6 | 3.9 | 18.9 |
| 3 | 60 | 16.4 | 16.0 | 16.2 | 3.5 | 3.1 | 12.9 |
| 4 | 80 | 20.4 | 19.8 | 20.0 | 3.0 | 2.9 | 3.4 |
| 5 | 100 | 24.5 | 22.5 | 21.8 | 6.0 | 5.9 | 1.7 |

Table 3. Statistical metrics for voltage measurement for mineral soil

| MD (cm) | Sta. dev | Mean | Variance (S^2) |
|---------|----------|-------|--------------------|
| 20 | 0.150 | 6.170 | 0.020 |
| 40 | 0.100 | 5.600 | 0.100 |
| 60 | 0.100 | 6.400 | 0.010 |
| 80 | 0.150 | 7.330 | 0.020 |
| 100 | 0.100 | 8.300 | 0.010 |

Table 4. Statistical metrics for voltage measurement for organic soil

| MD (cm) | Sta. dev | Mean | Variance (S^2) |
|---------|----------|--------|--------------------|
| 20 | 0.150 | 12.300 | 0.020 |
| 40 | 0.150 | 12.130 | 0.020 |
| 60 | 0.200 | 16.200 | 0.040 |
| 80 | 0.310 | 20.700 | 0.190 |
| 100 | 1.400 | 22.900 | 1.960 |

The outputs from organic soil, on the other hand, did not resemble those from mineral soil in terms of the relationship between the mean obtained voltage values and computed variance (S^2). According to the measurements made by the MPF5 probe sensors, the variance value (S^2) was found to be 2% (0.002) at 20 cm and 40 cm, 4% (0.04) at 60 cm, and 19.0% (0.190) and 196% (1.96) at MD of 80 cm and 100 cm (Table 4). In general, the sensor can accurately measure the volumetric water content of mineral soil when the soil moisture content is below 40%, however for organic soil, the instrument's performance can be deemed to be around average at the MD of 20 cm, 40 cm, and 60 cm. According to Munzon-Carpena (2021), the link holds true for the majority of mineral soils, but for moisture levels below 50%, it suggests that a particular recalibration is necessary. However, this depends on the instrument's input of the electromagnetic wave frequency (Munzon-Carpena, 2011).

Figures. 4 and 5 present the outputs of the voltage of the sensor against the soil moisture content (SMC) for mineral and organic soils. However, the two plots are very similar to each other. From the plots, it is shown that at higher SMC, the recorded voltage outputs are reduced. This may be due to the repelling of penetration of the voltage as a result of the dissolved salt contained in the soil moisture within the soil layers.

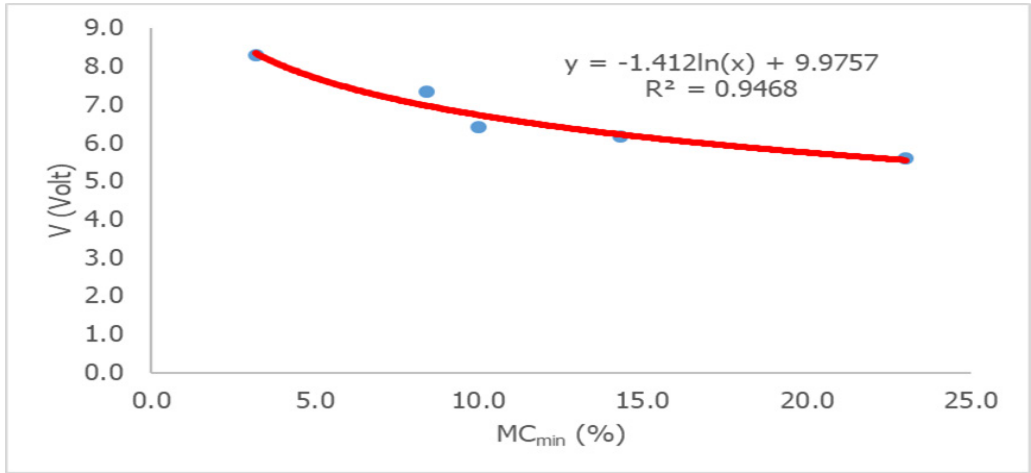


Figure 4. Voltage verse soil moisture of the mineral soil

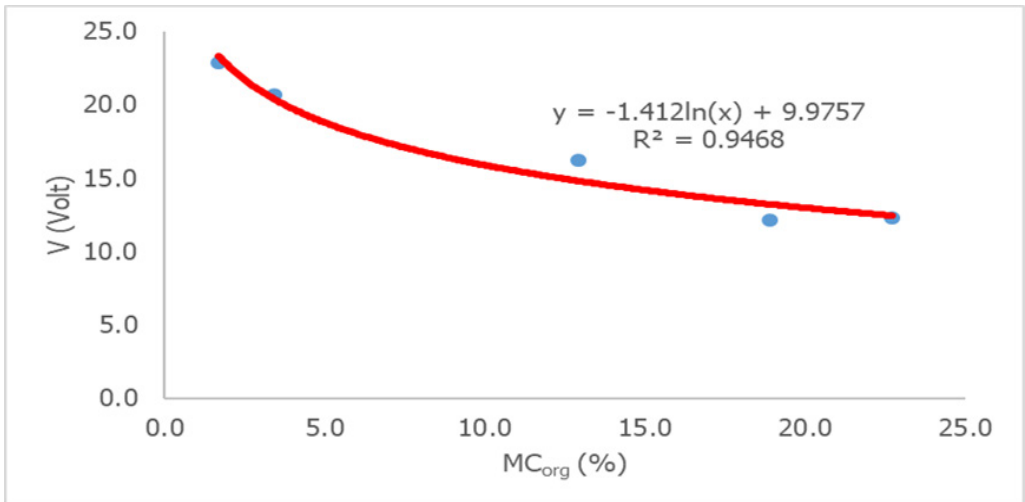


Figure 5. Voltage verse soil moisture of the organic soil

4. Conclusion

In this study, the performance of an integrated soil moisture meter called the MPF 5 was evaluated on both mineral and organic soils, with measurements being made from 20 cm to 100 cm below the surface. In order to facilitate signal reception, a pair of sensing probes (MPF5a and MPF5b) were used. By detecting changes in

SMC and transmitting the results in voltage format, the device operates on the electromagnetic induction principle. At each measuring depth, the device's output voltage was calibrated in response to the volumetric water content determined by the gravimetric method.

Therefore, at increasing SMC, the voltage gradually decreases for both soils, which may be caused by dissolved salt interfering with the electromagnetic process. In contrast, the voltage levels rose when the moisture content was low. The total results demonstrated that the device accurately measures soil moisture content between the MD of 20 cm and 100 cm beneath mineral soil at 40% SMC, while a realistic measurement could be achieved between the MD of 20 cm and 60 cm beneath organic soil at 30% SMC. Future research is required to increase the accuracy of quantifying organic soil.

Acknowledgment: The authors equally contributed to this study. The authors thank Ola and his group for the selection and building of sensors and transducers.

References

- [1] Bianca W.L., A Miniaturized Soil Moisture Sensor Based on Time Domain Transmissometry, *IEEE Institute of Microwave Systems*, SU-29(6), 2014, pp. 213-220.
- [2] Dingman S.L., *Physical Hydrology*, Prentice Hall, New Jersey, 1993.
- [3] Farshad A., *Analysis of Integrated Soil and Water Management Practices with different Agricultural System Under Semi-Arid Condition of Iran and Evaluation of their Sustainability*, Published PhD thesis, Fnschede, The Netherland, 1997.
- [4] Guneet M.M., *Design of Capacitive Sensor for Monitoring Moisture Content of Soil and Analysis of Analog Voltage with Variability in Moisture*, Proc. RA ECS UIET Panjab University Chandigarh, 2014.
- [5] Knight J.H., Sensitivity of Time Domain Reflectometry measurement to lateral variation in Soil Water Content. *Water resources. RES*, 28(4), 1992, pp. 2340-2353.
- [6] Munoz-Carpena F., Field Device for Monitoring Soil Water Content, UF/iFAS Extension, Gainesville, FL 32611, 2021.
- [7] Pulkit H., *Design of a central control unit and soil moisture sensor based irrigation water pump system*, IEEE Conference on. IEEE, 2013.
- [8] Rangan K.T.V., An Embedded systems approach to monitor greenhouse, *Recent Advances in Space Technology Services and Climate Change (RSTSCC)*, 20(4), 2010, pp.56-60.

- [9] Rishi R., Prototype Design of Indigenous GSM based Intelligent Irrigation System, *International Journal of Computer Applications* 73 (18), 2015, pp. 36-39.
- [10] Scott P., Maitre C., Interaction between vegetable and groundwater Research proprieties for South Africa, *Recent Advances in Space Technology Services and Climate Change (RSTSCC)*, 20(4), 1998, pp.56-60.
- [11] Zhang F., *Research on water-saving irrigation automatic control system based on internet of things*, Electric Information and Control Engineering (ICEICE), International Conference, 4(1), 2011, pp.2541-2544, 15- 17.
- [12] Zheng Y., Guohuan L., XiuLi Z., Qingxin, Z., *Research and development precision irrigation control system in agricultural*, Computer and Communication Technologies in Agriculture Engineering (CCTAE), International Conference, 3(1), 2010, pp.117- 120, 12-1.

Addresses:

- Dr. Engr. Yahaya Olotu, Auchu Polytechnic, Department of Agricultural & Bio-Environmental Engineering, Auchu, Edo State, Nigeria, olotu.abiodun@yahoo.com (*corresponding author)
- Engr. Reuben Ishiekwene, Delta State Polytechnic, Department of Electrical Engineering, Ogwashiku
- Engr. Mariam Abdul-Wajid Obomeghie, Auchu Polytechnic, Department of Electrical Engineering, Auchu, Nigeria
- Engr. Stephen Korede Abolaji, Auchu Polytechnic, Department of Electrical Engineering, Auchu, Nigeria
- Engr. Ferdinand Aleonokhu Aigbodoh, Auchu Polytechnic, Department of Electrical Engineering, Auchu, Nigeria

The influence of the Young modulus on two elements of a Warren truss on the dynamic behavior of the structure

Dan Alexandru Pirșan

Abstract. *The present work aims to determine the natural frequencies for a structure with Warren truss by changing the modulus of elasticity to two of the elements of the structure are keeping the same length of the elements. A numerical study is carried out by means of a 3D FE model of a Warren truss, simulating the dynamic interaction of beams with trusses.*

Keywords: *Warren truss, mode shape, natural frequency*

1. Introduction

Warren truss structures are popular construction used in various engineering fields and among them, steel rectangular tube trusses have been widely applied in large engineering structures, such as stadiums, bridges, concert halls, and offshore platforms, International Space Station because of their architecturally attractive shapes and favorable structural properties [1–2–4–5]. Is made up of longitudinal members linked only by angled cross-members that create successively inverted equilateral triangle-shaped sections along its length.

Loads on the diagonals vary between compression and tension, as they approach the center, with no vertical elements, but parts in the center must withstand both tension and compression in response to live loads [3]. Truss structures are popularly used in various engineering fields [1–4].

Many investigations have been carried out related to steel rectangular truss structures [6–7].

In this study, structural steel, from the Solidwork library, rectangular tubes with the dimensions of 50x30x2.6 mm and 120x80x8 mm were used.

With the help of Solidwork software we have found natural frequency and modal shapes for the first five vibration modes. Analyzed cases and the Young's modulus are given in table 1.



In case 1, the elements in the truss are of the same modulus of elasticity 210000N/mm^2 , the other cases 2...16 are with the modulus of elasticity different 160000 N/mm^2 . Warren truss is fixed at the both ends.

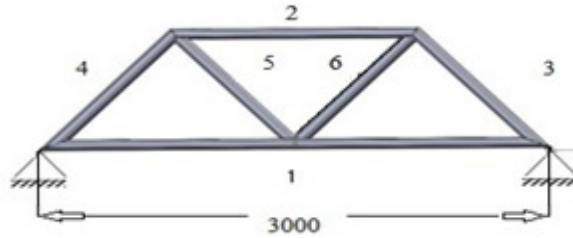


Figure 1. Six-bar truss

Length of span of the considered Warren truss is of 3000mm.

Table 1. Analyzed cases

| Case | Elements | Young's Modulus |
|------|----------|------------------------|
| 1 | - | 210000N/mm^2 |
| 2 | 1-2 | 160000 N/mm^2 |
| 3 | 1-3 | 160000 N/mm^2 |
| 4 | 1-4 | 160000 N/mm^2 |
| 5 | 1-5 | 160000 N/mm^2 |
| 6 | 1-6 | 160000 N/mm^2 |
| 7 | 2-3 | 160000 N/mm^2 |
| 8 | 2-4 | 160000 N/mm^2 |
| 9 | 2-5 | 160000 N/mm^2 |
| 10 | 2-6 | 160000 N/mm^2 |
| 11 | 3-4 | 160000 N/mm^2 |
| 12 | 3-5 | 160000 N/mm^2 |
| 13 | 3-6 | 160000 N/mm^2 |
| 14 | 4-5 | 160000 N/mm^2 |
| 15 | 4-6 | 160000 N/mm^2 |
| 16 | 5-6 | 160000 N/mm^2 |

2. Analytical approach

Elements are stressed in tension or compression for a double hinged truss. In this case the relationship of longitudinal vibrations will be used.

Applying the local coordinate system for the right (x, z) truss element shown in Fig. 2 [15].

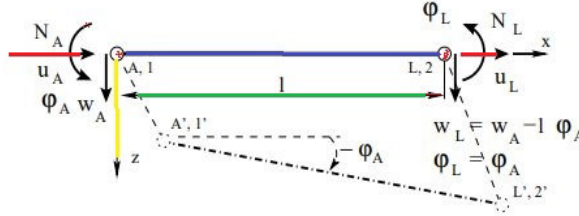


Figure 2. Truss bar

The transfer equations for longitudinal vibration of a truss bar are:

$$u_L = u_A \cos kl - \frac{N_A}{EA} \frac{1}{k} \sin kl \quad (1)$$

$$w_L = w_A - \phi_A l \quad (2)$$

$$\phi_L = \phi_A \quad (3)$$

$$N_L = -u_A E A k \sin kl - N_A \cos kl \quad (4)$$

where:

u_A, u_L – axial displacements at the beginning

w_A, w_L – transverse displacements at A and L;

ϕ_A, ϕ_L – rotation at A and L;

N_A, N_L – axial forces at A and L;

$\kappa = \omega \sqrt{m/EA} = \omega \sqrt{\rho/E}$ – wav enumber;

ω – frequency of vibration;

$m = \rho A$ – mass per unit length;

ρ – mass density;

A – cross-sectional area;

E – elastic or Young's modulus;

l – length of the element

2. Numerical modal analyzes

Solidworks is used to determine the natural frequencies and mode shapes which depend on the geometry of truss analyzed, material properties, and support condition.

It used a Warren-type truss, hinged at both ends, where it is changed the modulus of elasticity at two elements of the structure in order to determine the natural frequencies and mode shapes. The whole assembly was tested using gravitational acceleration. Figure 3 illustrates the first 5 vibration modes.

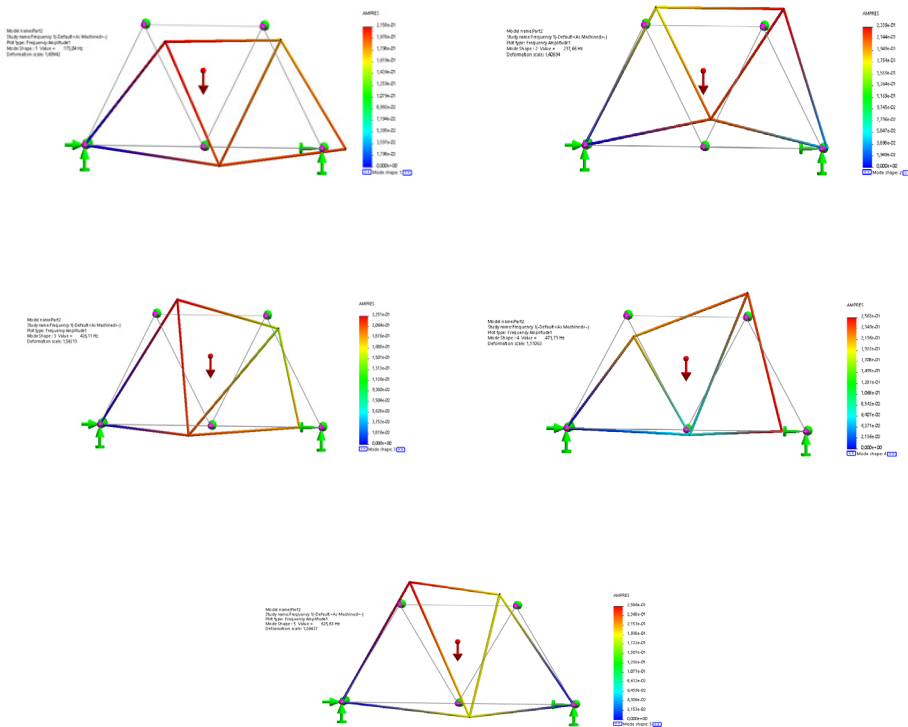


Figure 3. Mode shapes for seven elements warren truss.

Table 2 it shows the natural frequencies (f_n) for simulation for case of bars with section 50x30x2.6.mm Table 3 presents the relative frequencies shift (e_n) ($n=1, 2 \dots 5$), where e_n is calculated with the relationship:

$$e_n = \frac{f_{Un} - f_{Dn}}{f_{Un}} \quad (5)$$

f_{Un} – natural frequencies for the structure with $E=210000\text{N/mm}^2$
 f_{Dn} - the natural frequencies for the modified structure.

Table 2. Natural frequencies for truss bar with cross section 50x30x2.6mm

| Elements | F ₁ [Hz] | F ₂ [Hz] | F ₃ [Hz] | F ₄ [Hz] | F ₅ [Hz] |
|----------|------------------------|------------------------|------------------------|------------------------|------------------------|
| - | 52,183 | 54,8 | 61,89 | 68,08 | 72,57 |
| 1-2 | 49,499 | 51,64 | 58,55 | 65,04 | 66,86 |
| 1-3 | 49,087 | 50,93 | 58,93 | 67,41 | 68,08 |
| 1-4 | 49,125 | 50,93 | 58,85 | 67,43 | 68,08 |
| 1-5 | 49,8 | 50,72 | 58,73 | 65,31 | 67,96 |
| 1-6 | 49,778 | 50,71 | 58,7 | 65,31 | 68,1 |
| 2-3 | 49,43 | 53,71 | 59,35 | 64,97 | 69,04 |
| 2-4 | 49,47 | 53,71 | 59,26 | 64,97 | 69,1 |
| 2-5 | 49,668 | 53,74 | 59,18 | 62,68 | 70,24 |
| 2-6 | 49,638 | 53,73 | 59,2 | 62,68 | 70,3 |
| 3-4 | 49,847 | 52,56 | 59,5 | 64,079 | 69,45 |
| 3-5 | 50,008 | 52,73 | 59,23 | 65,35 | 70,49 |
| 3-6 | 49,548 | 52,87 | 59,77 | 65,32 | 70,33 |
| 4-5 | 49,604 | 52,87 | 59,69 | 65,32 | 70,29 |
| 4-6 | 50,022 | 52,73 | 59,14 | 65,35 | 70,62 |
| 5-6 | 50,245 | 52,58 | 59,48 | 62,9 | 71,19 |

Table 3. Relative frequency shift for truss bar cross section 50x30x2.6mm

| Elements | ε_1 [%] | ε_2 [%] | ε_3 [%] | ε_4 [%] | ε_5 [%] |
|----------|---------------------|---------------------|---------------------|---------------------|---------------------|
| - | 0 | 0 | 0 | 0 | 0 |
| 1-2 | 5,14 | 5,76 | 5,90 | 4,47 | 7,86 |
| 1-3 | 5,93 | 7,06 | 6,00 | 4,99 | 6,18 |
| 1-4 | 5,86 | 7,06 | 6,50 | 4,66 | 6,18 |
| 1-5 | 4,57 | 7,45 | 6,70 | 4,07 | 6,35 |
| 1-6 | 4,61 | 7,46 | 5,16 | 4,07 | 6,16 |
| 2-3 | 5,28 | 1,99 | 4,12 | 4,57 | 4,86 |
| 2-4 | 5,20 | 2,80 | 4,25 | 4,57 | 4,78 |
| 2-5 | 4,82 | 1,95 | 4,38 | 7,93 | 3,21 |
| 2-6 | 4,88 | 1,95 | 4,36 | 7,93 | 3,12 |
| 3-4 | 4,48 | 4,09 | 3,87 | 7,60 | 4,30 |
| 3-5 | 4,17 | 3,89 | 4,21 | 4,02 | 4,20 |
| 3-6 | 5,05 | 3,53 | 3,43 | 4,06 | 3,08 |
| 4-5 | 4,94 | 3,52 | 3,56 | 4,06 | 3,84 |
| 4-6 | 4,14 | 3,78 | 4,45 | 4,02 | 2,68 |
| 5-6 | 3,71 | 4,07 | 3,90 | 7,62 | 1,91 |

Tables 4 presents the natural frequencies for simulation for case of bars with section 120x50x8 mm and table 5 the relative frequency shift for this section.

Table 4. Natural frequencies for truss bar with cross section 120x80x8mm

| Elements | f ₁ [Hz] | f ₂ [Hz] | f ₃ [Hz] | f ₄ [Hz] | f ₅ [Hz] |
|----------|------------------------|------------------------|------------------------|------------------------|------------------------|
| - | 133,13 | 140,97 | 144,14 | 161,43 | 166,44 |
| 1-2 | 125,91 | 132,86 | 134,48 | 154,36 | 155,58 |
| 1-3 | 124,44 | 130,61 | 135,44 | 156,28 | 161,42 |
| 1-4 | 126,25 | 130,34 | 134,06 | 155,86 | 161,42 |
| 1-5 | 127,32 | 130,45 | 134,33 | 154,98 | 156,81 |
| 1-6 | 125,91 | 130,15 | 134,99 | 154,98 | 159,41 |
| 2-3 | 125,47 | 137,97 | 140,51 | 154,2 | 157,59 |
| 2-4 | 126,9 | 136,83 | 139,84 | 154,2 | 158,02 |
| 2-5 | 127,06 | 137,68 | 139,76 | 148,86 | 160,23 |
| 2-6 | 125,95 | 137,6 | 140,42 | 148,86 | 161,75 |
| 3-4 | 127,5 | 134,65 | 139,75 | 157,39 | 161,42 |
| 3-5 | 127,48 | 135,43 | 139,92 | 155,06 | 159,2 |
| 3-6 | 125,36 | 135,28 | 141,43 | 154,99 | 161,32 |
| 4-5 | 127,43 | 135,85 | 139,23 | 154,99 | 159,71 |
| 4-6 | 128,02 | 135,39 | 138,13 | 155,06 | 161,76 |
| 5-6 | 128,06 | 134,72 | 140,08 | 149,37 | 163,23 |

Table 5. Relative frequency shift for truss bar cross section 120x80x8mm

| Elements | ε_1 [%] | ε_2 [%] | ε_3 [%] | ε_4 [%] | ε_5 [%] |
|----------|---------------------|---------------------|---------------------|---------------------|---------------------|
| - | - | - | - | - | - |
| 1-2 | 5,42 | 5,75 | 6,70 | 4,38 | 7,00 |
| 1-3 | 6,53 | 7,35 | 6,04 | 4,60 | 5,89 |
| 1-4 | 5,60 | 7,54 | 6,99 | 4,16 | 5,56 |
| 1-5 | 4,36 | 7,46 | 6,81 | 4,00 | 5,79 |
| 1-6 | 5,42 | 7,68 | 6,35 | 4,00 | 4,22 |
| 2-3 | 5,75 | 2,13 | 3,90 | 4,48 | 5,32 |
| 2-4 | 4,68 | 2,94 | 4,00 | 4,48 | 5,06 |
| 2-5 | 4,56 | 2,33 | 3,04 | 7,79 | 3,73 |
| 2-6 | 5,39 | 3,78 | 3,48 | 7,79 | 4,00 |
| 3-4 | 4,23 | 4,48 | 3,05 | 2,50 | 4,02 |
| 3-5 | 4,24 | 3,93 | 4,20 | 3,95 | 4,35 |
| 3-6 | 5,84 | 4,04 | 3,20 | 3,99 | 3,08 |
| 4-5 | 4,28 | 3,63 | 3,41 | 3,99 | 4,04 |
| 4-6 | 3,84 | 3,96 | 4,17 | 3,95 | 2,81 |
| 5-6 | 3,81 | 4,43 | 3,50 | 7,47 | 1,93 |

Figure 4 shows the relative frequencies shift when 2 elements have the modulus of elasticity $E=160000 \text{ N/mm}^2$, respective: 1-2, 1-3, 1-4, 1-5, 1-6. With the black color we have the cross section $120 \times 80 \times 8 \text{ mm}$, and with yellow color we have cross section $50 \times 30 \times 2.6 \text{ mm}$.

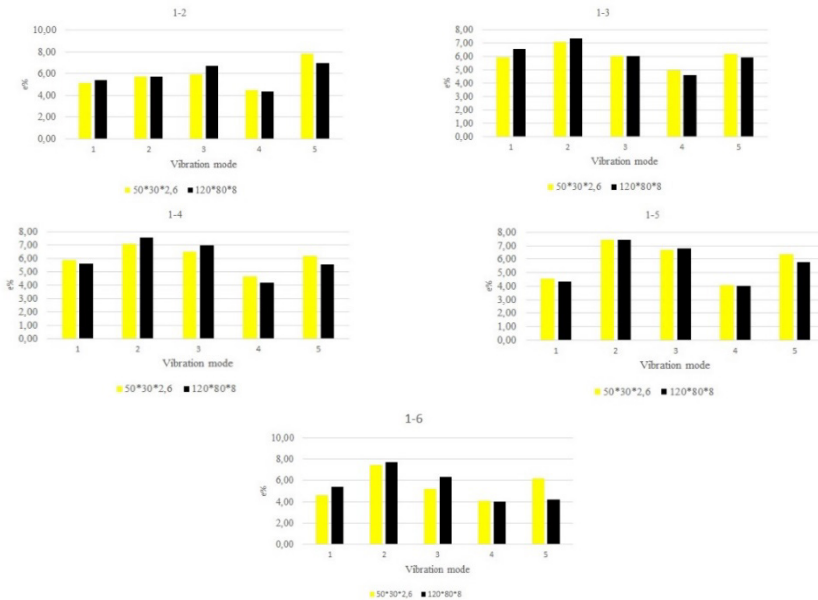


Figure 4. Comparison of the relative frequency shift in case of elements 1-2, 1-3, 1-4, 1-5, 1-6 have $E=160000 \text{ N/mm}^2$

Figure 5 shows the relative frequencies shift of the natural frequencies when elements 2-3, 3-4, 2-5, 2-6 have the modulus of elasticity $E=160000 \text{ N/mm}^2$.

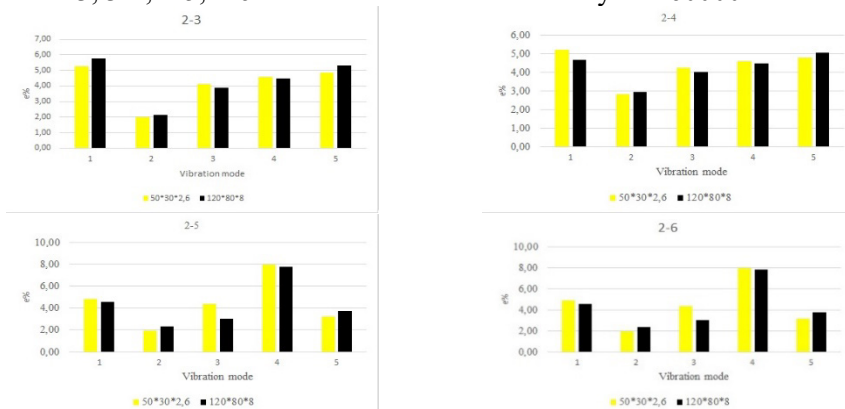


Figure 5. Comparison of the relative frequency shift in case of elements 2-3, 2-4, 2-5, 2-6, have $E=160000 \text{ N/mm}^2$

Figure 6 shows the relative deviations of the natural frequencies when 2 elements have the modulus of elasticity $E=160000 \text{ N/mm}^2$, respective: 3-4, 3-5, 3-6

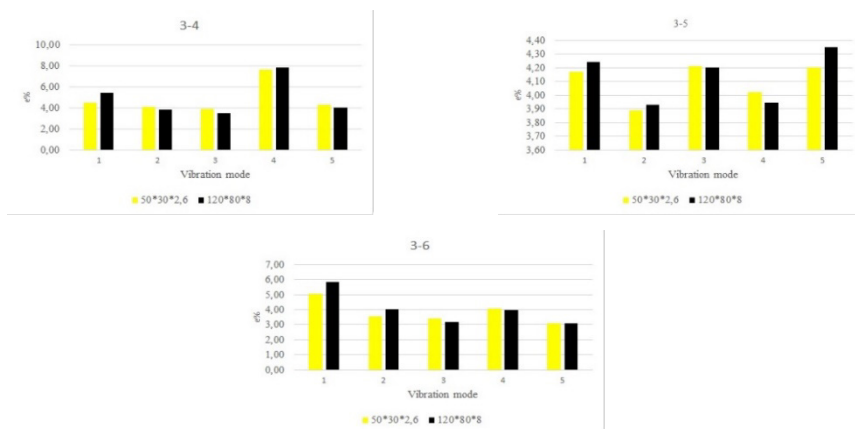


Figure 6. Comparison of the relative frequency shift in case of elements 3-4, 3-5, 3-6 have $E=160000 \text{ N/mm}^2$

Figure 7 shows the relative deviations of the natural frequencies when 2 elements have the modulus of elasticity $E=160000 \text{ N/mm}^2$, respective: 4-5, 4-6



Figure 7. Comparison of the relative frequency shift in case of elements 4-5, 4-6 have $E=160000 \text{ N/mm}^2$

Figure 8 shows the relative deviations of the natural frequencies when 2 elements have the modulus of elasticity $E=160000 \text{ N/mm}^2$, respective 5-6.

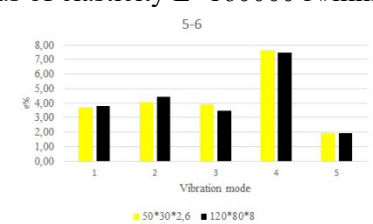


Figure 8. Comparison of the relative frequency shift in case of elements 5-6 have $E=160000 \text{ N/mm}^2$

4. Conclusion

A series of sixteen tests was performed on the Warren type beam elements to illustrate the influence of the modulus of elasticity in the behavior of the truss elements.

From figure 3, it follows that the allure of the vibration modes do not change regardless of whether the modulus of elasticity was reduced at the value of 1600000 N/mm².

The numerical modal analysis started from the structure with all the elements from the same material (structural steel $E=210000\text{N/mm}^2$) and natural frequencies were obtained.

Subsequently, 2 elements were modified where the modulus of elasticity was intentionally reduced to the value 160000 N/mm². The natural frequencies for the first 5 vibration modes were determined and their relative frequency shift was calculated.

From the analysis of figures 4 -8, it can be seen that the relative frequency shift is not influenced by the cross section chosen for the same length of the structural element.

References

- [1] Tiainen T., Mela K., Jokinen T., Heinisuo M., The effect of steel grade on weight and cost of warren-type welded tubular trusses. *Proc. Inst. Civ. Eng. Struct. Build.*, 170, 2017, pp. 815–883.
- [2] Gillman A., Fuchi K., Buskohl P.R., Truss-based nonlinear mechanical analysis for origami structures exhibiting bifurcation and limit point instabilities. *Int. J. Solids Struct.* 147, 2018, pp. 59–98.
- [3] Irvine T., Natural Frequencies of Beams Subjected to a Uniform Axial Load, Revision C, <http://www.vibration data.com>, 2011.
- [4] Jiang T., Wu Q., Wang L., Huo, L., Song G., Monitoring of Bolt Looseness-induced Damage in Steel Truss Arch Structure using Piezoceramic Transducers. *IEEE Sens. J.* 18, 2018, pp. 6660–6696.
- [5] Wardenier J., Packer J.A., Zhao X.L., Vegte G.J.V.D., *Hollow Sections in Structural Applications*, CIDECT: Geneva, Switzerland, 2010.
- [6] Yang W.W., Wang X.L., Wang D.D., Design of long-span and wave-shaped steel canopy structure of ningxia helan mountain stadium, *Adv. Mater. Res.* 2011, 243–249, 60–78.
- [7] Fenton M., McNally C., Byrne J., Hemberg E., McDermott J., O'Neill M., Automatic innovative truss design using grammatical evolution. *Autom. Constr.*, 39, 2014, pp. 50–70.

- [8] Lahe A., et al., *An exact solution of truss vibration problems*, Proceedings of the Estonian Academy of Sciences, 68(3), Sept. 2019, pp. 244+.Gale Academic OneFile

Address:

- PhD. Stud. Dan Alexandru Pîrșan, Babeș-Bolyai University, Department of Engineering Science, Cluj-Napoca, Romania
dan.pirsan@ubbcluj.ro

The influence of the change of the longitudinal modulus of elasticity on the dynamic behavior of a Warren truss

Zeno-Iosif Praisach*, Dan Alexandru Pîrșan

Abstract. *Trusses are commonly used structures and they are present in the most constructions because it use a small amount of material and for the loads they can support. The paper presents the dynamic behavior of a Warren truss with seven elements when for one member of the truss the modulus of elasticity is much different compared to the other elements. The relative frequency shift for the first seven vibration mode are calculated taking into consideration that the slenderness ratio has a constant value and the transverse section of the elements is changed. The conclusions reveal that by maintaining the constant value of a slenderness ratio, the relative frequency shift is not modified for the considered transverse sections of the elements of the Warren truss.*

Keywords: *Warren truss, slenderness ratio, modal analysis, relative frequency shift*

1. Introduction

Trusses are simple structures whose members are subject to axial compression and tension only [1]. Warren truss comprise of a series of equilateral triangles, that means that every member has the same length. In a truss, all the elements are pinned (hinged) at both ends.

A Warren truss is to be designed to achieve a definite set of natural frequencies to avoid resonance, or to provide study materials for certain critical computation of vibration instrumentation [2-3].

To calculate the natural frequency analysis assumes that a structure vibrates in the absence of excitation and damping [4].

The natural frequency depends upon stiffness and mass distributions, boundary conditions [5].

In this paper, the authors approach the numerical modal analysis for a single-span Warren truss with seven elements by calculating the natural frequencies and comparing them for the same structure, but in which for one element the elasticity modulus has been deliberately changed, considering this element as weakened or damaged.



2. Analytic approach

A single-span Warren truss with seven elements is illustrated in figure 1.

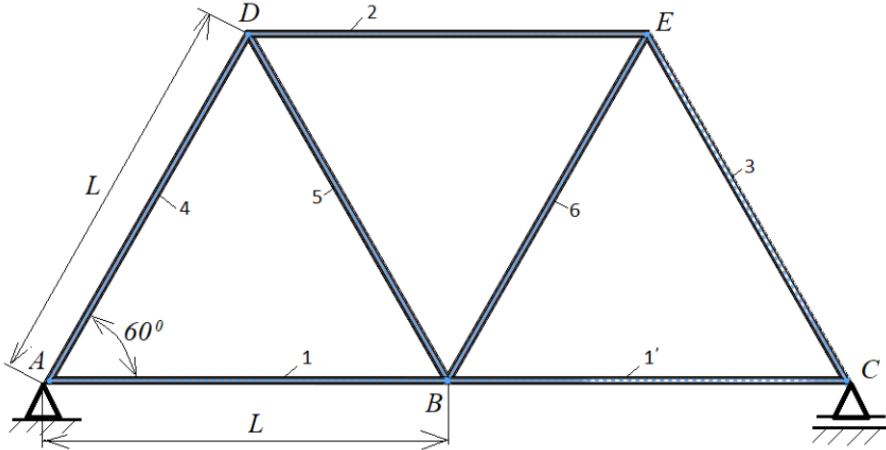


Figure 1. Warren truss with seven elements

It is known from the literature that in order to determine the longitudinal natural frequencies, the structural elements can have the following contour conditions:

- fixed at one end and free to the other with axial displacement $u(x)$:

$$u(x) = B \sin(k_L x) \quad (1)$$

where,

B is the integration coefficient,

k_L (2) are the eigenvalues for the considered natural frequencies (f_n) which can be computed with relation (3):

$$k_L = \frac{(2n-1)\pi}{2L} \quad (2)$$

$$f_n = \frac{(2n-1)\pi}{4L} \cdot \sqrt{\frac{E}{\rho}} \quad (3)$$

with,

L [m] is the length of the element,

E [N/m²] is the modulus of elasticity,

ρ [kg/m³] is the mass density of the element.

- free at both ends with axial displacement $u(x)$:

$$u(x) = A \cos(k_L x) \quad (4)$$

where,

B is the integration coefficient,

$$k_L = \frac{n \cdot \pi}{L} \quad (5)$$

are the eigenvalues for the considered natural frequencies (f_n) which can be computed with relation (6):

$$f_n = \frac{n}{2L} \cdot \sqrt{\frac{E}{\rho}} \quad (6)$$

- fixed at both ends with axial displacement given with (1) and k_L with (4);
- fixed at one end and free to the other with a mass. The axial displacement is given with (1) and the characteristic equation which permit us to calculate the eigenvalues is:

$$\cos(k_L \cdot L) - \frac{M}{m} (k_L \cdot L) \sin(k_L \cdot L) = 0 \quad (7)$$

here,

M [kg] is the mass at the free end,

m [kg] is the mass of the structural element.

For this case, the natural frequencies are given with (8):

$$f_n = \frac{k_L}{2\pi} \cdot \sqrt{\frac{E}{\rho}} \quad (8)$$

3. Numerical investigations

For the numerical investigations it was considered the Warren truss presented in figure 1. All the elements have the same cross section. By using FEM analysis it was obtained the first seven natural frequencies ($n=1, 2, \dots, 7$). The SolidWorks software were used to calculate the natural frequencies. By using this software and analyzing the structure as a truss, structural elements 1 and 1' will have the same material type.

The following cases were analyzed:

- all the elements are of the same material, structural steel with $E=2.1 \cdot 10^{11}$ N/m² and all the elements are the same. The natural frequencies f_U were determined;

- for each structural elements only the modulus of elasticity was changed to value of $E_I=1.6 \cdot 10^{11}$ N/m² considering it as a weakened or damaged structural element, and the natural frequencies f_D were determined;
- the natural frequencies obtained by modifying each structural element were compared with the natural frequencies obtained in the case of the structure made of the same material. The relative frequencies shift $\varepsilon = \frac{f_U - f_D}{f_U} \cdot 100$ [%] were calculated;
- for the cases mentioned above, three types of structural elements were considered, as follows: rectangular tube 120x80x8 mm; pipe 33,7x4 mm and square tube 80x80x5 mm;
- for these three types of structural elements, the length of the structural element was calculated so that the slenderness coefficient has the same value of: $\lambda = L \cdot \sqrt{\frac{A}{I}} = 0.01$, where A [m²] is the cross section area and I [m⁴] is the moment of inertia.

The results are presented in the tables below. In the first column, are indicated the truss bars for which the modulus of elasticity was reduced to E_I .

- Warren truss with truss bars of rectangular tube 120x80x8 mm with:
 - o $L=4265$ mm,
 - o $A=2779.19$ mm²,
 - o $I=4957718.55$ mm⁴.

The natural frequencies for the first seven vibration modes (f_1, f_2, \dots, f_7) are presented in table 1.

Table 1. Natural frequencies for Warren truss with rectangular tube 120x80x8 mm.

| Weakened element | f_1 [Hz] | f_2 [Hz] | f_3 [Hz] | f_4 [Hz] | | f_5 [Hz] | f_6 [Hz] | f_7 [Hz] |
|------------------|------------|------------|------------|------------|--|------------|------------|------------|
| - | 67.69 | 90.502 | 158.67 | 177.26 | | 227.76 | 263.57 | 284.78 |
| 1 | 61.595 | 89.193 | 153.900 | 169.12 | | 226.43 | 261.45 | 265.13 |
| 2 | 67.142 | 88.236 | 157.64 | 176.55 | | 218.49 | 250.91 | 284.43 |
| 3 | 65.569 | 89.817 | 151.05 | 175.09 | | 224.09 | 263.54 | 279.48 |
| 4 | 67.568 | 84.713 | 154.62 | 174.4 | | 222.02 | 263.46 | 284.76 |
| 5 | 67.645 | 87.289 | 157.59 | 173.81 | | 217.37 | 258.01 | 283.43 |
| 6 | 66.632 | 90.501 | 152.52 | 171.4 | | 226.36 | 254.77 | 282.81 |

- Warren truss with structural elements of pipe 33.7x4 mm with:
 - o $L=1070$ mm,
 - o $A=373.22$ mm²,
 - o $I=41898.28$ mm⁴.

Table 2 contains the natural frequencies for the first seven vibration modes.

Table 2. Natural frequencies for Warren truss with pipe 33.7x4 mm.

| Weakened element | f_1 [Hz] | f_2 [Hz] | f_3 [Hz] | f_4 [Hz] | f_5 [Hz] | f_6 [Hz] | f_7 [Hz] |
|------------------|------------|------------|------------|------------|------------|------------|------------|
| - | 269.48 | 360.44 | 632.67 | 705.58 | 907.74 | 1050.4 | 1133.7 |
| 1-1' | 245.21 | 355.12 | 613.75 | 673.07 | 902.42 | 1041.1 | 1056.6 |
| 2 | 267.27 | 351.45 | 628.55 | 702.74 | 870.97 | 999.87 | 1132.2 |
| 3 | 261.02 | 357.73 | 602.26 | 697.08 | 893.17 | 1050.3 | 1112.5 |
| 4 | 268.97 | 337.44 | 616.46 | 694.28 | 884.82 | 1050.0 | 1133.6 |
| 5 | 269.31 | 347.63 | 628.39 | 692.0 | 866.09 | 1028.4 | 1128.2 |
| 6 | 265.3 | 360.44 | 608.04 | 682.31 | 902.16 | 1015.2 | 1126.0 |

- Warren truss with structural elements of square tube 80x80x5 mm with:
 - o $L=3055$ mm,
 - o $A=1435.62$ mm²,
 - o $I=1314420.61$ mm⁴.

The natural frequencies for the first seven vibration modes are presented in table 3.

Table 3. Natural frequencies for Warren truss with square tube 80x80x5 mm.

| Weakened element | f_1 [Hz] | f_2 [Hz] | f_3 [Hz] | f_4 [Hz] | f_5 [Hz] | f_6 [Hz] | f_7 [Hz] |
|------------------|------------|------------|------------|------------|------------|------------|------------|
| - | 94.501 | 126.35 | 221.51 | 247.46 | 317.97 | 369.96 | 397.57 |
| 1-1' | 85.991 | 124.51 | 214.86 | 236.1 | 316.11 | 365.01 | 370.14 |
| 2 | 93.735 | 123.18 | 220.08 | 246.48 | 305.02 | 350.29 | 397.09 |
| 3 | 91.539 | 125.39 | 210.88 | 244.45 | 312.85 | 367.93 | 390.18 |
| 4 | 94.329 | 118.27 | 215.86 | 243.48 | 309.95 | 367.84 | 397.55 |
| 5 | 94.439 | 121.86 | 220.01 | 242.65 | 303.47 | 360.21 | 395.69 |
| 6 | 93.023 | 126.35 | 212.93 | 239.28 | 316.01 | 355.68 | 394.82 |

Table 4. The relative frequencies shift (ε_n) for $n = 1, 2, \dots, 7$ vibration modes.

| Weakened element | ε_1 [%] | ε_2 [%] | ε_3 [%] | ε_4 [%] | ε_5 [%] | ε_6 [%] | ε_7 [%] |
|------------------|---------------------|---------------------|---------------------|---------------------|---------------------|---------------------|---------------------|
| 1-1' | 9.0 | 1.46 | 3.0 | 4.6 | 0.58 | 0.8 | 6.9 |
| 2 | 0.8 | 2.5 | 0.7 | 0.4 | 4.1 | 4.8 | 0.1 |
| 3 | 3.1 | 0.8 | 4.8 | 1.2 | 1.6 | 0.0 | 1.9 |
| 4 | 0.2 | 6.4 | 2.6 | 1.6 | 2.5 | 0.0 | 0.0 |
| 5 | 0.1 | 3.6 | 0.7 | 1.9 | 4.6 | 2.1 | 0.5 |
| 6 | 1.6 | 0.0 | 3.9 | 3.3 | 0.6 | 3.3 | 0.7 |

The relative frequencies shift (ε) for the cases analyzed above are presented in the table 4 and illustrated in figure 2 for the weakened truss bar 1, 2, ..., 6.

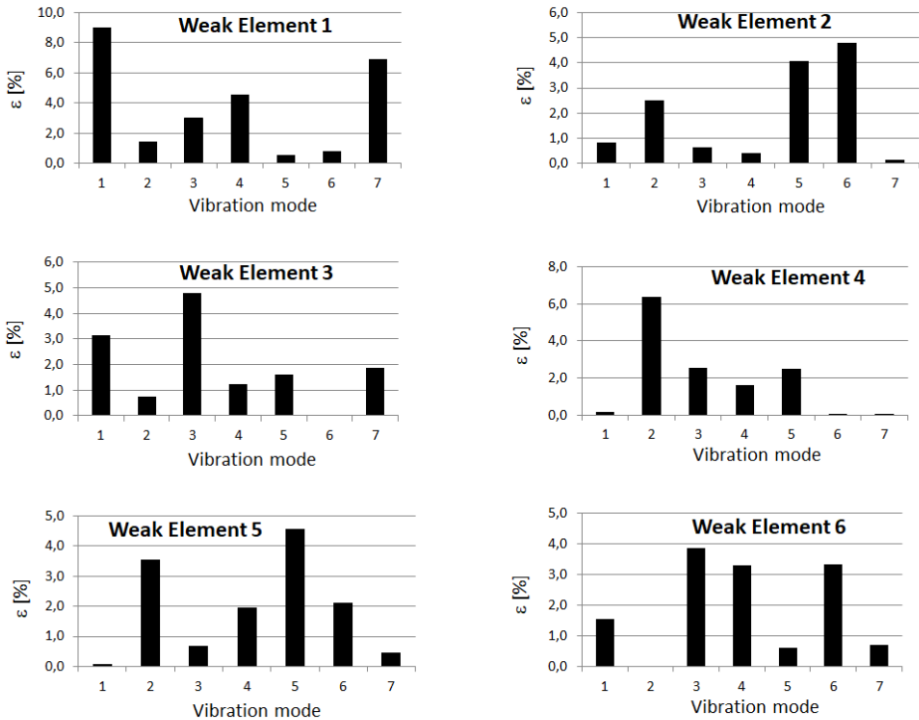
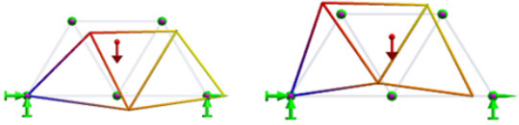
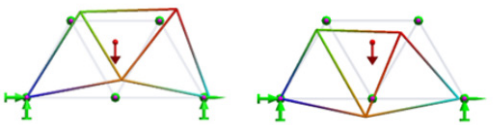
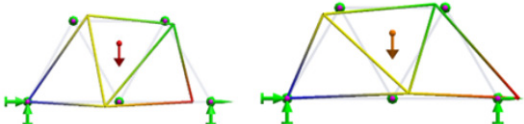
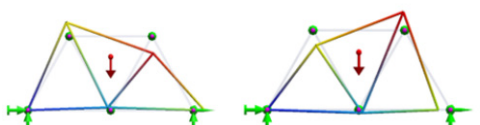
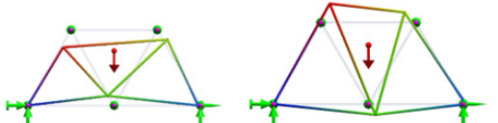
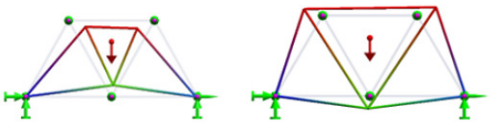
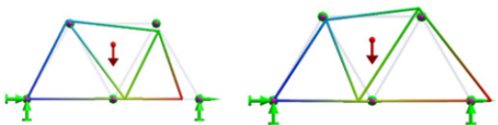


Figure 2. Relative frequencies shift for the first 7 vibration modes.

The mode shapes for the first seven vibration modes are illustrated in table 5.

Table 5. The first seven mode shapes for a single-span Warren truss

| Vibration mode | Mode shape | |
|----------------|--|--|
| 1 |  | |
| 2 |  | |
| 3 |  | |
| 4 |  | |
| 5 |  | |
| 6 |  | |
| 7 |  | |

4. Conclusions

The paper analyzed the dynamic behavior for a Warren truss in case an element is weakened by the forced modification of the modulus of elasticity. The material considered in the modal analysis is structural steel with $E=2.1 \cdot 10^{11}$ N/m², and the weakened structural element has the modulus of elasticity $E_I=1.6 \cdot 10^{11}$ N/m².

The modal analysis for three different cross-sections of the structural element, respectively rectangular tube 120x80x8 mm with $L=4265$ mm, pipe 33.7x4 mm with $L=1070$ mm and square tube 80x80x5 mm with $L=3055$ mm, with the constant slenderness ratio $i=0.01$, revealed the fact that the relative frequency shift ε (table 4), for each individual vibration mode, does not change.

This observation leads to the conclusion that if an element of the Warren truss is weakened, from the point of view of dynamic behavior, respectively by monitoring the natural frequencies, recognition patterns and identification of the weakened element can be obtained by drawing diagrams according to figure 2.

The mode shapes (table 5) obtained from the modal analysis have the same representation and do not take into account the change in the modulus of elasticity of the structural element in the Warren truss component.

References

- [1] Irvine, T., *Natural Frequencies of Beams Subjected to a Uniform Axial Load, Revision C*, vibrationdata.com, 2011.
- [2] Kanar A.K., *PhD. Thesis: Free Vibrations of 1-D and 2-D Skeletal Structures*, National Institute of Technology, Rourkela, India, 2013.
- [3] Fazli N., Malaek S.M.B., Abedian A., Teimouri H., Development of a new analytical tool to design hierarchical truss beam for natural frequency, *Journal of Mechanical Science and Technology*, 25 (10), 2011, pp. 2495-2503.
- [4] Lahe A., Braunbruck A., Klauson A., *An exact solution of truss vibration problems*, Proceedings of the Estonian Academy of Sciences, 2019, 68, pp. 244-263.
- [5] Millan-Paramo C., Millan-Romero E., Jove F., Truss optimisation with natural frequency constraints using Tiki-Taka algorithm, *PalArch's Journal of Archaeology of Egypt/Egyptology, PJAEE*, 18 (5), 2021, pp. 304-314.

Addresses:

- Lect. Dr. Eng. Habil. Zeno-Iosif Praisach, Babeş-Bolyai University, Department of Engineering Science, Cluj-Napoca, Romania, zeno.praisach@ubbcluj.ro
(* corresponding author)
- PhD. Stud. Dan Alexandru Pirsan, Babeş-Bolyai University, Department of Engineering Science, Cluj-Napoca, Romania, dan.pirsan@ubbcluj.ro

Simulation of electric field lines produced by electric point charges

Marius-Florian Predus, Cristian-Mircea Muscai*, Cornel Hatiegan

Abstract. *The paper proposes a method of solving differential equations using Runge-Kutta method and presents an application made in a Visual programming language that solves two differential equations step by step drawing the graph obtained for two electrically charged particles that interact by their electrical fields.*

Keywords: *differential equations, electrical field, simulation*

1. Introduction

Numerical methods are those techniques that allow the transformation of mathematical models into numerical models (operating on finite spaces) and assume algorithms that can be easily transformed into source codes, using different classical programming languages and, through them, solve real problems with the help of the computer [1], [2].

Numerical calculation methods often require retaining a very large number of terms and developing them in a Taylor series in order to obtain the best accuracy of the results. This is not always possible due to the large number of calculations required for each of the required points, especially if the integration step is constant and of very small value, these limitations being imposed by the memory space and the execution speed of these algorithm calculations [1], [2], [3].

Partial differential equations are often used in mathematically oriented scientific fields such as physics and engineering, aiding in the scientific understanding of phenomena in the fields of electrostatics, electrodynamics, thermodynamics and other physics-related phenomena modeling applications [1], [2], [4].

The integration of differential equations by numerical methods requires the creation of a program that will process the entered data and obtain a discrete string of values that represent an approximation of the exact solution requested. The accuracy of this solution depends on the solving method used but also on the chosen form of the equations subjected to numerical processing [3], [4].



The difficulty of creating computer programs that perform the integration of differential equations is to find a critical ratio between the processing precision and the speed of the program's execution, excluding the limit points where the defined functions do not make sense.

In order to obtain an algorithm as stable as possible, the time interval dt must be small but large enough for the method to be efficient from the point of view of the duration of the calculation [2], [3].

In general, integration methods are divided into two large categories: step-by-step methods and complex methods that take into account several previous values, not just one, as is the case with step-by-step methods [4].

2. The Runge-Kutta method

Runge-Kutta methods are iterative methods for solving ordinary differential equations used in setting initial value problems where we are given a differential equation $y'(t)=f(t,y(t))$ over a time interval $[t_0, t_1]$ with a starting point $y(t_0)=y_0$.

The Runge-Kutta method of the fourth degree performs four successive approximations, and the time interval dt must be chosen so that the integration is as precise as possible, being the most frequently used in practice [5], [6], [7].

Unlike Euler's Method, which calculates one slope at an interval, Runge-Kutta calculates four different slopes and uses them as weighted averages to better approximate the actual slope, the velocity, of the monitored body [6], [7].

These slopes are commonly named k_1 , k_2 , k_3 and k_4 , and must be calculated at each time step. Its position is then calculated using this new slope at each iteration. The Runge-Kutta's formula is defined as [4], [5], [6]:

$$y_{i+1} = y_i + \frac{1}{6}(k_1 + 2k_2 + 2k_3 + k_4) \quad (1)$$

Where each term is defined as:

$$k_1 = f(x_i, y_i) \quad (2)$$

$$k_2 = f(x_i + \frac{1}{2}h, y_i + \frac{1}{2}k_1h) \quad (3)$$

$$k_3 = f(x_i + \frac{1}{2}h, y_i + k_2h) \quad (4)$$

$$k_4 = f(x_i + h, y_i + k_3h) \quad (5)$$

Each of the Runge-Kutta terms has a well-defined role in the calculation method used: k_1 is the increment based on the slope at the beginning of the interval, k_2 is the increment based on the slope at the midpoint of the interval, k_3 is the increment based on the midpoint slope and k_4 is the increment based on the slope at the end of the interval [5], [6].

The method used has the advantage that during the integration, the step size is adapted so that the estimated error remains below a threshold defined by the user, thus solving the two distinct cases that may appear during the program run, i.e. if the calculated error is too large, it is repeated with a step of a smaller size, and if the error is much too small, the step size is increased to save processing time, thus helping the user who no longer has to identify the size suitable for processing [3], [5], [6].

3. Electric field line modeling application

The developed application calculates the steps required for the successive plotting of the solution for the electrostatic equations for the 3 distinct cases using the Runge-Kutta method of order 4, the standard variant of the method, and 13 necessary constants.

For the case of the two electrostatically charged particles, their modeling is done with the help of two differential equations [8] which have as boundary conditions $x(s_0) = x_0$ and $y(s_0) = y_0$:

$$\frac{dx}{ds} = \frac{-E_y}{\sqrt{E_x^2 + E_y^2}} \quad (6)$$

$$\frac{dy}{ds} = \frac{E_x}{\sqrt{E_x^2 + E_y^2}} \quad (7)$$

The first case is presented in Figure 1 where we considered two electrostatically charged point particles with charges of opposite signs, in which case the equipotential field lines and the field lines that close between the two electrostatically charged particles are drawn.

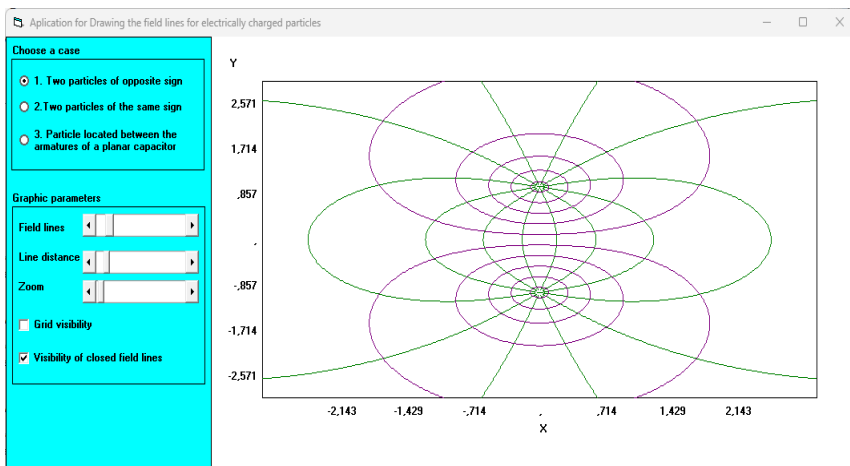


Figure 1. The two particles have opposite signs

The second case is somewhat similar, but the potentials of the two particles differ in the sense that they are now of the same sign, which can also be seen in Figure 2 where their field lines repel each other.

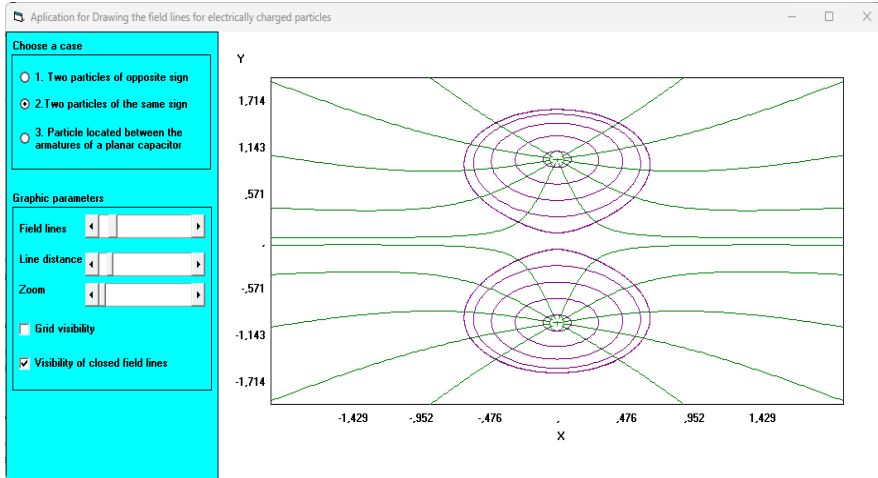


Figure 2. The two particles have same signs

The third case requires placing a single electrostatically charged particle between the armatures of a planar capacitor, as seen in Figure 3, and the field lines are drawn for this case, with the user being able to change the distance of the particle from the capacitor arms, represented as two parallel lines in the graphic.

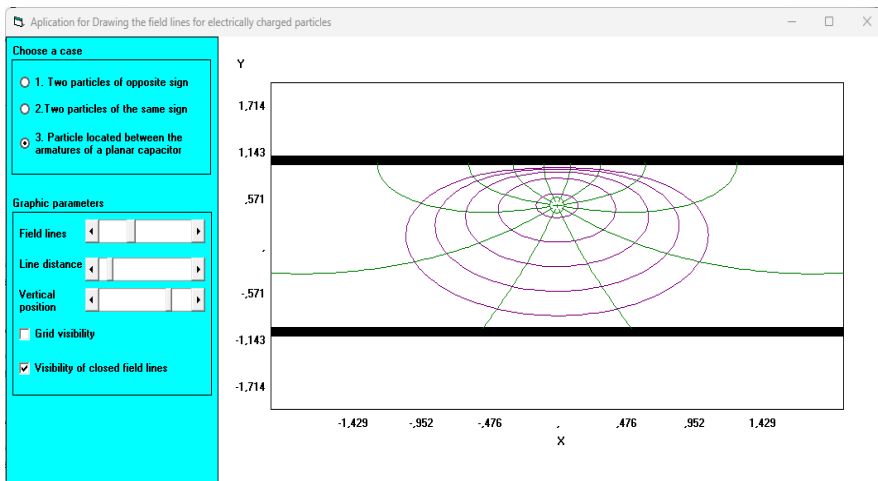


Figure 3. The particle placed between capacitor's armatures

The application allows changing the number of equipotential lines displayed, the size of the drawn plane, and the distance between successive field lines. For better visibility, the application window can be resized and the lines on the display grid can be hidden.

We often come across simulation applications made for didactic purposes using common programming languages in different technical fields [9], [10].

The program is made in the Visual Studio development environment, with the help of the Visual Basic programming language, in the form of a standard executable that allows it to run under Windows operating systems [11], [12]. The application consists of a module containing the graphics routines and a main window named Form1, on which several graphics controls are placed, including a PictureBox control that represents the display surface for graphic functions, and several HscrollBar controls for setting various display parameters like zoom or number of lines drawn.

To calculate the grid lines and the values displayed on the graph axes, we use a graphic routine called "Draw" which receives as values the limits, minimum and maximum values of the axes and the Form window that contains the graphic control on which the respective lines are drawn [13], [14].

The three cases are selected using a set of three RadioButton controls that allow individual selection of the drawn cases.

The starting point for the application is the main form. From the main form, based on our selected option, one of the two routines, "Afişez" or "Afisez1", is called, allowing the calculation of the derivatives and the point-by-point plotting of the graphs resulting from different scaling for each type of curve drawn on the screen [15].

```

Sub rezolv(ByRef hr As Double, ByRef x As Double, ByRef y_par() As Double)
Dim rk1(1 To 20) As Double
Dim rk2(1 To 20) As Double
Dim rk3(1 To 20) As Double
Dim rk4(1 To 20) As Double
Dim ry1(1 To 20) As Double

Form1.sist y_par(), rk1()
For j = 1 To 2
    rk1(j) = hr * rk1(j)
    ry1(j) = y_par(j) + rk1(j) / 2
Next j

Form1.sist ry1(), rk2()
For j = 1 To 2
    rk2(j) = hr * rk2(j)
    ry1(j) = y_par(j) + rk2(j) / 2
Next j

Form1.sist ry1(), rk3()
For j = 1 To 2
    rk3(j) = hr * rk3(j)
    ry1(j) = y_par(j) + rk3(j)
Next j

Form1.sist ry1(), rk4()
For j = 1 To 2
    rk4(j) = hr * rk4(j)
    y_par(j) = y_par(j) + (rk1(j) + 2 * (rk2(j) + rk3(j)) + rk4(j)) / 6
Next j

```

Figure 4. The routine that implements the Runge-Kutta method

The "Rezolv" subroutine shown in Figure 4 is the one that helps to implement the 4th order Runge-Kutta algorithm, which successively calculates k1, k2, k3 and k4, returning the new values to the calling routine with the help of the parameters passed by reference to it. To avoid getting stuck, the algorithm calculates, at each step, a reference value that represents the sum of the squared dx and dy. If this value is lower than a very small imposed limit, it stops the program because the desired precision has been reached or it has reached a point of singularity from where the created algorithm can no longer exit. The program can calculate only in one direction, based on the values already memorized, so a dead lock point can't be exited otherwise [11], [12].

The types of the variables used in the program are Double precision to keep the accuracy of the processed data within reasonable limits due to the small quantities used to model the two charged particles [10], [11], [12].

4. Conclusions

The advantage of implicit Runge-Kutta methods over explicit methods is their greater stability, especially when stiff equations are applied.

The application allows drawing of all existing field lines between electrostatically charged particles, both of the equipotential type that always have a closed contour, and of the others that originate in the vicinity of positive electric charges and close to negative electric charges.

The proposed application has a simple and intuitive interface and the results obtained can represent the basis of an understanding of the way of drawing the field lines and the way of interaction between electrically charged particles.

References

- [1] Demsoreanu B., *Metode numerice cu aplicații in fizică*, Editura Academiei-Române, 2005
- [2] Sorea, D., Lungoci, C., Scutaru G., *Metode numerice cu aplicații în ingineria electrică. Curs aplicativ*, Editura Universității Transilvania Brașov, 2009.
- [3] Burrage K., *Parallel and Sequential Methods for Ordinary Differential Equations, Numer. Math. Sci. Comput.*, Oxford University, New York, 1995.
- [4] Butcher J.C., *Numerical Methods for Ordinary Differential Equations*, 2nd ed., John Wiley & Sons, Chichester, 2003.
- [5] Shampine L.F., *Numerical Solution of Ordinary Differential Equations*, Chapman & Hall, New York, 1994.
- [6] Ketcheson D.I., BinWaheed U., A comparison of high-order explicit Runge-Kutta, extrapolation, and deferred correction methods in serial and parallel, *Communications in applied mathematics and computational science*, 9(2), 2014, pp.175 – 200.

- [7] Scutaru G., *Metode numerice*, Editura Universității Transilvania Brașov, 2003.
- [8] Hațiegan C., Sucișu L., *Fizică Tehnologică. Teorie și aplicații*, Editura Eftimie Murgu, Resita, 2010/
- [9] Hatiegan C., Stroia M.-D., Popescu C., Muscai C.-M., Application for Simulating and Analysis of a Serial R-L-C Circuit, *Analele Universității Constantin Brâncuși din Târgu-Jiu - Seria Inginerie*, 3, 2020.
- [10] Stroia M.-D., Hatiegan C., Muscai C.-M., Simulating an improved algorithm for propagation of transverse oscillations through a string, *Studia Universitatis Babeș-Bolyai Engineering*, 65(1), 2020.
- [11] Schneider D., *An Introduction to Programming Using Visual Basic*, 9th Edition, Pearson, 2013, USA.
- [12] Newsome B., *Beginning Visual Basic 2015*, Wrox, USA, 2015.
- [13] Alexander R., Diagonally implicit Runge–Kutta methods for stiff O.D.E.s, *SIAM J. Numer. Anal.* 14(6), 1977, pp. 1006–1021.
- [14] Zlatev Z., Dimov I., Faragó I., Havasi Á., *Richardson Extrapolation: Practical Aspects and Applications*, De Gruyter Ser. Appl. Numer. Math. 2, De Gruyter, Berlin, 2018.
- [15] Durham Jr. H.L., Francis Jr. O.B., Gallaher L.J., Hale Jr. H.G., Perlin I.E., *Final Report: Study of methods for the numerical solution of ordinary differential equations*: Final report. 9 Nov. 1963 - 8 Nov. 1964. NASA, Huntsville, AL, Georgia Institute of Technology, Engineering Experiment Station, Atlanta, Georgia, 1965.

Adresses:

- Dr. Eng. Marius-Florian Predus, Babeș-Bolyai University, Faculty of Engineering, Piața Traian Vuia, nr. 1-4, 320085, Reșița, Romania
marius.predus@ubbcluj.ro
- PhD. Stud. Eng. Cristian-Mircea Muscai, Polytechnic University of Bucharest, Faculty of Electrical Engineering, Splaiul Independenței 313, 060042, București, Romania
muscaicristian@yahoo.com
(* corresponding author)
- Lect. Dr. Eng Cornel Hatiegan, Babeș-Bolyai University, Faculty of Engineering, Piața Traian Vuia, nr. 1-4, 320085, Reșița, Romania
cornel.hatiegan@ubbcluj.ro

Design of low voltage electrical circuits for industrial receivers

Liviu-Bogdan Protea, Cristian-Mircea Muscai*

Abstract. *The paper presents the creation of a software for designing, verifying and analyzing voltage drops on electrical circuits, taking into account the classic design formulas and also the reactance of low-voltage electric cables. With the help of the application, it is possible to dimension and verify the existing electrical circuits as well as those of the single-wire schemes being designed as a result of the modernization or replacement of equipment in existing distribution networks. The application can be used for designing general consumers or for electrical equipment operated with direct start, star-delta or frequency converter electric motors.*

Keywords: *software, application, dimensioning, design, electrical circuits, electrical networks.*

1. Introduction

The design and dimensioning of low-voltage electric circuits requires the knowledge of the electrical parameters of the loads (receivers) in order to choose the protection apparatus and establish the right section of the electric cables based on their behavior.

Most of the length of the electrical circuit is outside the electrical panel, but the protection must be chosen according to the type of load in order to be able to properly dimension the protection of the cables used, this is done in the dimensioning of the electrical panels.[1]

Most of the length of the electrical circuit is outside the electrical panel, but the protection must be chosen according to the type of load and the type of consumer in order to be able to properly dimension the protection of the cables used, this is done in the dimensioning of the electrical panels. Electric consumers are described by specific parameters such as: current, voltage, nominal power, power factor, starting current, peak current and other parameters that must be taken into account when designing and resizing electrical networks.



From the supply point to the consumer, the effective value of the voltage decreases, due to the reactance of the supply circuit, characterized by the electrical resistance but also by the inductive and capacitive components specific to each supply line.

In the activity of designing electrical circuits, there is a need to determine the section of the cables and implicitly check the value of the voltage drops for the power lines, values imposed by the regulations but also by the proper operation of the powered electrical equipment.

In order to properly dimension the insulated power lines, the losses due to the insulation and its aging must also be taken into account, as is also presented in the work [2]. [3].

In the design of electrical circuits, exceeding the recommended voltage drop values negatively influences the operation of powered equipment and generates energy losses, reducing the total efficiency of the installation without bringing any benefits. In the design and verification process, verification formulas are used that require compliance with the limits imposed by local regulations like in the formula number (1).

$$\Delta U \leq \Delta U_{ad} \quad (1)$$

To analyze the operation of electrical circuits, modelling and simulation can be done using various dedicated programs [3]. To model the electrical supply circuits, we use the balanced three-phase alternating current line both in the case of internal and external networks because the receivers are symmetrical by their construction or are symmetrized by equal charging of the phases. That's why the distribution lines are modeled by a simplified scheme that takes into account only one of the phases in which the total reactance is presented with the help of the total resistance R in series with the total reactance X, according to Figure 1.

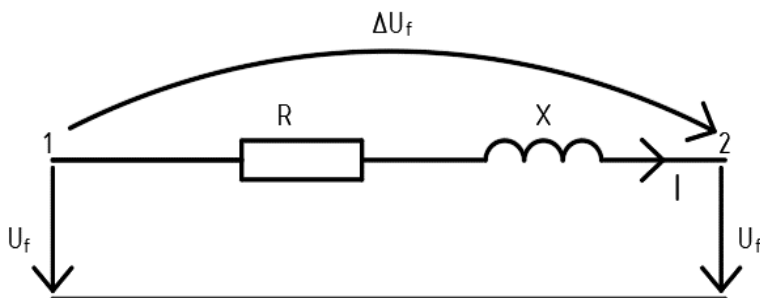


Figure 1. The typical model of a power line.

The voltage loss can be determined if the current through the respective line and the R and X parameters of the respective line are known using the formula (2, 3, 4)

$$\Delta U_f = RI \cos \varphi - XI \sin \varphi \quad (2)$$

$$R = \rho \frac{l}{s} = \frac{l}{\gamma \cdot s} \quad (3)$$

The electrical resistance parameter of a supply line R is determined based on the material characteristics of the conductors ρ used and the length of the respective line. For copper and aluminum cables, the conductivity values are $\gamma = 57$ and $\gamma = 34$, and "s" is the cable section.

The total reactance X of the line is calculated based on the data from the cable catalog sheets where it is described as the reactance per unit length.

The total reactance of the power line is distributed along the electrical cables, which helps to diagnose and detect damaged portions by using high-frequency sonar equipment as explained in the paper [4]

If the exact parameters of the line are not known or the data provided by the catalogs are not sufficient, then the unit reactance value can be approximated as $X_0 = 0.0001 \text{ } \Omega/\text{m}$. [5]

Substituting in the relation (2) the resistance and the reactance, the expression of the voltage drop for a three-phase alternating current line becomes one in which resistance and reactance are taken into account.

$$\Delta U\% = \frac{P \cdot l \cdot 10^5}{U^2} \cdot \frac{1}{\gamma \cdot s} \cdot (r_0 + x_0 \cdot \text{tg} \varphi) \quad (4)$$

If the real parameters of the cables to be used are not known from the design phase, the designer is forced to disregard the reactive components and take into account only the resistive component of the cables for the calculation of the voltage drop. (4)

During the course of the project, he can make any corrections especially for the longer lines after he makes a recheck of them right before the completion of the project.

$$\Delta U\% = \frac{P \cdot l \cdot 10^5}{U^2} \cdot \frac{1}{\gamma \cdot s} \quad (5)$$

To obtain the value of the relative error $\varepsilon\%$ we combine the two relations regarding the voltage drop obtained by the two methods, the one that takes into account the reactance of the cables and the one that does not take it into account. The obtained value can become significant for longer cables and larger sections.

$$\varepsilon\% = \frac{x_0 \cdot \operatorname{tg} \varphi}{r_0 + x_0 \cdot \operatorname{tg} \varphi} \quad (6)$$

For example, by adopting the permissible error $\varepsilon=0.05$ the sections of copper and aluminum cables expressed in Ω/m must satisfy the relations

$$s_{Cu} \leq \frac{9.93 \cdot 10^{-4}}{x_0 \cdot \tan \varphi} \quad (7)$$

$$s_{Al} \leq \frac{16.45 \cdot 10^{-4}}{x_0 \cdot \tan \varphi} \quad (8)$$

2. Example of application for the electrical design

A three-phase motor with the following nominal data is considered: power of 7.5 kW, power factor $\cos \varphi = 0.85$, line voltage of 400V.

The voltage loss between to the distribution board and the consumer where the circuit is made with copper cable with a section of 10 mm^2 and the circuit length l is 85m will be calculated in the following situations:

- a) Taking into account the inductive reactance of the cable
- b) Neglecting the inductive reactance of the cable.

First step is to calculate the specific resistance for the cable with a section of 10 mm^2 with the help of the next relation:

$$R_0 = \frac{1}{\gamma \cdot s} = \frac{1}{57 \cdot 10} = 0.175 \cdot 10^{-3}$$

Step two is to determine the specific reactance of the cable $x_0 = 0.1 \cdot 10^{-3} \Omega/\text{m}$

From the value of $\cos \varphi = 0.85$ corresponds to $\tan \varphi = 0.62$.

Step three is where we determine the voltage drop in the two considered situations with and without considering the influence of the inductive reactance of the cable. The voltage loss is calculated with the expression (4)

$$\Delta U\% = \frac{7.5 \cdot 85 \cdot 10^5}{400^2} \cdot (0.175 + 0.1 \cdot 0.62) \cdot 10^{-3} = 0.094$$

$$\Delta U\% = \frac{7.5 \cdot 85 \cdot 10^5}{400^2} \cdot 0.175 \cdot 10^{-3} = 0.069$$

The error is:

$$\varepsilon = \frac{0,069}{0.094} \cdot 100 = 26\%$$

The voltage drop obtained in this way falls within the limits allowed for normal operation and direct start-up of the verified electric motor type.

3. Description of the application

The proposed application is made using the Livecode Community Edition version 9 programming language, which allows the creation of rich and interactive graphical interfaces. Applications made with this programming language can be compiled directly without modification for other platforms such as Linux, Mac or HTML5. And with minimal changes it can be compiled for Android and iOS mobile platforms.

The developed application can be used for designing and checking three-phase electric lines based only on the behavior of the consumer connected to it.

The graphical interface of the application is intuitive and is based on a selection algorithm similar to the installation wizards, in which the user can choose one of the options available at a given time.

By choosing step by step different configurations the parameters and starting configurations are determined. The user must answer only the relevant questions about the configurations he choosed. The user is guided from the beginning to the result with precise steps being requested only the strict information necessary to configure the selected starting method.

When opening the application, we are greeted with a window that contains a brief description of the application and a series of buttons with which the user can navigate to the home page or to the previous page, as seen in Figure 2.

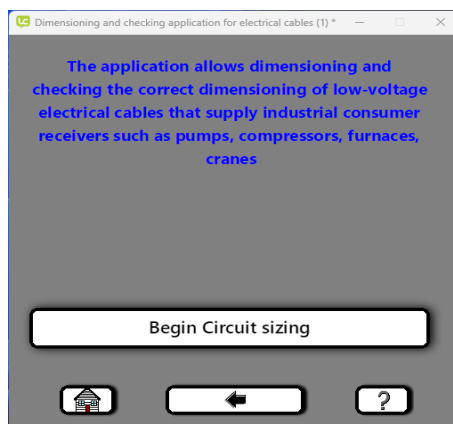


Figure 2. The welcome screen of the application.

In the following steps, the user will choose in small steps the desired drive type, the desired start type for the designed or verified application and then the nominal data of the drive motor of the designed equipment.

After entering all the necessary information according to the selected startup method, the application will determine the required theoretical section for the cable based on the entered data. After determining the corrected standardized section by the application, this new section is checked for the nominal regime, than for the starting regime. Checks are made both for the allowed current density and for the maximum allowed voltage drops in normal mode and in start-up mode for each section determined by the data supplied.

To exemplify the simple way of using the application, we will determine the section required for a three-phase power supply cable of a piece of equipment driven by a 7.5kW electric motor.

For this we will run the application where in the main window we will select the "Begin Circuit sizing" button, then from the displayed options we select "Classic electric drive" for direct start or star-delta as can be seen in Figure 3a.

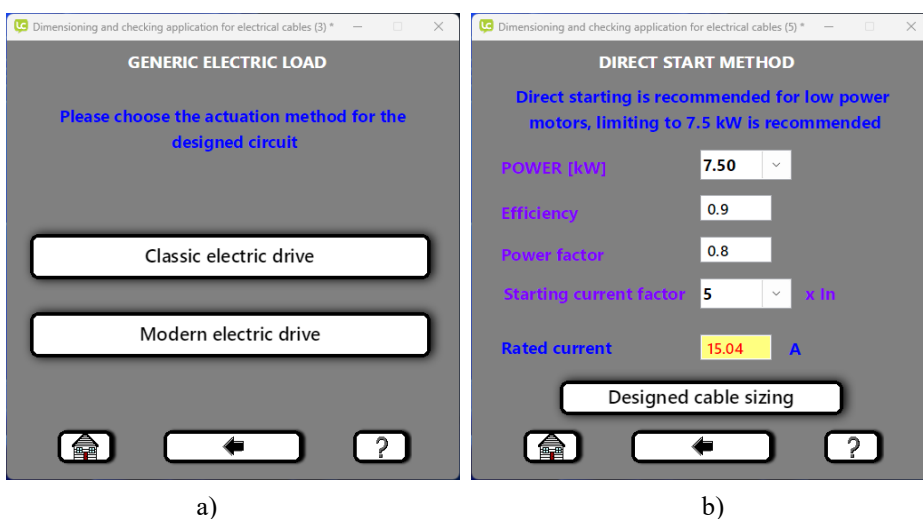
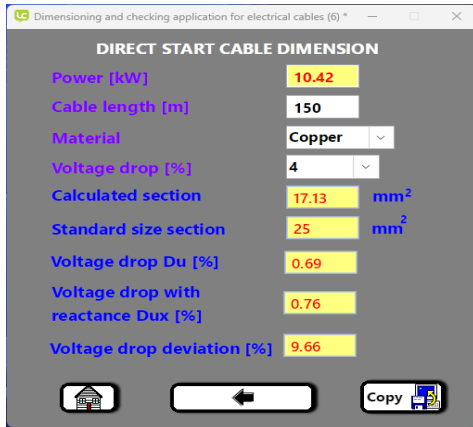


Figure 3. The page where you choose the drive method and motor parameters.

Figure 3b shows the area where the nominal parameters of the drive motor are entered, here the starting coefficient can also be selected depending on the actual starting regime of the application.



| | |
|----------------------------|------------------------------|
| Starting method | DIRECT START CABLE DIMENSION |
| Power [kW] | 10.42 |
| Power factor | 0.8 |
| Length [m] | 150 |
| Material | Copper |
| Voltage drop [%] | 4 |
| Calculated section [m] | 17.13 |
| Standard section [m] | 25 |
| Voltage drop Du [%] | 0.69 |
| Voltage drop Dux [%] | 0.76 |
| Voltage drop deviation [%] | 9.66 |

a)

b)

Figure 4. Calculation of the section and verification.

The following options clarify which of the two startup methods will be used in our project. The application recommends for powers of maximum 7.5kW the choice of direct starting method, but this is not mandatory.

After completing the information, we can press the "Designed cable sizing" button, which will redirect us to the final part of the cable sizing as seen in Figure 4a where we can select the length of the power supply circuit and the type of material it is made of. After establishing the parameters of the supply line we can impose a maximum voltage drop for the dimensioned circuit, a value between 1 and 10 % is allowed.

At any change made in every step the application calculates and checks a new section for the new data entered. If we want to return to some choices made, we can press the button symbolized by a black arrow, which will redirect us to the previous page as often as we need it, even to the home page. When returning to pages already visited, the information already entered is restored and we can resume the task with the new data or selections already made.

The final results of the application can be copied into the system's clipboard and after that pasted into a text editor or any word processor. The calculated values are returned in a tab formatted text as seen in Figure 4b.

4. Conclusion

The developed application allows the quick determination of the cable sections and its verification at voltage drop in normal mode and at start-up mode for electrical motors.

Compared to dedicated software, it has the advantage of calculating the electric circuit, without the need to describe the whole network from the power supply to the receiver.

The known data for the line parameters are entered manually or are selected from a list of predefined sizes of standardized powers to facilitate the operation.

The results obtained are validated by the application taking into account all the regulations and standards regarding the technical limits allowed.

The application allows the user to run multiple instances of the program to be able to simulate multiple scenarios side by side to compare the results obtained.

References

- [1] Protea B., Muscai C., Navrapescu V., Spunei E., Piroi I., Piroi F., *Computer assisted equipment selection for components of electric panels*, International Conference on Applied and Theoretical Electricity ICATE, 4-6 Oct., Craiova, 2018.
- [2] Preduș M.F., Spunei E., Roșu M., Prediction of power cables failures using a software application, *Studia Universitatis Babes-Bolyai Engineering*, 65(1), 2020, pp. 153-162.
- [3] Chioncel C.P., Spunei E., Anghel-Drugarin C.V., Piroi I., *Direct Self Control Structure for the Asynchronous Machine, Implemented in Scilab / Xcos*", 6th International Conference on Modern Power Systems, Cluj, 18-21 May 2015, Acta Electrotehnica, nr. 3, pp. 52-55.
- [4] Preduș M.F., Spunei E., Piroi I., Roșu M., *Diagnostic of Defects at Electric Lines in Cable*, Proceedings of 10th International Conference on Electromechanical and Power Systems SIELMEN 2015, Chișinău, 8-9 oct. 2015, pp. 518-521.
- [5] Piroi I., *Instalații electrice și de iluminat*, Editura Eftimie Murgu, Reșița, 2009.

Addresses:

- PhD. Stud. Eng. Liviu-Bogdan Protea, Politehnica University of Bucharest, Faculty of Electrical Engineering, Splaiul Independenței 313, 060042, București, Romania
bogdan.protea@gmail.com
- PhD. Stud. Eng. Cristian-Mircea Muscai, Politehnica University of Bucharest, Faculty of Electrical Engineering, Splaiul Independenței 313, 060042, București, Romania
muscaicristian@yahoo.com
(*corresponding author)

Study on the importance of upgrading public lighting systems

Elisabeta Spunei*, Arpad Csepei, Ion Piroi, Florina Piroi, Mihai Rotaru

Abstract. *The paper presents a case study which advocates for the adoption of smart outdoor illumination installations that come with energy management systems. To analyse the energy efficiency we carried out measurements on: a) a classical outdoor lighting system, with sodium vapour sources, b) the same system after the sodium vapour light sources were replaced with LEDs, and c) the same system with LEDs augmented with an energy management system. Our analysis shows that replacing the outdoor light-sources with LEDs, in combination with an energy management system, results in a reduction of 40% in energy consumption. At the same time, the luminance coefficients of the LED lighting system are significantly higher than the luminance coefficients of sodium vapour sources.*

Keywords: *illumination, LED, management system, electric energy reduction.*

1. Introduction

By definition, street lighting is “a fixed lighting installation designed to provide, during night-time, good visibility to users of public outdoor traffic areas in order to support the safety and flow of traffic as well as public safety” [1]. This definition includes both lighting of roadways as well as pedestrian and bicycle paths.

Studies have shown that, worldwide, lighting sources make about 19% of total electricity consumption [2]. In the context of the global economic crisis, replacing outdated lighting sources with highly energy-efficient ones is being widely implemented. The current lightsources of choice are LED sources [3], which achieve significant electricity savings [4].

In order to increase the lighting systems energy efficiency and increase their sustainability, certain criteria must be followed, such as:

- the choice of technologies must meet environmental requirements and use recyclable materials;
- a life cycle analysis of the lighting system and all necessary components must be done beforehand;



- an analysis of the impact of the lighting system on users and the environment must be available.

To reduce electricity consumption various solutions can and are implemented. For example, it has been established on a university campus that by applying a lighting enhancement scenario, in 12 years approximately 1.3 million euros can be saved [5]. The scenario envisages the replacement of existing lighting sources (metal halide) with LED sources and the adoption of a programmed switch-off of lighting sources and dimming with dimming modules.

For street lighting systems, the dimming modules are complemented by a system that monitors the number of vehicles which causes the luminous flux to be automatically adjusted depending on the traffic participants [6]. These systems can be powered by photovoltaic panels, by means of a battery and a controller, which monitors the lighting level, battery capacity, avoiding excessive battery discharges [7].

Lately, trends in outdoor lighting make use of artificial intelligence algorithm. For example, a rule-based algorithm has 213 rules and considers feedback from sensor systems to efficiently manage a lighting system. During the tests, which lasted for one semester, an average electricity saving of 33% was achieved [8, 9].

In order to get an overview of the energy efficiency of lighting systems, it was proposed to approach the analysis strategy at component and system level. At the component level the aim is to replace inefficient sources with LED sources and to optimise the performance of LED drivers. At the system level, through control strategies, the aim is to obtain real-time information about energy consumption and provide data about the operation of complete lighting systems [10].

In order to ensure the lighting coefficients, established by current in-force standards, it is necessary to pay more attention to the optimal design, to the appropriate location of lighting poles and crutches, to the choice of lighting sources with an appropriate photometric curve [11-15].

It is a known fact that, as the duration of use of lighting sources increases, their luminous flux decreases. In order to establish the efficiency of the lighting source/system, it is necessary to carry out light measurements at a certain, regular, time intervals [16]. At the same time, periodically, it is necessary to carry out proper maintenance so that the entire system is always in working order, ensuring the necessary quality coefficients [17].

The efficiency and sustainability analysis of lighting systems must also take into account the rather high cost of luminaires equipped with LED sources, especially in the case of high-power LEDs [18]. According to the previously mentioned research [19] where the outdoor lighting systems on a university campus combined LED sources with Smart Grid technologies, the payback period was 4 years and 10 months.

With the intention to reduce pollution, it is necessary to reduce or even eliminate light pollution through a management architecture that uses IoT (Internet of Things) technologies [20].

As the existing lighting system on the main road in the municipality was to be upgraded, it was necessary to identify the lighting and energy performance before and after the system change.

In order to analyse the lighting system efficiency, both from a lighting and energy point of view, this paper presents the lighting coefficients measured on a boulevard section where the light sources installed were sodium vapour based lights. After replacing these sources with LEDs, we carried out again photometric measurements for various values of luminous flux (nominal flux and nominal flux with a dimming system). This case study shows the energy efficiency that can be achieved by replacing sodium vapour sources with LED sources, and by additionally combining LED sources with an energy management system.

2. Analysis of the Lighting System Before the LED Modernisation

The lighting system we analysed is located on a boulevard in a municipality city. The light measurements were carried out on two sections between three lighting poles [21].

The roadway where the measurements were done, consists of a 5 m wide sidewalk (including a 1.5 m wide bike lane), followed by a 1.5 m wide green space and two lanes for motorized vehicles, each 3.5 m wide, on the direction of travel. The other traffic direction is separated from the one just described by a 5 m wide green space, and also consists of two traffic lanes and an additional bike lane.

The lighting poles illuminating the carriageway and pavement are placed in the view space, 2 m from the traffic lane, with 40 m between them. The pole height is 12.4 m, each pole has 2 arms of 4 m on which sodium vapour lamps powered at 230V and a power of 171 W (including ballast), luminous flux 17,700 lm and a power factor of 0.92 are mounted.

The photometric measurements were made with a luminance-meter and a lux-meter. The measurements were done at 9 regular intervals between the lighting poles, which constitute the measuring points. The following locations were selected for the light measurements:

- on the pole axis, on the green space separating the traffic directions;
- on the longitudinal axis separating the two traffic lanes in each direction;
- on the pavement;
- on each traffic lane direction, two measuring points at equal distances.

This resulted in a matrix with 63 measurement points. Table 1 shows the measured illuminance values and Table 2 the luminance values for the non-modernised, or classic, illumination system. We computed, for each measurement point, the average illuminance, and the average luminance as the arithmetic mean of the measurements.

Table 1. Illuminance values for the classic (sodium vapor-based) lighting system (“R” stands for “Direction”)

| Illuminance measurements for sodium vapor sources 171 W [lx] | | | | | | | | | | E_{med} [lx] |
|--|------|------|------|------|-----|------|-------|------|------|-------------------|
| Pole axis | 31.5 | 25.5 | 16.1 | 12.4 | 9.3 | 10.4 | 13.6 | 23.4 | 27.5 | 18.86 |
| Lane 1 R1 | 31.4 | 25.6 | 15.5 | 12.2 | 9.5 | 10.5 | 14.23 | 23 | 26.4 | 18.70 |
| Lane 1 R2 | 25.9 | 27.4 | 15.7 | 12 | 9 | 10.1 | 13.8 | 22.6 | 20.7 | 17.47 |
| Long. Axis | 27.6 | 26.6 | 15.4 | 12 | 9.4 | 10.4 | 13.2 | 21.9 | 22.5 | 17.67 |
| Lane 2 R1 | 25 | 22.2 | 15.6 | 11.5 | 9 | 8.5 | 11.8 | 19.6 | 23 | 16.24 |
| Lane 2 R2 | 21 | 20.3 | 14 | 11.3 | 8.5 | 7.9 | 10.6 | 15.7 | 20 | 14.37 |
| Side walk | 14 | 11.4 | 11.5 | 10.3 | 7.3 | 6.7 | 8 | 9.3 | 11 | 9.94 |

Table 2. Luminance values for the classic (sodium vapor-based) lighting system.

| Luminance measurements for sodium vapor sources 171 W [cd/m^2] | | | | | | | | | | L_{med} [cd/m^2] |
|--|------|------|------|------|------|------|------|------|------|---------------------------|
| Lane 1 R1 | 1.74 | 1.49 | 0.89 | 0.65 | 0.52 | 0.79 | 1.05 | 1.78 | 2.11 | 1.22 |
| Lane 1 R2 | 1.41 | 1.18 | 0.67 | 0.50 | 0.46 | 0.57 | 0.4 | 1.51 | 1.65 | 0.93 |
| Long. Axis | 1.07 | 1.08 | 0.52 | 0.37 | 0.44 | 0.29 | 0.68 | 1.11 | 1.30 | 0.76 |
| Lane 2 R1 | 0.93 | 0.80 | 0.44 | 0.34 | 0.32 | 0.47 | 0.62 | 1.10 | 1.24 | 0.70 |
| Lane 2 R2 | 0.93 | 0.81 | 0.54 | 0.40 | 0.39 | 0.44 | 0.76 | 1.13 | 1.29 | 0.74 |

The average illuminance calculated on the road surface is:

$$E_{med\ road} = \frac{E_{medPoleaxis} + E_{medL1R1} + E_{medL1R2} + E_{medLongaxis} + E_{medL2R1} + E_{medL2R2}}{6} = \frac{18.86 + 18.70 + 17.47 + 17.67 + 16.24 + 14.37}{6} = 17.22 \text{ [lx]} \quad (1)$$

and the average luminance is:

$$L_{med\ road} = \frac{L_{medL1R1} + L_{medL1R2} + L_{medLongaxis} + L_{medL2R1} + L_{medL2R2}}{5} = \frac{1.22 + 0.93 + 0.76 + 0.70 + 0.74}{5} = 0.87 \text{ [cd / m}^2\text{]} \quad (2)$$

The overall illuminance and luminance uniformity coefficients, calculated as the ratio of the measured minimum value to the calculated average value [22-24], for pavement and roadway are:

$$U_0(E)_{pavement} = \frac{E_{min}}{E_{med}} = \frac{6.7}{9.94} = 0.67 \quad (3)$$

$$U_0(E)_{road} = \frac{E_{min}}{E_{med}} = \frac{7.9}{17.22} = 0.46 \quad (4)$$

$$U_0(L)_{road} = \frac{L_{min}}{L_{med}} = \frac{0.29}{0.87} = 0.33 \quad (5)$$

The luminance longitudinal uniformity coefficient (on the road axis), computed as the ratio between the measured minimum illuminance and average value is:

$$U_1(L) = \frac{L_{min1}}{L_{max1}} = \frac{0.29}{1.3} = 0.22 \quad (6)$$

We found that the illuminance uniformity, the illuminance, and the average luminance are within the value ranges established by technical standards in force, but the overall and longitudinal luminance uniformity are not, as they are lower than the values in the standards (greater than 0.4 and 0.5 respectively).

Considering that a luminaire operates 10 hours a day, 30 days a month, the energy consumed by a luminaire in a month is:

$$W_{luminaire/month} = P_{luminaire} \cdot no\ hours \cdot no\ days = 171 \cdot 300 = 51.3 \text{ [kWh]} \quad (7)$$

As there are 52 poles on the section of road we measured, each with two luminaires, the monthly energy consumed is:

$$W_{\text{section/month}} = W_{\text{luminaire/month}} \cdot N_{o_{\text{luminaire}}} = 51.3 \cdot 52 \cdot 2 = 5335.2 \text{ [kWh]} \quad (8)$$

which is a substantial amount of energy consumed in the area analysed.

3. Analysis of the Upgraded Lighting System

The lighting system presented in Section 2 was upgraded by replacing the lighting fixtures with LEDs and installing an energy management system. The fixtures were placed on already existing street poles and positioned so that the central light flow falls perpendicular to the street surface, on the longitudinal axis separating the two traffic lanes.

The LEDs power is 140.5 W, they have a luminous flux of 12938 lm and have a power factor of 0.9. The LED sources are powered by a driver, monitoring the light installation is done through a communication and dimming module is used to monitor the lighting system. The street lighting system is divided into segments, controlled, and monitored by a segment controller. This controller transmits and receives information from the communication and dimming module and adjusts the light intensity from 10% to 100%.

After upgrading the lighting system, we took photometric at the same measurement points as previously established. The values of the measured illuminances are shown in Table 3 and of the luminances in Table 4.

Table 3. Illuminance values for LED system

| Illumination measurements for the 140.5 W LEDs [lx] | | | | | | | | | | E_{med} [lx] |
|---|------|------|------|------|------|------|------|------|------|--------------------------|
| Pole axis | 32.6 | 31.5 | 24.6 | 20.5 | 18.1 | 21.5 | 26.6 | 28.2 | 33.6 | 26.36 |
| Lane 1 R1 | 30.1 | 31.2 | 22.3 | 17.8 | 16.3 | 17.7 | 25.1 | 34.3 | 35.5 | 25.59 |
| Lane 1 R2 | 26 | 32.9 | 24.5 | 18.5 | 18.2 | 18.7 | 28.2 | 35.2 | 35.6 | 26.42 |
| Long. Axis | 24.8 | 37.6 | 23.5 | 21.2 | 20.7 | 23.2 | 23.8 | 33.9 | 34.5 | 27.02 |
| Lane 2 R1 | 23.8 | 21.4 | 19.8 | 18.4 | 16.5 | 18.7 | 21.6 | 24.4 | 26.2 | 21.20 |
| Banda 2 R2 | 20.2 | 18.7 | 18.1 | 16.9 | 14.2 | 15.8 | 17.7 | 20.2 | 12.4 | 17.13 |
| Side-walk | 9.6 | 8.4 | 7.3 | 6.5 | 5.2 | 6.4 | 7.9 | 8.3 | 9.16 | 7.64 |

Table 4. Luminance values for the LED street lighting system

| Luminance measurements for the 140.5 W LEDs [cd/m ²] | | | | | | | | | | L _{med} [cd/m ²] |
|--|------|------|------|------|------|------|------|------|------|--|
| Lane 1 R1 | 1.27 | 1.41 | 1.36 | 1.28 | 1.19 | 1.25 | 1.34 | 1.40 | 1.21 | 1.30 |
| Lane 1 R2 | 1.29 | 1.46 | 1.42 | 1.29 | 1.22 | 1.27 | 1.38 | 1.42 | 1.25 | 1.33 |
| Long. Axis | 1.31 | 1.48 | 1.45 | 1.36 | 1.25 | 1.30 | 1.44 | 1.47 | 1.32 | 1.38 |
| Lane 2 R1 | 1.25 | 1.37 | 1.23 | 1.21 | 1.17 | 1.21 | 1.31 | 1.45 | 1.24 | 1.27 |
| Lane 2 R2 | 1.02 | 1.13 | 1.06 | 1.01 | 0.95 | 1.05 | 1.22 | 1.36 | 1.15 | 1.11 |

The average illuminance and luminance calculated for the road surface are:

$$E_{med\ road} = \frac{26.36 + 25.59 + 26.42 + 27.02 + 21.20 + 17.13}{6} = 23.95 \text{ [lx]} \quad (9)$$

$$L_{med\ road} = \frac{1.30 + 1.33 + 1.37 + 1.27 + 1.11}{5} = 1.28 \text{ [cd / m}^2\text{]} \quad (10)$$

The overall illuminance and luminance uniformity coefficients for the pavement and road surface are:

$$U_0(E)_{pavement} = \frac{5.2}{7.64} = 0.68 \quad (11)$$

$$U_0(E)_{road} = \frac{12.4}{23.954} = 0.52 \quad (12)$$

$$U_0(L)_{road} = \frac{1.01}{1.277} = 0.79 \quad (13)$$

The luminance longitudinal uniformity coefficient is:

$$U_1(L) = \frac{1.25}{1.48} = 0.85 \quad (14)$$

Our analysis shows that all the quality coefficients of the lighting system analysed fall within the range set by the standards currently in force.

For the same length of time analysed in Section 2, the monthly electricity consumed by one luminaire and the electricity consumed by all luminaires in the area analysed are calculated by:

$$W_{luminaire/month} = 140.5 \cdot 10 \cdot 30 = 42.150 \text{ [kWh]} \quad (15)$$

$$W_{section/month} = 42.15 \cdot 104 = 4383.6 \text{ [kWh]} \quad (16)$$

which is 17.84% less than with sodium vapour lighting.

In order to determine whether the lighting system also meets the quality conditions for dimming, measurements were made under the same operating conditions and at the same measuring points for a dimming that considers the luminous flux reduction at 66% and 50% [21]. We present in this paper the photometric measurements made at a 50% dimming (Tables 5 and 6).

Table 5. Illuminance values for system with LED sources and 50% dimming

| Illuminance measurements for the 140.5 W and dimmed LEDs [lx] | | | | | | | | | | E _{med} [lx] |
|---|------|------|------|------|------|------|------|------|------|-----------------------|
| Pole axis | 22.8 | 23.6 | 16.7 | 13.3 | 10.7 | 14.1 | 16.4 | 19.2 | 24.7 | 17.94 |
| Lane 1 R1 | 20.6 | 21.7 | 17.8 | 13.9 | 11.9 | 12.4 | 17.5 | 21.8 | 21.5 | 17.38 |
| Lane 1 R2 | 20.4 | 22.2 | 18.8 | 14.5 | 12.5 | 13.5 | 18.8 | 24.6 | 25.3 | 18.96 |
| Long. Axis | 18.2 | 22.9 | 19.1 | 15.2 | 13 | 16.1 | 19 | 25 | 25.6 | 19.34 |
| Lane 2 R1 | 17.5 | 19.4 | 17.6 | 15 | 12.6 | 15.3 | 18 | 21.5 | 21.4 | 17.59 |
| Lane 2 R2 | 13.6 | 14.8 | 15.5 | 10.3 | 8.8 | 10.5 | 12.6 | 13.2 | 14.4 | 12.63 |
| Side walk | 7.1 | 6.2 | 5.6 | 4.5 | 3.7 | 4.6 | 5.2 | 5.8 | 6.9 | 5.51 |

Table 6. Luminance values for a LED lighting system, 50% dimmed

| Luminance measurements for 140.5 W LEDs [cd/m ²] dimmed | | | | | | | | | | L _{med} [cd/m ²] |
|---|------|------|------|------|------|------|------|------|------|---------------------------------------|
| Lane 1 R1 | 0.98 | 1.05 | 0.85 | 0.68 | 0.51 | 0.63 | 0.88 | 1.04 | 0.89 | 0.83 |
| Lane 1 R2 | 1.07 | 1.17 | 0.96 | 0.75 | 0.67 | 0.71 | 0.93 | 1.14 | 0.98 | 0.93 |
| Long. Axis | 1.12 | 1.21 | 1.04 | 0.78 | 0.77 | 0.82 | 1.01 | 1.23 | 1.07 | 1.001 |
| Lane 2 R1 | 1.09 | 1.11 | 0.97 | 0.67 | 0.51 | 0.64 | 0.86 | 0.95 | 0.88 | 0.85 |
| Lane 2 R2 | 0.89 | 0.93 | 0.72 | 0.51 | 0.44 | 0.47 | 0.56 | 0.77 | 0.62 | 0.66 |

The average luminance and illuminance values for this lighting system are then:

$$E_{med\ road} = \frac{17.94 + 17.68 + 18.96 + 19.34 + 17.59 + 12.63}{6} = 17.36 \text{ [lx]} \quad (17)$$

$$L_{med\ road} = \frac{0.83 + 0.93 + 1.01 + 0.85 + 0.66}{5} = 0.86 \text{ [cd / m}^2\text{]} \quad (18)$$

The general illuminance and luminance uniformity coefficients for the side walk and roadway and the longitudinal luminance uniformity coefficients are:

$$U_0(E)_{pavement} = \frac{3.7}{5.51} = 0.67 \quad (19)$$

$$U_0(E)_{road} = \frac{8.8}{17.36} = 0.51 \quad (20)$$

$$U_0(L)_{road} = \frac{0.44}{0.86} = 0.51 \quad (21)$$

$$U_1(L) = \frac{0.77}{1.23} = 0.63 \quad (22)$$

It is found that, even at 50 % dimming, the illumination uniformity on the roadway is superior to the situation where the lighting system had the sodium vapour sources and was operating at 100 % luminous flux. Additionally, the values of the lighting coefficients are higher than those required by the standards.

If we consider that the analysed lighting system operates according to a pre-set schedule (3 hours without dimming, 2 hours with a 66% reduction of luminous flux and 5 hours with a 50% reduction of luminous flux) for one luminaire, the energy consumed by it in one month at an operation of 10 hours/day is:

$$\begin{aligned} W_{lu\ min\ aire/month(100\%)} &= P_{lu\ min\ aire(100\%)} \cdot no\ hours \cdot no\ days = \\ &= 140.5 \cdot 3 \cdot 30 = 12.645 [kWh] \end{aligned} \quad (23)$$

$$\begin{aligned} W_{lu\ min\ aire/month(66\%)} &= P_{lu\ min\ aire(66\%)} \cdot no\ hours \cdot no\ days = \\ &140.5 \cdot 0.66 \cdot 2 \cdot 30 = 5.564 [kWh] \end{aligned} \quad (24)$$

$$\begin{aligned} W_{lu\ min\ aire/month(50\%)} &= P_{lu\ min\ aire(50\%)} \cdot no\ hours \cdot no\ days = \\ &140.5 \cdot 0.5 \cdot 5 \cdot 30 = 10.5275 [kWh] \end{aligned} \quad (25)$$

$$\begin{aligned} W_{lu\ min\ aire/month} &= W_{lu\ min\ aire/month(100\%)} + W_{lu\ min\ aire/month(66\%)} + W_{lu\ min\ aire/month(50\%)} = \\ &= 12.645 + 5.564 + 10.5275 = 28.7365 [kWh] \end{aligned} \quad (26)$$

which is 43.983% less than the energy consumed by conventional sources and 31.82% less than the case where the LED sources are operating non-dimmed.

The total energy consumed in one month, in the area analysed, when running with the previously mentioned schedule is:

$$W_{\text{section/month}} = W_{\text{luminaire/month}} \cdot N_{O_{\text{luminaire}}} = 28.7365 \cdot 104 = 2998.596 \text{ [kWh]} \quad (27)$$

4. Comparative Analysis of the Two Lighting Systems

We compared the classic lighting system with the LED lighting at 100% flux and scheduled operation. We looked at the quality parameters and at the energy consumed by the lighting system in these three scenarios, the results are shown in Table 7.

Table 7. Illuminance values for the LED system and 50% dimming

| Coefficient / measure | Standard reference value | Value for 171 W light sources | Value for 140.5 W LEDs | Value for 140.5 W LEDs and 50% dimming |
|---------------------------------------|--------------------------|-------------------------------|------------------------|--|
| E_{med} [lx] | 15.0 | 17.22 | 23.95 | 17.36 |
| L_{med} [cd/m ²] | 0.75 | 0.87 | 1.28 | 0.86 |
| $U_0(E)_{\text{road}}$ | > 0.4 | 0.46 | 0.52 | 0.51 |
| $U_0(L)_{\text{road}}$ | > 0.4 | 0.33 | 0.79 | 0.51 |
| $U_1(L)_{\text{road}}$ | > 0.5 | 0.22 | 0.85 | 0.63 |
| $W_{\text{luminaire/month}}$ [kWh] | - | 51.3 | 42.15 | 28.736 |
| $W_{\text{section/month}}$ [kWh] | - | 5335.2 | 4383.6 | 2998.596 |

Figure 1 shows a graph of the electricity consumption of the analysed luminaires for an operation of 10 hours/day, 30 days/month. The analysis shows that, for all three scenarios examined in this work, the average illuminances and luminances correspond to the values required by the standards. At the same time, we found that the average illuminance for the operation using LED sources and 50% dimming is 0.8% higher than the average illuminance with sodium vapour sources.

With regard to the uniformity coefficient of the illuminance, in all three analysed cases, its value corresponds to the requirements of the in-force standards. At the same time, it was found that at a dimming of 50%, the uniformity coefficient is 10.46% higher than the coefficient computed for the installation using sodium vapour light sources.

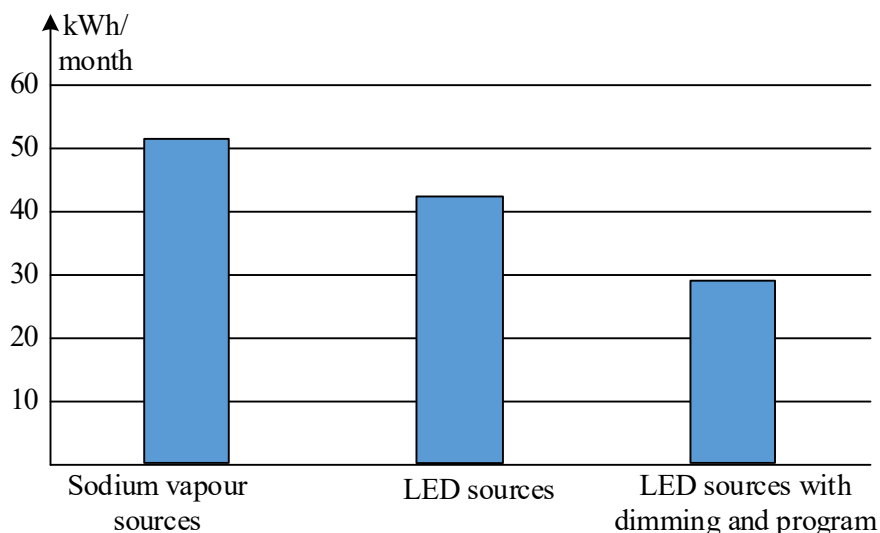


Figure 1. Monthly energy consumption for the examined lighting installations.

Our analysis shows that, for sodium vapour sources, the luminance uniformity coefficient and the luminance longitudinal uniformity coefficient are 16.75% lower and 55.4% lower than the values requested by the current technical standards in force, respectively. After replacing the lighting sources with modern LEDs, these coefficients are higher than the minimum required values, so even at a dimming of 50% the coefficients are 28.5% respectively 25.2% higher.

Regarding the electricity consumption, compared to the use of sodium vapour sources, LED sources bring a 17.84% reduction in electricity consumption. When an energy management system is used and the lighting system is operated on predefined schedules, the electricity reduction is of 43.98%.

4. Conclusion

The analysis we carried out emphasizes the need to modernize street lighting systems, by replacing energy inefficient sources and appliances with LED sources and high-performance lighting appliances that ensure the correct distribution of the light flow. Furthermore, the modernisation of lighting systems through the use of an energy management system allows the creation of different operating scenarios, which contribute to a substantial reduction in electricity consumption. At the same time, the management system allows remote control and monitoring, as well as providing information on the operating status of the installation.

In the context of the current energy crisis, the modernisation of lighting systems is a necessity, which must be supported by various government, European and global programmes.

References

- [1] Technical Documentation Guidelines for Public Illumination Calls, <https://www.electricianul.ro/wp-content/uploads/2019/12/Ghid-pentru-%C3%AEntocmirea-documenta%C8%9Biilor-tehnice-pentru-licita%C8%9Biile-de-iluminat-stradal-1.pdf> (downloaded at July 28rd, 2022)
- [2] National Integrated Plan for Energy and Climate Changes 2021-2030, https://ec.europa.eu/energy/sites/ener/files/documents/ro_final_necp_main_ro.pdf (downloaded at July 28rd, 2022).
- [3] Proiect act normativ – implementarea iluminatului LED în România, <http://www.ensola.ro/proiect-act-normativ-implementarea-iluminatului-led-romania/> (downloaded at July 28rd, 2022).
- [4] Shahzad K., Cucek L., Sagir M., Ali N., Rashid M.I., Nazir R., Nizami A.S., Al-Turaif H.A., Ismail I.M.I., An ecological feasibility study for developing sustainable street lighting system, *Journal of cleaner production*, 175, 2018, pp. 683-695.
- [5] Gorgulu S., Kocabey S., An energy saving potential analysis of lighting retrofit scenarios in outdoor lighting systems: A case study for a university campus. *Journal of cleaner production*, 290, 121060, 2020.
- [6] Pavlov N., Bachurin A., Siemens E., *Analysis of Outdoor Lighting Control Systems and Devices for the Creation of Outdoor Lighting Automatic Control System Using the Traffic Flow Value*. 5th International Conference on Applied Innovations in IT (ICAIIIT), Mar. 16, 2017, Koethen, Germany.
- [7] Kiwan S., Mosali A.A., Al-Ghasem A., Smart Solar-Powered LED Outdoor Lighting System Based on the Energy Storage Level in Batteries. *Buildings*, 8(9), 119, 2018.
- [8] Wojnicki I., Ernst S., Kotulski L., Economic Impact of Intelligent Dynamic Control in Urban Outdoor Lighting, *Energies*, 9(5), 314, 2019.
- [9] Atis S., Ekren N., Development of an outdoor lighting control system using expert system, *Energy and buildings*, 130, 2016, pp. 773-786.
- [10] Farahat A., Florea A., Lastra J.L.M., Branás C., Sanchez F.J.A., Energy Efficiency Considerations for LED-Based Lighting of Multipurpose Outdoor Environments, *IEEE Journal of emerging and selected topics in power electronics*, 3(3), 2015, pp. 599-608.
- [11] Farahat A., Florea A., Lastra J.L.M. Reyes C.B., Azcondo F.J., *Energy efficient outdoor lighting: an implementation*, IEEE 15th Workshop on Control and Modeling for Power Electronics (COMPEL), Jun 22-25, 2014, Univ. Cantabria, Santander, Spain.

- [12] Spunei E., Piroi I., Piroi F., Brebenariu D., The Importance of Optimal Design in Outdoor Light Source Positioning, *Analele Universității „Eftimie Murgu” Reșița, Fascicula de Inginerie*, 25(2), 2018, pp. 127-137.
- [13] Spunei E., Piroi I., Piroi F., Optimizing Street Lighting Systems Design, *Analele Universității „Eftimie Murgu” Reșița, Fascicula de Inginerie*, 21(3), 2014, pp. 257-268.
- [14] Spunei E., Piroi I., Piroi F., Notes on LED Installations in Street Illumination, *Analele Universității „Eftimie Murgu” Reșița, Fascicula de Inginerie*, 21(3), 2014, pp. 269-280.
- [15] Spunei E., Piroi I., Chioncel C.P., The experimental determination of the luminous flux emitted by a few types of lighting sources, *IOP Conference Series: Materials Science and Engineering*, 163, May 25–27, 2016, Hunedoara, Romania.
- [16] Kaleem Z., Yoon T.M., Lee C., Energy Efficient Outdoor Light Monitoring and Control Architecture Using Embedded System. *IEEE Embedded systems letters*, 8, 2016, pp. 18-21.
- [17] Ullman I., Bos P., Ullman J., *New Outdoor Lighting - Operation and Maintenance*. 17th International Scientific Conference on Electric Power Engineering (EPE), May 16-18, 2016, Prague, Czech Republic.
- [18] Boxler L., *Optical Design and Lighting Application of an LED-Based Sports Lighting System*. 11th International Conference on Solid State Lighting, Aug 22-24, 2011, San Diego, C.A.
- [19] Filimonova A.A., Barbasova T.A., Shnayder D.A., *Outdoor lighting system upgrading based on Smart Grid concept*. 8th International Conference on Sustainability in Energy and Buildings (SEB), Sep. 11-13, 2016, Politecnico Torino, Turin, Italy.
- [20] Escriva D.M.L., Berlanga-Llavori R., Torres-Sospedra J., Smart Outdoor Light Desktop Central Management System. *IEEE Intelligent transportation systems magazine*, 10(2), 2018, pp. 58-68.
- [21] Piroi I., *Instalații electrice și de iluminat*, Editura Eftimie Murgu, Reșița, 2009.
- [22] Mogoreanu N., *Iluminatul Electric*, Editura Lumina, 2013.
- [23] Bianchi G., Mira N., Moroldo D., Gheorghescu A., Moroldo H., *Sisteme de iluminat interior si exterior*, Editura Matrixrom, 2001.
- [24] Csepei A., *Studiu privind eficiența sistemului de iluminat public dintr-o zona a Municipiului Reșița*, Master of Science Thesis, Reșița, 2022.

Addresses:

- S.L. Dr. Eng. Elisabeta Spunei, Babeş-Bolyai University, Faculty of Engineering, Piaţa Traian Vuia, nr. 1-4, 320085, Reşiţa, Romania
elisabeta.spunei@ubbcluj.ro
(* *corresponding author*)
- Eng. Csepei Arpad, Babeş-Bolyai University, Faculty of Engineering, Piaţa Traian Vuia, nr. 1-4, 320085, Reşiţa, Romania
arpad.csepei@stud.ubbcluj.ro
- Prof. Dr. Eng. Ion Piroi, Babeş-Bolyai University, Faculty of Engineering, Piaţa Traian Vuia, nr. 1-4, 320085, Reşiţa, Romania
ion.piroi@ubbcluj.ro
Dr. Florina Piroi, Technische Universität Wien, Institute for Information Systems Engineering, Favoritenstrasse 9-11, 1040, Vienna, Austria
florina.piroi@tuwien.ac.at
- Drd. Eng. Mihai Rotaru, Polytechnic University of Bucharest, Faculty of Electrical Engineering, Sp. Independenţei 313, 060042, Bucharest, România
mihai.rotaru2002@stud.electro.upb.ro

Application for speech assistance of people with hearing disability

Mihaela Dorica Stroia, Cornel Hațiegan*, Bogdan Daniel Borcilă

Abstract. *Worldwide, there are many people with hearing impairments. Depending on its severity, hearing impairment can be solved using a more or less performant hearing device, according to one's needs, but in the case of a total loss of hearing, these devices are rather expensive and not affordable for everyone. With these situations in mind, we developed a simple application, named Talky, which can be used to assist people with hearing disabilities, mostly total hearing loss, in order to facilitate the communication process with others. Talky is simple to use and may be useful for people who have difficulty speaking.*

Keywords: *speech, disability, hearing, framework, React*

1. Introduction

Statistics show that worldwide, 5% of the global population, representing 360 million of people, suffer from a variable degree of hearing impairment [1]. In Romania, in 2018, more than 23 thousand of people were declared with total hearing loss, of which almost 2000 were children. And we are talking only about people registered with the Romanian National Association of the Deaf. Whatever the cause of the hearing loss, not being able to communicate as a human is not only frustrating but also causes a great deal of suffering [2].

Hearing device technology has undergone a significant development in the past several years. With a small device implanted in the auditory canal, a person with a total hearing loss would be able to hear [3]. However, one issue arises. This type of technology, though performant, is quite expensive and not affordable for the average person.

With the above situations in mind, we thought of finding a solution that might come in handy of people with hearing loss and not only, with speech impairment as well, a solution that can be affordable and come in handy to everyone. Considering that, nowadays, everyone has a smartphone or a computer device that supports writing and audio software, we developed an application we named Talky, one that is simple, easy to use, has portability and has a friendly interface for the user with hearing or speech impairment [4].



2. Developing Talky application using specific programming languages

Talky is thought to function on a desktop, tablet and smartphone, all of these devices allowing for writing and audio [5,7]. From the user's point of view, the application has two main parts:

- when he wants to communicate, to “talk”, he uses the “text to speech” component of the application, which converts the written text to audio sound;
- when he wants to “hear” what the other person is saying, he uses the “speech to text” component, which converts the audio sound into text that the user can read.

Both components of the application were built using the React framework, which allows dividing the code in fragments that can be written and debugged independently from one another [5,6]. For the design of the application's interface, we used Bootstrap's facilities.

```
1 import React,{Fragment} from 'react';
2 import logo from "../src/components/images/Logo@2x.png";
3 import microphone from "../src/components/images/Microphone@2x.png";
4 import "../App.css";
5 import SpeechToText from './components/SpeechToText/SpeechToText';
6 import Speech from './components/TextToSpeech/TextToSpeech'
7
8 const App=()=>{
9   return(
10     <Fragment>
11       <div className='container-fluid mt-3 mt-sm-5'>
12         <header>
13           <img className='img-fluid logo' src={logo} />
14           <img className='img-fluid justify-content-end micro' src={microphone} />
15         </header>
16         <div className='container text-center'>
17           <h1 className='title '>Communication is the key</h1>
18         </div>
19         <div className='container-fluid d-block d-sm-flex mt-5'>
20           <SpeechToText className="justify-content-center"/>
21           <Speech className="justify-content-center"/>
22         </div>
23       </div>
24     </Fragment>
25   )
26 }
```

Figure 1. Main code of Talky application.

For programming code, we used the Visual Studio Code editor, which comes with IntelliSense for JavaScript, TypeScript, CSS and HTML, as well as debugging support for Node.js [4,7,9], languages we needed for developing Talky. The application supports the English language, but the support for additional languages is provided by extensions, available with no charge on the VS Code Marketplace.

The code for the main component of the application Talky, as depicted in figure 1, is used to import the “Text-to-speech” and “Speech-to text” code parts and the buttons the user will see on the interface. Both components will return the results to the main application.

2.1. Talky “Speech-to-text” component

For building the “Speech-to-text” component of the Talky application, we have used both JavaScript and HTML languages. Part of the JavaScript programming code for this functionality is shown in figure 2.

```
function SpeechToText() {
  const [isListening, setIsListening] = useState(false)
  const [note, setNote] = useState(null)

  useEffect(() => {
    handleListen()
  }, [islistening])

  const handlelisten = () => {
    if (isListening) {
      mic.start()
      mic.onend = () => {
        console.log('continue..')
        mic.start()
      }
    } else {
      mic.stop()
      mic.onend = () => {
        console.log('Stopped Mic on Click')
      }
    }
  }
}
```

Figure 2. “Speech-to-text” JavaScript code.

The main function of this component is connected to the “Start/Stop” button function. The HTML code, as presented in figure 3, of “Speech-to-text”, will make visible the button “Start/Stop” on the user’s interface. When the user presses the “Start/Stop” button on the screen, the application will check whether the device’s microphone is activated or not, and if not, the application will take action in that direction, preparing the microphone. After this step, the application will start recording the audio, exactly what the other person is saying, until the user presses the “Start/Stop” again.

The application will proceed to convert the sound into text. The resulted text will be shown on the device’s screen to the user. The JavaScript function `setIsListening` will convert the recorded audio into a text array (list), and this array will be available to the user in a paragraph format [7]. The paragraph in the HTML code will not appear until the recording event is closed.

```
return (
  <Fragment>
    <div className='container-fluid text-center'>
      <div className="container mt-4">
        <div className="box col-lg-5">
          <h2 className='subtitle'>Speech-Text</h2>
          {islistening ? <span>🔊</span> : <span>🔇</span>}
          <button onClick={handleDeleteNotes} disabled={!note}>
            Delete Note
          </button>
          <button className='start_stop' onClick={() => setIsListening(prevState => !prevState)}>
            Start/Stop
          </button>
          <p className='note'>{note}</p>
        </div>
      </div>
    </div>
  </Fragment>
)
```

Figure 3. “Speech-to-text” HTML code.

We also implemented a “Delete” button that is designed for deleting previous “conversations”. While the processes of recording or converting are ongoing, the “Delete” button will be inactive.

2.2. Talky “Text-to- speech” component

For building the “Speech-to-text” component of the Talky application, we have used JavaScript and HTML languages, but both in a single function, as can be seen in figure 4. The logic for this component is the same as for the previous one.

We are using a JavaScript function that aims to play the audio of whatever word the user enters into the input HTML element [7,9]. The audio playback function of the input data is assigned to the “Speech” button. After the user writes a text, he will press the “Speech” button. We have used a value type command with the purpose of listening to any event as input the user will give and trigger the playback audio function.

This component has available, as the previous one, the “Delete” option that works similarly. When the user writes his message, the text converted in audio, he is able to delete it or correct it.

```
const Speech = () => {
  const [value, setValue] = React.useState("");
  const { speak } = useSpeechSynthesis();
  const handleDeleteNotes = () => {
    setValue(" ")
  }
}

return (
  <div className="container text-center mt-4 ">
    <div className="group d-block text-center align-middle">
      <h2 className="txt-title ">Text-Speech</h2>
      <input className="input"
        type="text"
        value={value}
        placeholder="Write something"
        onChange={(e) => setValue(e.target.value)}
      />
      <button className="text-center btn" onClick={() => speak({ text: value }, )}>Speech</button>
      <button onClick={handleDeleteNotes} disabled={!value}>
        Delete Note
      </button>
    </div>
  </div>
)
```

Figure 4. “Text-to-speech” code.

3. Talky interface and functioning

The first impact of the user with the Talky application is the one presented in figure 5. In the upper left corner, we can notice the application’s logo, designed using Adobe XD software [8].

Both “Speech-to-text” and “Text-to-speech” components appear on the user’s device, but only one can be used at a time, according to the user’s needs. If the user wants to “listen”, he will work on the left side of the application. In a similar manner, if the user wants to “talk”, he will work with the right side of the application.

As we can observe, to use Talky, one does not need special skills or knowledge, because the application is simple, easy to install on a laptop, desktop, tablet or smartphone, and is user friendly. Simply by touching a button, a person with hearing loss can be able to “communicate” with others, whether he chooses to “talk” or to “listen”.

In the following, we will explain in detail how the two components contained within the Talky application can be used.

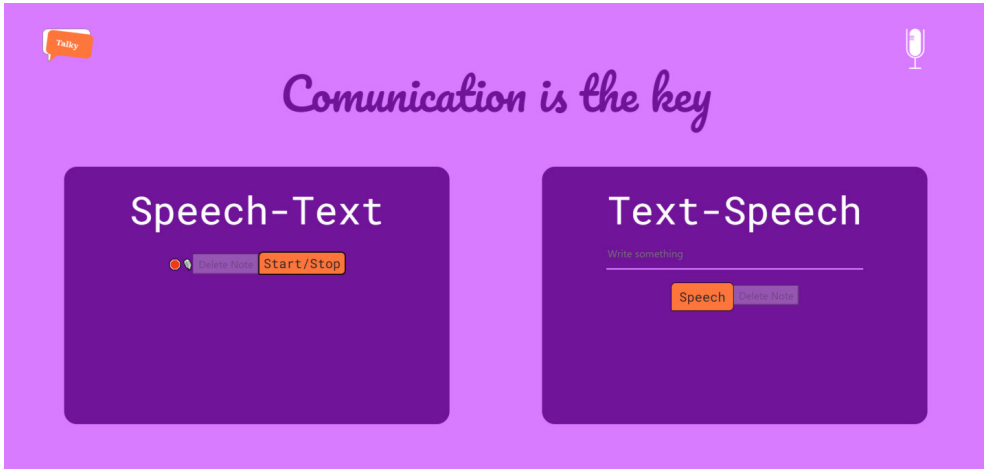


Figure 5. Talky user interface.

In figure 6, we have a better view of the “Speech-to-text” component while it is being used. When the user presses the “Start/Stop” button, the application will start recording the speaker’s voice. We have added a red icon on the left side of the “Speech-to-text” that has the role of indicating the user if the component is activated or not. If the red icon is not present on the screen, it indicates the user that the recording has started and the audio conversion is in progress.

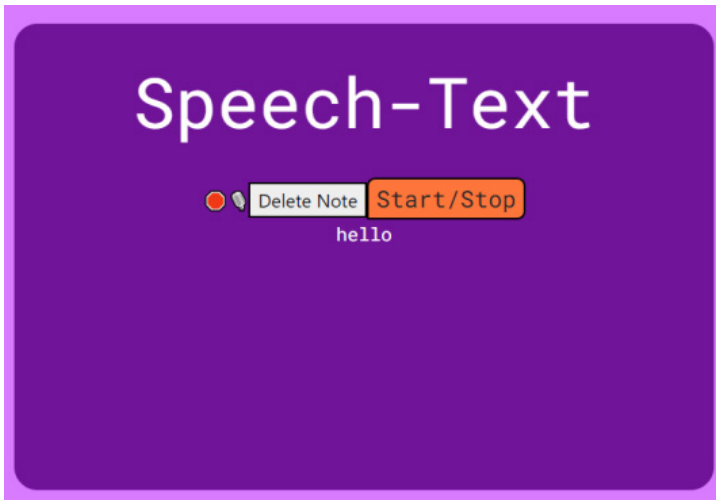


Figure 6. Speech-to-text user interface.

When the user presses the “Start/Stop” button once again, the text of the converted audio will display on the screen. In the process of recording and audio conversion, the “Delete” button is grey-colored, thus inactive. When the process stops, the “Delete” button is white-colored, thus active and the user can delete data.

As we show in figure 6, we spoke the word “Hello”, which appeared on the screen as text.

For the “Text-to-speech” component from figure 7, we have the text area where initially appears “write something”, the “Speech” button and the “Delete” button. The user writes his message in the text area and presses the “Speech” button for the text to sound conversion and audio play events to take place. The other person will be able to hear what the user has written. We can notice that the “Delete” button is active while writing a text.

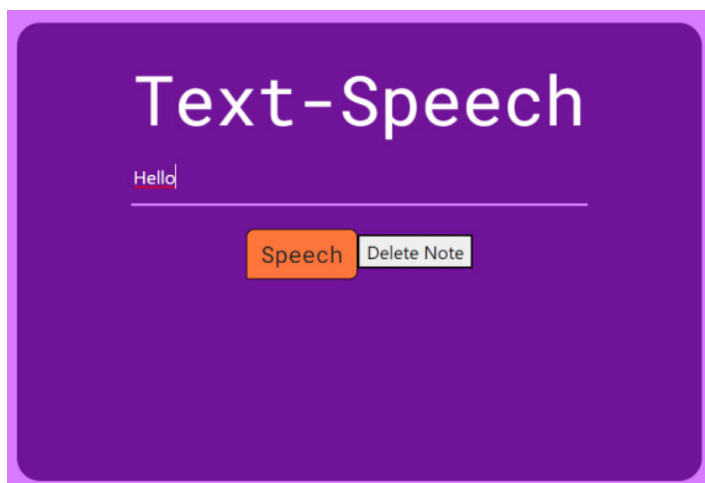


Figure 7. Speech-to-text user interface.

4. Conclusions

Hearing loss can cause plenty of suffering to a person, and there are cases where this issue cannot be solved by medical intervention. Although the technology of hearing devices has evolved so much in the past years that with a small device implanted in the ear canal, one can hear again, it is not yet affordable for the average person. We thought and developed the Talky application to come to the aid of the average person with loss of hearing. Talky is not a healing solution but a mean to help people integrate in everyday life. We have used simple technology and our programming skills to develop an affordable product.

References

- [1] Lin F.R., Niparko J.K., Ferrucci L, Hearing Loss Prevalence in the United States, *Arch Intern Med.*, 20.11, 171(20): 1851–1853, doi: 10.1001/archinternmed.2011.506
- [2] Newton VE, Shah SR. Improving communication with patients with a hearing impairment, *Journal of Community Eye Health*, 10(3), 2013, 26(81): 6-7. PMID: 23840079; PMCID: PMC3678307
- [3] Cox R.M., Johnson J.A., Xu J., Impact of Hearing Aid Technology on Outcomes in Daily Life I: the Patients' Perspective, *Ear and Hearing-The official journal of the American Auditory Society*, 37(4), 2016, pp. 224-237, doi: 10.1097/AUD.0000000000000277.
- [4] Stroia M.D., Hațiegan C., Popescu C., Bugar S.V., System design for improving our home comfort, *Annals of the „Constantin Brancusi” University of Targu Jiu, Engineering Series*, issue 2, 2021, pp. 19-23.
- [5] Accomazzo A., Murray N., Lerner A., *Fullstack React: The Complete Guide to ReactJS and Friends*, Publishing House FullStack.IO, 2017.
- [6] Vipul A., *ReactJS by Example - Building Modern Web Applications with React*, Publishing House Packt Publishing Limited, 2016.
- [7] Lopez L., *React: QuickStart Step-By-Step Guide to Learning React JavaScript Library*, Publishing House Createspace Independent, 2017.
- [8] Schwarz D., *Jump Start Adobe XD*, Publishing House Site Point, 2017.
- [9] Duckett J., *HTML and CSS: Design and Build Websites*, Publishing House Wiley, 2011.

Addresses:

- Lect. Dr. Eng. Mihaela-Dorica Stroia, Babeş-Bolyai University, Faculty of Engineering, Piața Traian Vuia, nr. 1-4, 320085, Reșița, Romania
mihaela.stroia@ubbcluj.ro
- Lect. Dr. Fiz. Cornel Hațiegan, Babeş-Bolyai University, Faculty of Engineering, Piața Traian Vuia, nr. 1-4, 320085, Reșița, Romania
cornel.hatiegan@ubbcluj.ro
(*corresponding author)
- Stud. Bogdan Daniel Borcilă, Babeş-Bolyai University, Faculty of Engineering, Piața Traian Vuia, nr. 1-4, 320085, Reșița, Romania
bogdan.daniel.borcila@stud.ubbcluj.ro

Robot for tracking rectilinear motion

Stelică Timofte, Lenuța Cîndea*, Cornel Hațiegan

Abstract. *The aim of the research work is to deepen and acquire new practical and technical knowledge about how to work with the Arduino platform, the Android operating system and related technologies. Uniformly varied rectilinear motion monitoring can be done optimally using a robot via Bluetooth. The operation of the system can be easily modified and this mini robot can be used for a variety of purposes. Making adjustments in the design and body of the system will allow this vehicle to serve as a remote control robot to perform a wide range of operations.*

Keywords: *robot, straight motion, Arduino, monitoring.*

1. Introduction

The aim of this work was to develop a Line Follower device that involves the tracking of a black line on a white background (or vice versa) by means of light sensors, and its applicability makes it easier to study uniform rectilinear motion in laboratory conditions for the practical study of students in the Mechanical Engineering Specialization [1], [6], [7].

The use of a mobile phone during the application is an advantage to be able to control the robot, which would replace a conventional remote control by which it would normally have to be controlled. Another big advantage is the Android operating system which has helped to make the control interface a reality, as the Android operating system covers a wide range of devices and applications and is very widespread and new utilities are always emerging through its operation.

Arduino is an open source platform used for building electronic projects. Arduino consists of both a physical programmable circuit board (often referred to as a microcontroller) and a piece of software or IDE (Integrated Development Environment) that runs on the initiator computer, used to write and upload source code to the physical board [1].



Arduino has been refined at the Ivrea Interaction Design Institute as an easy rapid prototyping tool for students without a background in electronics and programming. As soon as it reached a wider community, the Arduino board began to change to adapt to new needs and challenges, differentiating its offerings from simple 8-bit boards to products for IoT, 3D printing and embedded environment applications. All Arduino boards are completely open, giving users the ability to build them independently and eventually tailor them to their specific needs. The software, too, is open-source, and is growing through user contributions from around the world.

The Arduino software is easy to use for beginners, but flexible enough for advanced users. It runs on Mac, Windows and Linux. Teachers and students use it to build inexpensive scientific instruments, prove principles of chemistry and physics, or get started with programming and robotics [3].

2. Choice of components. Hardware architecture

An early Arduino board with an RS-232 serial interface (top left) and an Atmel ATmega8 microcontroller (black, bottom right); the 14 digital I/O pins are at the top, the 6 analog input pins at the bottom right and the power connector at the bottom left. Most Arduino boards consist of an 8-bit ATM AVR microcontroller (ATmega8, ATmega168, ATmega328, ATmega1280, ATmega2560) with varying amounts of flash memory, pins and features. The 32-bit Arduino Due, based on the Atmel SAM3X8E, was introduced in 2012. The boards use single or double line pins or female headers that facilitate connections for programming and embedding in other circuits. They can connect with add-on modules called shields [2].

Multiple and possibly stacked shields can be individually addressed via an I2C serial bus. Most boards include a 5 V linear regulator and a 16 MHz crystal oscillator or ceramic resonator. Some models, such as the LilyPad, operate at 8 MHz and are taken off the on-board voltage regulator due to specific factory restrictions.

Arduino microcontrollers are pre-programmed with a bootloader that simplifies loading programs onto the chip's flash memory. The default bootloader of the Arduino UNO is the optiboot bootloader. The boards are loaded with program code via a serial connection to another computer. Some Arduino serial boards contain a level shift circuit to convert between RS-232 logic levels and transistor-transistor logic (TTL) level signals [4].

Current Arduino boards are programmed via the Universal Serial Bus (USB), implemented using USB-to-serial chips such as the FTDI FT232. Some boards, such as the latest generation Uno boards, replace the FTDI chip with a separate AVR chip containing USB-to-serial firmware, which is reprogrammable via its own ICSP header. Other variants, such as the unofficial Arduino Mini and Boarduino, use a USB adapter board or detachable cable, Bluetooth or other methods.

When used with traditional microcontroller tools, standard In-System Programming (ISP) is used instead of Arduino IDE programming [5].

2.1. Arduino UNO V3

It consists of a small platform (68mm/53mm - the most common variant) built around a signal processor and is capable of taking data from the environment through a series of sensors and performing actions on the environment through lights, motors, servomotors and other types of mechanical devices.

The processor is capable of running code written in a programming language that is very similar to the C++ language, the specifications of the Arduino development board are given in Tab. 1. [6].

Table 1. Development board specifications Arduino UNO V3

| | |
|-----------------------------|---|
| Microcontroller | ATmega328 |
| Working voltage | 5 V |
| Input voltage (recommended) | 7 – 12 V |
| Input voltage (limit) | 6 – 20 V |
| Digital pins | 14 (6 PWM output) |
| Analogue pins | 6 |
| Output intensity | 40 mA |
| Output current on 3.3 V | 50 mA |
| Flash memory | 30 KB (ATmega328) 0.5 KB for bootloader |
| SRAM | 2 KB (ATmega328) |
| EEPROM | 1 KB (ATmega328) |
| Clock speed | 16 MHz |

2.2. Engine drivers L298

It is used to control DC motors using the Arduino board. The Arduino is capable of putting out very little power on its ports, totally insufficient to turn a motor.

To avoid burning out the processor, an amplifier has been used to take power from the power supply (in the case of the battery) and transmit it to the motors via commands received from the Arduino board.

The amplifier is called a motor driver based on the L298 integrator, and is a mid-level driver in terms of power conducted. It can control motors requiring 2A or less.

The driver contains a jumper that allows the Arduino board to be powered directly from the power supply, as shown in Fig.1.

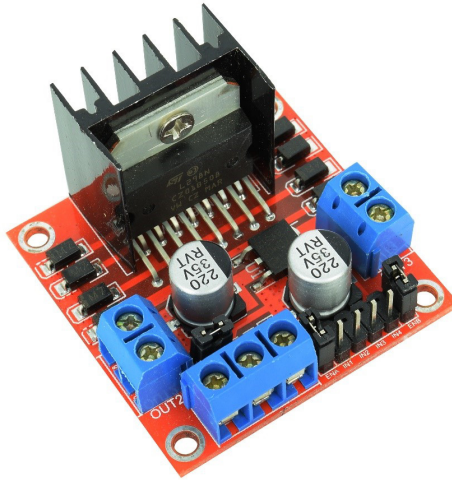


Figure 1. Engine drivers L298 [2]

The HC-05 bluetooth module is a high performance module and consumes very little power. It is also small in size. The product can be used in projects where data needs to be easily transmitted, but not by cable, over reasonable distances, Fig.2.

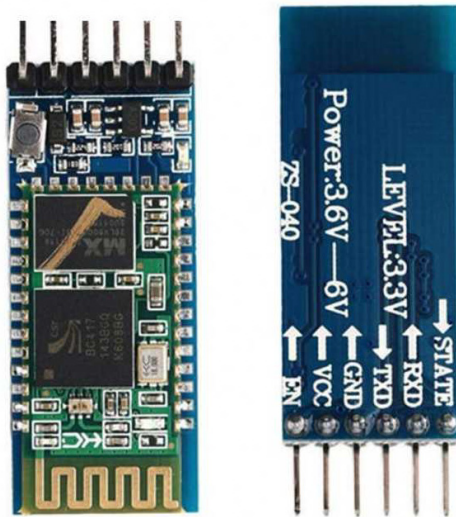


Figure 2. Modulul bluetooth HC-05 [2]

The HC-05 bluetooth module is a slave bluetooth module designed for wireless serial communications. It is a slave module, which means that it can receive serial data when serial data is sent from a master Bluetooth device (device capable of sending serial data over the air: smart phones, PCs). When the module receives wireless data, it is sent through the serial interface right on reception.

No Bluetooth module-specific source code is required at all in the arduino chip. An app on the phone is used to send inputs to the receiving module and then transfers them to the arduino. In turn, the arduino and actuators respond accordingly, as specified in the source code.

When the module is not in a paired state, the LED on the module flashes rapidly, while when paired with the app on the phone, the LED on the module is steady red.

2.3. Line tracking sensor mode TCRT5000

With this module you can detect the distance to an object or follow a black line with infrared sensors. Therefore the module is used to build a line-following robot, which has both infrared line-following sensors, oriented downwards, and a sensor oriented forwards so that the robot can also detect obstacles on the path.

Connecting the TCRT5000 line tracking sensor module together with the Arduino is shown in Fig. 3.

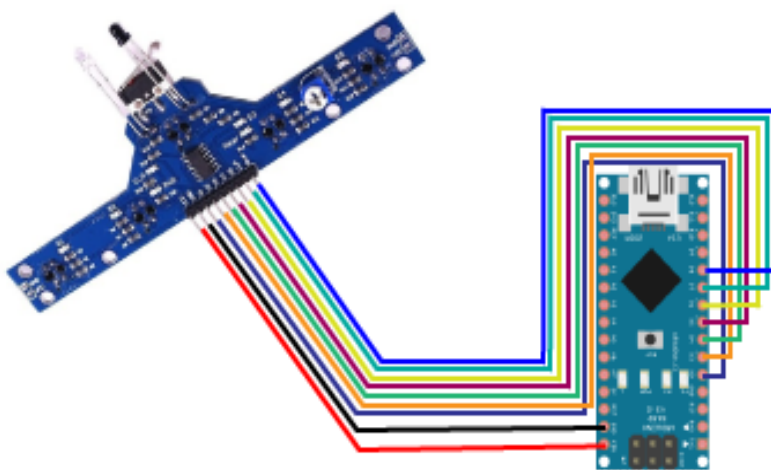


Figure 3. TCRT5000 module connections with Arduino

3. Finite element model of the robot chassis

3D simulation of the chassis, Fig. 4, was developed in the SOLIDWORKS 2016 software program, going through the simulation steps, of which the most relevant were selected: The material 2018 Alloy was chosen from the SOLIDWORKS 2016 material library.

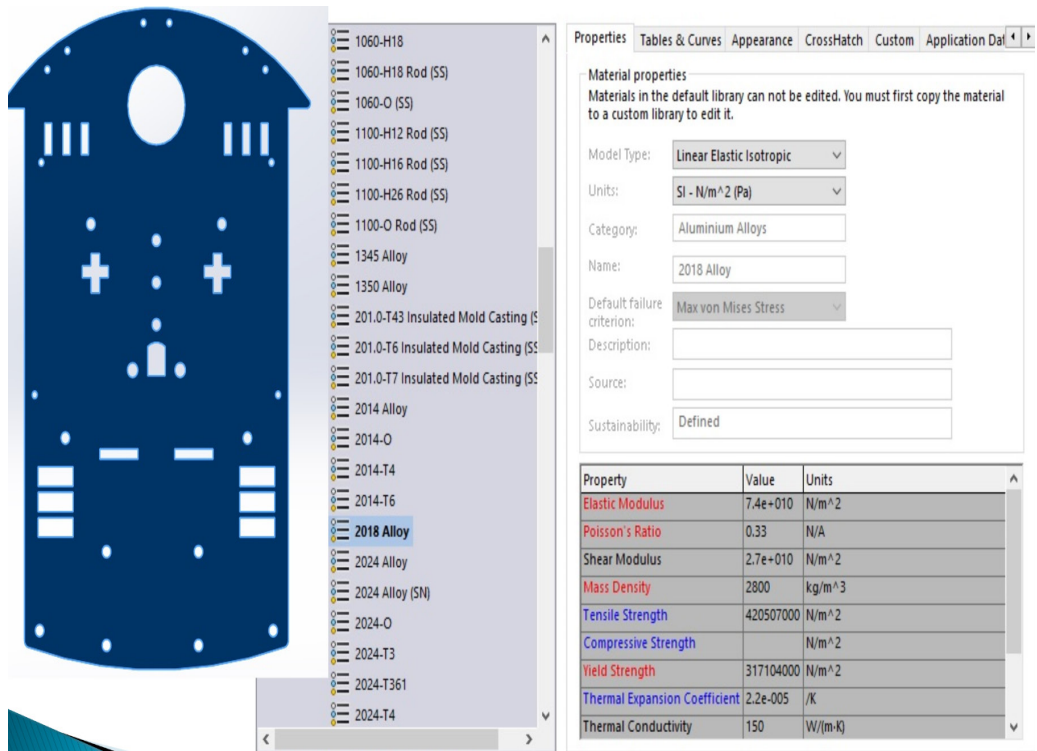


Figure 4. Choice of chassis material

The model was discretized in finite elements by applying Mesh for solid discretization, the chassis was fixed in the motor clamping area and a force of 100 N was applied in the driven wheel clamping area in order to carry out the analysis and simulation study on the mini robot chassis, Fig. 5 [4].

This stage of the simulation is part of the processing stage of the results, and we also set the regime to be static and dynamic by analysing the von Mises stresses.

Before starting the processing stage, the program transferred the boundary conditions and the loads applied on the geometrical elements to the nodes of the discretized model.

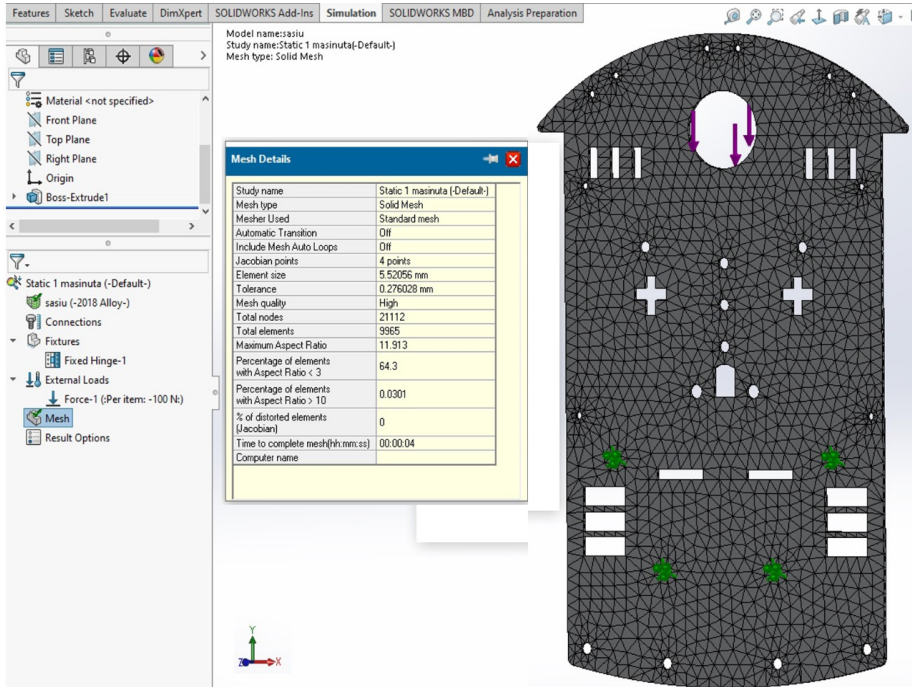


Figure 5. Discretizing the chassis

4. Usefulness of the robot for the study of uniform rectilinear motion

It is known that on the same trajectory, e.g. in a straight line, a mobile can travel at the same speed for several seconds or change speed.

In this case the robot plays the moving mobile. With the help of the apparatus in the Mechanics laboratory, made up of sliders that are placed along a track, the robot moves, under the control of the phone, over certain distances depending on the length of the track. The main condition is the perpendicularity of the light barriers equipped with an LED and the data acquisition device.

For distances travelled in 10 cm increments, the corresponding time is timed to cover the distance.

To save time, one can let the supplied trolley and the built robot pass through the two light barriers at the same distance on both speed settings one after the other.

Knowing the space covered, from 0.1m for each measurement, the time is timed at each step so that the time covered can be calculated for each measurement.

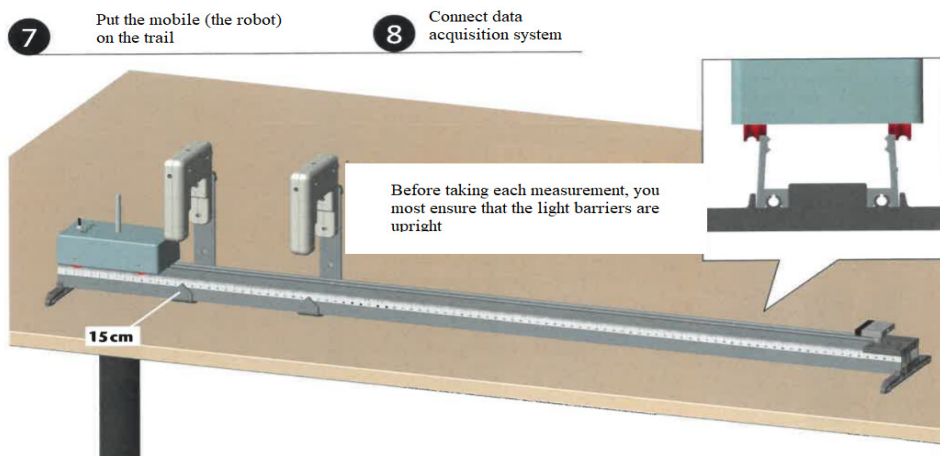


Figure 6. The experimental stand

For example, for the space $s=0.4\text{m}$, $t=3.44\text{s}$ was obtained, resulting in velocity:

$$v_4 = \frac{s}{t} = \frac{0,4}{3,44} = 0,116\text{m/s} \quad (1)$$

In this way the velocities are calculated for each value of the space travelled by both moving mobiles.

Both the robot and the motorised trolley move at constant speed on both speed settings. The actual speed may differ slightly from trolley to trolley, which means that the result of different groups is likely to differ between them.

For both speeds, the distance versus time plot should lead to a straight line through the too high degree of accuracy of the origin, Fig. 7.

A sample measurement of travel time between 25cm and 80cm at both speeds gave the following results:

$$t_1 = \frac{0,80\text{m} - 0,25\text{m}}{0,116\text{m/s}} \cong 4,74\text{s} \quad (2)$$

$$t_1 = \frac{0,80\text{m} - 0,25\text{m}}{0,153\text{m/s}} \cong 3,59\text{s} \quad (3)$$

The deviation between the two time measurements of 4.76 and 3.61 is about 0.5%.

Table 2. Measurement results

| The mobile | Δs [m] | 0,1 | 0,2 | 0,3 | 0,4 | 0,5 | 0,6 | 0,7 |
|----------------|----------------|------|------|------|------|------|------|------|
| Velocity v_1 | Δt [s] | 0,88 | 1,73 | 2,58 | 3,44 | 4,31 | 5,19 | 6,04 |
| Velocity v_2 | Δt [s] | 0,67 | 1,32 | 1,97 | 2,63 | 3,27 | 3,93 | 4,59 |

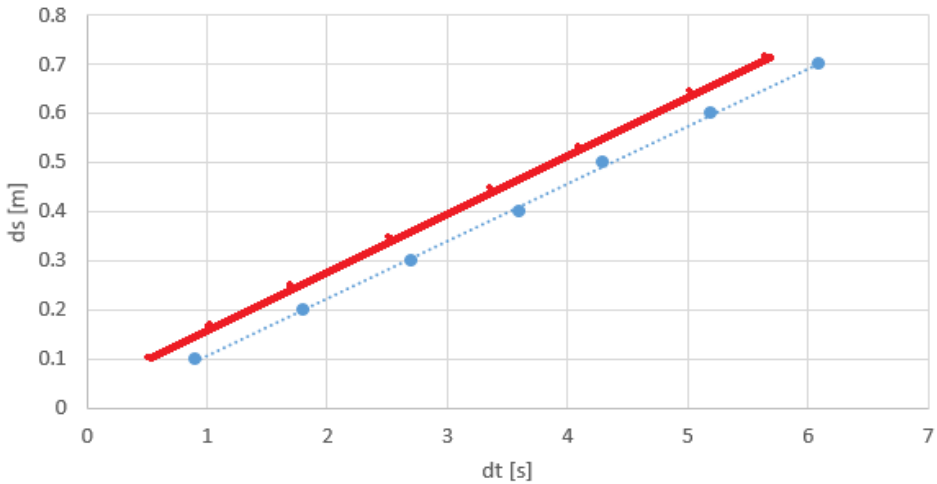


Figure 7. Distance versus time graph

5. Conclusion

The construction and testing of the robot involved three different phases: perception, processing and action.

Depending on the trajectory chosen to study a type of movement, it can be used in several applications, including monitoring different types of movements.

Studying rectilinear motion with this robot can improve students' ability to explain the phenomenon in practice. The construction of the robot is inexpensive and relatively fast and allows experiments to be carried out in the laboratory, comparing the measurement results with the analytical results given in the literature. The geometry of the trajectory is dependent on the time parameter in this type of application, and the errors resulting from comparisons are relatively small. The benefit of this type of robot is that it can be adapted to independently drivable vehicles. In this case, the sensors enable independent travel. Programming allows the robot to adapt to new requirements or to change certain parameters in a short time.

References

- [1] Stroia M.D., Derbac D., Hațiegan C., Cîndea L., Thermostat model with Arduino uno board for controlling a colling system, *Annals of the „Constantin Brancusi” University of Targu Jiu, Engineering Series*, 3, 2018, pp.73-77.
- [2] Doroftei I., Marta C., Hamat C., Suciu L., Prisacaru Gh., A hybrid wheel-leg mobile robot, *Annals of DAAAM & Proceedings*, 2008, pp. 213.
- [3] Timofte S., Cîndea L., Hațiegan C., Control of a vehicle through a smartphone application, *Annals of the „Constantin Brancusi” University of Targu Jiu, Engineering Series*, 2, 2021, pp. 39-43.
- [4] Ward J.R.; Phillips M.J., Digitizer Technology: Performance Characteristics and the Effects on the User Interface, *IEEE Computer Graphics and Applications*. Spectrum.ieee.org. 2014.
- [5] Alfred A. (n.d.), How to Interface XBEE with Arduino., <http://www.engineersgarage.com/embedded/arduino/how-to-interface-xbee-witharduino-tutorial>.
- [6] Stroia M.-D., Hatiegan C., Popescu C., Virtual instrument designed for data acquisition, *Studia Universitatis Babeş-Bolyai Engineering*, 65(1), 2020. pp.179-186.
- [7] The Android Debug Bridge(ADB), Android Open Accessory Development Kit", <http://developer.android.com/guide/topics/usb/adk.html>, 2012.

Addresses:

- Ph.D. Stud. Eng. Stelică Timofte, Babeş-Bolyai University, Faculty of Engineering, Piața Traian Vuia, nr. 1-4, 320085, Reșița, Romania
stelică.timofte@ubbcluj.ro
- S.L. Dr. Eng. Lenuța Cîndea, Babeş-Bolyai University, Faculty of Engineering, Piața Traian Vuia, nr. 1-4, 320085, Reșița, Romania
(*corresponding author).
lenuta.cindea@ubbcluj.ro
- S.L. Dr. Eng. Cornel Hațiegan, Babeş-Bolyai University, Faculty of Engineering, Piața Traian Vuia, nr. 1-4, 320085, Reșița, Romania
cornel.hatiegan@ubbcluj.ro

Electromechanical engineering education and science in Republic of Moldova

Petru Todos, Ilie Nuca, Andrei Chiciuc, Vadim Cazac,
Marcel Burduniuc*

Abstract. *The work is a summary of the history of the industry and education development of electrotechnics in the Republic of Moldova during the independence period. With the national renaissance, the process of professional training in the electrotechnical field began to take on a natural national face - training in the Romanian language. Scientific research is determined by the subject of special submersible and permanent magnet electric machines, renewable energy sources, but also by new directions such as the development of adjustable electromechanical systems for the automation and efficiency of technological processes and traction systems of electric passenger vehicles.*

Keywords: *electromechanical engineering, education, science*

1. Introduction

Electrotechnics is an important branch in any country's economy. In a previously published paper [1], a series of problems was related to the appearance of the electrotechnical field in the Republic of Moldova industry, the formation of the electrotechnical school in education and research were elucidated. The electrotechnical industry in Moldova (within the former USSR) had a considerable weight during a long period in the national economy. In the period after 1990, the role of this industry, was significantly reduced, but at the same time other branches of electrical engineering appeared, such as electric transport, the automotive industry and others. Thus, for a correct planning of the next steps, regarding the development of the field in its entirety, but also of the Technical University, including the Department of Electrical Engineering, as an indispensable part of it, a deep and multilateral analysis of both the previous period and the situation in the current period is necessary [1].



2. The history of the industry development during the period of independence of the Republic of Moldova

With the dissolution of the Soviet Union (USSR), or more precisely since 1990 (1989 was recognized as a pre-crisis year), the annual volume of production began to decrease, which led to the degradation of the industry. The economic situation in the country was aggravated by the 1992-armed conflict in Transnistria, the consequences of which are still felt today. Structurally, the economy of the republic gradually began to lose its industrial character: the share of industry in GDP fell to 31,8% (in 1995), and the number of people employed in industry decreased by 50%. At the same time, another structural change occurred – the reduction of the share of the machine-building industry (mainly electrotechnical), both in production and in exports. In the year (1995), in which the real reform of the republic's industry began, the volume of industrial production, compared to the level of 1990, was 44,2% [2].

What were the causes of the electrical industry catastrophe in the period immediately following the collapse of the USSR? Most of the companies in this branch were part of the group of those with Union subordination. The economic value of these enterprises for the Republic of Moldova, of course, was enormous. In 1990, the share of the Union subordinate industry in the whole sector of the republic, in terms of production was 29%, in terms of the number of staff – 36%, and after the cost of basic production funds – 48%. These largely determined the scientific and technical potential of the Republic of Moldova. However, for these enterprises the ministries and party structures of the USSR in Moscow adopted all decisions. There, the nomenclature and volume of production, the sources of raw materials, the way of production, and the financing were planned. The Republic of Moldova was responsible for the social part and waste. Persons brought from Russia exclusively supplemented the leading and scientific staff. It should be noted that the share of military-industrial complex enterprises in these five years has decreased from 11,4% to 0,77% in 1995 [2].

Towards the year 2000, the decline of industrial production stopped and the gradual increase in the production of electrical and electronic equipment began (figure 1).

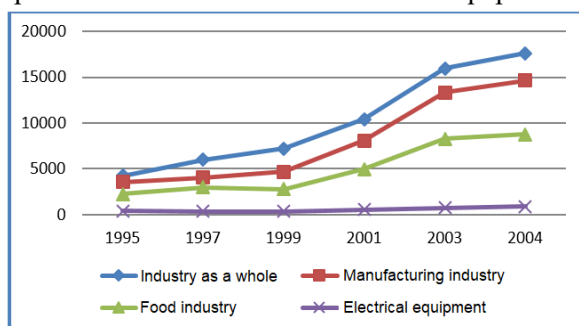


Figure 1. Volume of industrial production-by-production sectors in million MDL [3] (processed by authors).

3. The dynamics of the current electrotechnical industry transformations

After the years 2003-2005, there was a slow increase in industrial production overall, and some structural changes took place: the share of manufacturing industry production increases (83,3%) [4-6]. After a long period of slow growth, on the background of stagnation of traditional electrotechnical productions (figure 2) there is an explosive development of a specific sector related to the automotive industry - the manufacture of wires, cables and other equipment for assembling cars. Small and medium enterprises in the electrotechnical field have developed in recent years

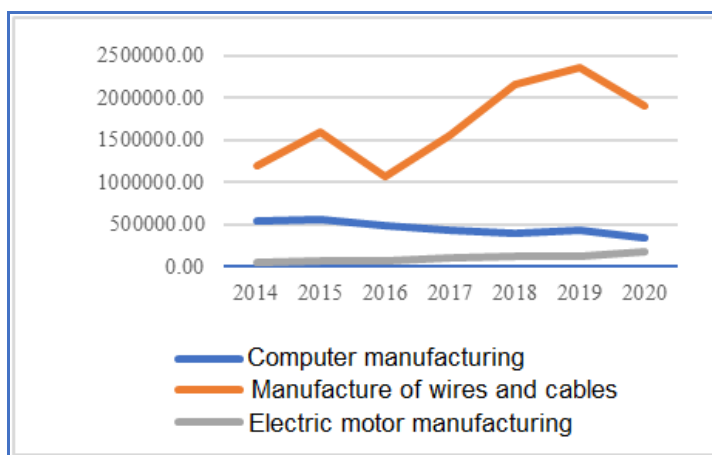


Figure 2. Dynamics of the manufacture of electrical and electronic equipment, 2014-2020 [7, 8] (processed by authors).

There are also other characteristic moments of the current economic development of the country. If in 1990 the GDP of the services chapter accounted for 20%, for 2020 their rate is 60%. The complexity of services, for example, urban electric transport, vertical transport in multi-storey buildings, automatic water supply systems and others has changed a lot, which requires a higher degree of qualification of specialists.

4. Modification of the process of specealists preparation

The changes in the economy of the Republic of Moldova imposed essential reorientations in the policy of training the specealists - the transition to wider specializations for a wide range of enterprises. What does our faculty, our department, do in these circumstances?

After several attempts, in 1988, the establishment of a new study program „Electric drive and automation of technological processes” was accepted. This was a real test for the department. In addition to the traditional courses of Electrical Engineering, Electric cars, Electrical appliances, in a short time, we had to learn many new disciplines specific to the specialty mentioned.

In parallel, groups with teaching in Romanian had to be formed, the library filled with literature in Romanian. Here we could mention the special contribution of some teachers who were directly involved in the teaching process: Professors Lorin Cantemir, Alexandru Simion (UTIs), Aurel Câmpeanu and Gheorghe Manolea (UCr); Carmen Golovanov, Mihai Covrig, Valentin Năvrănescu (UPB), Elena Helrea and Mihai Cernat (UTBr), Adrian Graur (USV). This collaboration is continued by the next generation (Dorin Lucache, Iulian Birou, Sergiu Ivanov, Vasile Horga, and Calin Munteanu). We will also mention, on this occasion, the special contribution of the people coming from the research: dr. conf. Tudor Ciuru - specialist in the field of electric drives, Valeriu Blaja dr. conf. – electronist, Vladimir Gutic – former chief engineer.

In 2015, the „Electromechanical” bachelor program was accredited by the AQAS quality assurance Agency in Germany.

In 2017, was approved the current specialty nomenclature, according to which the program was renamed into „Electromechanical systems Engineering” (ISEM). At the current stage the ISEM program has the mission to train specialists – integrators of programmable electromechanical systems (starting-protection equipment, electromechanical converters, static converters, sensors-transducers, PLC, SCADA) for the automation and efficiency of working machines or technological processes.

Due to the reduction in the number of high school graduates in 2019 was proposed joint trunk for two years of studies in full, and at the years three and four they have a common trunk that constitutes 30-40%.

For over 55 years, within the department over 1800 highly qualified electromechanical engineers have been trained for the national economy. Former electromechanical students represent the core of the production/repair of equipment and electrical machines (Hidromaş, Electromeaş, Energorotor, Electromotor-Service), electrotechnical enterprises (Volta, TehElectro-SV, EltroTehnImport, Salonix) or provides the installation and exlocation of auatomatize technological lines from the most diverse fields (glass container Company, Franzeluţa, Vitanta, Orhei-Vit etc.). It is gratifying that several electro-emcanic graduates have founded their own national and multinational enterprises, which successfully deal with the development and production of modern technological lines based on automated electromechanical systems with PLC and SCADA control (Alex Dragomir, Alexandru Jalba, Artiom Moldovan, Nicolae Prisacaru, Vladimir Ivanov, etc.).

5. Organizing scientific research under new conditions

The topic of scientific research within the department has also undergone essential changes, dictated by those changes that took place in the economy, on the labor market (the needs of our partners), but also in the study process.

A significant orientation toward the issues of sustainable development occurred both in the study programs and in the topic of scientific research at the department. Thus, in the bachelor programs the fundamental course of „renewable energy sources” is studied, at cycle II – Master studies was introduced the module „project Management” which was supplemented with a course „Environmental impact assessment of development projects”. The doctoral school proposes to all doctoral students to study the „methodological foundations of sustainable development” and to argue the topic of its research on its principles.

Currently, the scientific research of the department is focused on the following priority directions „*Renewable Energy Sources*”, „*Special Electric and Electromechanical Converters*”, „*Traction systems for urban passenger electric transport*”, „*Adjustable electromechanical systems for the automation and energy efficiency of technological processes*”.

Research direction „Renewable Energy Sources”. As early as 80 years of the last century, the team of researchers Petru Todos, Iurii Mindru, Iurii Soloviov and the student Ion Moldovanu developed an autonomous system for supplying electricity to a hail protection equipment, using wind energy. Next, the department had several researches and elaborations related to the valorization of renewable energy sources through research projects within state programs, European projects and cooperation Moldova Romania.

The results of the research carried out within the projects Tempus („Creation of a Center for Higher Education in the Area of Renewable Energies” in collaboration with the French Agency for Energy and Environment, leader Ion Sobor, 1996-1998; „MSC programme in Environment and Clean technologies”, grant holder: Royal technological Institute in Stockholm, coordinator Petru Todos, 2004-2006), two projects funded under the United Nations Framework Convention on Climate change, were developed courses and textbooks for students [9-10] related to the conversion and efficient use of the most widely used renewable energy sources in the Republic of Moldova (wind, sun, biomass, flowing water).

Another research project was carried out between 2001-2003 „Elaboration of the wind energy cadastre of the Republic of Moldova”, financed by the national Council for Science and technological Development (research team: Petru Todos, Ion Sobor, Andrei Chiciuc and the student Mihai Grosu). These team laid the methodological foundations for studying the wind energy potential, elaborated the data instrumentation and processing system, the calculation algorithm, the methodology for interpreting and graphical presentation of the results. A first map of the

wind energy potential at height was drawn up (figure 3). The most important success of this project was the breaking of the dogma, promoted by the traditional energy lobbyists, that Moldova does not have wind energy potential.

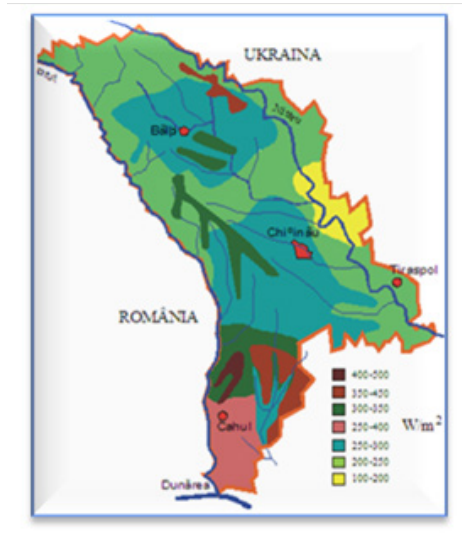


Figure 3. Map of wind energy potential of RM (height 70 m from ground)

Another research project was carried out between 2014-2017, (coordinator Ion Sobor), financed from the energy efficiency fund of the Republic of Moldova, was completed with the elaboration and editing of „Atlas of wind energy resources of the Republic of Moldova”, authors Ion Sobor, Andrei Chiciuc and Vasile Rachier.

Research direction „Special Electrical and Electromechanical converters”.

Projects carried out under this theme relate to the development of methodologies, devices and systems aimed at enhancing energy efficiency and energy conservation, which is included in the sustainable development goals declared in the United Nations Development Strategy 2030, which is also reflected in the development strategy of the Republic of Moldova.

The project „*Elaboration and production in series of small and special transformers from reconditioned materials (2002-2015)*” had as research objective the development of the technology for the reuse of the electrotechnical materials obtained when the power transformers are dismantled at the end of their term of use. Research team: prof. dr. Ion Stratan, prof. dr. Tudor Ambros, Alexandr Gorceac, Vladimir Olhovschii, Marcel Burduniuc, Valeriu Bordian, Natalia Chirița. Based on the technical documentation and the developed technology, the company S.A. “RED-Nord” manufactures a wide range of single-phase and three-phase power transformers from 10 kVA to 250 kVA (figure 4).



Figure 4. Transformers produced from reconditioned materials

The project “Submersible pumps with electromagnetic action”, realized in the period 1997-2004, the research team: Ion Sobor, Nicolae Kobîleaţkii, Abdel Wahhab, Corneliu Gherţescu, Iaroslav Kobîleaţchii, the objective of the research was to modernize the electromagnetic action of household submersible pumps in order to reduce the costs of electrotechnical steel, copper and increase the efficiency. An electromagnetic pumping system for irrigation of small areas, powered by photovoltaic panels, was developed and implemented.

Between 2004 and 2008, the team of professors, engineers and students from the department (I. Sobor, T. Ambros, N. Kobîleaţkii, conf., dr. ing. A. Chiciuc, conf., L. Iazloveţchii, M. Burduniuc, V. Bordian, A. Dragomir) have done more research on synchronous machines with permanent magnets. Industrial prototypes of the synchronous motor with permanent magnets of 7,5 kW were made for the operation of submersible pumps, of the permanent magnet generator for the wind turbine of 10 kW, 136 rpm and direct coupling with the wind turbine rotor, a series of permanent magnet generators for micro-hydropower plants (figure 5) with rated power 3 kW, rotational speed 375 rpm.



Figure 5. Generators with permanent magnets of 3 kW

Research direction „Traction systems for urban electric passenger transport”.

An indisputable way to solve environmental pollution problems and reduce fossil consumption is to use electric motor transport units [11, 13, 14]. Public electric transport, electric cars, vertical transport are today elements, which without urban life cannot be imagined [12].

The research teams of the department and the Informbusiness enterprise studied the traction systems of urban electric vehicles [15, 16]. In the period 2005-2008, the structure and control algorithms were developed and the company INFORMBUSINESS produced/produces in series DC/DC static converters for equipping or upgrading trolleybuses and trams from Ukraine, Romania, Russia and the Republic of Moldova. In 2008-2010, the structure and vector control algorithms of traction inverters for trolleybuses with asynchronous engines were developed [15, 16]. At the exhibition „Made in Moldova-2010”, the INFORMBUSINESS campaign presented the first Moldovan trolleybus with asynchronous engine and vector control. Over the past 5-7 years, the focus has been on the development of traction and power systems of batteries for electrolip batteries (figure 6). As a result, in Chişinău the electric buses provide eight connecting routes with the suburbs over 150 km long.



Figure 6. The traction and battery supply system for electric buses

Within the cooperation project between the Polytechnic University of Timisoara (prof. Sorin Deaconu-director) in association with the Technical University Gh. Asachi of Iași (dr.conf. Vasile Horga) and Technical University of Moldova (dr. conf. Ilie Nuca-director, Vadim Cazac, Marcel Burduniuc, Petru Virlan, Iurie Nuca, Adrian Turcan) „Performance systems of hybrid and electric vehicles with a dual-rotor axial synchronous machine, a single stator and inverter HELSAX (2016-2018) were developed and researched electric propulsion systems based on a single-stator and two rotors axial electric car and a single static converter with two independent output frequencies [16].

In the period of 2020-2022, the Technical University of Moldova of Chisinau in partnership with the Technical University „Gheorghe Asachi” of Iasi had realized the project of cross-border cooperation RO-MD EMS-ENI 2SOFT/3.1/54 „Improving the cross-border public transportation using electric buses supplied with renewable energy”. In the project were carried out extensive studies of the traction systems of electric motor electrobuses, electronic power converter and battery accumulators, of vector control methods, intelligent and energy efficient, a mixed automated system was developed to supply battery accumulators of electric mains batteries and solar panel farm [17, 18].

Since 2020, within the State Program, the team of the Department of Electrical Engineering (dr. conf. Ilie Nuca-director, prof. Petru Todos, prof. Tudor Ambros, dr. conf. Vadim Cazac, dr. conf. Alexandru Tarlajanu, Marcel Burduniuc, Cornel Gherțescu, Ghendie Terteia, Iurie Nuca, and Alexandru Motroi) carries out the research project no. 20.80009.5007.29PS „Integrated autochthonous electric traction systems for urban passenger vehicles”. The aim of the project is to develop integrated domestic electric traction systems with increased energy efficiency and reliability for urban passenger vehicles, based on the associated use of the electronic static converter and the asynchronous motor, both with six phases. At the current stage, models of static converter and hexafazate asynchronous motor (figure 7)

have been developed and manufactured, in-depth experimental research is carried out to test the topological structures of the motor and inverter, as well as the optimal control methods.

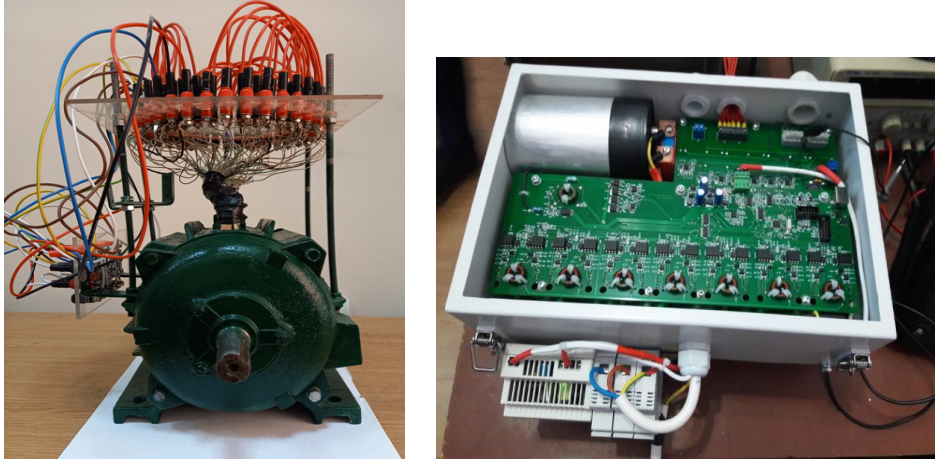


Figure 7. Models of the hexafazate asynchronous motor and inverter

Research direction „Electromechanical adjustable systems for Automation and Energy efficiency of technological processes” It is fully in line with the national Program for Energy efficiency. Within the national research project „Toward an Energy autonomy of the Republic of Moldova (AUTOEN)” the team of the department (prof. Tudor Ambros, dr. conf. Ilie Nuca, dr. conf. Leonid Iazlovețchi, Marcel Burduniuc, Iurie Nuca, Adrian Țurcan) have developed and researched various electromechanical converters with low power loss, adjustable electromechanical systems to increase the energy efficiency of pumping/ventilation technological processes, industrial technological processes and common technological installations [19].

6. Conclusions.

During the period of independence of the Republic of Moldova, the industry underwent many transformations. In accordance with the requirements of the industry, the study programs at the Electrical Engineering department were, also, modified. Science, in the field of electromechanical, is developing in step with the development of technologies used in the industry.

Acknowledgment. This work was supported by a grant of the National Agency of Research and Innovation (ANCD), project number 20.80009.5007.29.

References

- [1] Todos P., Nuca I., Nuca I., *Development of Electrotechnical Industry, Research and Education in the Republic of Moldova*, International Conference on Electromechanical and Energy Systems 2019 (SIELMEN).
DOI: [10.1109/SIELMEN.2019.8905848](https://doi.org/10.1109/SIELMEN.2019.8905848);
- [2] Mihail P., *Promyshlennosti Moldovy vcera, segodnea.* / Evonomica, 30 iulie 2008. <https://ava.md/2008/07/30/promyshlennost-moldovy-vchera-segodnya/>;
- [3] Anuarul statistic al Republicii Moldova/Biroul Național de Statistică al Republicii Moldova; – Ch.: Statistica, 2005
- [4] Anuarul statistic al Republicii Moldova, 2003 / Departamentul Statistică și Sociologie al Republicii Moldova. – Ch.: Statistica, 2003.
- [5] Anuarul statistic al Republicii Moldova / Biroul Național de Statistică al Republicii Moldova; – Ch.: Statistica, 2021.
- [6] Banca de date statistice a Republicii Moldova. Industrie. Valoarea producției industriale, pe tipuri de activitate, 1997-2004. <http://date.gov.md/ro/content/banca-de-date-statistice-republicii-moldova>;
- [7] Banca de date statistice Moldova. Industria. Producția principalelor produse industriale 2004-2021, <http://statbank.statistica.md/pxweb/pxweb/ro>;
- [8] MEI. *Strategia industrializării Republicii Moldova 2019-2030*. Document operațional analitic. Chișinău, 2018.
- [9] Ambros T., Arion V., Guțu A., Sobor I., Todos P., Ungureanu D., *Surse Regenerabile de Energie*, Editura „Tehnica-Info” Chișinău. 1999.
- [10] Sobor I., Caraghiaur D., Nosadze S., *Surse Regenerabile de Energie. Curs de prelegeri*. Ministerul Educației și Tineretului. Universitatea Tehnică a Moldovei, Chișinău, 2006.
- [11] Motroi A., Eșanu V., Nuca I., Olevschi G., Nuca I., *Development of electronic equipment for trolleybuses with autonomous power source*. Proceeding of the 5th International Conference „Telecommunications, Electronics and Informatics”, May 20-23, 2015, Chișinău, Moldova, pp. 98-101.
- [12] European Commission. Mobility and transport. https://transport.ec.europa.eu/index_en (accessed on 21 august 2021);
- [13] 30% of city buses registered in Europe is now zero emissions. <https://www.sustainable-bus.com/news/electric-bus-market-europe-half-2022-vdl/>
- [14] Esanu V., Motroi A., Nuca I., Nuca I., *Electrical Buses: Development and Implementation in Chisinau Municipality*, Moldova: 2019 International Conference on Electromechanical and Energy Systems (SIELMEN)
<https://ieeexplore.ieee.org/document/8905794>

- [15] Produse ale companiei Informbusiness pentru transportul electric. <http://trans-electro.com/ro/product.html>
- [16] Deaconu S., Topor M., Horga V., Marignetti F., Tutelea L., Nuca I., Light-weight high efficiency power train propulsion with axial flux machines for electric or hybrid vehicles, *New Trends in Electrical Vehicle Powertrains - Reliability and Resilience*, 2019, pp.153-174.
- [17] Nițucă C., Nucă I., Pleșca A.-T., Chiriac G., Cazac V., Burduniuc M., *Improving the cross-border public transportation using electric buses supplied with renewable energy*, Editura Tritonic, București, 2022.
- [18] Mallon K.R., Assadian F., Bo Fu. Analysis of On-Board Photovoltaics for a Battery Electric Bus and Their Impact on Battery Lifespan, *Energies*, 2017, 10, 943; doi:10.3390/en10070943
- [19] Cazac V., Nuca I., Todos P., *AC Drive Control System of the Wire Drawing Machine with DTC Control and Fuzzy Controller*. 13th International Conference on Development and Application Systems, Suceava, Romania, May 19-21, 2016. pp.126-129, <http://ieeexplore.ieee.org/document/7492560/>

Addresses:

- Prof. Dr. Eng. Petru Todos, Technical University of Moldova, Faculty of Energetics and Electrical Engineering, Department of Electrical Engineering, Chisinau, Republic of Moldova.
petru.todos@ie.utm.md
 - Conf. Dr. Eng. Ilie Nuca, Technical University of Moldova, Faculty of Energetics and Electrical Engineering, Department of Electrical Engineering, Chisinau, Republic of Moldova.
ilie.nuca@ie.utm.md
 - Conf. Dr. Eng. Andrei Chicviuc, Technical University of Moldova, Faculty of Energetics and Electrical Engineering, Department of Electrical Engineering, Chisinau, Republic of Moldova.
andrei.chicviuc@ie.utm.md
 - Lect. Dr. Eng. Vadim Cazac, Technical University of Moldova, Faculty of Energetics and Electrical Engineering, Department of Electrical Engineering, Chisinau, Republic of Moldova.
vadim.cazac@ie.utm.md
 - Lect. Marcel Burduniuc, Technical University of Moldova, Faculty of Energetics and Electrical Engineering, Department of Electrical Engineering, Chisinau, Republic of Moldova.
marcel.burduniuc@ie.utm.md
- (* corresponding author)

Geometry influence of stator and rotor armatures on energy efficiency of induction motors

Ion Voncilă, Elena Selim, Ion Paraschiv

Abstract. *This paper presents the geometry influence of stator and rotor armatures on induction motor energy efficiency. The entire work is analyzed using a Motor-CAD programming environment. In principle, in the first stage, the influence of each armature is distinctly visualized upon loss level, for given effective power and given cooling algorithm through geometry changes that concern aspects related to the dimensions of the ferromagnetic core and the notches practiced within it. Afterwards, in a second stage, a synergistic modification of the induction motor geometry is carried out by cumulating the changes (cooperative effect) at the level of the two armatures, aiming to find the topology that provides – for some given effective power, and cooling algorithm – the highest energy efficiency.*

Keywords: *induction motor, energy efficiency, geometrical optimization*

1. Introduction

Induction motors have a wide applicability in industry, being used in electric drive systems from low power (hundreds of W) to high power (tens of MW). In these circumstances, the visualization of the energy efficiency of this motor has a great importance for practice, because reducing the impact on the environment calls for an overall increase in efficiency. It is worth noting that the power of electric motors, according to the classic design algorithm, is proportional to their volume. Therefore, a structure of a certain volume, in the vision of some smooth armature/ without notches, allows the development of a particular global power; being a conservative system, each motor, at an effective power developed at the shaft, will also claim an amount of losses in the electromechanical conversion process. The real induction motor has notched armatures and contains, within its structure, both windings, placed in these notches, and ferromagnetic core (into which the notches are made). Thus, the issue of conversion becomes more complicated, the technical and energetic performances of the engine being strongly influenced by the geometrical particularities of the two armatures. The influence of the stator and rotor armature



geometry on the technical performance of the squirrel cage rotor induction motor is highlighted in various specialized works [1], [2], [3]. The visualization of energy performances is presented, as an historical evolution for induction motors - in the paper [4], which also highlights the importance of armatures geometry and the materials embedded within the structures of electromechanical conversion, to ensure a high efficiency of these motors.

Of course, knowing these influences on the technical and energetical performances of the geometry of the stator and rotor armatures, in the case of induction motors, many works also deal with the ways in which these performances can be improved [5], [6], [7], [8]. Defining new classes of energy efficiency as well as finding new applications for induction motors is a continuous concern of both the academic world and industry specialists, highlighted in works [9], [10], [11]. This paper studies how the structural modifications of the two armatures of the induction motor (modification of the notches number, modification of the shape of the notches and, implicitly, the teeth) influence the losses quantity developed within it (ultimately influencing the efficiency /motor energy efficiency).

2. Determination of energy efficiency for the reference geometry of the induction motor

To view the total losses within the structure of an induction motor, related to reference geometry, the Motor-CAD programming environment was used. The defining sizes of the structure and the cross-section of the reference geometry of the induction motor chosen for the study are shown in Figure 1. Figure 2 shows a detailed view regarding the internal structure of the two armatures of the motor, with the stated purpose of visualizing the particularities of the notches (and teeth) on the stator and rotor armatures (which constitute the reference for the following analyzes within the work).

As can be seen from Figures 1 and 2, in the case of the reference geometry, the stator and rotor notches are trapezoidal in shape, while the teeth on the two armatures are rectangular. The number of notches on the two armatures, in the case of the reference geometry, has the following values (Fig. 1): $Z_1=18$, $Z_2=26$ respectively.

Next, in the case of reference geometry, the level and distribution of losses within the constituent elements of the induction motor were evaluated in two cases: a) for given cooling (natural convection at the limit value, from a temperate-continental climate, of the ambient temperature, respectively, $T_a = 40^0$ C) – without taking into account the variation of losses with temperature (Table 1); b) for given cooling (natural convection at the limit value, from a temperate-continental climate, of the ambient temperature, respectively, $T_a = 40^0$ C) - taking into account the variation of losses with temperature (Table 2).

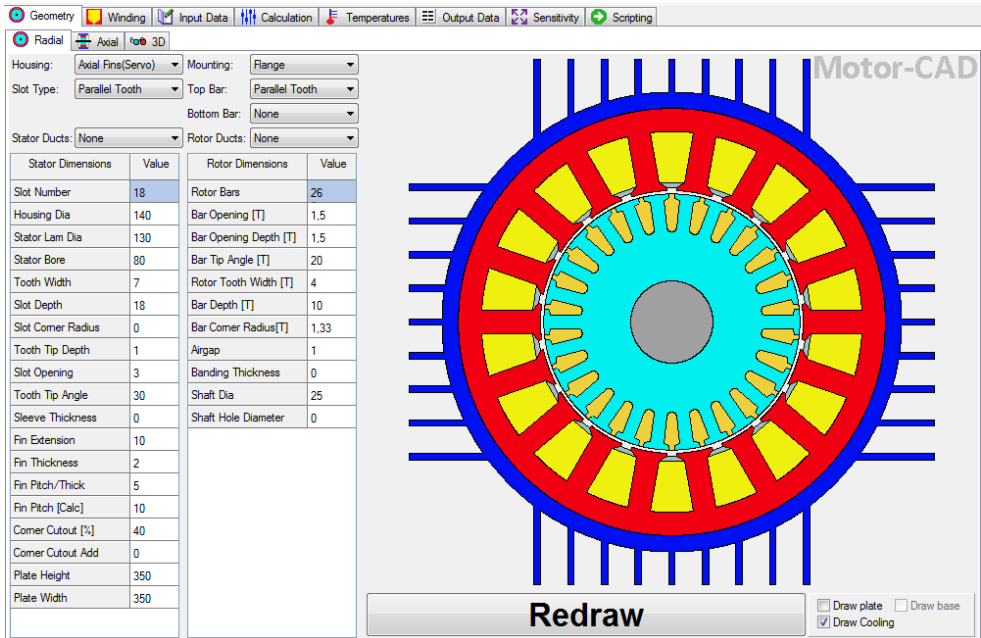


Figure 1. Reference geometry of analyzed induction motor



Figure 2. The shape of teeth and notches in the analyzed induction motor – reference geometry

In the case of considering the variation of losses with temperature, the following were used:

- The variation of the conductive material resistivity with temperature (copper for the stator winding, respectively aluminum for the rotor winding), in the form of:

$$\rho_T = \rho_{20}(1 + \alpha(T - 20)) \quad (1)$$

where: ρ_T - is the resistivity value of the material at a working temperature T.

ρ_{20} - is the value of the resistivity of the material at the reference temperature, indicated in the standards ($\rho_{20_{Copper}} = 1,72 \times 10^{-8}[\Omega m]$, $\rho_{20_{Al}} = 2,82 \times 10^{-8}[\Omega m]$);

a - is the coefficient of variation with temperature of the resistance of the conductive materials used for analysis ($\alpha_{Copper} = 4 \times 10^{-3} [1/^\circ C]$, $\alpha_{Al} = 4,3 \times 10^{-3} [1/^\circ C]$).

- Variation of shaft speed losses in the form of:

$$P_{speed} = P_{input} \times \left[\frac{Shaft\ speed}{Speed[REF]} \right]^{coef[A]} \quad (2)$$

where: $Speed[REF] = 3000[rpm]$; $coef[A] = 1,5$, values valid for the variation of losses in the stator ferromagnetic core; $Speed[REF] = 3000[rpm]$; $coef[A] = 1$ - for variation of bearing losses.

Table 1 shows both the distribution of losses developed within the structure of electromechanical conversion (without considering variation with temperature) and distribution of dissipated losses to the environment, to achieve thermal equilibrium with it, in the case of reference geometry, with the number of notches mentioned in Figure 1 and the shape of the notches and teeth, on the two armatures, highlighted in Figure 2.

Table 1. Distribution of losses within the induction motor structure, for reference geometry, without considering variation with temperature

| Developed losses Z1=18; Z2=26 | | Dissipated losses in the environment Z1=18; Z2=26 | |
|-----------------------------------|--------------|--|--------------|
| Variable | Value [W] | Variable | Value [W] |
| Loss [Stator Copper] | 120 | Main Winding (Copper Loss Multiplier) | 1 |
| Loss [Stray Load Stator Copper] | 0 | Stall Operation (Copper Loss Multiplier) | 1 |
| Loss [Stator Copper] (Active) | 63,55 | Fault Operation (Copper Loss Multiplier) | 1 |
| Loss [Stator Copper] (EWdg Front) | 28,22 | Loss[Stator Back Iron] Schematic Addition | 0 |
| Loss [Stator Copper] (EWdg Rear) | 28,22 | ----- | |
| ----- | | Dissipation - Housing - Active [Con] | 27,37 |
| Loss [Stator Back Iron] | 30 | Dissipation - Housing - Active [Rad] | 28,86 |
| Loss [Stator Tooth] | 40 | Dissipation - Front Housing OH [Con] | 14,53 |
| ----- | | Dissipation - Front Housing OH [Rad] | 15,44 |
| Loss [Rotor Cage] | 50 | Dissipation - Rear Housing OH [Con] | 16,13 |

| Developed losses Z1=18; Z2=26 | | Dissipated losses in the environment Z1=18; Z2=26 | |
|-----------------------------------|--------------|--|--------------|
| Variable | Value [W] | Variable | Value [W] |
| Loss [Rotor Cage] (Active) | 42,36 | Dissipation - Rear Housing OH [Rad] | 17,03 |
| Loss [Rotor Cage] (EndRing Front) | 3,818 | Dissipation - Front Endcap [Con] | 1,009 |
| Loss [Rotor Cage] (EndRing Rear) | 3,821 | Dissipation - Front Endcap [Rad] | 1,409 |
| ----- | | Dissipation - Rear Endcap [Con] | 7,546 |
| Loss [Stray Load Iron] | 0 | Dissipation - Rear Endcap [Rad] | 9,612 |
| Loss [Stray Load Stator Iron] | 0 | Dissipation - Plate [Con] | 44,4 |
| Loss [Stray Load Rotor Iron] | 0 | Dissipation - Plate [Rad] | 69,42 |
| Loss [Rotor Tooth] | 20 | Total Dissipation to model ambient node | 260 |
| Loss [Total] | 260 | | |

Table 2 underlines the same data, as shown in Table 1, but considers variation in relation to the temperature of the losses developed within the analyzed induction motor.

Table 2. Distribution of losses within the induction motor structure, for reference geometry, considering variation with temperature

| Developed losses Z1=18; Z2=26 | | Dissipated losses in the environment Z1=18; Z2=26 | |
|-----------------------------------|--------------|--|--------------|
| Variable | Value [W] | Variable | Value [W] |
| Loss [Stator Copper] | 176,8 | Main Winding (Copper Loss Multiplier) | 1 |
| Loss [Stray Load Stator Copper] | 0 | Stall Operation (Copper Loss Multiplier) | 1 |
| Loss [Stator Copper] (Active) | 93,61 | Fault Operation (Copper Loss Multiplier) | 1 |
| Loss [Stator Copper] (EWdg Front) | 41,57 | Loss [Stator Back Iron] Schematic Addition | 0 |
| Loss [Stator Copper] (EWdg Rear) | 41,57 | ----- | |
| ----- | | Dissipation - Housing - Active [Con] | 37,36 |
| Loss [Stator Back Iron] | 30 | Dissipation - Housing - Active [Rad] | 39,3 |
| Loss [Stator Tooth] | 40 | Dissipation - Front Housing OH [Con] | 19,79 |
| ----- | | Dissipation - Front Housing OH [Rad] | 20,78 |
| Loss [Rotor Cage] | 80,3 | Dissipation - Rear Housing OH [Con] | 22 |
| Loss [Rotor Cage] (Active) | 68,03 | Dissipation - Rear Housing OH [Rad] | 23,12 |
| Loss [Rotor Cage] (EndRing Front) | 6,13 | Dissipation - Front Endcap [Con] | 1,326 |
| Loss [Rotor Cage] (EndRing Rear) | 6,135 | Dissipation - Front Endcap [Rad] | 1,846 |

| Developed losses Z1=18; Z2=26 | | Dissipated losses in the environment Z1=18; Z2=26 | |
|----------------------------------|--------------|--|--------------|
| Variable | Value [W] | Variable | Value [W] |
| ----- | | Dissipation - Rear Endcap [Con] | 10,04 |
| Loss [Stray Load Iron] | 0 | Dissipation - Rear Endcap [Rad] | 13,04 |
| Loss [Stray Load Stator Iron] | 0 | Dissipation - Plate [Con] | 58,23 |
| Loss [Stray Load Rotor Iron] | 0 | Dissipation - Plate [Rad] | 90,65 |
| Loss [Rotor Tooth] | 20 | Total Dissipation to model ambient node | 347,0 54 |
| Loss [Total] | 347,054 | | |

There is a strong variation with temperature of the losses of the two windings: stator and rotor, respectively. On the other hand, it is noted that the cooling process is sufficient to eliminate the developed losses, without being able to specify the thermal time constant to achieve the balance with the environment. The energy efficiency assessment will be made based on a comparative analysis, which is ultimately the case for given technical characteristics when balancing the losses developed within the structure.

3. Determination of energy efficiency for changes in the geometry of stator and rotor armatures of the induction motor

By means of Motor-CAD programming environment, were analyzed the effects generated at the level of the total losses in the motor, but also on the components of the losses developed in the constitutive subassemblies of the induction motor, by changing the geometry of each armature, but also by a synergistic change, cumulative, of the two basic armatures of such type of motor. First, the results are presented for the losses within the induction motor, losses based on which, for a given effective shaft power, the efficiency of this motor can be determined (the classic formulation of the concept of energy efficiency).

As stated above, the evaluation is done by effectively comparing the total losses within the conversion structure.

In the following, the obtained results are presented in an analytical manner, by quantifying the level of losses at the variation of the geometry of each armature of the motor (cases A and B), followed by the case of the synergistic, cumulative change of the global geometry of the induction motor (case C). It is worth mentioning that the geometry of the motor still retains cylindrical symmetry on a macroscopic level, the changes being aimed at the internal components of the induction motor structure (ferromagnetic core, geometry of the notches, etc.).

A. Stator armature geometry modification

a) Increasing the number of stator notches $Z1 = 24$

For this case, the distribution of the main losses within the structure of the induction motor is comparatively presented, in the case of considering the variation of losses with temperature, with the distribution of the same categories of losses for the reference geometry, in Table 3.

Table 3. Distribution of losses within the structure of the induction motor, modified stator geometry (notches number), considering variation with temperature

| Developed losses for reference geometry $Z1=18; Z2=26$ | | Losses developed for modified stator geometry $Z1=24; Z2=26$ | |
|---|--------------|---|--------------|
| Variable | Value [W] | Variable | Value [W] |
| Loss [Stator Copper] | 176,8 | Loss [Stator Copper] | 175,5 |
| Loss [Stator Copper] (Active) | 93,61 | Loss [Stator Copper] (Active) | 81,12 |
| Loss [Stator Copper] (EWdg Front) | 41,57 | Loss [Stator Copper] (EWdg Front) | 47,18 |
| Loss [Stator Copper] (EWdg Rear) | 41,57 | Loss [Stator Copper] (EWdg Rear) | 47,18 |
| Loss [Rotor Cage] | 80,3 | Loss [Rotor Cage] | 80,09 |
| Loss [Rotor Cage] (Active) | 68,03 | Loss [Rotor Cage] (Active) | 67,85 |
| Loss [Rotor Cage] (EndRing Front) | 6,13 | Loss [Rotor Cage] (EndRing Front) | 6,114 |
| Loss [Rotor Cage] (EndRing Rear) | 6,135 | Loss [Rotor Cage] (EndRing Rear) | 6,119 |
| Loss [Total] | 347,054 | Loss [Total] | 345,563 |

b) Modification of stator notch shape, rectangular notches: $Z1 = 18$

The new shape of the stator notches is exemplified in the detail shown in Figure 3.

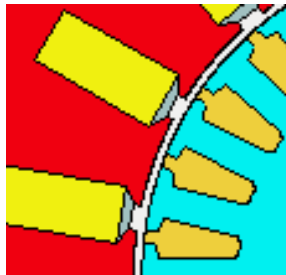


Figure 3. The shape of teeth and notches for the analyzed induction motor, modified stator geometry

Table 4 shows, also through comparative analysis regarding the reference geometry, the distribution of the main losses within the structure of the induction motor, considering the variation of these losses with temperature, for the case of changing the shape of the stator notches.

Table 4. Distribution of losses within the structure of the induction motor for modified stator geometry (notch shape), considering variation with temperature

| Developed losses for reference geometry Z1=18; Z2=26 | | Losses developed for modified stator geometry (notch rectangular shape) Z1=18, Z2=26 | |
|---|--------------|--|--------------|
| Variable | Value [W] | Variable | Value [W] |
| Loss [Stator Copper] | 176,8 | Loss [Stator Copper] | 175,8 |
| Loss [Stator Copper] (Active) | 93,61 | Loss [Stator Copper] (Active) | 76,01 |
| Loss [Stator Copper] (EWdg Front) | 41,57 | Loss [Stator Copper] (EWdg Front) | 49,9 |
| Loss [Stator Copper] (EWdg Rear) | 41,57 | Loss [Stator Copper] (EWdg Rear) | 49,9 |
| Loss [Rotor Cage] | 80,3 | Loss [Rotor Cage] | 79,99 |
| Loss [Rotor Cage] (Active) | 68,03 | Loss [Rotor Cage] (Active) | 67,77 |
| Loss [Rotor Cage] (EndRing Front) | 6,13 | Loss [Rotor Cage] (EndRing Front) | 6,107 |
| Loss [Rotor Cage] (EndRing Rear) | 6,135 | Loss [Rotor Cage] (EndRing Rear) | 6,112 |
| Loss [Total] | 347,054 | Loss [Total] | 345,799 |

B. Modification of rotor armature geometry

a) Reducing the number of rotor notches: $Z2 = 22$

For this case, taking into account that for the same number of stator notches it is possible to choose of a number of rotor notches, within a relatively wide range, the choice consisted in a decrease of the of rotor notches number in relation to the reference geometry.

The new distribution of the main losses within the structure (the losses in the iron and those in the bearings being influenced, only, by the speed at the shaft; the regime analysis was done for the shaft speed equal to the synchronism speed, respectively, 3000 rpm). Table 5 presents the analysis comparison developed in case A for the new value of the number of rotor notches.

Table 5. Distribution of losses within the induction motor structure, for modified rotor geometry (lower number of rotor notches), considering the variation with temperature

| Developed losses for reference geometry Z1=18; Z2=26 | | Losses developed for modified rotor geometry Z1=18, Z2=22 | |
|---|--------------|--|--------------|
| Variable | Value [W] | Variable | Value [W] |
| Loss [Stator Copper] | 176,8 | Loss [Stator Copper] | 174,7 |
| Loss [Stator Copper] (Active) | 93,61 | Loss [Stator Copper] (Active) | 92,51 |
| Loss [Stator Copper] (EWdg Front) | 41,57 | Loss [Stator Copper] (EWdg Front) | 41,08 |
| Loss [Stator Copper] (EWdg Rear) | 41,57 | Loss [Stator Copper] (EWdg Rear) | 41,08 |
| Loss [Rotor Cage] | 80,3 | Loss [Rotor Cage] | 80,06 |
| Loss [Rotor Cage] (Active) | 68,03 | Loss [Rotor Cage] (Active) | 66,5 |
| Loss [Rotor Cage] (EndRing Front) | 6,13 | Loss [Rotor Cage] (EndRing Front) | 6,777 |
| Loss [Rotor Cage] (EndRing Rear) | 6,135 | Loss [Rotor Cage] (EndRing Rear) | 6,782 |
| Loss [Total] | 347,054 | Loss [Total] | 344,734 |

b) Increasing the number of rotor notches: Z2 = 30

Increasing symmetrically the number of rotor notches in relation to the reference geometry, the situation highlighted in Table 6 was obtained for the distribution of the main losses developed within the structure.

Table 6. Distribution of losses within the structure of the induction motor, for modified rotor geometry (larger number of rotor notches)

| Developed losses for reference geometry Z1=18; Z2=26 | | Losses developed for modified rotor geometry Z1=18, Z2=30 | |
|---|--------------|--|--------------|
| Variable | Value [W] | Variable | Value [W] |
| Loss [Stator Copper] | 176,8 | Loss [Stator Copper] | 176,8 |
| Loss [Stator Copper] (Active) | 93,61 | Loss [Stator Copper] (Active) | 93,61 |
| Loss [Stator Copper] (EWdg Front) | 41,57 | Loss [Stator Copper] (EWdg Front) | 41,57 |
| Loss [Stator Copper] (EWdg Rear) | 41,57 | Loss [Stator Copper] (EWdg Rear) | 41,57 |
| Loss [Rotor Cage] | 80,3 | Loss [Rotor Cage] | 80,29 |
| Loss [Rotor Cage] (Active) | 68,03 | Loss [Rotor Cage] (Active) | 69,4 |
| Loss [Rotor Cage] (EndRing Front) | 6,13 | Loss [Rotor Cage] (EndRing Front) | 5,438 |
| Loss [Rotor Cage] (EndRing Rear) | 6,135 | Loss [Rotor Cage] (EndRing Rear) | 5,443 |
| Loss [Total] | 347,054 | Loss [Total] | 347,043 |

c) Changing the shape of the rotor notch, round/circular notches: $Z_2 = 26$

The new geometry of the rotor notches (for the same number of notches on the rotor armature, with the one in the reference geometry) is shown in Figure 4.



Figure 4. Shape of teeth and notches at the analyzed induction motor - modified rotor geometry

The distribution of losses developed, in the new configuration, is presented in Table 7.

Table 7. Distribution of losses within the induction motor, for modified rotor geometry (notch shape), considering variation with temperature

| Losses developed for reference geometry $Z_1=18; Z_2=26$ | | Losses developed for modified rotor geometry (round/circular notches) $Z_1=18,$ $Z_2=26$ | |
|---|--------------|--|--------------|
| Variable | Value [W] | Variable | Value [W] |
| Loss [Stator Copper] | 176,8 | Loss [Stator Copper] | 176,7 |
| Loss [Stator Copper] (Active) | 93,61 | Loss [Stator Copper] (Active) | 93,6 |
| Loss [Stator Copper] (EWdg Front) | 41,57 | Loss [Stator Copper] (EWdg Front) | 41,57 |
| Loss [Stator Copper] (EWdg Rear) | 41,57 | Loss [Stator Copper] (EWdg Rear) | 41,57 |
| Loss [Rotor Cage] | 80,3 | Loss [Rotor Cage] | 80,06 |
| Loss [Rotor Cage] (Active) | 68,03 | Loss [Rotor Cage] (Active) | 71,94 |
| Loss [Rotor Cage] (EndRing Front) | 6,13 | Loss [Rotor Cage] (EndRing Front) | 4,057 |
| Loss [Rotor Cage] (EndRing Rear) | 6,135 | Loss [Rotor Cage] (EndRing Rear) | 4,065 |
| Loss [Total] | 347,054 | Loss [Total] | 346,79 |

C. Synergistic modification of induction motor geometry

In this last analysis of the paper, radical structural changes were made, aiming at a synergistic change of the geometry (either a stator-rotor synergistic change that targets only the simultaneous modification of the notches number on the two armatures, or a synergistic change only at the level of the rotor armature, that aims both the changing the notches number at the level of this armature, in relation to the reference geometry as well as the change in the shape of the rotor notches).

a) Total modification of stator and rotor geometry (number of notches only)

Table 8 presents the results obtained regarding the distribution of the main losses within the induction motor structure, for stator-rotor synergistic modification (simultaneous modification of the notches number on the two armatures).

Table 8. Distribution of losses within the structure of the induction motor, for modified stator and rotor geometry, considering variation with temperature

| Losses developed for reference geometry Z1=18; Z2=26 | | Losses developed for total modification of stator and rotor geometry Z1=24; Z2=22 | |
|---|--------------|--|--------------|
| Variable | Value [W] | Variable | Value [W] |
| Loss [Stator Copper] | 176,8 | Loss [Stator Copper] | 175,9 |
| Loss [Stator Copper] (Active) | 93,61 | Loss [Stator Copper] (Active) | 81,34 |
| Loss [Stator Copper] (EWdg Front) | 41,57 | Loss [Stator Copper] (EWdg Front) | 47,3 |
| Loss [Stator Copper] (EWdg Rear) | 41,57 | Loss [Stator Copper] (EWdg Rear) | 47,3 |
| Loss [Rotor Cage] | 80,3 | Loss [Rotor Cage] | 80,15 |
| Loss [Rotor Cage] (Active) | 68,03 | Loss [Rotor Cage] (Active) | 66,52 |
| Loss [Rotor Cage] (EndRing Front) | 6,13 | Loss [Rotor Cage] (EndRing Front) | 6,811 |
| Loss [Rotor Cage] (EndRing Rear) | 6,135 | Loss [Rotor Cage] (EndRing Rear) | 6,817 |
| Loss [Total] | 347,054 | Loss [Total] | 346,088 |

b) Changing only the rotor geometry (notches number and shape)

In the case of synergistic modification only at the level of the rotor armature (notches number and shape), the new distribution of the main losses within the engine is presented in Table 9.

Table 9. Distribution of losses within the structure of the induction motor - for changing only the rotor geometry - considering the variation with temperature

| Losses developed for reference geometry Z1=18; Z2=26 | | Losses developed for changing only the rotor geometry Z1=18; Z2=22 (round/circular notches) | |
|---|--------------|---|--------------|
| Variable | Value [W] | Variable | Value [W] |
| Loss [Stator Copper] | 176,8 | Loss [Stator Copper] | 174,6 |
| Loss [Stator Copper] (Active) | 93,61 | Loss [Stator Copper] (Active) | 92,49 |
| Loss [Stator Copper] (EWdg Front) | 41,57 | Loss [Stator Copper] (EWdg Front) | 41,07 |
| Loss [Stator Copper] (EWdg Rear) | 41,57 | Loss [Stator Copper] (EWdg Rear) | 41,07 |
| Loss [Rotor Cage] | 80,3 | Loss [Rotor Cage] | 79,79 |
| Loss [Rotor Cage] (Active) | 68,03 | Loss [Rotor Cage] (Active) | 72,84 |
| Loss [Rotor Cage] (EndRing Front) | 6,13 | Loss [Rotor Cage] (EndRing Front) | 3,472 |
| Loss [Rotor Cage] (EndRing Rear) | 6,135 | Loss [Rotor Cage] (EndRing Rear) | 3,48 |
| Loss [Total] | 347,054 | Loss [Total] | 344,4 23 |

Remark. Within the total losses, captured in tables 3-9, are integrated the main losses that vary with temperature and the constant value of losses in iron (from the stator yoke and stator and rotor teeth) that do not register variations with temperature, losses mentioned in Tables 1 and 2 (a constant value of 90 W).

4. Obtained results. Discussions

The results of the comparative analysis, summarized in Tables 3-9, can be viewed further easily, to highlight the particularities regarding the distribution of the main losses within the induction motor (and, by extrapolation, the energy efficiency/yield of this motor), through the graphical representations in Figures 5-7.

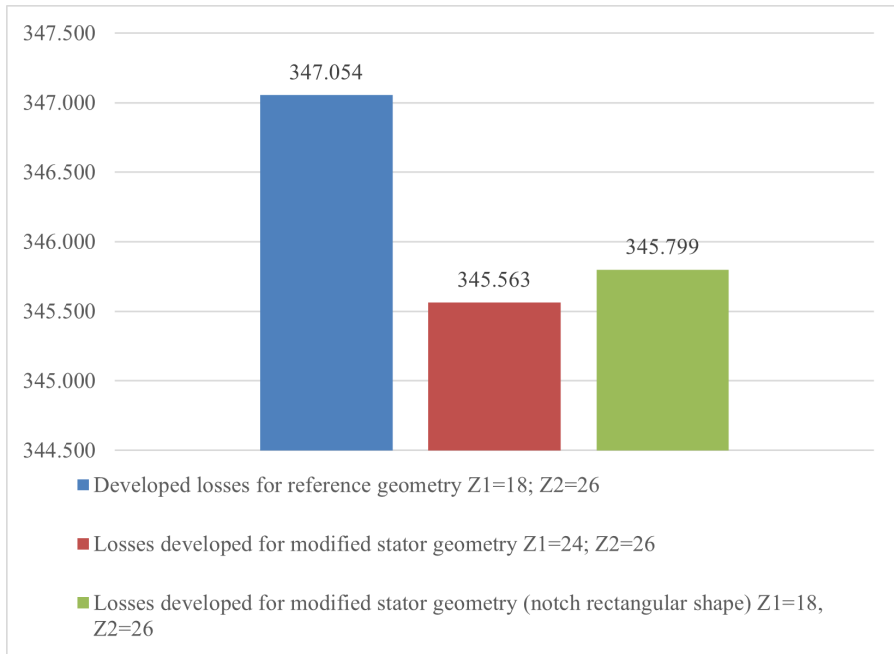


Figure 5. The Influence of stator geometry changes on induction motor losses

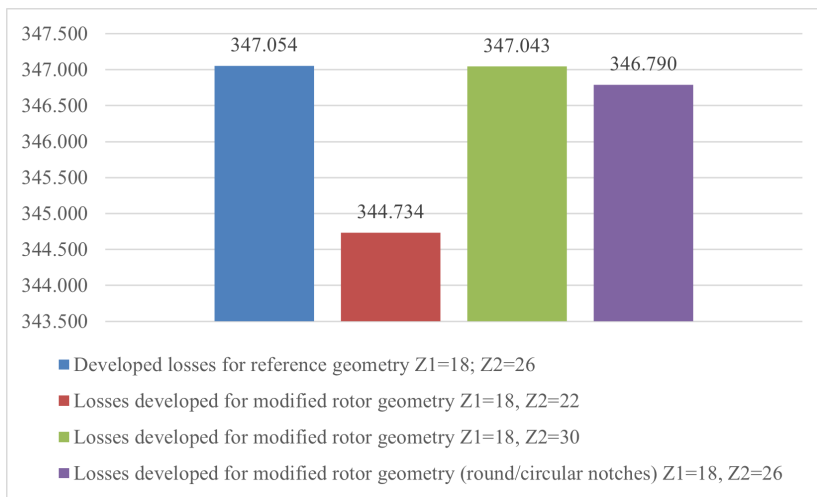


Figure 6. The Influence of rotor geometry changes on induction motor losses

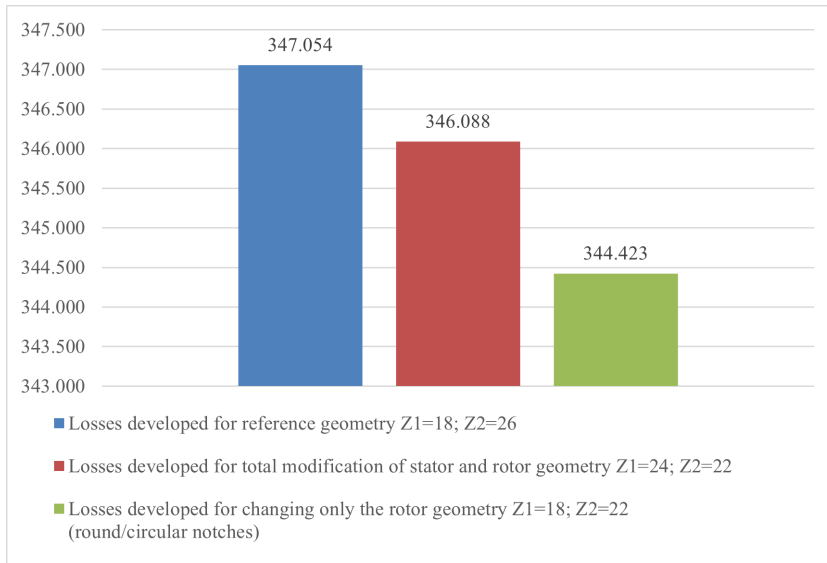


Figure 7. The influence of synergistic geometric changes on induction motor losses

This analysis shows that:

- Modification of the geometry of the stator and rotor armatures at the induction motor, for given technical and ventilation characteristics, leads to a modification of the level and the distribution of losses within the structure and, implicitly, to a change its energy efficiency.
- Unilateral changes in the geometry of the induction motor (of each armature, independently) slightly affect the level of losses and change the induction motor efficiency in a small proportion.
- Synergistic changes in the induction motor geometry affect to a greater extent the losses level developed within the structure and substantially modifies the induction motor efficiency.
 - Rotor geometry modifications (unilateral or synergistic), at the induction motor, lead to a significant reduction of the motor losses level and, thus, to an efficiency increase.
 - Changes in the geometry of the stator and rotor armatures significantly influence the losses in the windings and much less the losses in the ferromagnetic core.

5. Conclusions

Following the study undertaken, we can conclude:

- Increasing the energy efficiency of induction motors can be achieved, relatively easily, by radically changing the rotor geometry - as it resulted from the analysis carried out: in principle, in induction motors with a cage rotor, by changing the number of bars/notches rotors, but also by changing the geometry/shape of the notches of this armature.

- The geometric changes of the rotor armature certainly, unfortunately, also affect the technical characteristics of this motor and not only those of energy performance, because the torque developed by the induction motor strongly depends on the electrical resistance of the rotor cage, a resistance that changes, along with the change in the geometry of the notches and rotor teeth. As a result, in the design process, it is necessary to continuously weigh the technical performances (especially the torque developed by the engine) and those of energy efficiency.

Of course, this work opened a path, on which, along with companies that design and produce induction motors, concrete steps can be taken to develop, soon, induction motors that perform technically, economically and with a low impact on the environment, whilst also implementing the concept of saving electricity.

References

- [1] Gundogdu T., Zhu Z. Q., Mipo J. C., Personnaz S., Influence of stator and rotor geometric parameters on rotor bar current waveform and performance of IMs, *The Journal of Engineering*, 2019, Vol. 2019, Iss. 17, pp. 3649-3654.
- [2] Purwanto W., Risfendra, D.S., *Effect of Stator Slot Geometry on High Speed Spindle Motor Performance*, Proceedings of 2018 International Conference on Information and Communications Technology, pp. 560-564.
- [3] Tezcan M.M., Yetgin A.G., Influencies of the Slits on Magnetic Flux Density for Induction Motors Having Different Rotor Slot Geometries, *Journal of Multidisciplinary Engineering Science and Technology (JMEST)*, 3(12), 2016, pp. 6226-6229.
- [4] Ferreira de Souza D., Marino Salotti F.A., Sauer I.L., Tatizawa H., Traça de Almeida A., Kanashiro A.G., A Performance Evaluation of Three-Phase Induction Electric Motors between 1945 and 2020, *Energies* 2022, 15, 2002, pp. 1-31.
- [5] Khoury G., *Energy efficiency improvement of a squirrel-cage induction motor through the control strategy*, thèse doctorale de l'Université de Toulouse, 2018.

- [6] Gundabattini E., Kuppan R., Solomon D. G., Kalam A., Kothari D.P., Abu Bakar R., A review on methods of finding losses and cooling methods to increase efficiency of electric machines, *Ain Shams Engineering Journal* 12 (2021), pp. 497–505.
- [7] Rezaiee Nakhaei M., Roshanfekar R., Optimal Design of 3-phase Squirrel Cage Induction Motors Using Genetic Algorithm Based on the Motor Efficiency and Economic Evaluation of the optimal Model, *Balkan Journal of electrical & Computer Engineer*, 9(1), 2021, pp. 59-68.
- [8] Nehete M. K., Kulkarni S.U., Design Improvement of the Premium Efficiency Induction Motor for Higher Efficiency & Cost Reduction, *International Journal of Applied Engineering Research*, 13(10), 2018, pp. 8596-8600.
- [9] *Premium efficiency motor selection and application guide - a handbook for industry*, U.S. Department of Energy, February 2014.
- [10] Zeaiter A., *Thermal modeling and cooling of electric motors. Application to the propulsion of hybrid aircraft*, thèse doctorale de l'Ecole Nationale Supérieure de Mécanique et d'Aérotechnique, 2016.
- [11] Lan B., *Design Simulation and Experiments on Electrical Machines for Integrated Starter - Generator Applications*, Doctoral Thesis, University of Sheffield, 2018.

Addresses:

- Conf. Dr. Eng. Ion Voncila, Dunarea de Jos University, Faculty of Automation, Computers, Electrical Engineering and Electronics, Str. Științei nr. 2, Galați - 800146, România, ion.voncila@ugal.ro (*corresponding author)
- Assist. Dr. Eng. Elena Selim, Dunarea de Jos University, Faculty of Automation, Computers, Electrical Engineering and Electronics, Str. Științei nr. 2, Galați - 800146, România elena.selim@ugal.ro
- S.L. Dr. Eng. Ion Paraschiv, Dunarea de Jos University, Faculty of Automation, Computers, Electrical Engineering and Electronics, Str. Științei nr. 2, Galați - 800146, România, ion.paraschiv@ugal.ro